



Campos Domínguez, Candela, Dipl.- Ing.

# **Process Intensification for Supercritical Fluid Fractionation by Means of Micro-Mixers**

## **DOCTORAL THESIS**

to achieve the university degree of  
Doktor der technischen Wissenschaften  
submitted to

**Graz University of Technology**

Supervisor

Gamse, Thomas, Ao.Univ.-Prof. Dipl.-Ing. Dr.techn.  
Institute of Chemical Engineering and Environmental Technology

Graz University of Technology

Graz, October 2016

## **AFFIDAVIT**

I declare that I have authored this thesis independently, that I have not used other than the declared sources/resources, and that I have explicitly indicated all material which has been quoted either literally or by content from the sources used. The text document uploaded to TUGRAZonline is identical to the present doctoral thesis.

---

Date

---

Signature

*To my family and friends*

*The mind is like a parachute;  
it doesn't work unless it is open.*

Frank Zappa or Albert Einstein?



The authors want to thank the Marie Curie Initial Training Networks (ITN) for the financial support of the project "DoHip - Training Program for the Design of Resource and Energy Efficient Products by High Pressure Processes", project number PITN-GA-2012-316959).

## DoHip Training

- Workshop I. **Project Management, Intellectual Property Rights (IPR) and Tools for Literature and Patent Survey.** Bochum, Oberhausen (Germany), Valladolid (Spain), Graz (Austria), Maribor (Slovenia) and Budapest (Hungary). November 20 - December 6, 2013.
- LLL Intensive Course „**Process Intensification by High Pressure Technologies – Actual Strategies for Energy and Resources Conservation**“, University of Strathclyde, Glasgow (Scotland). June 29-July 16, 2014.
- Workshop II. „**DoHip Analytical Course**“, Maribor (Slovenia). July 21-16, 2014. **“Business and Communications Skills**“, Graz (Austria). July 28-31, 2014.
- Workshop III. **“Academic Career Planning**“, Frankfurt/Darmstadt (Germany). June 15-19, 2015.

## Publications

Campos Dominguez, C., Gamse, T., 2015 Prozessintensivierung der Hochdruckextraktion flüssiger Ausgangsmaterialien durch Mikromischer. *Chemie Ingenieur Technik*, 87(8), 1074-1075.

Domínguez Campos, C., Gamse, T., 2016. Process intensification by the use of micro devices for liquid fractionation with supercritical carbon dioxide. *Chemical Engineering Research and Design*, 108, 139-145.

## Contributions

- Process Intensification of Liquid Fractionation with Supercritical Fluids by Use of Micro Devices. Campos Dominguez, C., Gamse, T. *Jahrestreffen der Fachgruppe Hochdruckverfahrenstechnik (DECHEMA), Merseburg (Germany). March 13-14, 2014.* – **Poster presentation.**
- Process Intensification of Liquid Fractionation with Supercritical Fluids by Use of Micro Devices. Campos Dominguez, C., Gamse, T. *10. Minisymposium Verfahrenstechnik, Wien (Austria). June 17-18, 2014.* – **Poster presentation.**
- Process Intensification of Liquid Fractionation with Supercritical Fluids by Use of Micro Devices. *Campos Dominguez, C.*, Gamse, T. *Jahrestreffen der Fachgruppe Hochdruckverfahrenstechnik (DECHEMA), Darmstadt (Germany). March 3-5, 2015.* – **Poster Presentation.**
- Process Intensification of Liquid Fractionation with Supercritical Fluids by Use of Micro Devices. Campos Dominguez, C., Gamse, T. *Hungarian National Conference on Supercritical Fluids, Budapest (Hungary). May 21, 2015.* – **Oral presentation.**

- Process Intensification of Liquid Fractionation with Supercritical Fluids by Use of Micro Devices. Campos Dominguez, C., Gamse, T. *15th European Mixing Conference, St. Petersburg (Russia). June 28–July 3, 2015.* – **Oral presentation.**
  
- Process Intensification of Liquid Fractionation with Supercritical Fluids by Using of Micro Devices. Campos Dominguez, C., Gamse, T. *Jahrestreffen der Fachgemeinschaft Fluidodynamik und Trenntechnik (DECHEMA), Bamberg (Germany). September 9–11, 2015.* – **Oral presentation.**
  
- Supercritical CO<sub>2</sub> Extraction of Liquid Mixtures by Micro-Devices. Campos Dominguez, C., Gamse, T. *Jahrestreffen der Fachgruppe Mikroverfahrenstechnik. Frankfurt (Germany). September 14, 2015.* – **Poster Presentation.**
  
- Supercritical Fluid Extraction of Ethanol from Aqueous Solutions Using Micro-Devices. Campos Dominguez, C., Gamse, T. *10th European Congress on Chemical Engineering (ECCE10), Nice (France). September 28–October 1, 2015.* – **Poster presentation.**
  
- Continuous Supercritical Fluid Extraction of Liquids Using Micro-Mixers. Campos Dominguez, C., Gamse, T. *12. Minisymposium Verfahrenstechnik, Graz (Austria). March 30-31, 2016.* – **Poster presentation.**
  
- Utilization of Micro-Devices for Supercritical Extraction of Liquids. Campos Dominguez, C., Gamse, T. *15<sup>th</sup> European Meeting on Supercritical Fluids, Essen (Germany). May 8-11, 2016.* – **Oral presentation.**

# Acknowledgements

First of all, I would like to thank my supervisor, Prof. Thomas Gamse, for giving me the chance to complete my PhD within the framework of DoHip project and to develop myself (personally and professionally) during the last 3 years. Thank you for always having a smile and such a good mood every time I was going to your office for help, advice and/or support!

I would also take the chance to thank Prof. Siebenhofer, for thinking of me when this position came up and for his recommendation. But especially for his support and his encouraging words (particularly in the last months), and for his “Buenos días” with a smile every day.

Thank you to Bettina Koch and Jutta Freißmuth for their help in all the administrative matters and their patient with my issues with the German language. Thank you to Rene, Herta and Peter Letonja, too, for their help with the technical and scientific issues. I would also like to express my thanks to Ricardo Santos and his research group from University of Porto for making me feel so welcome while I was with them, but especially, for all their extraordinary work.

A special, warm thanks to the DoHip family. Especially to the DoHippies. Thank you for all the moments, the amazing trips and experiences that we have lived together. Without any of you, these 3 years definitely would not have been the same. And a special thanks to my DC: Dániel. For all the support, the screwing, and help.

To all the students who were part of this, thank you for your work and motivation: Taru, Petra, Sebastian, María, Carlos and Andressa.

Thank you to all my colleagues and friends in Graz, for being part of this adventure and making these last three years so special and unique.

Thank you very much to my family: to my parents and my sister. For being always my biggest support despite the distance (anytime, anywhere). For always listening to me (and to my complaints and frustrations) and for being such an inspiration. And last but not least, the most special thanks to Rafa, for being always by my side, no matters what. For being my partner, my colleague, my psychologist, my friend, and the most important: my adventure mate. I know you have *suffered* this thesis as much as I have. Thank you for all your support, comprehension, help and encouragement.

# Abstract

The utilization of micro-mixers for Supercritical Fluid Extraction (SFE) and Supercritical Fluid Fractionation (SFF) was investigated in this work. A fully new high-pressure experimental apparatus was designed and assembled. Two different mixing principles were tested: multi-lamination and T-type lamination. The extraction of ethanol from aqueous solutions by supercritical carbon dioxide (scCO<sub>2</sub>) was chosen as the model system. The influence of different parameters on the extraction process was studied: feed concentration, solvent flow rate and Solvent-to-Feed ratio, length of the capillary placed between the micro-mixer and separator, and overall flow rate. The phase equilibria behaviour of the CO<sub>2</sub>-ethanol-water system was modelled in ASPEN Plus® using the Peng-Robinson EoS at the experimental conditions chosen (101 bar and 60 °C). Experimental results showed that one theoretical stage was always reached at the different ethanol feed concentrations and Solvent-to-Feed ratios studied. Nevertheless, the study of capillary length showed that the K-factor slightly decreased as the capillary length increased. These results confirmed that, at the flow rates considered, the mixing in the micro-mixers was enough to reach the thermodynamic equilibrium. In order to assess the extraction process in micro-mixers under different hydrodynamic conditions, the extraction of FFA from olive oil with micro-mixers was also investigated. The results proved that equilibrium could be achieved as well at distinct physical properties. It was therefore concluded then that one micro-mixer can be equivalent of a theoretical extraction stage. By comparing the results obtained with both mixing principles studied here, it was observed that the extraction results were not influenced by the mixing principle.

The mixing of liquids with scCO<sub>2</sub> was also studied. The multiphase flow behaviour of scCO<sub>2</sub> with different liquid mixtures (ethanol-water mixtures and olive oil) in a capillary placed at the outlet of the micro-mixer was observed. Results showed that the mixing principle as well as the physical properties influences the flow behaviour of the fluids through the mixing process and in the capillary. Experimental results were compared with CFD simulations.

Aspects such as the design of a multi-stage extraction process with micro-mixers as well as the scale-up of the process have also been discussed.

# Kurzfassung

Die Prozessintensivierung der Hochdruckextraktion flüssiger Ausgangsmaterialien durch die Nutzung von Mikromischern wurde untersucht. Zur Untersuchung der Durchführbarkeit des Extraktionsprozesses mittels Mikromischern wurde eine Hochdruckanlage konzipiert und im Technikum aufgebaut. Bei dieser Anlage ist der Mikromischer das Kernstück, in dem das Lösungsmittel (überkritisches  $\text{CO}_2$ ) und das flüssige Ausgangsmaterial intensiv gemischt werden. Zwei unterschiedliche Mikromischer (sowie Mischprinzipien) wurden verglichen: Multilaminations-Mischprinzip und T-Mischer. Um die Wirtschaftlichkeit der Mikromischer-Hochdruckextraktionsanlage zu ermitteln, wurde die Ethanol - Wasser Trennung mit überkritischem  $\text{CO}_2$  als Lösungsmittel gewählt. Experimente wurden bei 101 bar,  $60^\circ\text{C}$ , unterschiedlichen Feedzusammensetzungen sowie verschiedenen Lösemittel zu Feed Verhältnissen durchgeführt. Der Einfluss der Kapillarlänge zwischen Mischer und Abscheider sowie der Durchflussrate auf die Extraktionseffizienz wurden ebenfalls untersucht. Die Phasengleichgewichtsberechnungen erfolgten mit der Peng-Robinson-Zustandsgleichung in ASPEN Plus<sup>®</sup>, um zu prüfen, ob eine theoretische Trennstufe in der Mikromischeranlage erreicht wird, und um die experimentellen Ergebnisse mit der Modellierung zu vergleichen. Um die Wirtschaftlichkeit der Mikromischer-Hochdruckextraktionsanlage unter verschiedenen hydrodynamischen Bedingungen zu ermitteln, wurde auch die Gewinnung von Olivenöl untersucht. Die Ergebnisse demonstrieren, dass in der Mikromischeranlage eine theoretische Stufe erreicht werden kann.

Das Fließverhalten verschiedener Flüssigkeitsgemische (wässrigen Ethanol Lösungen und Olivenöl) mit überkritischem  $\text{CO}_2$  wurde untersucht. Die Ergebnisse bestätigten, dass das Strömungsprofil von der Durchflussrate (Fließgeschwindigkeit) sowie der Eigenschaften der Lösungssysteme beeinflusst werden. Experimentelle Ergebnisse wurden mit CFD-Modellierung verglichen.

Design und Modellierung von Mehrstufen-Extraktionsprozesse durch die Nutzung von Mikromischern wurde durchgeführt. Das Konzept zum Scale-up vom Labor- zum Pilotanlagen-Maßstab wurde für größere Durchsätze diskutiert.

# Table of Contents

1. Introduction.....	1
2. State-of-the-art.....	4
2.1. Supercritical fluids.....	4
2.1.1. Supercritical carbon dioxide.....	9
2.2. Supercritical Fluid Extraction (SFE).....	11
2.2.1. SFE of ethanol from aqueous solutions.....	15
2.2.2. SFE of free fatty acids from olive oil.....	19
2.3. Microfluidics technology.....	21
2.3.1. Mixing principles under study.....	23
2.3.1.1. T-type lamination mixing.....	23
2.3.1.2. Multi-lamination mixing.....	24
2.3.2. Micro-mixers for extraction purposes.....	25
2.3.2.1. Micro-mixers for liquid-liquid extraction.....	25
2.3.3. Micro-mixers and supercritical fluids.....	26
2.4. CFD and supercritical fluids.....	28
3. Experimental section.....	30
3.1. Experimental setup.....	30
3.1.1. SFE experimental setup.....	30
3.1.2. Visualization experimental setup.....	32
3.1.3. Micro-devices description.....	33
3.2. Experimental procedures.....	35
3.2.1. SFE experiments.....	35
3.2.2. Visualization experiments.....	36
3.3. Materials and methods.....	36
3.3.1. Experiments on the extraction of ethanol from aqueous solutions (system A).....	36
3.3.1.1. Chemicals.....	36
3.3.1.2. Sampling.....	37
3.3.1.3. Analytical methods.....	37
3.3.2. Experiments on the extraction of FFA from olive oil (system B).....	37
3.3.2.1. Chemicals.....	37
3.3.2.2. Sampling.....	38
3.3.2.3. Analytical methods.....	38
3.3.3. Experiments on the visualization of multiphase flows of scCO <sub>2</sub> and liquid mixtures.....	39
3.3.3.1. Chemicals.....	39
3.3.3.2. Optical system.....	39
4. Model system: CO <sub>2</sub> -ethanol-water. SFE of ethanol from aqueous solutions.....	40
4.1. Phase behaviour.....	40
4.1.1. Experimental data.....	40
4.1.2. Modelling.....	47

4.2. Physical properties.....	50
4.2.1. Supercritical CO <sub>2</sub> .....	51
4.2.2. CO <sub>2</sub> -water system.....	51
4.2.3. Ethanol-water system.....	53
4.2.4. CO <sub>2</sub> -ethanol system.....	57
4.2.5. CO <sub>2</sub> -ethanol-water system.....	59
4.3. Experimental results.....	62
4.3.1. Influence of the feed concentration.....	64
4.3.2. Influence of the solvent flow rate.....	66
4.3.3. Influence of the Solvent-to-Feed ratio (S-to-F).....	68
4.3.4. Influence of the capillary length.....	69
4.3.5. Influence of the overall volume flow rate.....	74
4.3.5.1. Feed with 10 wt.% ethanol.....	74
4.3.5.2. Feed with 50 wt.% ethanol.....	78
4.3.5.3. Feed with 90 wt.% ethanol.....	81
4.4. Process design of a micro-mixer multi-stage extraction process and comparison with SFE in an extraction column.....	82
5. SFE of free fatty acids from olive oil.....	92
5.1. Phase behaviour.....	92
5.2. Physical properties.....	98
5.2.1. Supercritical CO <sub>2</sub> .....	98
5.2.2. Olive oil.....	100
5.2.3. CO <sub>2</sub> + olive oil.....	101
5.3. Experimental results.....	105
5.4. Validation of the model.....	108
6. Visualization of multiphase flows of supercritical carbon dioxide and liquid mixtures.....	110
6.1. Fluid behaviour of supercritical carbon dioxide with ethanol-water liquid mixtures (system A).....	111
6.1.1. Mixing in HPIMM micro-mixer.....	113
6.1.2. Mixing in Tee-mixer.....	116
6.1.3. Comparison HPIMM micro-mixer vs. Tee-mixer.....	120
6.2. Fluid behaviour of supercritical carbon dioxide with olive oil (system B).....	121
6.2.1. Mixing in HPIMM micro-mixer.....	122
6.2.2. Mixing in Tee-mixer.....	123
6.2.3. Comparison HPIMM micro-mixer vs. Tee-mixer.....	124
6.3. Comparison of the fluid behaviour of system A and system B.....	125
7. CFD modelling of the multiphase flow of supercritical carbon dioxide and liquid mixtures.....	126
7.1. CFD model of the flow behaviour.....	126
7.1.1. 3D domain.....	126
7.1.2. VOF model.....	128
7.2. CFD model of the mass transfer.....	134



7.2.1. Eulerian-Eulerian model.....	135
7.2.2. Eulerian model with Multi-fluid VOF.....	138
8. Conclusions, remarks and outlook.....	142
8.1. Conclusions.....	142
8.2. Remarks.....	144
8.3. Outlook.....	145
9. Summary.....	150
Abbreviations & Nomenclature	
References	

# 1. Introduction

Process intensification was defined by Stankiewicz and Moulijn (2000) as “the development of novel apparatus and techniques that, compared to those commonly used today, are expected to bring dramatic improvements in manufacturing and processing, substantially decreasing equipment size/production capacity ratio, energy consumption, or waste production, and ultimately resulting in cheaper, sustainable technologies”. Terms such as “micro-process technology” or “microfluidics” are strongly linked to the conception of process intensification, as it has been proved that it can provide the opportunity to perform chemical processes as well as plant designs faster, resulting therefore in lower operating costs and investment (Becht et al., 2007). Within the last decades, different applications of micro-process technology have been developed: micro-mixers, micro heat exchangers, micro-evaporators, micro-extractors, micro-distillators or micro-membrane devices. The utilization of micro-mixers in particular has been demonstrated to be very advantageous in processes such as chemical reaction or extraction. As Assmann, Ładosz and Rudolf von Rohr (2013) stated, liquid-liquid extraction benefits from microfluidics as the short path lengths and large interfacial area between the two liquid phases can enhance the extraction efficiency and equilibrium can be reached within seconds. Nevertheless, the utilization of micro-mixers for Supercritical Fluid Extraction (SFE) and Supercritical Fluid Fractionation (SFF) has been barely investigated to date (Assmann et al., 2012; Assmann, Werhan, Ładosz, et al., 2013). In the last decades, SFE and SFF processes are becoming a convenient, significant alternative to other conventional separation techniques. The use of supercritical solvents provides enhanced extraction rates and solvent-free extracts and raffinates, as product recovery happens via pressure reduction. Besides, Assmann, Ładosz and Rudolf von Rohr (2013) affirmed that, despite the benefits of microfluidics for liquid-liquid extraction, the separation of the phases still constitutes a difficulty. However, in SFE and SFF, the phase separation is not an issue, as the separation of the solvent from the extract happens via pressure reduction, causing the phase change from supercritical to gas.

In this work, the applicability and efficiency of micro-mixers in SFE and SFF processes was investigated. For this purpose, a fully new high-pressure experimental apparatus was designed and assembled. Besides, the extraction of ethanol from aqueous solutions by

supercritical carbon dioxide (scCO<sub>2</sub>) was chosen as a model system due to that it is a widely studied process for applications such as dealcoholisation of beverages, ethanol production or ethanol recovery from fermentation broth. The influence of different parameters on the extraction process was studied: feed concentration, solvent flow rate and Solvent-to-Feed ratio, length of the capillary placed between the micro-mixer and separator, and overall flow rate. Moreover, the Equilibrium Stage Model Concept was used to assess the experimental results and confirm whether equilibrium was reached through the extraction process.

Further on, for a better comprehension and knowledge of the extraction process in micro-mixers, a second extraction system was investigated: the extraction of free fatty acids (FFA) from olive oil. This second system presents physical properties very different from the first one. Moreover, the extraction conditions were also different, which allowed us to assess the extraction process in micro-mixers under different hydrodynamic conditions.

Besides the extraction process, the mixing of liquids with scCO<sub>2</sub> was also studied. Processes which involve supercritical fluids (SCFs) consequentially involve high-pressure as well. High-pressure processes usually take place in the interior of solid stainless steel apparatuses capable to withstand the pressure, which restricts the optical access and hinders the observation and the study of the mechanism taking place. Thus, the data available in literature for supercritical fluid flow behaviour in micro-mixers is very limited. Furthermore, one of the features of the SCFs is that their physical and chemical properties assume intermediate values of those of liquids and gases and, moreover, near the critical point, they are very sensitive to minor changes in pressure and temperature. These facts made the study and knowledge of the flow behaviour and hydrodynamics of SCFs of great interest for the comprehension of several processes. Here, the multiphase flow behaviour of scCO<sub>2</sub> with different liquid mixtures (ethanol-water mixtures and olive oil) in a capillary was observed. Moreover, the multiphase flow of scCO<sub>2</sub> with water and ethanol-water mixtures was modelled by Computational Fluid Dynamics (CFD). One of the main and most important advantages of CFD is that it allows to reduce the number of experiments or to design more precisely the experiments performed. Nonetheless, the number of CFD models or simulations on processes which involve SCFs that can be openly found in literature is very scarce. In this study, a model for the flow behaviour of scCO<sub>2</sub> with water was described. Likewise, the mass

transfer of ethanol from water to scCO<sub>2</sub> has been also studied, although the model still needs to be improved.

On the other hand, some other aspects such as the design of a multi-stage extraction process with micro-mixers as well as the scale-up of the process have been also discussed.

## 2. State-of-the-art

### 2.1. Supercritical fluids

A supercritical fluid (SCF) is defined as any substance or pure component at pressure and temperature conditions above its thermodynamic critical point. A typical phase diagram for a pure substance is shown in Figure 2.1, where the critical point (C) corresponds to the higher values of pressure and temperature at which liquid-vapour equilibrium can coexist. Above this critical point, there is a region called supercritical fluid region, in which distinct liquid and gas phases do not exist. In the supercritical region, the physical and chemical properties assume intermediate values of those of liquids and gases, as shown in Table 2.1 (Vázquez da Silva, 2010). In other words, supercritical fluids present unique chemical and physical properties which make them distinctive solvents. In Table 2.1 is observed that SCFs present a liquid-like density and a gas-like viscosity, while the diffusion coefficients of SCF intermediate between those of liquids and gases. This means, as Vázquez da Silva (2010) described, that the SCFs possess a dissolution power similar to those of liquids but their properties of mass transfer are much more favourable, which makes them very good solvents.

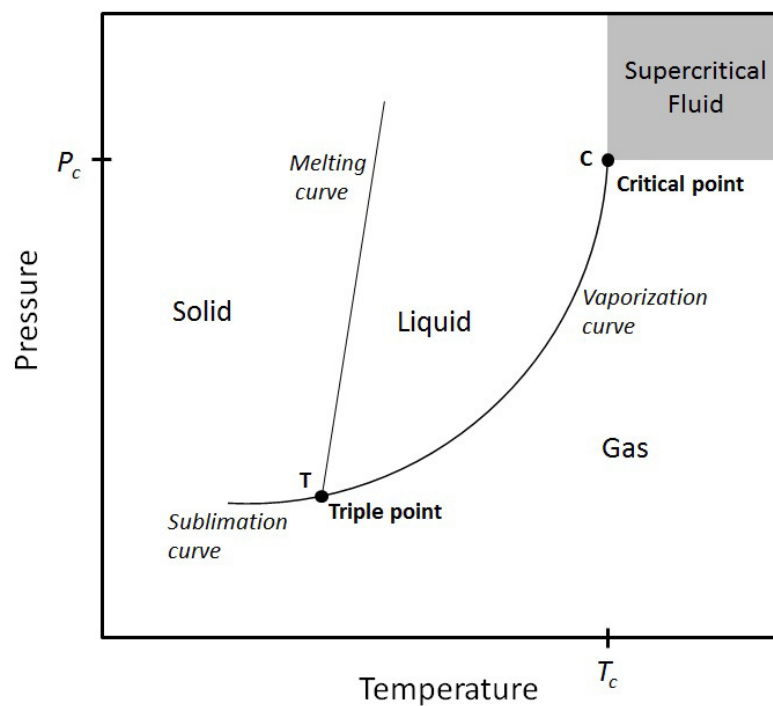


Figure 2.1. PT-phase diagram for a pure substance.

Table 2.1. Comparison of the liquids, gases and SCFs properties.

	Liquid	SCF	Gas
Density (kg/m <sup>3</sup> )	600-1600	200-900	0.6
Viscosity (Pa·s)·10 <sup>5</sup>	20-300	1-9	1-3
Diffusion coefficient (m <sup>2</sup> /s)·10 <sup>9</sup>	0.2-20	20-70	10000-40000

Another special characteristic of the SCFs is that, near the critical point the density is extremely sensitive to minor changes in pressure and temperature. Figure 2.2 (de la Ossa and Serrano, 1990) shows very clearly the behaviour of the SCFs properties. In the figure, the reduced pressure ( $P_r$ ) is represented as a function of the reduced density ( $\rho_r$ ) and the reduced temperature ( $T_r$ ). As defined by Equations (2.1)-(2.3), a reduced property is the quotient of the value of the property and its value at the critical point. Therefore, the critical point in Figure 2.2 is the point in which  $T_r = P_r = \rho_r = 1$ . It is observed that in the vicinity of the critical point, small changes in the reduced pressure and reduced temperature cause large changes in the reduced density and, consequently, in all the substance properties and behaviour.

$$P_r = \frac{P}{P_c} \quad (2.1)$$

$$T_r = \frac{T}{T_c} \quad (2.2)$$

$$\rho_r = \frac{\rho}{\rho_c} \quad (2.3)$$

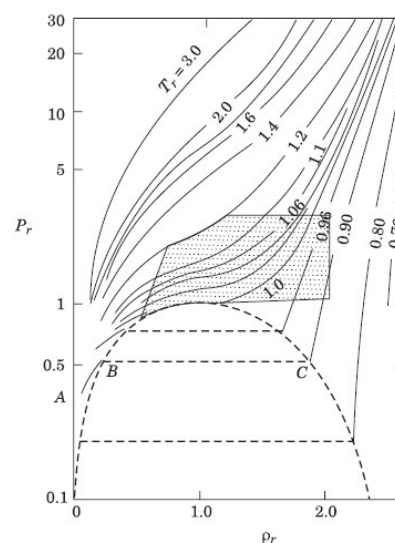


Figure 2.2. Representation of the reduced pressure ( $P_r$ ) of a pure substance as a function of the reduced density ( $\rho_r$ ) and the reduced temperature ( $T_r$ ). Source: de la Ossa and Serrano (1990).

This unique behaviour of their chemical and physical properties makes the SCFs of high interest for many different applications. According to Vázquez da Silva (2010), the supercritical fluid extraction (SFE) was for many years the main area of application of the SCF. However, the energetic crisis of the 70s fomented the development of alternative technologies with a lower energy demand. At this point, the interest in SCFs increased remarkably, spreading their application to new areas of processing.

Nowadays SCFs are applied in many different areas and applications. As mentioned above, for some decades, their main application was the supercritical fluid extraction (SFE), which is extensively described in *Section 2.2*.

Furthermore, the particles formation and design of solid particles has been one of the major developments of the supercritical fluids technology. The main techniques developed to date: Rapid Expansion of Supercritical Solutions (RESS), Particles from Gas-Saturated Solutions (PGSS), Concentrated Powder Form (CPF), and the different Gas Anti-Solvent processes (GAS, GASR, GASP, SAS, PCA, SEDS) were described and evaluated by Knez and Weidner (2003), and Weidner et al. (2003).

Another application of SCFs is the supercritical fluid chromatography (SFC), in which the supercritical fluid is used as the mobile phase. This technique was discovered by Klesper et al. (1962), who described in 1962 the separation of thermo-labile porphyrin derivatives using supercritical chlorofluoromethanes at pressures up to 140 bar and temperatures from 150 to 170 °C. However, it was in the 80s when SFC started to be used as an analytical method. As concluded by Taylor (2009), at the moment, SFC is currently on the strongest foundation and vendors are strongly committed to advancing the technology.

Moreover, SCFs are also attractive as media for chemical reactions. As explained by Savage et al. (1995), conducting chemical reactions at supercritical conditions enables to manipulate the reaction environment by changing the reaction conditions (i.e. pressure) to enhance the solubility of reactants and products. This allows the elimination of interphase transport limitations on reaction rates and moreover can integrate the reaction and separation unit operations. The diversity of chemical reactions which can benefit of a supercritical medium is quite wide: Diels-Alder reactions, organometallic reactions,

heterogeneously catalysed reactions, fuels processing, oxidation chemistry, electrochemistry, biomass utilization, polymerization, and materials synthesis are some examples.

SCFs can also be utilized for impregnation purposes. In the supercritical impregnation process, a substance which is dissolved in the supercritical fluid is adsorbed or deposited on/into a porous solid material, namely matrix. This step is followed by a de-pressurization step that causes the CO<sub>2</sub> phase change from supercritical to gas, leaving the matrix impregnated with the active substance. The main advantage of this technique is that no liquid effluents are produced during the process, so the liquid consumption, as well as the waste production, is extremely reduced or completely eliminated. In the last decades, the supercritical impregnation of different materials such as wood (Kjellow and Henriksen, 2009) or polymers (Kikic and Vecchione, 2003) has been widely studied.

Besides, supercritical fluids are also used for drying. The supercritical drying is an alternative drying technique to remove liquid in a precise, controlled way. This technique is not only for dry cleaning of clothes but also for food drying (Brown et al., 2008).

Table 2.2. Critical data for pure components (NIST, 2016).

	T <sub>c</sub> (K)	P <sub>c</sub> (bar)
Carbon Dioxide	304.18	73.80
Methane	190.6	43.1
Ethylene	282.5	50.6
Propane	369.9	42.5
Propene	365.2	46.0
Ethane	305.3	49.0
Cyclohexane	554.0	40.7
Isopropanol	509.0	49.0
Benzene	562.0	48.9
Toluene	593.0	41.0
p-Xylene	617.0	35.0
Chlorotrifluoromethane	301.8	38.85
Trichlorofluoromethane	471.1	44.66
Ammonia	405.4	113.0
Ethanol	514.7	63.0
Water	647.0	220.64



On the other hand, regarding the substances that are frequently used as SCF, Table 2.2 gives the critical data of many common SCFs. By comparing the values, it is observed that the carbon dioxide presents moderate critical parameters: 304.18 K and 73.8 bar. This, together with the facts that it is not toxic or flammable or corrosive, it is considered an environmentally friendly solvent and it has a low price, makes the CO<sub>2</sub> the most popular supercritical fluid at the moment. On the other hand, in spite of its high critical parameters, supercritical water has also many applications, such as reaction media and treatment of toxic wastewater. Moreover, in the last years, supercritical water biomass valorisation (SCBV) processes are being studied as an alternative way to produce biogas, biofuels, and valuable chemicals (Loppinet-Serani et al., 2008).

In spite of all the applications described above for supercritical fluids, their presence in industrial processes is still limited. The main reason of this is the large capital investment required, due to the high values of pressure and, in some cases, temperature, that the equipment must withstand. Perrut (2000) discussed that supercritical and high pressure processes are not always the best choices, but should be considered as alternatives among others, with their own advantages and limitations. He concluded that it is false both to underestimate the final operating cost and to overestimate it because the high-pressure technology continues to appear “exotic”. Moreover, he affirmed to be confident that the global trend to “green” technologies would create favourable conditions to move to supercritical fluid solvents and reaction media. Furthermore, Brunner (2010) covered the industrial and near-to-industry applications of supercritical fluids, highlighting that although the properties of supercritical fluids are well known, they are yet not fully exploited for industrial applications. The main industrial applications of SCFs included in Brunner (2010) are: extraction of essential oils, special oils, and edible oils; cork treatment; spent rubber tires; supercritical drying, cleaning and degreasing; impregnation with SCFs (e.g. processing of wood to protect it from deterioration), dyeing and tanning; processes for particle formation, encapsulation and coating, widely applied in pharmaceutical industry; and polymer processing, emulsions and micro-emulsions. All these processes mainly use scCO<sub>2</sub> as SCF. However, as Brunner (2010) remarks, supercritical water has also some industrial applications at the moment, mainly focused on the supercritical water oxidation (SCWO), a method to destroy toxic and dangerous compounds and to clean liquids and solids.

Nevertheless, for the purpose of the further development and utilization of the SCFs technology, the research on high pressure processes and supercritical fluids is focused at the moment on a wide variety of applications, such as SFE of emulsions (Lévai et al., 2015), supercritical impregnation into polymers (Varga et al., 2016) or aerogels (Pantić et al., 2016), supercritical fluid chromatography (Ortega et al., 2016), the study of scCO<sub>2</sub>/ionic liquids systems (Lopes et al., 2016), and many more.

### 2.1.1. Supercritical carbon dioxide

As discussed above, carbon dioxide is the most popular supercritical fluid at the moment. Besides its moderate critical pressure and temperature (31.1 °C and 73.8 bar), as shown in Figure 2.3., scCO<sub>2</sub> is attractive because of its “green” properties: it is environmentally benign, non-toxic, non-flammable and chemically relatively inert (this latter will be further discussed below). Moreover, its mutual solubility in water is very small, which makes the extraction of organic products from aqueous solutions with scCO<sub>2</sub> as solvent possible. Furthermore, CO<sub>2</sub> solubilises the low molecular weight hydrocarbons and oxygenated compounds. Besides, its enthalpy of vaporization is low, especially near the critical point, which makes the energy requirements quite low. Some of the advantages of the use of scCO<sub>2</sub> as solvent were emphasized by Eckert (1996): milder conditions, and higher yield and selectivity by adjusting temperature and pressure conditions or the use of co-solvent in small amounts. Later on, De Simone (2002) discussed different opportunities for the practical implementation of green solvents as a solution to the contamination of our air, land and water because of the difficulties to contain and recycle the traditional solvents. De Simone highlighted the potential of alternative solvents and drew special attention to scCO<sub>2</sub>, since processes that use CO<sub>2</sub> do not contribute directly to the greenhouse effect and most CO<sub>2</sub> sold today is isolated as a by-product from primary sources (such as ethanol, ammonia and hydrogen).

Regarding the CO<sub>2</sub> solvent power, Hyatt (1984) studied and compared the solvent strength of CO<sub>2</sub> in liquid and supercritical state. The author proposed that although it was understood that scCO<sub>2</sub> offers advantages over liquid CO<sub>2</sub> as a solvent (for instance, higher solubility with increasing pressure, wider range of operating temperatures and pressures available, and density variable over a wide range), it had not been proved that the solvent behaviour of supercritical CO<sub>2</sub> differs from that of subcritical CO<sub>2</sub>. His results suggested that

liquid and supercritical CO<sub>2</sub> have dipolarities close to those of hydrocarbons, but have polarizabilities which are even lower than those of fluorocarbon solvents. Thus CO<sub>2</sub> could be considered a solvent which bridges the gap in polarizability between fluorocarbons and the gas phase. Therefore, the author concluded that CO<sub>2</sub> in these both states exhibits properties typical of hydrocarbon solvents (such as toluene) with a very low polarizability. No significant difference in polarity was detected between the liquid and supercritical phases. On the other hand, the author also observed that CO<sub>2</sub> provides more H bonding basicity for basic molecules than hydrocarbon solvents do.

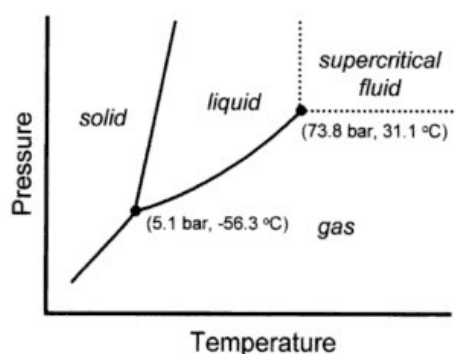


Figure 2.3. Phase diagram of pure CO<sub>2</sub>. Source: DeSimone and Tumas (2003).

Nevertheless, despite the numerous advantages that the scCO<sub>2</sub> presents, it can also suffer from some inconvenient physicochemical properties for a good, effective solvent in certain processes, as Peach and Eastoe (2014) discussed. Lower viscosity, dielectric constant and surface tension in comparison to other common solvents are its main drawbacks for given applications. Nevertheless, due to the necessary movement towards green chemistry and that scCO<sub>2</sub> can be a significant factor on it, several researchers have focused on enhancing these properties of the scCO<sub>2</sub>. Peach and Eastoe (2014) examined these attempts and breakthroughs, focusing mainly on the factors that impact solubility of polar and ionic species and the attempts to enhance scCO<sub>2</sub> viscosity. The authors concluded that, over the last 20 years, significant developments have been achieved, especially on identifying factors to enhance the CO<sub>2</sub>-philicity in additives as well as on the development of CO<sub>2</sub> viscosifiers. Moreover, the authors also considered that the properties of scCO<sub>2</sub> as a solvent could be enhanced further through the use of ionic liquids (IL)-in-CO<sub>2</sub> systems, thus combining with the positive properties of ILs as solvents.

Besides, although CO<sub>2</sub> has been commonly considered to be highly chemically inert, recently it is being proved that the reactivity of the CO<sub>2</sub> molecule might have been underestimated due to its high chemical stability. Müller and Leitner (2015) highlighted that CO<sub>2</sub> is isoelectronic to highly reactive molecules such as isocyanates and ketenes. Moreover, the authors presented a Thematic Series, which consisted of a remarkable overview of opportunities in the field of CO<sub>2</sub> chemistry.

In any case, along with its advantages and drawbacks, the scCO<sub>2</sub> is the most popular and used supercritical fluid nowadays both in research and industry. In fact, in the last decades, scCO<sub>2</sub> has become the ideal SCF in food industry due to its characteristics. Factors such as the solvent toxicity and flammability are of crucial importance in food industry. And, in that regard, scCO<sub>2</sub> seems to be the perfect choice for several processes. Raventós et al. (2002), Rozzi and Singh (2002) and Omprakash (2016) covered most of the applications of scCO<sub>2</sub> in food industry nowadays: extraction and fractionation; recovery of natural compounds such as food colorants with high antioxidant activity, for instance; supercritical drying; or analytical uses for the detection of fat content or pesticide residues are some of them.

## 2.2. Supercritical Fluid Extraction (SFE)

Supercritical Fluid Extraction (SFE) is the separation technique in which the solvent or extractant is a SCF, i.e. a “fluid” at temperature and pressure conditions above its critical point, and the materials to be extracted from are liquid or solid. The use of supercritical solvents provides enhanced extraction rates and solvent-free extracts and raffinates, as the product recovery happens via simple pressure reduction. Besides, because generally no high temperatures are required, less degradation of solutes occurs during SFE in comparison with other separation techniques. McHugh and Krukoni (1994) explained the fundamentals and industrial applications of SFE. Moreover, Reverchon and De Marco (2006) reported the supercritical fluid extraction and supercritical fluid fractionation techniques of natural matter carried out within the last decades.

For decades, SFE was the main application of SCFs, and it was suggested by the researches to be the solution for many of the challenging separations problems. On the other hand, designers and, in general, people from industry were averse to this new technique, due to the

high capital costs and safety problems. Nevertheless, as affirmed by Brennecke and Eckert (1989), SFE is neither a panacea nor a hazard. Brennecke and Eckert highlighted that SFE is probably the best solution for difficult separations, especially on relatively low-volume, high-value products. However, in cases that separation can be achieved by either liquid-liquid extraction or any type of distillation, it is almost always cheaper to choose the latter ones over SFE. Still, exceptions exist in processes with environmental concerns or governmental regulations, in which SFE with  $\text{scCO}_2$  is more attractive than conventional separation methods. On the contrary, SFE processes require special training for engineers and workers in industry in order to learn how to deal with moderate/high pressures.

Focusing on the advantages, Brennecke and Eckert (1989) summarized the important characteristics of SCFs for extraction as follows:

- SCFs have a very high capacity for solutes: the usual solubility is about  $10^3$ - $10^6$ , or even  $10^8$  (greater than one would expect in an ideal gas).
- Compounds can be separated not only by differences in vapour pressure, but also by specific interactions with well-chosen solvent components (by the use of entrainers or co-solvents), thus combining the advantages of both distillation and extraction processes.
- SCFs can be easily adapted to very difficult separations: facile separation of thermally-labile materials at low temperature is possible and, moreover, because of the high compressibility and exponential solubility, good separations with very small pressure variations can be performed. (See Figure 2.2, where the shaded area represents the region where most extraction processes take place. Note that in this area the solvent density is high - liquid-like, and the compressibility is very high, which means that very small pressure changes give large density deviations)

Nevertheless, for a proper application and design of SFE processes, the knowledge of the phase equilibria of the system is essential. In this regard, SCFs present some difficulties: on one hand, the proximity to the critical point makes the modelling very challenging. On the other hand, what was defined by Brennecke and Eckert (1989) as a “great asymmetry” of the most SCF systems of interest, which means that the SCF systems present large differences in both size and force constant of the molecules involved, makes the modelling more difficult

too. For this reason, Brennecke and Eckert (1989) covered the experimental and analytical data on phase equilibrium thermodynamics of SCF systems and discussed the importance of a fundamental understanding of molecular behaviour in SCFs to develop predictive models.

In this work, micro-mixers were employed and therefore, due to the small size of the micro-channels, it is important that neither solids nor small particles are present in the extraction systems in order to avoid plugging or fouling. For this reason, the study was focused on the SFE from liquid mixtures, also known as Supercritical Fluid Fractionation (SFF). This technique is usually used to fractionate mixtures which have been already extracted by conventional methods, and is normally performed in counter-current. As explained by Brunner (2013), the equipment for a counter-current multistage extraction process consists of (see Figure 2.4) a separation column (1) where both phases (liquid and gas – or supercritical, in this case) are contacted counter-currently; a separator (2) for separating solvent and extract; and devices for feeding reflux to the column (3), for recovering the extract (4), for delivering feed to the column (e.g. pump) (5), for recovering the raffinate at the lower end of the column (6), and for recycling the solvent (7). The separation column consists of two separation cascades: in the upper one (enriching section) the bottom product compounds are separated from the top product compounds and rejected to the lower section (stripping section); whereas in the stripping section the top product compounds are separated from the bottom product compounds and transported to the enriching section. At the top of the column, the separation of the extract and solvent occurs by changes of pressure and temperature in the separator.

Furthermore, Bejarano et al. (2016) focused on the fractionation technologies studied and developed for liquid mixtures using  $scCO_2$  in the last decades. Although counter-current SFF in packed columns is the most used technique, the authors also discussed less common SFF technologies such as membrane contactors, mixer-settler arrangements, and spray processes. If we focus only on the mixers, the authors found in literature several different mixer-settler equipment and configurations but the principle was always the same, a separation process that consists of two steps: (1) mixing of the solvent with the solution containing the solute(s) of interest and (2) a quiescent settling to separate the phases by gravity. Bejarano et al. (2016) highlighted that the use of mixer-settler arrangements in SFF is desirable when: (a) the liquid phase flow rate is low and does not cover all the mass transfer equipment, thus leading

to a limited mass transfer rate; (b) the liquid phase viscosity is high, even when the solvent (SCF) is dissolved in this phase; (c) the S-to-F is very large, compromising then stable operation of the column; and (d) there are small density differences between phases causing limited flow in columns driven by gravity. On the other hand, the main drawback of this technology is the limitation to systems which require a relative small number of stages. In Figure 2.5 (from Bejarano et al., 2016), a SFE process in a mixer-settler arrangement is described, where it is shown that each stage requires at least one mixing device and one separator. Side channel pumps with a diffuser or static mixers are usually used as mixing devices.

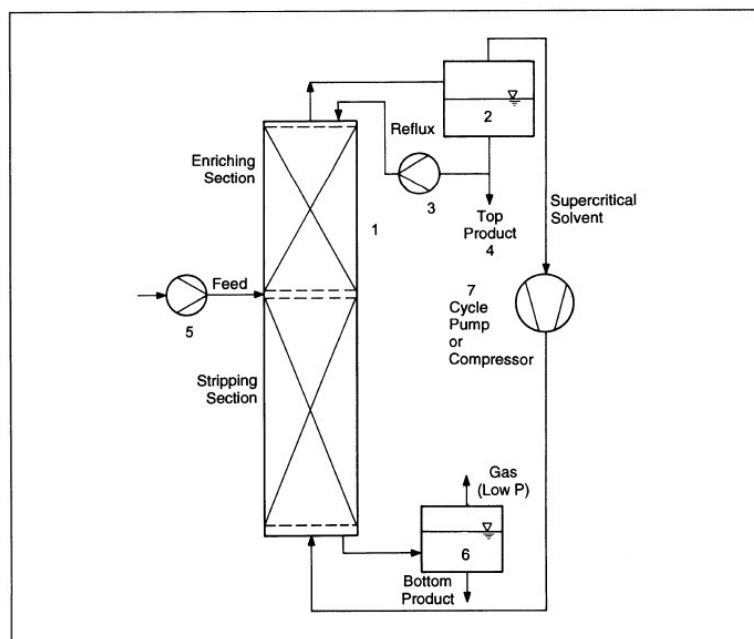


Figure 2.4. Process scheme of a counter-current SFE. Source: Brunner (2013).

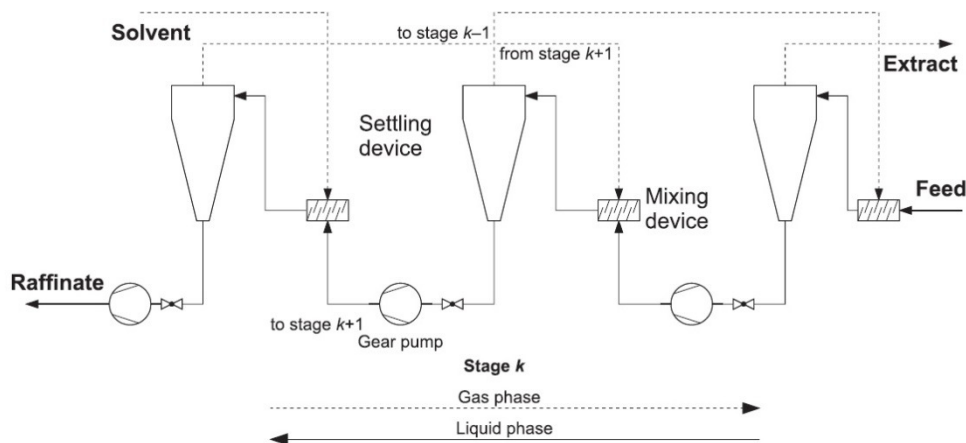


Figure 2.5. Schematic flow diagram of a mixer-settler arrangement of (k+1) stages. Source: Bejarano et al. (2016).

Focusing mainly on the use of static mixers as mixing device, Catchpole et al. (2000) studied and compared the fractionation of lipids in a static mixer and in a packed column to obtain squalene from shark liver oil and olive oil deodorizer distillate. Experiments were carried out in a laboratory/pilot-scale static mixer and compared with that achieved in laboratory- and pilot-scale packed columns. The authors concluded that the separation that can be achieved with a static mixer is less than that with a laboratory- or pilot-scale packed column for shark liver oil (which they considered as an easily fractionated mixture). On the contrary, it is similar for the olive oil deodorizer distillate (considered as a mixture difficult to fractionate), due to the very low separation factor of squalene in olive oil deodorizer distillate. Moreover, their results showed that even though the static mixer presented higher extraction efficiency per transfer unit, the yield of extraction was higher in the packed column, as the counter-current packed column had a higher number of transfer units than the static mixer.

In spite of the different examples of mixer-settler arrangements that they found in literature, Bejarano et al. (2016) commented that there are only few comparisons between the different technologies for SFF.

On the other hand, Bejarano et al. (2016) identified two main categories among SFF applications: fractionation of non-aqueous and aqueous mixtures. Moreover, they distinguished three major areas of intense scientific research in SFF: lipids, essential oils, and alcoholic beverages. Taking this into account and bearing in mind that for a better comparison and evaluation of our experimental results the use of model systems was the best and the easiest, the SFF systems studied here are the following:

- System A: extraction of ethanol from aqueous solutions using scCO<sub>2</sub> as solvent
- System B: extraction of free fatty acids from olive oil using scCO<sub>2</sub> as solvent

The extraction of these two mixtures will be further described and explained in the next sections.

### **2.2.1. SFE of ethanol from aqueous solutions**

The removal or extraction of ethanol by scCO<sub>2</sub> is a widely studied process for applications such as dealcoholisation of beverages (Gamse et al., 1999; Fornari et al., 2009), ethanol production or ethanol recovery from fermentation processes (Güvenc, et al., 1998).



Therefore, the CO<sub>2</sub>–ethanol–water ternary mixture has been extensively investigated: both the phase equilibrium behaviour of the system (which is reviewed in detail in *Section 4.1*) and the extraction and mass transfer rates. For several years, the ethanol–water azeotrope, with a composition of 89.4 mol% (i.e. 95.5 wt.%) of ethanol (DDBST GmbH, in press), had been a perpetual limit of the distillation: a concentration of ethanol higher than the azeotrope composition could not be achieved within one distillation column. Lim et al. (1994) determined that the upper limit of ethanol concentration in the scCO<sub>2</sub> phase was attributed to the existence of a plait point, the point in which both liquid and vapour phases coincide and therefore no separation is possible. Hence, they postulated that ethanol could be concentrated above its atmospheric azeotropic composition if the extraction is performed below the critical pressure of the CO<sub>2</sub>–ethanol system at the given temperature.

Bernad et al. (1993) studied the extraction of this system and compared the experimental results with simulations. The authors evaluated the mass transfer coefficient in the extraction of ethanol from an aqueous solution by scCO<sub>2</sub> at a pressure of 100 bar and a temperature of 40 °C in a pilot plant equipped with a 1.4 m high, 54 mm ID column packed with stainless steel BX 64 Sulzer packing. The column was operated both in bubble flow (i.e. interface in the upper head, continuous aqueous phase), and in trickle flow (i.e. liquid interface in the lower head, continuous scCO<sub>2</sub> phase). In their experiments, the feed composition was always about 30 wt.% ethanol. Furthermore, the extract obtained had an ethanol content of about 90 wt.% (i.e. lower than the azeotrope point) and the raffinate composition was between 15 to 27 wt.%, depending on the S-to-F ratio, which was always lower than 10. Regarding the simulations, the Redlich-Kwong-Soave EoS modified by Schwartzentruber and Renon was used for the determination of the equilibrium compositions. Extraction efficiency was calculated in terms of HETS and the overall mass transfer coefficient. The HETS values were obtained by three different methods: SIMCO, PROSIM and the Kremser equation. For the feed composition studied and the different values of S-to-F ratio, the authors obtained values of HETS between 0.5 to 1 m. Furthermore, the values for overall mass transfer coefficient obtained were  $k_{Ga} = 4 \cdot 10^{-3}$  to  $12 \cdot 10^{-3} \text{ s}^{-1}$ .

On the other hand, Ikawa et al. (1993) studied the separation process of ethanol from aqueous solutions using scCO<sub>2</sub> with the purpose of concentrating more than 99mol% ethanol in the extract. The authors chose the experimental conditions (60 °C and 100 bar) based on

the phase equilibrium data from Furuta et al. (1990), the ethanol feed composition was 83.5mol%. The experiments were carried out in a bench scale test plant. The extraction column had a height and a diameter of 2.48 m and 60 mm, respectively. The column had sieve trays (5 mm hole diameter and 50 mm tray spacing) to enhance the contact between the liquid solution and CO<sub>2</sub>. Moreover, a separation column was used to purify the carbon dioxide, which was used for recycling. In this separation column, the ethanol (extract) was obtained from the bottom, whereas the purified carbon dioxide was obtained at the top. The column was a high pressure distillation column packed with 1/8" DIXON packing. The experimental results showed that the concentration of ethanol in the extract increases dramatically as the reflux ratio increased up to 10, and that more than 99 mol% of ethanol could be concentrated using this test plant (see Figure 2.6). Therefore, the authors proved that the ethanol-water azeotrope limit could be crossed by SFE using scCO<sub>2</sub> as the solvent.

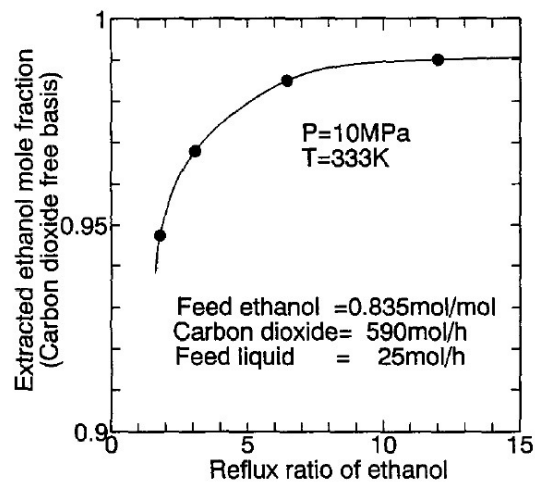


Figure 2.6. Experimental results from Ikawa et al. (1993). Effect of reflux ratio of ethanol on extracted ethanol concentration in the extraction column. Source: Ikawa et al. (1993).

Lim et al. (1995) studied and compared the mass-transfer efficiency and the hydraulic characteristics in a spray column and in a packed column for extracting ethanol from aqueous solutions with scCO<sub>2</sub>. Their experiments were performed at 35, 40 and 50 °C and at pressure range from 91 to 122 bar. The influence of fluid properties, phase flow rates, column internals, and phase dispersion were studied and discussed. HETS and volumetric mass-transfer coefficients ( $K_{od}a$ ) were calculated. The authors concluded that the values of HETS for the spray column are approximately two times higher than those for packed column. Moreover, the mass-transfer efficiency was found to be about 65% lower in the case of

dispersing the aqueous phase in comparison to dispersing the scCO<sub>2</sub> phase. The authors also observed that, at a constant temperature (40 °C), the recovery fraction (defined by Equation (2.4)) increases with the pressure. This fact was attributed to effects of the distribution coefficient on the recovery fraction, and not to effects of the volumetric mass-transfer coefficient.

$$\text{Recovery fraction} = \frac{\text{Total amount of extracted solute}}{\text{Total amount of solute in feed}} = 1 - \frac{X_R}{X_F} \quad (2.4)$$

Later on, Budich and Brunner (2002) investigated the recovery of ethanol from aqueous solutions by scCO<sub>2</sub> at the same conditions than Ikawa et al. (1993), i.e. 60 °C and 100 bar. The authors measured vapour-liquid equilibrium data of the ternary mixture at the extraction conditions for the calculation of theoretical equilibrium stages, and results were compared with counter-current column experiments. Separation of extract and solvent was carried out by multistage solvent distillation. The counter-current multistage extraction was performed in an extraction column of 6 m height and 25 mm ID, equipped with 4 m of Sulzer EX packing. The distillation column for the separation of the extract from the solvent had a height of 1.5 m and 35 mm ID, and was filled with stainless steel mesh packings. The number of theoretical stages was calculated by the Ponchon-Savarit method. The authors found that HETS values are a function of the percentage of water in the liquid phase, obtaining values between 0.33 m (when a feed with 94 wt.% ethanol was used) and 1 m (with feed mixtures of low ethanol content). Comparing their results with previous results from literature, the authors concluded that HETS is influenced by many different factors such as the type of packing, the cross-section capacity, the method to evaluate the number of stages, and the transport properties of both phases (e.g. viscosity and interfacial tension). Moreover, flooding point measurements were carried out with ethanol-water mixtures of different composition.

Recently, Pieck et al. (2015) used the fractionation of ethanol-water mixtures by scCO<sub>2</sub> as a model system to compare experimental extract and raffinate compositions at laboratory, pilot and industrial scales to contribute toward a sizing methodology for counter-current SFF columns. Three different columns, with an ID of 19, 58 and 126 mm and a height of 2, 5 and 8 m were used for the different scales: lab, pilot and industrial scale, respectively. The mass S-

to-F ratio was varied between 5.2 and 78.8 and different feed compositions were considered. In total, 42 experiments were taken into account, including 6 at pilot scale and 2 at industrial scale. All the experiments were performed at 60 °C and 101 bar. The conditions at the cyclonic separator for the separation of the extract and the solvent were 20 °C and 45 bar. The experimental results at the different scales were analysed and compared from the thermodynamic, mass transfer and column hydrodynamics points of view.

### 2.2.2. SFE of free fatty acids from olive oil

Traditionally, hexane has been one of the most used organic solvents for the extraction of fats and oils. However, due to the government restrictions for the last years concerning the organic solvents because of safety and environmental reasons, the use of scCO<sub>2</sub> is gaining relevance as an alternative to organic solvents for the processing of fats and oils.

Temelli (2009) focused on the perspectives of supercritical fluids for processing of fats and oils. The author discussed not only the fundamental aspects to understand and design the processes, but also the commercialization and future outlook of this technology. Moreover, he summarized the different supercritical separation processes of fats and oils developed so far, such as extraction, fractionation and coupling with membrane systems.

Among the different fats and edible oils which can be fractionated by SFF, in this work the SFE from olive oil with scCO<sub>2</sub> was performed. This system has been extensively studied for different applications: deacidification of oils or extraction of minor components such as sterols (Hurtado-Benavides et al., 2004), tocopherols (King et al., 1996; Ibanez et al., 2000), squalene (Ruivo et al., 2001; Ruivo et al., 2002; Stavroulias and Panayiotou, 2005), etc. However, for the purposes of simplicity, the deacidification of olive oil was chosen for this study, i.e. the extraction of free fatty acids (FFA) from olive oil. This process has been studied by different authors in the last decades, both the phase equilibrium behaviour of the system (which is described in detail in *Section 5.1*) and the extraction process.

Firstly, Brunetti et al. (1989) investigated the application of scCO<sub>2</sub> extraction for the deacidification of olive oils. The extraction was performed on samples with different FFA content at 200 and 300 bar, and at 40 and 60 °C. The SFE was in batch process, carried out in an extractor, and the fluid dynamics of the system were studied to determine the optimal

operating flow rate of solvent (scCO<sub>2</sub>). The extraction results suggested that the selectivity factor for FFA is higher than 5 and increases significantly as the FFA content in the oil decreases. Moreover, it was found that the solvent selectivity increases with temperature, whereas it decreases as pressure increases. The authors concluded that SFE with scCO<sub>2</sub> could be a suitable technique for the deacidification of olive oil, especially for oils with relatively high FFA (i.e. FFA content lower than 10%, in weight percentage).

Bondioli et al. (1992) investigated the refining of lampante olive oil by scCO<sub>2</sub>. The influence of different factors such as pressure (in a range between 80 and 150 bar), temperature (40 and 60 °C), as well as temperature gradient along the length of the column and CO<sub>2</sub>/oil ratio (between 10 and 170 kg CO<sub>2</sub>/kg oil) was studied. The extraction was performed in a packed column with Sulzer packing material and a height and ID of 3 m and 30 mm, respectively. Their extraction results showed that by increasing the pressure, the solvent power of the scCO<sub>2</sub> was enhanced, with an evident reduction in the yield of refined oil. Regarding the influence of the temperature, it was observed that with an increase of 20 °C, the density of the scCO<sub>2</sub> decreased remarkably and therefore its solvent power as well. This decrease in density could be avoided by increasing the pressure in a parallel manner, but that would have severe economic consequences in the process. On the other hand, for flux ratios higher than 100 kg CO<sub>2</sub>/kg oil, the desired reduction of acidity was obtained and moreover, the FFA content in the extract reached a maximum at a flux ratio of 80 kg CO<sub>2</sub>/kg oil. The authors observed that for values higher than 80, a balance between yield, reduction of acidity in the product and acidity of the extract could be reached.

On the other hand, De Lucas et al. (2002) studied the influence of operating variables in SFE of olive husk on the yield and quality parameters. The effects of pressure (100-300 bar), temperature (40-60 °C), solvent flow (1-1.5 L/min), and particle size (0.30-0.55 mm) on the extraction yield and three oil-quality parameters (acidity, phosphorus content and peroxide value) were analysed. The authors used a response surface methodology based on statistical analysis of the experimental data to obtain mathematical expressions relating the operational variables and parameters studied. The results were compared to those obtained by hexane Soxhlet extraction and it was concluded that the quality of the product from SFE was superior, requiring only simple refining.

Vazquez et al. (2009) investigated the deacidification of olive oil by scCO<sub>2</sub> in a counter-current packed column, comparing experimental data with thermodynamic modelling. The experiments were performed at 40 °C and pressure of 180, 234 and 250 bar, considering crude oils of different acidity content (between 0.5 and 4.0 wt.%) as feed. On the other hand, the separation process was simulated using the Group Contribution EoS (GC-EoS). The experimental data obtained were in good agreement with the model.

### 2.3. Microfluidics technology

In the last years, micro-process technology has gained more attention because of its advantages in different processes. Microfluidics can be defined as the science and engineering of systems in which fluid behaviour differs from conventional flow theory primarily due to the small length scale of the system. Recently, Nguyen (2012) set out the fundamentals of microfluidics and described in detail its various applications in chemical engineering at the moment, focusing mainly on micro-valves, micro-pumps, micro-flow sensors, micro-needles, micro-mixers, micro-dispensers, micro-reactors and micro-separators. Nguyen (2012) highlighted that the small scale and the high surface-to-volume ratio in microfluidics offer numerous advantages for chemical processes. For instance, in chemical and biochemical analysis, scaling down the analysis allows to integrate all process steps on a single chip, for a faster handling of the samples. Analytical chemists, biochemists, and chemical engineers came to microfluidics to take advantage of the new effects and better performance, primarily interested in shrinking down the pathway of the chemicals. All this led to a remarkable increase in the use, sales and production of microfluidic systems and devices, as shown in Figure 2.7 (from Nguyen, 2012). However, when beginning to work in the field of micro-fluidics, it must always be asked whether working at microscopic length scale is really beneficial for the process.

Hessel and Noël (2012) described the different applications of micro-process technology in chemical engineering, focusing mainly on micro-mixers, micro heat exchangers, micro-evaporators, micro-extractors, micro-distillators (or rectifiers), micro chromatography devices and micro membrane devices.

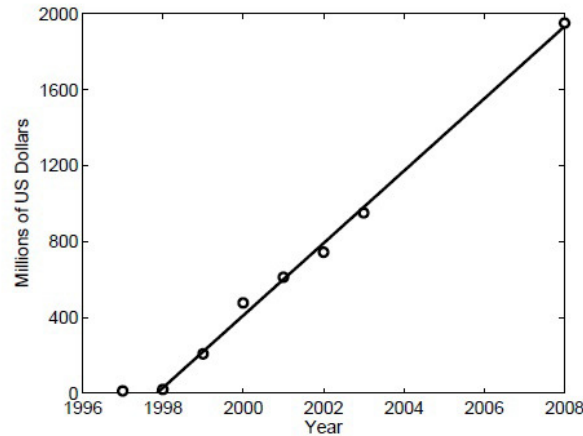


Figure 2.7. Actual worldwide sales of micro-fluidic systems and devices for 1997 through 2003 and projected sales for 2008. Source: Nguyen (2012).

Here, micro-mixers and their application in SFE processes were investigated. First of all, micro-mixers are classified mainly as active and passive micro-mixers. Hessel et al. (2005) made a review on micro-structured mixer devices and their mixing principles. As they described, due to the absence of turbulence in micro-fluidic devices, mixing relies merely on molecular interdiffusion, and two basic principles are followed to induce this mixing at micro-scale: *active mixing*, when energy input from the exterior is used; and *passive mixing*, when the flow energy (e.g. due to pumping action or hydrostatic potential) is used to restructure a flow in a way that results in faster mixing. Different examples of both active and passive mixing are given in Figure 2.8 (from Hessel et al., 2005). In this work uniquely passive mixing was considered, in particular, T-type lamination mixing and multi-lamination principle.

ACTIVE MIXING – external energy input	PASSIVE MIXING – Energy input by pumping power
<ul style="list-style-type: none"> <li>● Ultrasound</li> <li>● Acoustically induced vibrations</li> <li>● Electrokinetic instabilities</li> <li>● Periodical variation of pumping capacity</li> <li>● Electrowetting induced joint of droplets</li> <li>● Piezoelectrically vibrating membrane</li> <li>● Magneto-hydrodynamic action</li> <li>● Small impellers</li> <li>● Integrated micro valves / pumps</li> </ul>	<ul style="list-style-type: none"> <li>● Interdigital multi-lamellae arrangements</li> <li>● Split-and-Recombine concepts (SAR)</li> <li>● Chaotic mixing by eddy formation and folding</li> <li>● Nozzle injection in flow</li> <li>● Collision of jets</li> <li>● Specialties, e.g. Coanda-effect</li> </ul>

Figure 2.8. Scheme of the main mixing classification and examples. Source: Hessel et al. (2005).

### 2.3.1. Mixing principles under study

In this work, two different passive mixing principles were studied. Because of the experimental conditions required (high pressures), the selection was quite limited. In the end, a multi-lamination micro-mixer and a Tee-mixer were chosen. The mixing principles are represented (see Figure 2.9) and further explained below.

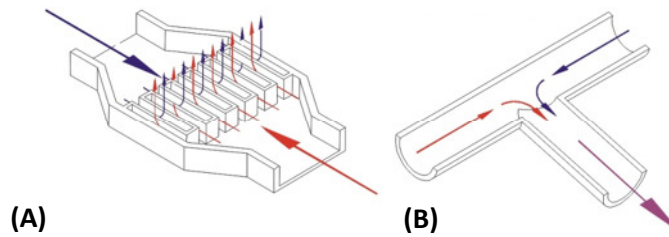


Figure 2.9. Description of the mixing principles studied in this work: multi-lamination (A) and T-type lamination (B). Source Löwe et al. (2000).

#### 2.3.1.1. T-type lamination mixing

In a T-type lamination mixer, the mixing occurs by contacting both streams together on a third perpendicular jet. As described by Hessel and Noël (2012), these mixers are typically used for simple and undemanding mixing tasks, as they use diffusion in laminar regimes for mixing, by virtue of decreasing the distances within a bilayer.

T-type is one of the simplest geometries for mixers and it is been extensively studied, especially for liquid mixing. For instance, Wong et al. (2004) studied four T-channel micro-mixers of different hydraulic diameter and concluded that the smaller the hydraulic diameter, the shorter the mixing time. Moreover, it was found that the millisecond mixing times are orders of magnitude faster than those calculated by Fick's law for diffusion, proving that convection mixing also contributes and not only diffusion mixing. The authors also observed the distinct mixing flows at different Reynolds numbers: for  $Re < 150$ , bilaminated streams were found; for  $Re = 150-400$ , striations were observed; whereas for  $Re > 400$  homogeneous colour textures were obtained, i.e. the two phases were completely mixed.



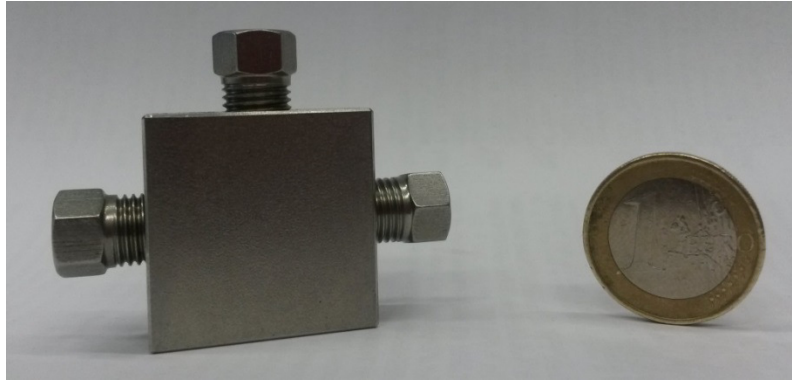


Figure 2.10. Tee-junction manufactured by Nova Swiss.

The Tee-mixer used in this work was manufactured by Nova Swiss and is shown in Figure 2.10. Its three channels (or jets) have an inner diameter of 1 mm and a length of about 2.4 mm.

#### 2.3.1.2. Multi-lamination mixing

The multi-lamination mixing principle consists of the generation of an alternating arrangement of thin fluid compartments – *multilamellae* – which are mixed by diffusion. Multi-lamination is arranged by alternating feed arrays, followed by a mixing chamber, creating the *multilamellae* pattern with steep concentration gradients for fast mixing by diffusion, as described by Hessel and Noël (2012). There are various feed schemes for this type of mixing, such as bifurcation multilamellae arrangement or interdigital multilamellae arrangement. Moreover, the interdigital designs can also differ in the flow-through mixing chamber. Hessel et al. (2003), for instance, studied the laminar mixing in interdigital micro-mixers with three different mixing chamber geometries: rectangular, triangular and slit-type. In this work, the HPIMM (High-Pressure Interdigital Micro-Mixer), manufactured by Fraunhofer ICT-IMM, was chosen (see Figure 2.11). This micro-mixer presents an interdigital multilamellae arrangement, as shown in Figure 2.9(A), with slit-type mixing chamber geometry.



Figure 2.11. HPIMM manufactures by Fraunhofer ICT-IMM.

## 2.3.2. Micro-mixers for extraction purposes

Recent works proved that extraction processes can benefit from microfluidics, as mass transfer is enhanced and equilibrium can be reached within seconds due to the short path lengths and the large interfacial area in micro-devices. However, as explained below, most of the data available in literature is focused on micro liquid-liquid extraction, whereas the data on SFE with micro-devices is still very scarce.

### 2.3.2.1. Micro-mixers for liquid-liquid extraction

In the last decade, many authors have studied the liquid fluid behaviour in microfluidics for extraction applications. In 2001, Benz et al. (2001) already proved the utilization of micro-mixers for liquid-liquid extraction processes, evaluating the extraction performance of different micro-mixers and micro-mixers arrays. The authors studied the extraction of four different systems and found the extraction performance to be function of the volume flow rate. Lately, Assmann, Ładosz and Rudolf von Rohr (2013) gave an overview on different examples of continuous micro liquid-liquid extraction, and distinguish and compare the different multiphase flow patterns and their characteristics, advantages and disadvantages for the liquid-liquid extraction process. The authors focused on the parallel flow, slug flow and dispersed flow as they are the most common flow patterns in liquid-liquid systems. They highlighted that, although the mass transfer performance of slug flow is usually better than of parallel flow, slug flow presents a more challenging phase separation, as both phases are combined within the channel. Furthermore, Zhao et al. (2007) studied the liquid-liquid two-phase mass transfer in T-junction micro-channels for the system water-succinic acid-n-butanol. The authors divided the entire extraction process in five different mass transfer

zones: (1) T-junction mass transfer zone, (2) mixing channel transfer zone, (3) outlet conduit mass transfer zone, (4) droplets mass transfer zone and (5) sampling mass transfer zone. Moreover, they studied the effect of different parameters such as the height and length of the microchannel and the volumetric flux ratio. Zhao et al. (2007) observed that the T-junction microchannel design, the input oil (n-butanol) volume fraction, the mixture Reynolds number, and the dimensions of the microchannel are factors which define the liquid-liquid flow regimes observed (parallel flow with smooth interface, parallel flow with wavy interface and chaotic thin striations flow). Besides, they concluded that a decrease in the height or the length of the mixing channel at constant  $Re_M$  (mixture Reynolds number) results in an increase in the overall volumetric mean mass transfer coefficient. On the other hand, Jovanovic et al. (2011) studied the influence of the flow rate and the capillary length on the hydrodynamics of liquid-liquid flow patterns. The authors also evaluated the extraction performance for different liquid-liquid flows in a capillary micro-reactor for the extraction of 2-butanol from toluene using water as the solvent. They observed that in the cases that slug or bubbly flow regimes had been observed, equilibrium was achieved. However, when the flow regime in the capillary was parallel or annular, equilibrium could not be reached and the thermodynamic extraction efficiency was limited to 60% and 90% for the parallel and annular flow regimes, respectively.

### 2.3.3. Micro-mixers and supercritical fluids

All the examples given above were focused only on liquid-liquid extraction. As discussed by Luther and Braeuer (2012), the high-pressure processes usually take place in the interior of solid stainless steel apparatuses capable to withstand the pressure, which restricts the optical access and hinders the observation and the study of the mechanism taking place. Thus, the data available in literature for supercritical fluid flows in microfluidics are very limited. Consequently, in order to extend and promote the study of SCFs behaviour in micro-devices, the development of new techniques or technologies for the fabrication of micro-channels and micro-devices with high-pressure resistance and which also permit the optical access is imperative. In recent years, some publications have focused on this (Lorber et al., 2011; Luther and Braeuer, 2012; De Marco et al., 2014).

Nonetheless, the fluid behaviour of scCO<sub>2</sub> with water in micro-channels or microfluidic chips has been lately under study by different authors. Marre et al. (2009) demonstrated the possibility to generate stable droplets and reversible dripping to jetting transitions at micro-scale in scCO<sub>2</sub>-liquid water microflows at different pressure (from 80 to 180 bar) and temperature (from 40 to 80 °C) conditions. Furthermore, Ogden et al. (2014) investigated the fluid behaviour of scCO<sub>2</sub> with water in a double-Y-channel microfluidic chip. Three flow regimes in the scCO<sub>2</sub>-liquid water two-phase microfluidic system were mapped at 100 bar and 50 °C: parallel, segmented and wavy. Moreover, the effect of both total flow rate and relative flow rate ( $Q_{rel}=Q_{CO_2}/Q_{water}$ ) on the flow regime was also evaluated. The authors observed that an increase in the total flow rate shifts the flow regime from segmented to parallel flow. Moreover, at a high total flow rate, a low  $Q_{rel}$  is destabilizing and the parallel flow shifts to wavy flow. Latterly, Knaust et al. (2015) studied and modelled the influence of different parameters (such as flow rate, temperature, pressure, and flow ratio) on the flow of scCO<sub>2</sub> and water. They found that the flow ratio as well as the flow rate influenced both the parallel length and the segments size, and that a higher pressure resulted in shorter parallel lengths. Moreover, a higher temperature as well as a higher Weber number (see Equation (6.3)) for water (liquid phase) resulted in longer CO<sub>2</sub> segments.

On the other hand, the flow of CO<sub>2</sub>-ethanol in a microfluidics T-junction at high pressures was studied by Blanch-Ojea et al. (2012). The operating conditions ranged from 70 to 180 bar, and from 21 to 201 °C. CO<sub>2</sub> was either in liquid, gas or supercritical state; and the mixtures experienced a miscible single phase or a vapour-liquid equilibrium, with two separated phases. Plug flow (named Taylor by Blanch-Ojea et al., 2012), annular flow and wavy flow were the two-phase flow regimes observed in the VLE region.

Regarding extraction in micro-devices with scCO<sub>2</sub>, Ohashi et al. (2011) is, to our best knowledge, the only work available in literature focused on measuring the distribution behaviour between scCO<sub>2</sub> and water. The authors measured the distribution behaviour of tris(acetylacetonato)cobalt(III) (Co(acac)<sub>3</sub>) from scCO<sub>2</sub> phase to aqueous phase in a parallel flow regime at the conditions of 100 bar and 45 °C. Luther et al. (2013) also investigated the mass transfer in compressible multi-phase systems composed of oil, water and carbon dioxide at elevated pressures. However, the application of this work is more focused on emulsions. Furthermore, Assmann et al. (2012) and Assmann, Werhan, Ładosz, et al. (2013) studied the

SFE of vanillin and lignin oxidation products, respectively, in a microfluidic device. In the first case, for the extraction of vanillin,  $\text{scCO}_2$  was used as solvent at pressures from 80 to 110 bar. The authors manufactured an integrated silicon/glass micro-extractor for the continuous SFE, which permits the efficient contact of the supercritical solvent and the liquid phase. The further separation was achieved by capillary forces and adjusted pressure drops, enabling this way the complete integration of the SFE process into one micro-device. Further on, the same channel design was adapted for the evaluation of the extraction of aromatic products from lignin oxidation using a continuous microfluidic device, in which equilibrium concentrations were reached in less than 10 s (Assmann, Werhan, Ładosz, et al., 2013).

Several authors pointed out that the separation of the both phases (solvent and liquid phase) after the extraction in micro-devices can be challenging, especially when the flow regime is slug or plug flow. However, this does not pose a problem in SFE, as the separation of the supercritical and the liquid phases happens via simple pressure reduction, turning the solvent from supercritical into gas form.

## 2.4. CFD and supercritical fluids

The data available in literature on modelling of supercritical fluid processes with Computational Fluid Dynamics (CFD) is very scarce. To our best knowledge, the following are the main research works carried out combining SCFs and CFD.

Martín and Cocero (2004) described a mathematical model for the SAS process. This model considered the main physical phenomena involved in the SAS, including: jet hydrodynamics, mass transfer, phase equilibrium, nucleation and crystal growth kinetics. Focusing on the phase equilibrium, the hydrodynamics and the mass transfer modelling; the first one was modelled using the Peng-Robinson EoS modified by Stryjek and Vera with quadratic mixing rules. On the other hand, the hydrodynamics of the process was modelled applying standard CFD techniques using the Launder-Sharma model to solve the motion equation. The mass transfer was modelled considering the effect of turbulence and the equation of continuity was solved combining the Maxwell-Stefan equations and the Fick's law. The model was compared with experimental results, showing that it predicts correctly the variation of particle size with the operating parameters, but it fails to predict the value of the

mean particle size. The main reason of this failure is that the interfacial tension between the solid and the fluid phase was not known.

Fernandes et al. (2008) and Fernandes et al. (2009) applied CFD for the calculation of dry pressure drops and wet pressure drops, respectively, in a SFE column with structured packing. In both cases the VOF model was used for the calculations. In the latter work, Fernandes et al. (2009), 2D and 3D simulations were performed in a pressure range of between 80 and 260 bar, and at temperature between 40 and 120 °C. The authors considered the effects of surface tension and contact angle between the phases for the system scCO<sub>2</sub> and water. The data used in the simulations were taken from Egger and Jaeger (1994).

Besides, CFD was also used for modelling diverse applications of the SCFs. For instance, Han et al. (2002) simulated the contraction flow in the extrusion die for the polystyrene foam extrusion with scCO<sub>2</sub> applying a Fluent computational code to predict profiles of pressure, temperature, viscosity and velocity. Furthermore, a 3D CFD study of the impeller of a centrifugal compressor operating with scCO<sub>2</sub> was carried out by Pecnik et al. (2012).

On the other hand, regarding the modelling of heat transfer, He et al. (2005), for instance, simulated the turbulent convection heat transfer of scCO<sub>2</sub> in a vertical mini-tube. The thermal efficiency of a Kenics® KM static mixer as a heat exchanger for scCO<sub>2</sub> was studied using CFD, and compared to a conventional empty tube heat exchanger. The results showed that the static mixer has a thermal efficiency more than three times higher than that of the empty tube.

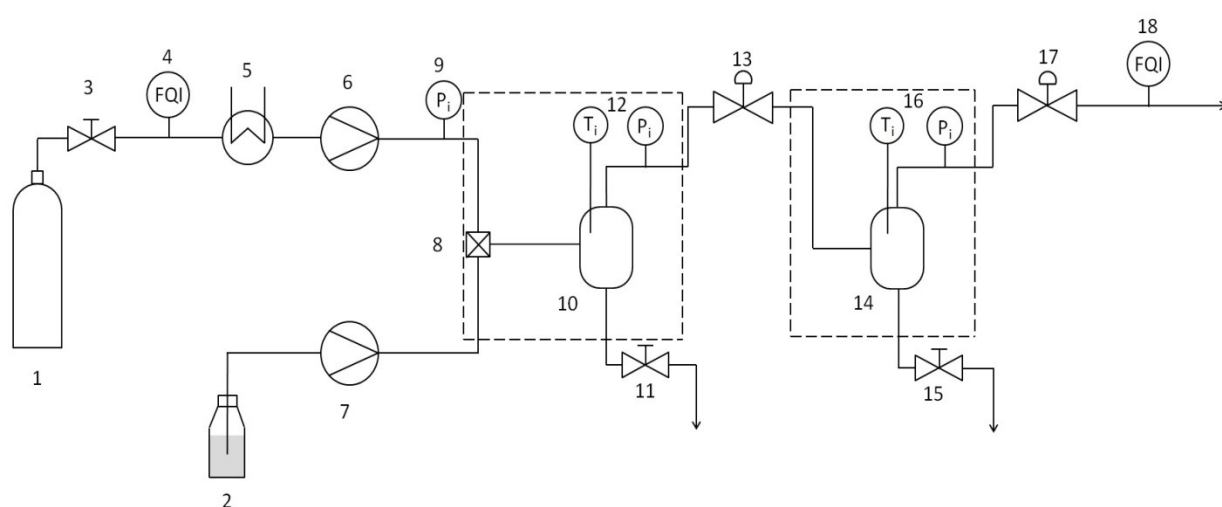
## 3. Experimental section

### 3.1. Experimental setup

#### 3.1.1. SFE experimental setup

The entire design and assembly of an experimental setup for SFE of liquids with micro-mixers was carried out within the framework of this project. A picture of the SFE experimental apparatus is presented in Figure 3.2. It mainly comprises two 305 Gilson HPLC pumps, a micro-mixer, two separators, placed in two different thermostated water baths, and two regulation valves. A schematic diagram of the SFE experimental apparatus is shown in Figure 3.1. The CO<sub>2</sub> cylinder (1) is stored in the lab inside an Asecos EN14470-2 safety storage cabinet for safety reasons. A check-valve (3) avoids the CO<sub>2</sub> back-flow to the bottle. Carbon steel Swagelok tubing ASTM A179 (1/2" OD) is used for the moderate-pressure CO<sub>2</sub> (55 bar) in the section from the check valve (3) to the heat exchanger (5). The CO<sub>2</sub> flow rate is controlled by a Coriolis mass flow meter Model D6 from Micro Motion (4). A heat exchanger (5), connected to a LAUDA Ultra-Kryomat® RUK 40 S which supplies an isopropanol-water mixture as refrigerant, cools down the CO<sub>2</sub> before being pumped by the HPLC pump (6). Moreover, in order to maintain the CO<sub>2</sub> in liquid state when pumped, a special cooling device was coupled to the HPLC pump head. This cooling device was designed and manufactured in our lab. Due to manufacturer's instructions, a Gilson HPLC pump 10SC Piston Pump Head, with a flow rate limit of 10 mL/min, is used for pumping the CO<sub>2</sub>; whereas the liquid feed (2) is pumped using a Gilson 50SC Piston Pump Head, with a flow rate limit of 50 mL/min. Stainless steel Swagelok tubing ASTM A269 (1/16" OD) was installed in the section from both HPLC pumps (6, 7) to the first separator (10). Stainless steel Swagelok tubing ASTM A269 (1/8" OD) was installed in the section from the outlet of the first separator (10) to the second regulation valve (17). Both micro-mixers under study in this work, either the Tee mixer or the HPIMM micro-mixer (8), can be interchangeably installed in the experimental apparatus. The separators (10, 14), with an inner volume of 0.14 L, are able to withstand up to 400 bar and 100 °C. The pressure in the separators is regulated by two Kämmer valves® (13, 17) set up at the outlet of each separator. The temperature is maintained constant by thermostated water baths, represented by the dotted lines in Figure 3.1, in which it is observed that the micro-mixer and the first separator

are both placed in the same thermostated water bath. Thereby it is ensured that both micro-mixer (8) and first separator (10) are at the same temperature and pressure conditions. Pressure and temperature are measured at different points of the experimental apparatus setting thermometers and PMR pressure transmitters connected to Lumel N30U indicators (9, 12 and 16). Nova Swiss® LHP valves (11, 15) are installed to withdraw the raffinate and extract samples collected in the first and second separator, respectively. At the outlet of the SFE experimental setup, a Ritter volumetric gas flow meter (18) measures the CO<sub>2</sub> flow to double check the CO<sub>2</sub> flow rate through the system.



**Figure 3.1.** Schematic diagram of the SFE apparatus. (1) CO<sub>2</sub> cylinder, (2) liquid feed flask, (3) check valve, (4) flow meter, (5) heat exchanger (cooler), (6, 7) HPLC pumps, (8) micro-mixer, (9, 12, 16) pressure indicators, (10, 14) separators, (11, 15) valves, (13, 17) regulation valves, (18) gas meter.

As it is observed in Figure 3.1, in the SFE apparatus designed in this work, the micro-mixer (either the HPIMM micro-mixer or the Tee-mixer) is the unit where the solvent and the liquid feed come into contact. After this contact, the feed and solvent mixture flows through a capillary with an inner diameter of 0.5 mm, and enters the first separator for separation of the raffinate. The solvent phase is then expanded into a second separator for separating the extract. In this way, the separation of both phases, liquid and vapour, is achieved by changes of temperature and pressure, obtaining a raffinate and an extract.

As mentioned, the Gilson 10SC Piston Pump Head used to pump the CO<sub>2</sub> has a flow rate limit of 10 mL/min. However, in the series of experiments performed to study the influence of the overall flow rate on the extraction performance (explained in *Section 4.3.5*), CO<sub>2</sub> flow



rates higher than 10 mL/min were required. For these experiments, the Gilson HPLC pump was replaced by a liquid CO<sub>2</sub> pump (Haskel ASF-100, USA), which can reach the desired CO<sub>2</sub> flow rates.



Figure 3.2. High pressure micro-device apparatus for SFE in our lab.

### 3.1.2. Visualization experimental setup

For the experiments on the visualization of the flow pattern in different multiphase systems of scCO<sub>2</sub> and liquid mixtures (ethanol aqueous solutions and olive oil), some changes were made in the SFE apparatus. Figure 3.3 shows the modifications done in the experimental setup for the assembly of the visualization section (located in the first thermostated water bath), the rest of the experimental setup stayed as it was (see Figure 3.1).

As indicated in Figure 3.3, the Stainless steel Swagelok tubing ASTM A269 (1/16" OD) placed between the micro-mixer and the first separator is replaced by a Radel® Tubing 1/16" OD with the same diameter as the stainless steel tubing used in the SFE experiments (i.e. 0.5mm). The transparent Radel® Tubing can withstand up to 862 bar. The capillary is placed above a white background for a better visualization of the multiphase flow in the capillary. The flow pattern hydrodynamics is visualized and recorded by a microscope (DigiMicro Profi) at 30 frames per second. The microscope is connected to a laptop and the software Microcapture Pro is used to capture the videos and images during the experiments.

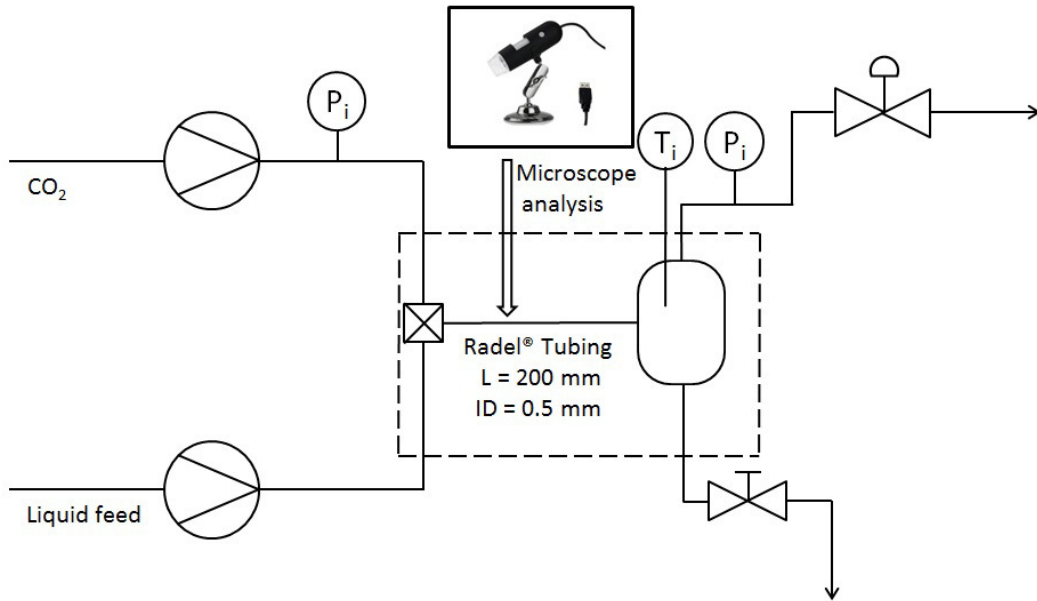


Figure 3.3. Visualization section integrated in the SFE experimental apparatus.

### 3.1.3. Micro-devices description

As explained in *Section 3.1.1*, either the Tee-mixer or the HPIMM micro-mixer can be installed in the experimental apparatuses (SFE experimental setup and visualization experimental setup) for the study and comparison of the two mixing principles. The HPIMM (High-Pressure Interdigital Micro-Mixer) presents a interdigital multi-lamellae arrangement (see mixing element in Figure 3.4) and a mixing chamber, namely the fluid passage following the start of contacting, which has a slit-type shape, as described in Figure 3.5. The Figure 3.4 shows a disassembled HPIMM micro-mixer so the different parts are distinguished, and the mixing element is schematically illustrated.

On the other hand, the mixing in the Tee-mixer (T-type lamination) occurs by contacting both streams together on a third perpendicular jet. The three jets (or channels) of the Tee-mixer used in this work have an inner diameter of 1 mm. The inlet configuration in the Tee-mixer is shown in Figure 3.6.

Operating conditions of both micro-mixers are compared in Table 3.1. It is observed that inner volumes are similar but the HPIMM micro-mixer presents some limitations on flow rate and viscosity. Besides, it must be mentioned that high-pressure 1/16" OD tubes with an ID of 0.5 mm were connected at the inlets and outlet of both micro-devices.

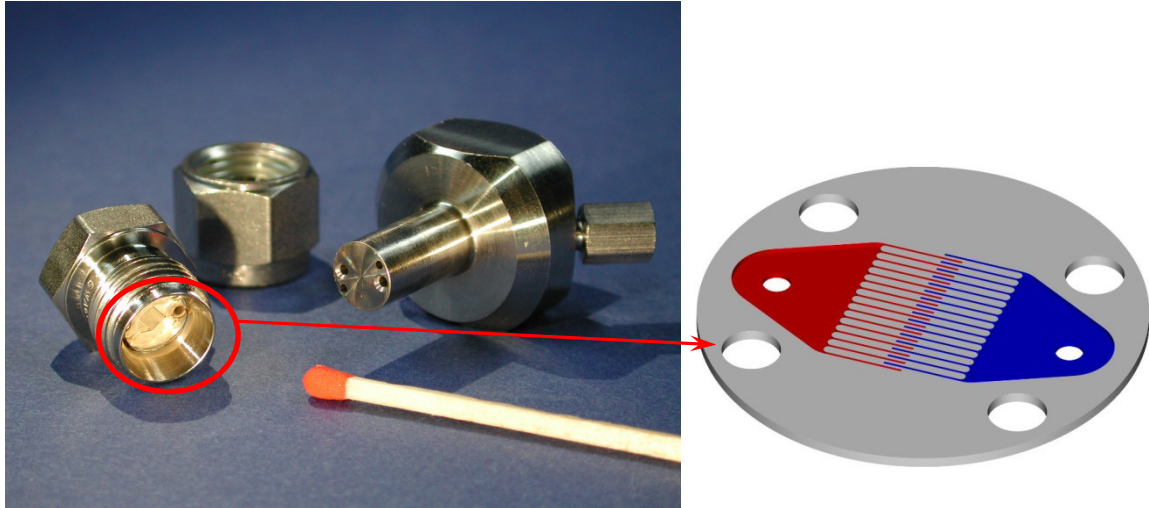


Figure 3.4. HPIMM micro-mixer de-assembled (left side) and schematic illustrating the mixing element inside the HPIMM consisting of 2 x 15 interdigitated micro-channels (right side). Source: Copyright Fraunhofer ICT-IMM.

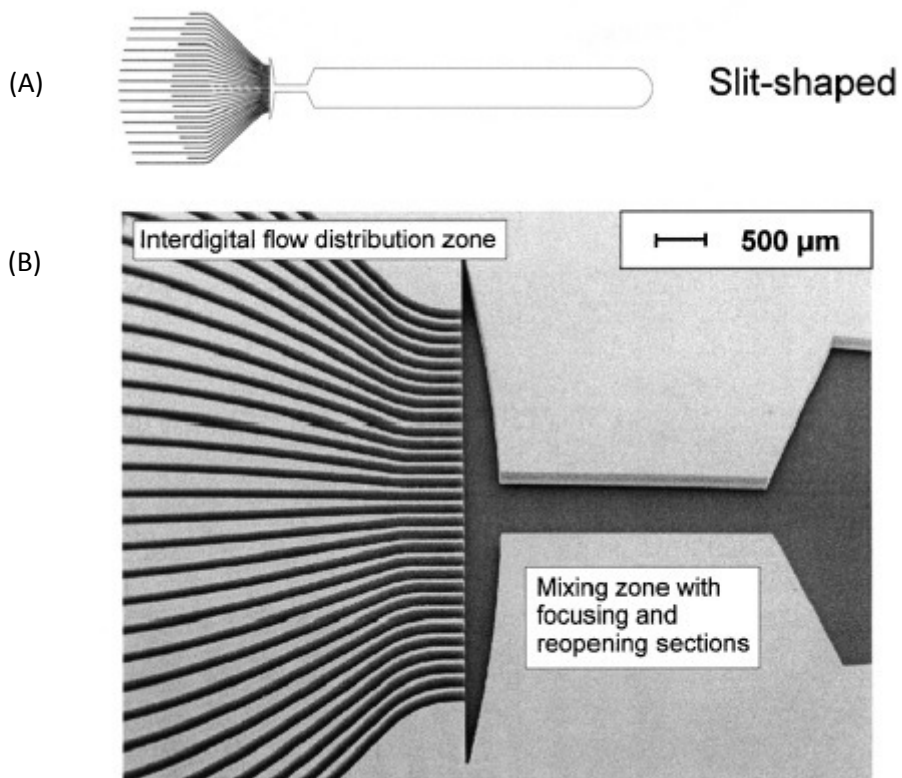


Figure 3.5. (A) Design of the slit-shape mixing chamber geometry. (B) SEM image of one micro-structured layer building the slit-shaped interdigital micro-mixer. Source: Hessel et al. (2003).

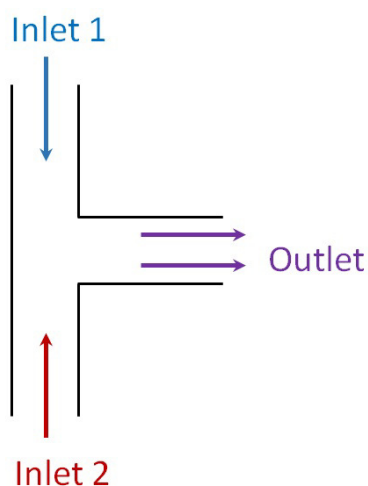


Figure 3.6. Inlet configuration of the Tee-mixer in our experiments.

Table 3.1. Comparison of operating conditions of HPIMM micro-mixer and Tee-mixer.

	HPIMM micro-mixer	Tee-mixer
Temperature range (°C)	-40 – 500	-50 – 180
Pressure stability (up to)	600	1000
Flow rate (L/h)	0.04 – 2.5	-
Residence time (ms)	27 – 1350	-
Mixing channels WxL (µm)	45 x 200	-
Inner volume (µL)	15	12.1
Max. viscosity (mPa·s)	1000	-

## 3.2. Experimental procedures

### 3.2.1. SFE experiments

SFE experiments were carried out as follows. Liquid CO<sub>2</sub> from the bottle (at approx. 50 bar) is cooled to 5 °C in the heat exchanger (5 in Figure 3.1) before being pumped and heated to the working temperature. Once the system is pressurized and heated at the desired experimental conditions (see Table 3.2), the experiment is started and liquid feed is fed into the system. Both solvent and feed are pumped continuously by two Gilson 305 HPLC pumps (6 and 7 in Figure 3.1) and flow rate of CO<sub>2</sub> is double-checked at the entrance and the exit of the system (4 and 18 in Figure 3.1). The continuous extraction experiments performed in this work lasted between 3 and 7 hours (depending on the flow rates and feed compositions),

raffinate and extract samples were regularly collected through two valves (11 and 15, respectively, in Figure 3.1).

**Table 3.2. Experimental conditions for the SFE experiments.**

Extraction system	1 <sup>st</sup> separator		2 <sup>nd</sup> separator	
	P (bar)	T (°C)	P (bar)	T (°C)
Ethanol+water/CO <sub>2</sub> (system A)	101	60	45	20
Olive oil/CO <sub>2</sub> (system B)	150-180	40	55	40

### 3.2.2. Visualization experiments

In the visualization experiments performed in this work, the preparation was similar to that of the SFE experiments: liquid CO<sub>2</sub> from the bottle (at approx. 50 bar) is cooled to 5 °C in the heat exchanger (5 in Figure 3.1) before being pumped and heated to the working temperature. Once the system is pressurized and heated at the desired experimental conditions, the experiment was started and liquid feed is fed into the system. As the purpose of these experiments was to study the influence of the flow pattern on the extraction performance, the experimental conditions chosen were the same as in the SFE experiments (see Table 3.2). During the experiments, both the solvent and the feed are pumped continuously and flow rate of CO<sub>2</sub> is double-checked at the entrance and the exit of the system. At the same time, images and videos are captured by the microscope (see Figure 3.3). The system was running for about 15-30 minutes. Then, the pumps were stopped and the entire procedure was repeated to start a new experiment.

## 3.3. Materials and methods

### 3.3.1. Experiments on the extraction of ethanol from aqueous solutions (system A)

#### 3.3.1.1. Chemicals

Distilled water and high-purity ethanol (>99.9 %) were used for the preparation of feed solutions. Technical grade carbon dioxide (>99.5%) supplied by Linde was used as the solvent.

### 3.3.1.2. Sampling

During the experiments on the extraction of ethanol from ethanol-water mixtures, the raffinate and extract samples were collected through valves 11 and 15 in Figure 3.1, respectively. Samples were taken regularly to make sure that steady-state was achieved. Feed samples were also taken at the beginning and at the end of each experiment to double check. Furthermore, extract and raffinate samples were weighed and the mass of feed consumed during the experiment was measured so the mass balance of the system could be calculated. During sampling, although it was tried to withdraw all the liquid contained in the separators, sometimes small amount of sample was remaining in the vessels. Nevertheless, more than 90% of the samples was recovered in most of the cases. This small error caused by sampling was taken into account in the mass balance calculations.

### 3.3.1.3. Analytical methods

All water-ethanol compositions were determined by density measurements. The ethanol mass fraction of feed, extract and raffinate was calculated from literature density tables (Perry and Green, 1997). Before analysis, extract and raffinate samples were treated by ultrasound to remove excess carbon dioxide. The density measurements were made using an Anton Paar SVM300. All samples, when possible, were measured twice. However, in the cases that the sample amount was less than 3 mL, e.g. experiments at very low flow rates (~300 mL/h) and when using a feed of 10 wt.% ethanol (see *Section 4.3.5.1*), an Anton Paar DM45 was used for the density measurements, as the sample volume required for this device was less than 2 mL.

The viscosity of several ethanol-water solutions of different concentration was also measured for the discussion in *Section 4.2.3* using the Anton Paar SVM 300.

## 3.3.2. Experiments on the extraction of FFA from olive oil (system B)

### 3.3.2.1. Chemicals

Mani® extra virgin olive oil purchased at the supermarket and high-purity oleic acid (>99.9%) were used for the preparation of feed solutions. Technical grade carbon dioxide (>99.5%) supplied by Linde was used as the solvent. The initial FFA content in the olive oil was 0.5 wt.%.

The feed solutions were enriched on FFA content by adding high-purity oleic acid to the olive oil to achieve the desired FFA concentration.

### 3.3.2.2. Sampling

During the extraction experiments of FFA from olive oil, the raffinate and extract samples were collected every hour through valves 11 and 15 in Figure 3.1, respectively. Furthermore, extract and raffinate samples were weighed and the mass of feed consumed during the experiment was measured so the mass balance of the system could be calculated.

### 3.3.2.3. Analytical methods

The acidity of the feed, raffinate and extract samples was determined according to the DGF Standard Method C-V 2 (06) for the determination of acid value and free fatty acid content in fats and oils. Before analysis, extract and raffinate samples were treated by ultrasound to remove excess carbon dioxide. Then, the samples were dissolved in a solution of isopropanol-water (9:1 in volume). The acid value was measured by potentiometric titration of the samples with an ethanolic solution of potassium hydroxide (0.1N). The titration system consisted of the TIM900 Titration Manager, the ABU 93 Triburette and the SAM55 Sample Station from Radiometer Copenhagen. The acidity or FFA content was calculated as a percentage by mass using the Equation (3.1), where  $V$  is the volume (mL) of the standard volumetric KOH solution,  $c$  is the concentration (mol/L) of the standard KOH solution,  $m$  is the weight (g) of the sample and  $M$  is the molar mass of oleic acid (282.45 g/mol). Every raffinate sample was analysed twice. Extract samples were analysed only once due their small amount.

$$FFA (\% \text{ oleic acid}) = \frac{V \cdot c \cdot M \cdot 100}{1000 \cdot m} \quad (3.1)$$

The density and viscosity of the olive oil used as feed were also measured for the discussion in Section 5.2.2 using an Anton Paar SVM 300.

### 3.3.3. Experiments on the visualization of multiphase flows of scCO<sub>2</sub> and liquid mixtures

#### 3.3.3.1. Chemicals

Distilled water and high-purity ethanol (>99.9%) were used for the preparation of ethanol-water binary mixtures of different concentration: 10, 50 and 90 wt.% of ethanol.

Mani® extra virgin olive oil purchased at the supermarket with a FFA content of 0.5 wt.% and high-purity oleic acid (>99.9 %) were used in the experiments for the visualization of the multiphase flow of olive oil and scCO<sub>2</sub>. The olive oil was enriched on FFA content by adding high-purity oleic acid to the olive oil to achieve the desired FFA concentration: 2.4 wt.% olive oil.

Technical grade carbon dioxide (>99.5%) supplied by Linde was used for the supercritical phase.

#### 3.3.3.2. Optical system

Shadowgraph technique was used to visualize the multiphase flow inside the capillary at different locations: in the section close to the outlet of the micro-mixer (at approx. at 30 mm from the outlet), and in the middle section of the capillary (at approx. 100-120 mm from the outlet of the micro-mixer). As described by Merzkirch (1987), in this technique, which is the simplest form to observe a flow exhibiting variations of the fluid density, the use of a point-shaped light source is essential. The light diverging from this source is transmitted through the test field, and the shadow picture produced by the inhomogeneous density field can be reflected in a plane placed at a distance behind the test field. In our experiments, an intense white light incorporated into the microscope was used as the light source. Furthermore, the transparent Radel® tubing was placed over a white background for a better visualization of the different phases.



## 4. Model system: CO<sub>2</sub>-ethanol-water. SFE of ethanol from aqueous solutions

As commented in *Section 2.2.1*, the removal or extraction of ethanol by scCO<sub>2</sub> is a widely studied process for applications such as dealcoholisation of beverages, ethanol production or ethanol recovery from fermentation processes. Therefore, the CO<sub>2</sub>-ethanol-water ternary mixture has been extensively investigated, as well the phase equilibrium behaviour of the system as the extraction and the mass transfer rates. All these reasons, together with the fact that the analysis of the samples is very simple (density measurements and comparison with tabulated data), led us to choose the continuous extraction of ethanol from aqueous solutions by scCO<sub>2</sub> as the model system to study the feasibility and applicability of micro-mixers for SFE application.

One of the first objectives of this work was to determine whether the equilibrium was reached and therefore one theoretical stage could be achieved within the extraction process in the micro-device apparatus. Therefore, the phase behaviour of the CO<sub>2</sub>-ethanol-water mixture was deeply studied and modelled using ASPEN Plus<sup>®</sup>, as described below in this chapter.

Furthermore, in order to have a better understanding of the hydrodynamics of the system and study its influence in the mixing and extraction processes considered here, fluid properties such as density, viscosity, interfacial tension and diffusion coefficient were studied in detail and are explained below.

### 4.1. Phase behaviour

#### 4.1.1. Experimental data

The vapour-liquid equilibria for a three-component system are normally represented in a triangular diagram. Every point of the diagram corresponds to a possible composition of a ternary mixture and each corner of the triangle represents a pure component. In the typical triangular phase equilibrium diagram (Figure 4.1 from Müller et al., 2012), the *binodal curve* is made up of the equilibrium points. Every point on the *binodal curve* is in equilibrium with another binodal point and these two points in equilibrium are connected by a *tie line*.

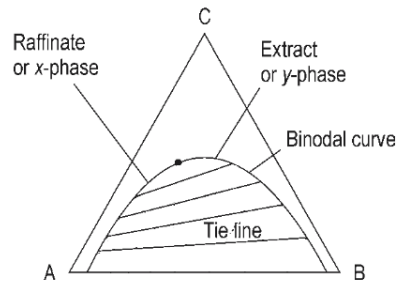


Figure 4.1. Typical triangular diagram for phase equilibria of a ternary system. Source: Müller et al. (2012).

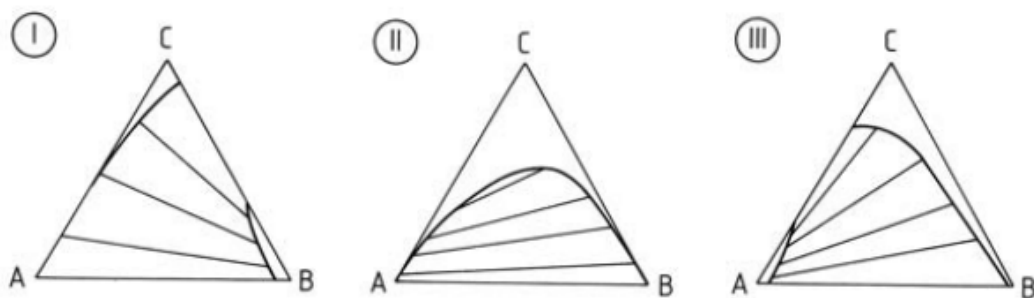


Figure 4.2. Three different types of phase equilibria in ternary systems. Source: Müller et al. (2012).

Three different types of phase equilibria behaviour are shown in Figure 4.2, where *type I* corresponds to an open system with a miscibility gap between B and C; *type II* is a closed system, in which C is completely miscible with A and B; and *type III* is an open system which presents a miscibility gap between the components A and C (Müller et al., 2012). These triangular diagrams will be alluded to for the description and explanation of the phase equilibria behaviour of the ternary mixture studied here.

The phase equilibria of the system CO<sub>2</sub>-ethanol-water has been widely studied in the last 60 years, even at high pressures, due to the feasibility of the SFE process, which has been proved to provide a better, cleaner and most efficient extraction of ethanol from aqueous solutions. For several years, the ethanol-water azeotrope, with a composition of 89.4 mol% (or 95.5 wt.%) of ethanol (DDBST), had been a perpetual limit of the distillation: an ethanol concentration higher than the azeotrope composition could not be achieved within one distillation column.

In the 50s, Baker and Anderson (1957) already reported experimental data at temperatures in the range of 10 and 50 °C and pressures up to 200 bar. It was confirmed that

pure water and pure CO<sub>2</sub> present very limited mutual solubility but CO<sub>2</sub> was found to be completely miscible with ethanol: within the conditions cited, a 95 wt.% solution of ethanol in water was completely miscible with CO<sub>2</sub>. This means that the phase equilibria diagram of this ternary mixture looks normally like the diagram *type II* in Figure 4.2, in which A represents water, B represents CO<sub>2</sub> (solvent) and C represents ethanol (solute). In this type of phase equilibrium diagram, the end point of the tie lines draw to become closer until they fit together at the plait point, i.e. the point in which both liquid and vapour phases coincide and therefore no separation is possible.

**Table 4.1. Estimated plait point concentrations at 35 °C by Gilbert and Paulaltis (1986).**

Pressure (bar)	Plait point concentrations (mole fraction)		
	Ethanol	Water	Carbon Dioxide
102	0.163	0.062	0.775
136	0.194	0.082	0.724
170	0.212	0.102	0.686

30 years later, Takishima et al. (1986) reported experimental data of this ternary system, measured at temperatures near the critical point of CO<sub>2</sub>. From their data, it was found that a high selectivity of ethanol can be expected in SFE with CO<sub>2</sub> at low concentrations of ethanol, whereas the complete dehydration was not be achieved due to the existence of an upper limit of ethanol concentration (azeotrope point). By the same time, Gilbert and Paulaltis (1986) presented a study of the vapour-liquid equilibria at different conditions of temperature (35, 50 and 65 °C) and pressure (102, 136, and 170 bar), in which phase equilibria compositions for the two coexisting fluid phases as a function of temperature and pressure are reported. From their results, it was concluded that the higher the pressure, the higher the mole fraction of ethanol at the plait point composition. This is shown in Figure 4.3(A), in which it is seen that the extent of the two-phase region decreases by increasing the pressure. Besides, these results were confirmed by their calculations using an estimation method based on the Patel-Teja equation of state (results in Table 4.1). Gilbert and Paulaltis (1986) also observed that the higher the CO<sub>2</sub> density, the better the solubility of ethanol in CO<sub>2</sub> (greater solvent capacity). However, lower ethanol selectivity was observed with greater solvent capacities. Nevertheless, ethanol concentrations greater than that corresponding to

the ethanol-water azeotrope could not be obtained by extraction with CO<sub>2</sub> at the temperatures and pressures conditions studied in Gilbert and Paulaltis (1986).

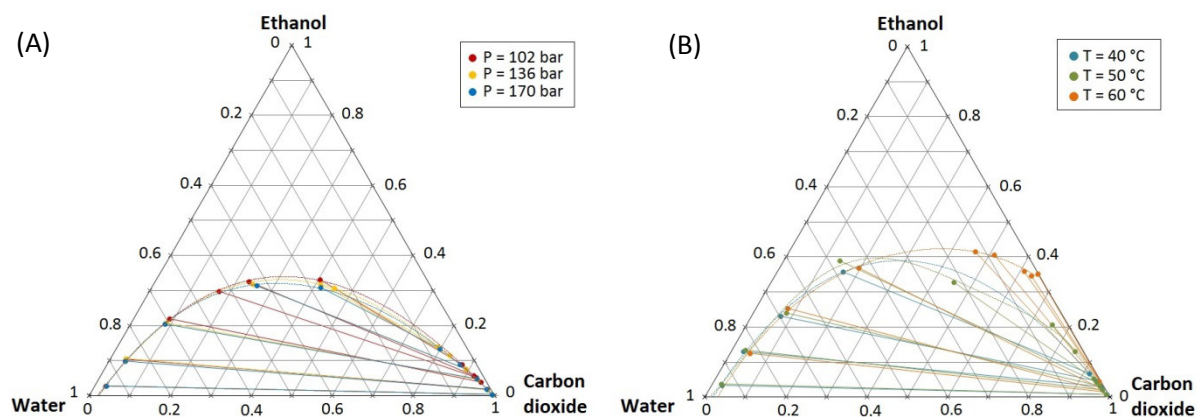


Figure 4.3. (A) Experimental data (mole basis) on the phase equilibrium of the system CO<sub>2</sub>-ethanol-water at 35 °C and 102, 136, 170 bar (data from Gilbert and Paulaltis, 1986). (B) Experimental data (mole basis) on the phase equilibrium of the system CO<sub>2</sub>-ethanol-water at 100 bar and 40, 50 and 60 °C (data from Furuta et al., 1989).

On the other hand, Furuta et al. (1989) measured the vapour-liquid equilibrium of this ternary system in the ranges of temperature and pressure of 30 - 90 °C and 56 - 132 bar (see Figure 4.3(B)), and obtained ethanol concentrations higher than the ethanol-water azeotrope. The optimum extraction conditions were determined to be a temperature in the range of 30 – 60 °C and a pressure of 100 bar: the ideal extraction temperature increases as the ethanol concentration in the liquid phase increases. Summarizing, azeotropic limit was broken by Furuta et al. (1989) but the requisites to break this limit were not certainly explained. It was actually Lim et al. (1994) who investigated and explained the conditions needed to break the azeotropic limit. They measured the vapour-liquid equilibria for the ethanol-water-CO<sub>2</sub> ternary system at 40, 50, 60 and 70 °C and pressures up to 185 bar. In Figure 4.4(A), ethanol concentrations in a CO<sub>2</sub>-free basis at 60 °C and different pressures are represented and it is observed that in some cases (at pressures of 101 bar and 105 bar), the highest attainable concentration of ethanol goes over 90 mol%. This confirms that the azeotropic limit can be broken and therefore it is possible to concentrate ethanol above the atmospheric azeotropic composition (89.4 mol%). For a better understanding of the phase equilibria of the system at these conditions, ternary diagrams of the system at the constant temperature of 60 °C and different pressures are represented in Figure 4.4(B). It is easily discernible that at 101 and 105 bar, the both pressures at which the highest ethanol concentration obtained goes over the atmospheric azeotropic composition, the binodal curves of the system are different and they

do not present a plait point (as it also occurs in the results obtained by Furuta et al. (1989) at 60 °C and 101 bar - Figure 4.3(B)). This means that ethanol and CO<sub>2</sub> are partially miscible (and not totally miscible as they are in the diagram *type II* represented in Figure 4.2 - with plait point).

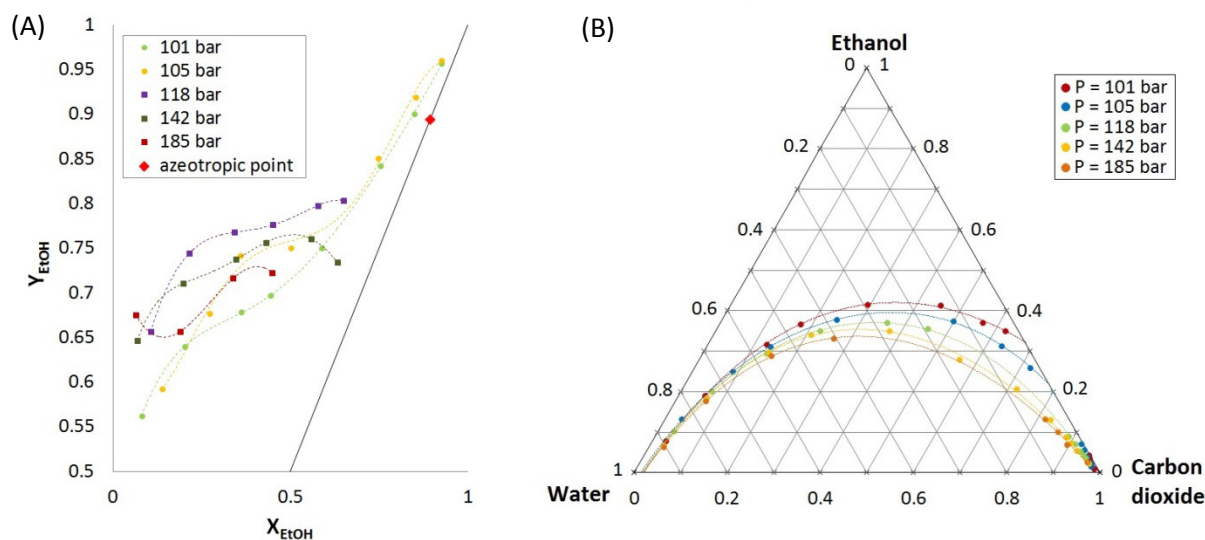


Fig 4.4. (A) Ethanol concentrations (in mole fractions and CO<sub>2</sub>-free basis) in phase equilibria of the CO<sub>2</sub>-ethanol-water ternary system at 60 °C (data from Lim et al., 1994). (B) Experimental data (mole basis) on the phase equilibrium of the system CO<sub>2</sub>-ethanol-water at 60 °C and 101, 105, 118, 142, 185 bar (data from Lim et al., 1994).

From these results, Lim et al. (1994) determined that the upper limit of ethanol concentration in the scCO<sub>2</sub> phase was attributed to the existence of a plait point, i.e. the point in which both liquid and vapour phases coincide and therefore no separation is possible. Hence, they postulated that ethanol could be concentrated above its atmospheric azeotropic composition if the extraction was performed below the critical pressure of the CO<sub>2</sub>-ethanol system at a given temperature. Moreover, they correlated the critical pressure of the binary system CO<sub>2</sub>-ethanol with the temperature (for the range of 300 – 350 K), as shown in Equation (4.1). Experimental conditions considered for the extraction of ethanol from aqueous solutions in the work presented here have been chosen in accordance with this equation to ensure that no azeotrope limit exists in our experiments.

$$P_{c,m}(\text{MPa}) = 0.1203 T(\text{K}) - 28.44 \quad (4.1)$$

Furthermore, Fornari et al. (2009) focused on proving that the solvent power depends on the CO<sub>2</sub> density and that selectivity can be turned according to CO<sub>2</sub> density as well. They established temperature and pressure so as supercritical and subcritical CO<sub>2</sub> exhibited the same density (780 kg/m<sup>3</sup>) and comparison of ethanol content in the initial mixture with that obtained in the equilibrium liquid phase was made. The results, shown in Table 4.2, indicated that the degree of dealcoholisation achieved was nearly the same when either supercritical or subcritical CO<sub>2</sub> was the solvent used.

Table 4.2. Removal of ethanol from ethanol + water mixtures using subcritical CO<sub>2</sub> (T = 25 °C, P = 90 bar) or supercritical CO<sub>2</sub> (T = 35 °C, P = 125 bar) with the same density (780 kg/m<sup>3</sup>). Data from Fornari et al. (1998).

	Ethanol content (wt.%)	
	Ethanol-water mixture loaded to the equilibrium cell	Dealcoholized equilibrium liquid phase (CO <sub>2</sub> free)
Subcritical CO <sub>2</sub>	40.0	34.9
	25.0	17.9
Supercritical CO <sub>2</sub>	40.0	35.0
	25.0	18.3

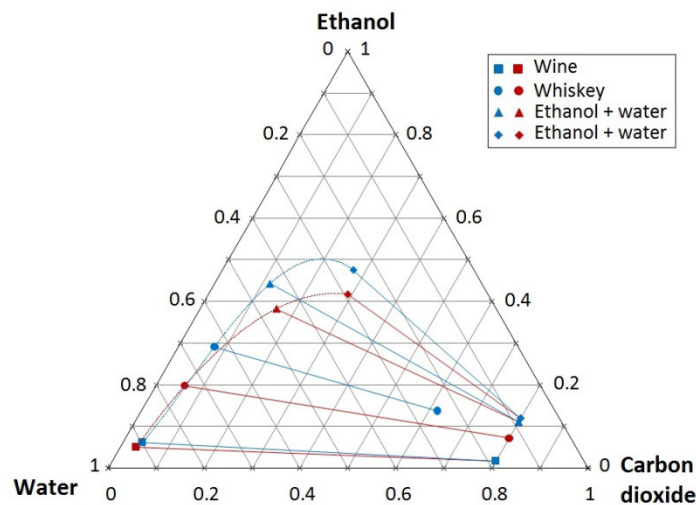


Figure 4.5. Phase equilibria ternary diagram (mass fractions) for the pseudo-ternary CO<sub>2</sub>+alcoholic beverage mixtures at constant CO<sub>2</sub> density. Red symbols: CO<sub>2</sub> density = 850 kg/m<sup>3</sup>. Blue symbols: CO<sub>2</sub> density = 600 kg/m<sup>3</sup>. (Data from Fornari et al., 2009).

Fornari et al. (2009) also carried out the comparison of the phase equilibria behaviour of different alcoholic beverages and ethanol-water mixtures with scCO<sub>2</sub>. Temperature and pressure conditions were set so as to maintain exactly the same CO<sub>2</sub> density. Two different densities were studied: 850 and 600 kg/m<sup>3</sup>. The results (Figure 4.5) show that regardless of

the alcoholic beverage or temperature and pressure conditions employed, the binodal curve was mainly determined by the CO<sub>2</sub> density.

Once the phase behaviour of the mixture was deeply studied, the extraction experimental conditions in this work were decided to be fixed at 60 °C and 101 bar. These values were chosen based on the results of Furuta et al. (1989) in addition to the statement of Lim et al. (1994) about the conditions required to break the azeotrope limit and the Equation (4.1). Moreover, it was found that different studies on the extraction of ethanol from aqueous solutions with scCO<sub>2</sub> were also performed at these or very similar conditions (Budich and Brunner, 2003; Pieck et al., 2015), which made the comparison of our extraction method (micro-mixers) with the conventional method (extraction column) easier and more reliable. In Figure 4.6, the experimental data on the phase behaviour of the ternary mixture from Lim et al. (1994), Furuta et al. (1989) and Budich, Brunner (2003) at the experimental conditions chosen in this work are compared. It is observed that the data from these authors fit pretty well together, so it was decided to consider the combination of all these data as the experimental values used in this work for the characterization of phase behaviour of the mixture CO<sub>2</sub>-ethanol-water.

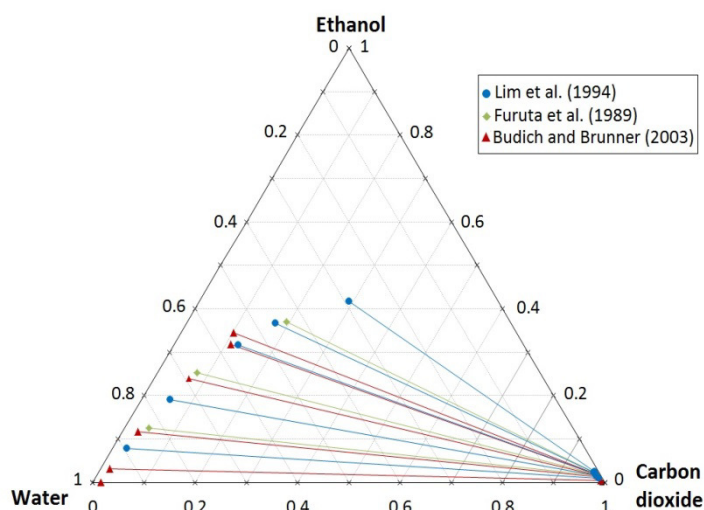


Figure 4.6. Experimental data (mole basis) on the phase equilibrium of the system CO<sub>2</sub>-ethanol-water at 60 °C and 101 bar (data from Lim et al., 1994; Furuta et al., 1989; and Budich and Brunner, 2003).

### 4.1.2. Modelling

The phase behaviour of the CO<sub>2</sub>-ethanol-water system has been modelled by different authors within the last decades. Table 4.3 shows a brief summary of the equations of state and mixing rules used to date to model this ternary mixture.

After the analysis and comparison of the different models available in literature included in Table 4.3, it was concluded that the most accurate equation of state to predict the phase equilibrium of CO<sub>2</sub>-ethanol-water system at high pressure conditions is the Peng-Robinson EoS. Therefore, this equation of state was chosen to model the phase behaviour of the ternary mixture. The model was performed using the ASPEN-Plus® software, in which the PR EoS is defined as follows in Equations (4.2)-(4.12) (Peng, Robinson, 1976; Matthias et al., 1991; Knapp et al., 1982).

**Table 4.3. Summary of the equations of state and mixing rules used in literature for the system CO<sub>2</sub>-ethanol-water.**

Equation of State	Mixing rule(s)	References
Patel-Teja EoS	Wilson	Takishima et al. (1985) Yoon et al. (1994)
Modification of the EoS proposed by Bryan and Prausnitz (1987)	-	de la Ossa et al. (1990)
Patel-Teja EoS	Conventional mixing rule Wilson mixing rule Yu et al. mixing rule Adachi and Sugie mixing rule	Lim et al. (1994)
GCA-EoS	-	Gros et al. (1997)
SAFT-EoS	-	Zhang et al. (2000)
PR-EoS & PRSV-EoS	Panagiotopoulos-Reid	Li et al. (2005)
CPA-EoS	Van der Waals one-fluid mixing rule	Perakis et al. (2006)
PR-EoS	Wong-Sandler Quadratic	Durling et al. (2007)

$$P = \frac{RT}{(c + V_m) - b} - \frac{a}{(V_m + c)(V_m + c + b) + b(V_m + c - b)} \quad (4.2)$$

where,

$$b = \sum_i x_i b_i \quad (4.3)$$



$$c = \sum_i x_i c_i \quad (4.4)$$

$$a = a_0 + a_1 \quad (4.5)$$

$$a_0 = \sum_i \sum_j x_i x_j (a_i a_j)^{0.5} (1 - k_{ij}) \quad (4.6)$$

$$k_{ij} = k_{ij}^{(1)} + k_{ij}^{(2)}T + \frac{k_{ij}^{(3)}}{T} \quad k_{ij} = k_{ji} \quad (4.7)$$

$$a_1 = \sum_{i=1}^n x_i \left( \sum_{j=1}^a x_j \left( (a_i a_j)^{1/2} l_{ij} \right)^{1/3} \right)^3 \quad (4.8)$$

$$l_{ij} = l_{ij}^{(1)} + l_{ij}^{(2)}T + l_{ij}^{(3)}/T \quad l_{ij} \neq l_{ji} \quad (4.9)$$

$$a_i = fnc(T, T_{ci}, p_{ci}, \omega_i) \quad (4.10)$$

$$b_i = fcn(T_{ci}, p_{ci}) \quad (4.11)$$

$$c_i = 0.40768 \left( \frac{RT_{ci}}{P_{ci}} \right) (0.29441 - z_{RAi}) \quad (4.12)$$

The factor  $z_{RAi}$  in Equation (4.12) represents the Rackett parameter, which estimates the molar volume. The estimation of the binary interaction parameters ( $k_{ij}$ ,  $l_{ij}$  and  $l_{ji}$ ) was made using experimental data on the phase behaviour of the mixture at the experimental conditions chosen in this work (101 bar, 60 °C) from different authors (Furuta et al., 1989; Lim et al., 1994 and Budich and Brunner, 2003) as already discussed in *Section 4.1.1*. The calculations were performed according to the procedure shown in Figure 4.7. The obtained values are shown in Table 4.4.

**Table 4.4.** Calculated binary interaction parameters for the PR EoS at 101 bar and 60 °C.

	CO <sub>2</sub> -ethanol	CO <sub>2</sub> -water	Ethanol-water
$k_{12} = k_{21}$	0.11196	-0.01950	-0.09680
$l_{12}$	-0.08228	0.13973	0.02310
$l_{21}$	0.02295	-0.37128	0.11160

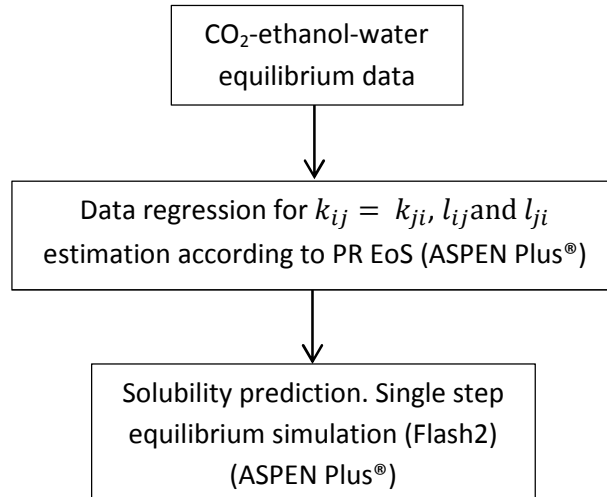


Figure 4.7. Process scheme followed in this work to obtain binary interaction parameters.

In Figure 4.8, the model is represented together with the experimental data and it is observed that the model calculated here fits the experimental results from the authors well. However, looking at the slope of the tie lines and comparing the model with the experimental results, it is seen that the model fits the liquid phase better than the vapour phase compositions. In order to assess the model, the relative deviation (RD) was used as an error criterion. RD is defined in Equation (4.13), where  $N$  is the number of data point,  $x_{exp}$  is the experimental value and  $x_{calc}$  corresponds to the value calculated with the model.

$$RD = \frac{100}{N} \sum \frac{|x_{EtOH\ exp} - x_{EtOH\ calc}|}{x_{EtOH\ exp}} \quad (4.13)$$

The relative deviation of the vapour phase and the liquid phase data is 18% and 4%, respectively. Thus, we assumed that the raffinate composition (liquid phase) was more representative than the extract composition (vapour phase) for comparison of our experimental extraction results with the model. Further on it was found that the worst accuracy of the prediction of the extract phase occurs at very low (~10 wt.%) and very high (~90 wt.%) concentration of ethanol.

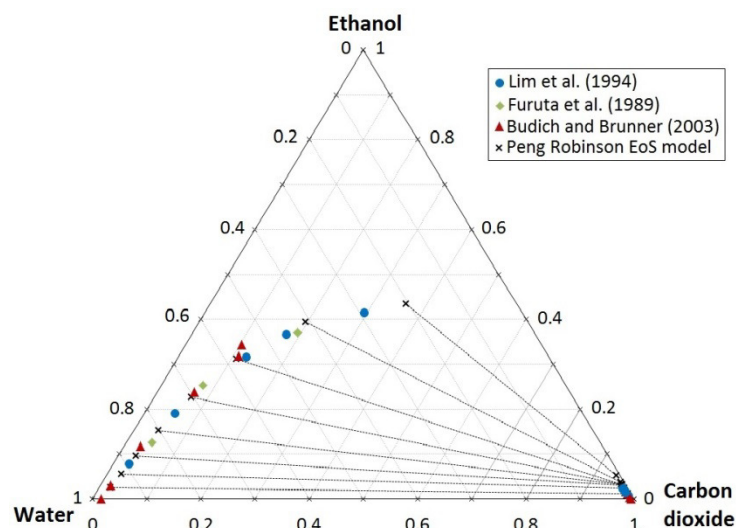


Figure 4.8. Phase behaviour of the ternary mixture CO<sub>2</sub>-ethanol-water at 60°C and 101 bar: comparison of model and experimental data from different authors.

## 4.2. Physical properties

It is known that the fluid physical properties such as density, viscosity and surface or interfacial tension rule the behaviour of the fluids and certainly influence most of the chemical and physical processes. Therefore, the fluid dynamic properties of every binary and ternary system involved in the extraction of ethanol from aqueous solutions, namely CO<sub>2</sub>-water, CO<sub>2</sub>-ethanol, ethanol-water (binary systems) and CO<sub>2</sub>-ethanol-water (ternary system) were strongly studied, and described here in order to have a better overview of their influence and to understand the effect that they have on the mixing and the extraction processes investigated in this work. Moreover, as SCFs presents unique properties in comparison with other fluids, physical properties of scCO<sub>2</sub> and their dependence with the pressure are also briefly described in this chapter. Properties such as density, viscosity and interfacial tension are of great importance to define the behaviour of the fluids in the mixing, and the flow pattern along the micro-channel at the outlet of the micro-mixer. On the other hand, diffusion coefficients are important for a better comprehension of the mass transfer. These properties are highly dependent on pressure and temperature conditions as well as composition; therefore all the data used in our calculations and reported here were taken at the conditions of 60 °C and 101 bar. In case that data at 60 °C and 101 bar were not found or could not be measured, data on very similar conditions were used.

### 4.2.1. Supercritical CO<sub>2</sub>

In the extraction process studied here, scCO<sub>2</sub> was chosen as the solvent. Therefore its fluid dynamic properties play an important role. It is known that the density and some others properties of the supercritical fluids are extremely sensitive to minor changes in pressure and temperature near the critical point. This is seen in Figures 4.9 and 4.10, in which the density and the viscosity of scCO<sub>2</sub> are represented as a function of pressure. Thus, the experimental conditions (P and T) chosen for the extraction experiments are of great importance.

Table 4.5. CO<sub>2</sub> density and viscosity at the experimental extraction conditions (NIST, 2016).

Temperature (°C)	Pressure (bar)	Density (kg/m <sup>3</sup> )	Viscosity (mPa·s)
60	101	296.13	0.024128

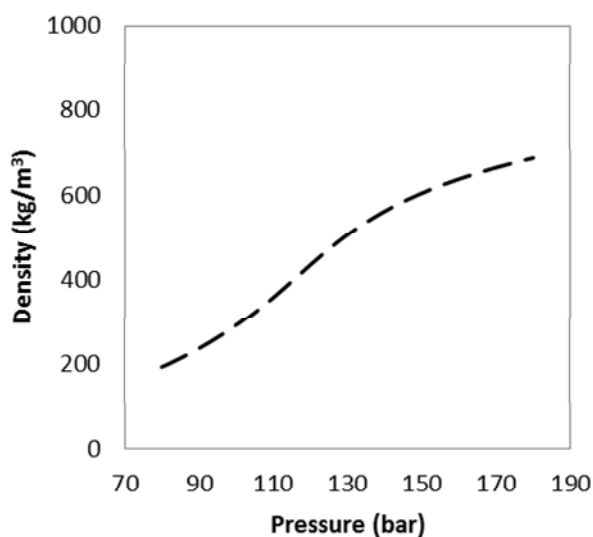


Figure 4.9. Density of scCO<sub>2</sub> as a function of the pressure at 60 °C. Data from NIST (2016).

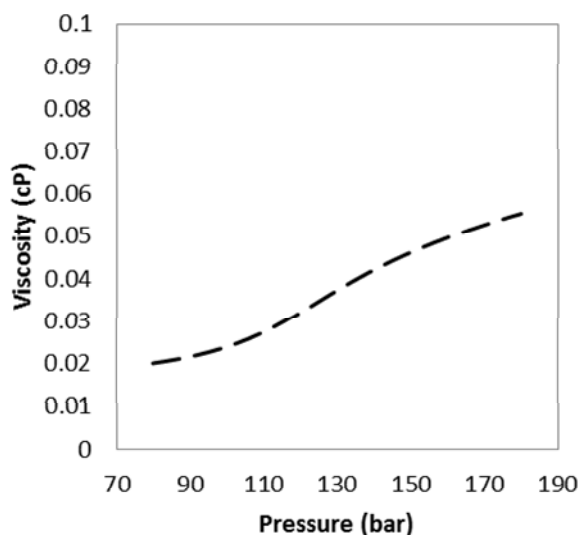


Figure 4.10. Viscosity of scCO<sub>2</sub> as a function of the pressure at 60 °C. Data from NIST (2016).

The conditions of pressure and temperature for the extraction of ethanol from aqueous solutions chosen in this work are 101 bar and 60 °C. The CO<sub>2</sub> density and viscosity values at these conditions are shown in Table 4.5.

### 4.2.2. CO<sub>2</sub>-water system

CO<sub>2</sub> and water are the two key components in the extraction process studied here. Water is the key component of the phase from which the solute (ethanol) is extracted, whereas the scCO<sub>2</sub> (the solvent) is the key component of the phase into which the solute is extracted. Due to their low mutual solubility, it was considered that, in our extraction experiments, after the

mixing step inside the micro-mixer, both aqueous and supercritical phases were mutually saturated and hence, ethanol was the only diffusing specie in the mass transfer unit. For the purpose of knowing the main fluid properties of the two key components in the extraction process, the density of the saturated and the unsaturated phases were compared. In Table 4.6 and Figure 4.11 (NIST, 2016; Bikkina et al., 2011), the density values for the following phases are represented as a function of pressure: (1) pure water, (2) pure CO<sub>2</sub>, (3) saturated water with CO<sub>2</sub> and (4) saturated CO<sub>2</sub> with water. If phases (1) and (3) are compared, namely pure water and saturated water with CO<sub>2</sub>, no remarkable differences are observed. The same happens when comparing phases (2) and (4), i.e. pure CO<sub>2</sub> and CO<sub>2</sub> saturated with water. Therefore, as no significant differences are observed between the saturated and unsaturated phases, and based on the low solubility of CO<sub>2</sub> in water and vice versa, the influence of the dissolved CO<sub>2</sub> in the liquid mixture was assumed to be negligible for the calculation and determination of the fluid properties of the feed mixtures in our extraction experiments (i.e. ethanol-water binary mixtures).

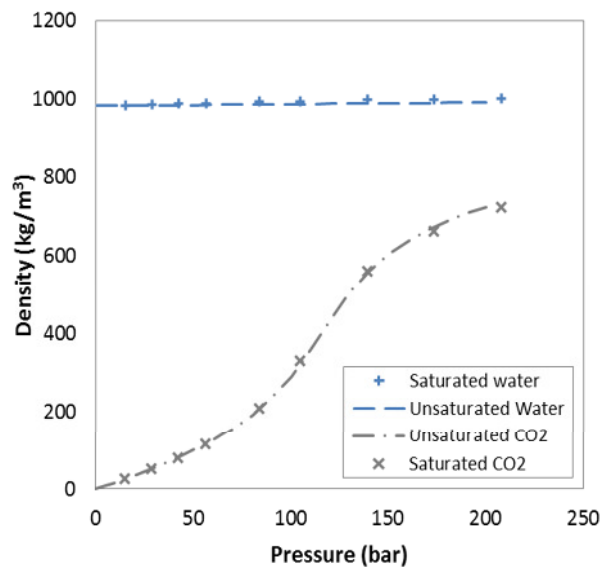


Figure 4.11. Comparison of density values as a function of the pressure: the lines represent the density of pure water and pure CO<sub>2</sub> (data from NIST, 2016), whereas the symbols represent the density of water saturated with CO<sub>2</sub> (water-rich phase) (+) and CO<sub>2</sub> saturated with water (CO<sub>2</sub>-rich phase) (x) (data from Bikkina et al., 2011).

Table 4.6. Density of both aqueous and supercritical saturated and unsaturated phases at 104 bar and 60 °C. Data from NIST (2016) and Bikina et al. (2011).

Phase	Density (kg/m <sup>3</sup> )
Saturated CO <sub>2</sub> with water	328.8
Unsaturated CO <sub>2</sub>	315.5
Saturated water with CO <sub>2</sub>	995.7
Unsaturated water	987.6

### 4.2.3. Ethanol-water system

The feed solutions used in the extraction experiments of ethanol from aqueous solutions performed in this work were binary mixtures of ethanol and water of different concentrations: between 10 and 90 wt.% of ethanol. Obviously, the ethanol concentration of these liquid mixtures certainly influences the solution's fluid properties, as observed in Figures 4.12 and 4.13, in which the density and viscosity of ethanol-water mixtures are represented as a function of the ethanol concentration.

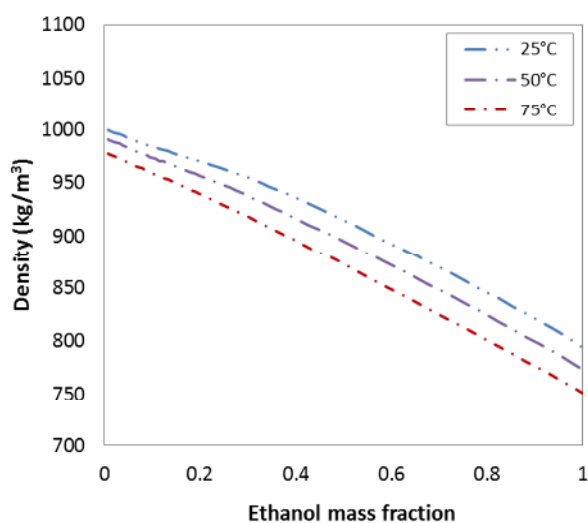


Figure 4.12. Density of ethanol aqueous solutions as a function of the ethanol mass fraction at 100 bar and different temperatures (25, 50 and 75 °C). Data from Pečar and Doleček (2005).

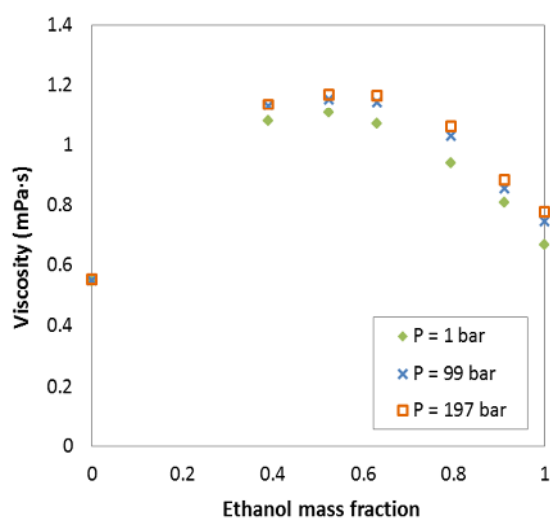


Figure 4.13. Viscosity of ethanol aqueous solutions as a function of the ethanol mass fraction at 50 °C and different pressures (1, 99 and 197 bar). Data from Tanaka et al. (1987).

Pečar and Doleček (2005) measured the density of ethanol-water mixtures at 25, 50 and 75 °C and at pressures up to 400 bar (see Figure 4.12). As our experiments were performed at 101 bar and 60 °C, a linear regression was made using Pečar and Doleček's data in order to

estimate the density of ethanol aqueous solutions at our experimental conditions (the results of this linear regression are shown in Figure 4.15 and Table 4.7).

On the other hand, Tanaka et al. (1987) measured the viscosity of water-ethanol binary mixtures at high pressure conditions. As it is observed in Figure 4.13, the viscosity of each concentration barely changes in a range of 200 bar. For this reason, it was considered that the influence of the pressure on the viscosity in our experiments (carried out at 101 bar) might be neglected. The viscosity of several ethanol-water solutions was then measured in our lab using a viscosity meter Anton Paar SVM 300. First of all, the viscosity of ethanol-water mixtures of different concentrations was measured at 50 °C and values were compared with the values from Tanaka et al. (1987). As shown in Figure 4.14, our measurements at 50 °C fit the data from Tanaka et al. (1987) perfectly. Then, the viscosity of ethanol-water mixtures at 60 °C was also measured (see Figure 4.14). Due to the minor influence of the pressure on the viscosity, as noted in Figure 4.13, we assumed the values of the viscosity of ethanol-water mixtures at 60 °C and atmospheric pressure measured in our lab to be the viscosity of the ethanol-water mixtures at our experimental conditions, data are shown in Table 4.7.

**Table 4.7. Calculated or estimated values of density and viscosity of ethanol-water mixtures at 100 bar and 60 °C.**

Ethanol mass fraction	Density (kg/m <sup>3</sup> )	Viscosity (mPa·s)
0	987.48 <sup>1</sup>	0.4687 <sup>1</sup>
0.1	971.05	0.6463 ± 0.0214
0.2	948.90	0.7489 ± 0.0166
0.3	926.75	0.8497 ± 0.0173
0.4	904.60	0.9006 ± 0.0076
0.5	882.45	0.9172 ± 0.0023
0.6	860.30	0.8959 ± 0.0077
0.7	838.15	0.8404 ± 0.0003
0.8	816.00	0.7684 ± 0.0077
0.9	793.85	0.6843 ± 0.0171
1	764.14 <sup>2</sup>	0.5850 ± 0.0108

<sup>1</sup> Data from NIST (2016)

<sup>2</sup> Data from Dortmund Data Bank (DDBST)

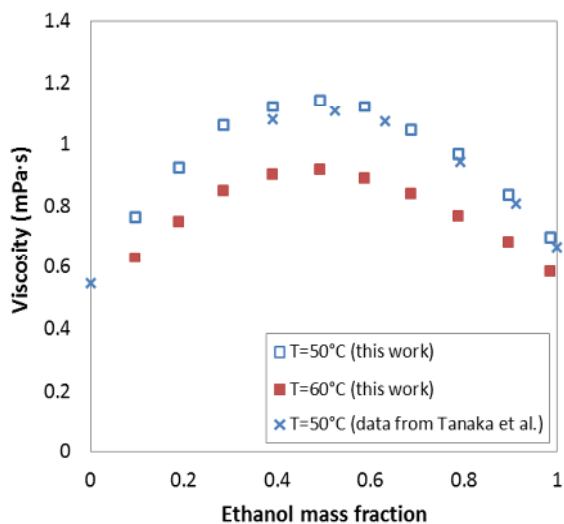


Figure 4.14. Viscosity of ethanol aqueous solutions as a function of the ethanol mass fraction at atmospheric pressure and at 50 and 60 °C.

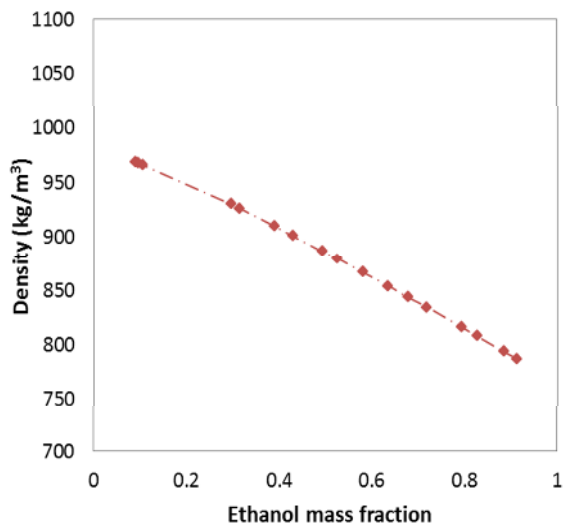


Figure 4.15. Density of ethanol aqueous solutions as a function of the ethanol mass fraction at 100 bar and 60 °C. Values estimated using data from Pečar and Doleček (2005).

Regarding the diffusion coefficient of ethanol in water, Easteal and Woolf (1985) studied the pressure and temperature dependence of tracer diffusion coefficients of some alcohols in water, ethanol among them. They proved that, for a given temperature, the effect of the pressure in the diffusion coefficient is very low (see Table 4.8). Furthermore, Pratt and Wakeham (1974) measured the mutual diffusion coefficients for liquid mixtures of ethanol and water over the entire range of composition, for temperatures from 25 to 65 °C and at atmospheric pressure (Figure 4.16). According to Easteal and Woolf's results, it was assumed in this work that the influence of the pressure in the diffusion of ethanol in water is negligible. Thus, the mutual diffusion coefficients of ethanol in water mixtures at 60 °C and atmospheric pressure were calculated by correlating Pratt and Wakeham's data and the results obtained were assumed to be the diffusion coefficients of ethanol in water at our experimental conditions (see results in Figure 4.17, Table 4.9).



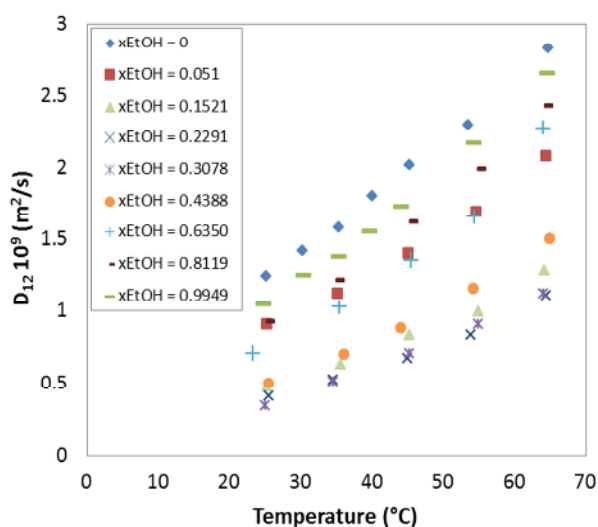


Figure 4.16. Mutual diffusion coefficient for ethanol-water mixtures as a function of temperature for different mole fractions of ethanol and atmospheric pressure. Data from Pratt and Wakeham (1974).

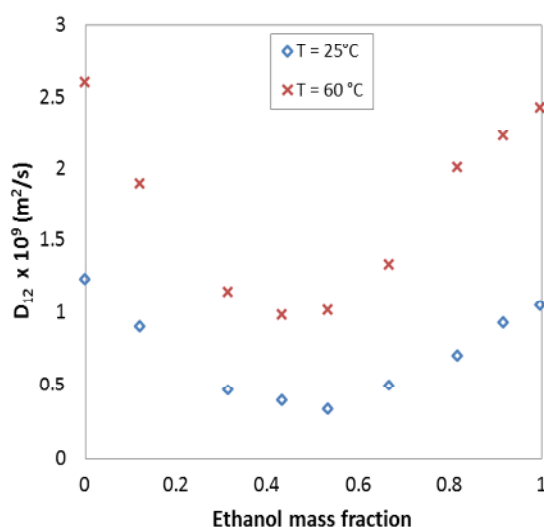


Figure 4.17. Mutual diffusion coefficient for ethanol-water mixtures as a function of the ethanol mass fraction at 25 and 60 °C. Data from Pratt and Wakeham (1974).

Table 4.8. Tracer diffusion coefficients of ethanol in water. Data from Easteal and Woolf (1985).

T = 5 °C		T = 15 °C		T = 25 °C	
P (bar)	$D_{12} \cdot 10^9$ (m <sup>2</sup> /s)	P (bar)	$D_{12} \cdot 10^9$ (m <sup>2</sup> /s)	P (bar)	$D_{12} \cdot 10^9$ (m <sup>2</sup> /s)
1	0.53	1	0.88	1	1.22
473	0.62	580	0.87	552	1.20
527	0.61	1300	0.89	1276	1.16

Table 4.9. The mutual diffusion coefficients considered for ethanol-water mixtures at 60 °C and 101 bar.

Ethanol mass fraction	$D_{12} \cdot 10^9$ (m <sup>2</sup> /s)
0	2.60
0.1208	1.89
0.3144	1.15
0.4318	0.98
0.5320	1.02
0.6666	1.34
0.8165	2.01
0.9169	2.23
0.9979	2.43

#### 4.2.4. CO<sub>2</sub>-ethanol system

As explained above, ethanol is the specie diffusing from the liquid phase into the supercritical phase. Therefore, to study the mass transfer, it is also important to know the diffusion coefficient of ethanol in CO<sub>2</sub>. Kong et al. (2006) measured the diffusion coefficients of ethanol in supercritical CO<sub>2</sub> at 40 °C and different pressures. Unfortunately, no data of diffusion coefficients of ethanol in scCO<sub>2</sub> had been found in literature at 60 °C. Thus, a predictive equation (Equations (4.15)-(4.21)), based on the Stokes-Einstein equation and developed by He (1998) was chosen to predict the diffusion coefficient of ethanol in scCO<sub>2</sub> at our experimental conditions. Among the predictive equations developed for diffusion coefficients in supercritical fluids, this one was chosen due to its low average absolute deviations (AAD) from experimental results (Medina, 2012). The Stokes-Einstein equation is commonly used for the estimation of diffusion coefficients in liquids and it describes the diffusion coefficient as shown in Equation (4.14) (Miller 1924),

$$D = \frac{RT}{N} \frac{1}{6\pi Zr} \quad (4.14)$$

where R is the gas constant ( $m^3 \cdot Pa \cdot K^{-1} \cdot mol^{-1}$ ), N Avogadro's number ( $mol^{-1}$ ), T the absolute temperature (K), r is the radius of a diffusing particle (m) and Z is the viscosity of the diffusion medium (Pa·s).

$$D_{21} = A \cdot 10^{-9} (V_1^k - B) T M_2^{-0.5} \exp[n(1 - T_{c1}/T)] \quad (4.15)$$

$$k = 1 \quad \rho_{r1} \geq 1.2 \quad (4.16)$$

$$k = 1 + (\rho_{r1} - 1.2) M_1^{-0.5} \quad \rho_{r1} < 1.2 \quad (4.17)$$

$$n = 0.8 \quad \text{for non - associating solvent} \quad (4.18)$$

$$n = 2 \quad \text{for associating solvent} \quad (4.19)$$

$$A = 7.5888 \cdot 10^{-4} + 0.60165 / (V_{c1} - 38.02) \quad (4.20)$$

$$B = (5.13 - 0.755V_{c1}/M_1)M_1^{0.5} \quad (4.21)$$

Table 4.10. Estimated diffusion coefficient of ethanol in scCO<sub>2</sub> at 60 °C using He's predictive equation (He, 1998).

P (bar)	D <sub>12</sub> · 10 <sup>8</sup> (m <sup>2</sup> /s)
95	4.97 ± 0.10
97.2	4.83 ± 0.10
100	4.66 ± 0.10
101	4.60 ± 0.10
104.9	4.40 ± 0.10
110	4.15 ± 0.10

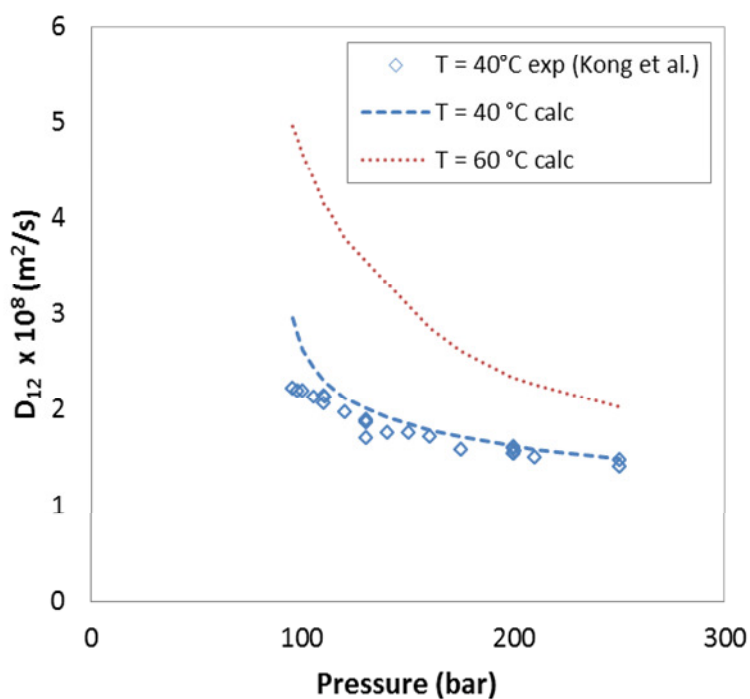


Figure 4.18. Diffusion coefficient of ethanol in scCO<sub>2</sub> as a function of the pressure. Experimental data from Kong et al. (2006). Calculated data using C.H. He's predictive equation (He, 1998).

In Figure 4.18, experimental data (Kong et al., 2006) on diffusion coefficient of ethanol in scCO<sub>2</sub> are compared with the values obtained by the predictive equation from He (1998) at 40 °C. Moreover, the predicted values by He's equation at 60 °C are also shown. As it is observed, the calculated values fit with experimental data well, except at pressures of about

90-100 bar, which is actually the range of our experimental conditions. The predictive equation was tested with different components (benzene and naphthalene) and at different conditions (115-260 bar and 40-60 °C), and experimental and calculated values were compared. Results were very satisfactory, especially at 60 °C: an AAD lower than 10% was obtained. Therefore and due to the reliable prediction of the diffusion coefficient in scCO<sub>2</sub> of different solutes, the calculated value using the He's equation was assumed to be the diffusion coefficient of ethanol in scCO<sub>2</sub> at our experimental conditions (results are shown in Table 4.10).

#### 4.2.5. CO<sub>2</sub>-ethanol-water system

The ternary system CO<sub>2</sub>-ethanol-water comprises the three fundamental components (key components and solute) for the extraction process of ethanol from water into scCO<sub>2</sub> studied here. As described above, water and scCO<sub>2</sub> are considered immiscible fluids so ethanol is the only diffusing specie in the mass transfer unit. Fluid properties such as viscosity and density of both fluids (ethanol-water solutions and scCO<sub>2</sub>) have been explained above (see *Sections 4.2.1. and 4.2.3.*). These properties, together with the interfacial tension between the two phases define the behaviour of the fluids in the mixing process and the flow pattern. The interfacial tension of CO<sub>2</sub>-water-alcohol mixtures was studied by Chun and Wilkinson (1995) at different pressures and temperatures: in Figure 4.19, the interfacial tension of ethanol-water mixtures of different composition (in mole fractions) at 65 °C is represented as a function of the pressure. Moreover, the interfacial tension of pure water and pure ethanol in CO<sub>2</sub> at 60°C are also shown for comparison. In this work, a regression was made using the data from Chun and Wilkinson (1995) to estimate the interfacial tension of ethanol-water mixtures in CO<sub>2</sub> at our experimental conditions (101 bar and 60 °C), results are shown in Figure 4.20 and Table 4.11. The interfacial tension of pure ethanol and water at those conditions were estimated using data from Dittmar et al. (2002) and Bikkina et al. (2011), respectively. It is observed that, the interfacial tension clearly decreases as the pressure and the ethanol concentration in the solution increase. This is an important factor to bear in mind for extraction processes since, as Dittmar et al. (2002) stated, during a counter-current extraction of an ethanol-water mixture, the extraction of ethanol leads to a rising interfacial tension. Likewise, as the ethanol is extracted from the water phase into the scCO<sub>2</sub> phase, the composition of both liquid and supercritical phases vary with the time, which leads

to changes in their fluid properties as well. In Section 4.2.3., the influence of the ethanol concentration on the liquid phase's density and viscosity is given. As explained in Section 4.2.2, the influence of the dissolved CO<sub>2</sub> in the liquid phase is assumed negligible. On the other hand, the changes in the density of the supercritical phase as the ethanol is extracted are shown in Figure 4.21. Budich and Brunner (2003) studied the equilibrium behaviour of the ternary mixture CO<sub>2</sub>-ethanol-water and measured the density of the vapour phase at equilibrium conditions. Figure 4.21 shows how the density of the vapour phase changes with the mass fraction of ethanol: the density clearly increases as the amount of ethanol in the vapour phase increases.

Table 4.11. Estimated interfacial tension of ethanol-water mixtures at 101 bar and 60 °C.

Ethanol mass fraction	Interfacial tension (mN/m)
0	32.15
0.2135	29.24
0.3657	21.89
0.5641	16.36
0.7371	12.25
1	1.03

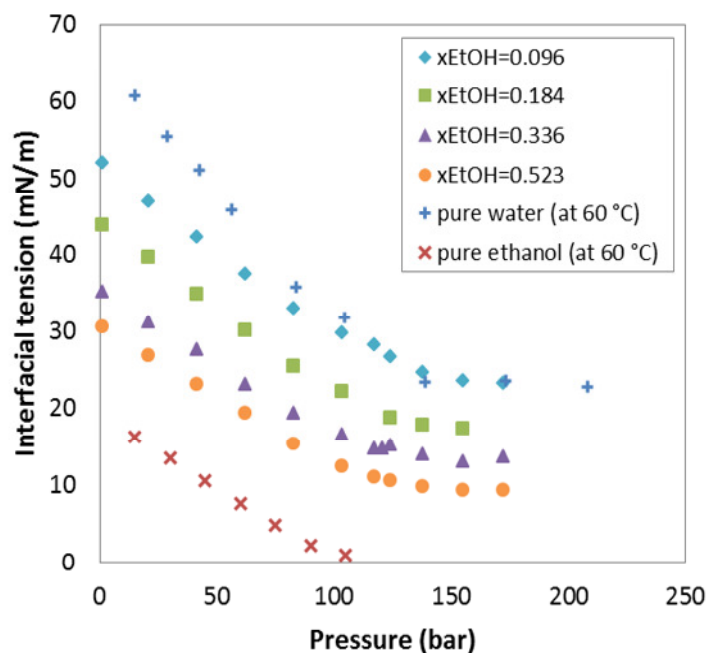


Figure 4.19. Interfacial tension of water in CO<sub>2</sub> (Bikkina et al., 2011), ethanol in CO<sub>2</sub> (Dittmar et al., 2002) at 60 °C and ethanol-water mixtures of different composition (mole fractions) in CO<sub>2</sub> (Chun and Wilkinson, 1995) at 65 °C as a function of the pressure.

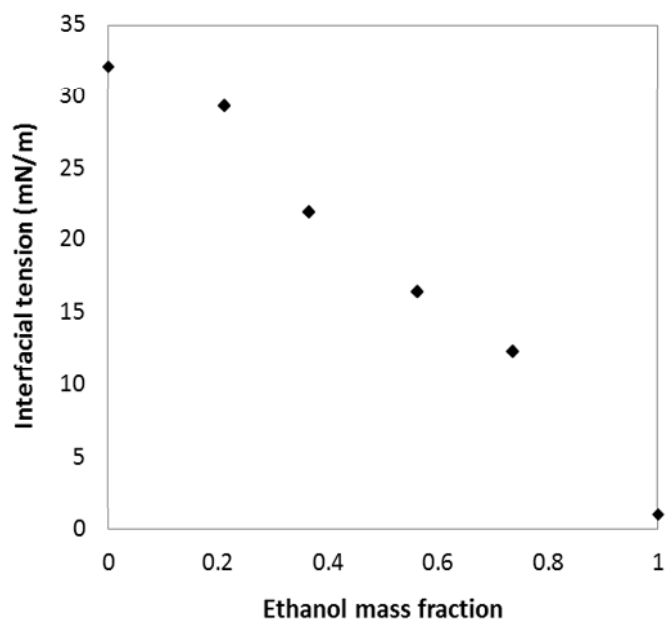


Figure 4.20. Estimated interfacial tension values of ethanol-water mixtures at 101 bar and 60 °C.

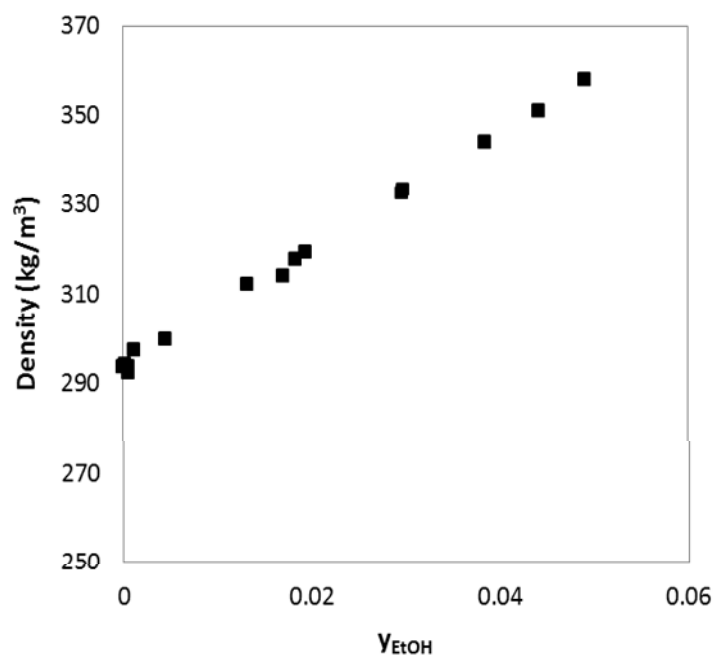


Figure 4.21. Vapour phase density in the VLE of CO<sub>2</sub>-ethanol-water as a function of the mass fraction of ethanol at 100 bar and 60 °C. Data from Budich and Brunner (2003).

### 4.3. Experimental results

Experiments on the extraction of ethanol from aqueous solutions were carried out in the experimental apparatus described in *Chapter 3* to study the feasibility of micro-mixers for SFE purposes. The experimental conditions chosen in this work are given in Table 4.12.

Table 4.12. Experimental conditions for the extraction of ethanol from aqueous solutions by scCO<sub>2</sub>.

	Pressure (bar)	Temperature (°C)
1 <sup>st</sup> separator	101	60
2 <sup>nd</sup> separator	45	20

As explained in *Chapter 3*, the micro-mixer is the only point in which solvent and feed get into contact. Thus, only one theoretical stage of extraction can be achieved within the extraction process. The first objective was to determine whether the equilibrium was reached and therefore one theoretical stage could be achieved within the extraction process in the high pressure micro-device apparatus. By knowing this, extraction processes which require more than one single stage could simply be designed as a number of micro-mixers (the same number as extraction stages are required) placed in series. The Equilibrium Stage Model Concept (see Figure 4.22 and Equations (4.22)-(4.26)) was used in this work to assess the experimental results and confirm the achievement of the equilibrium state.

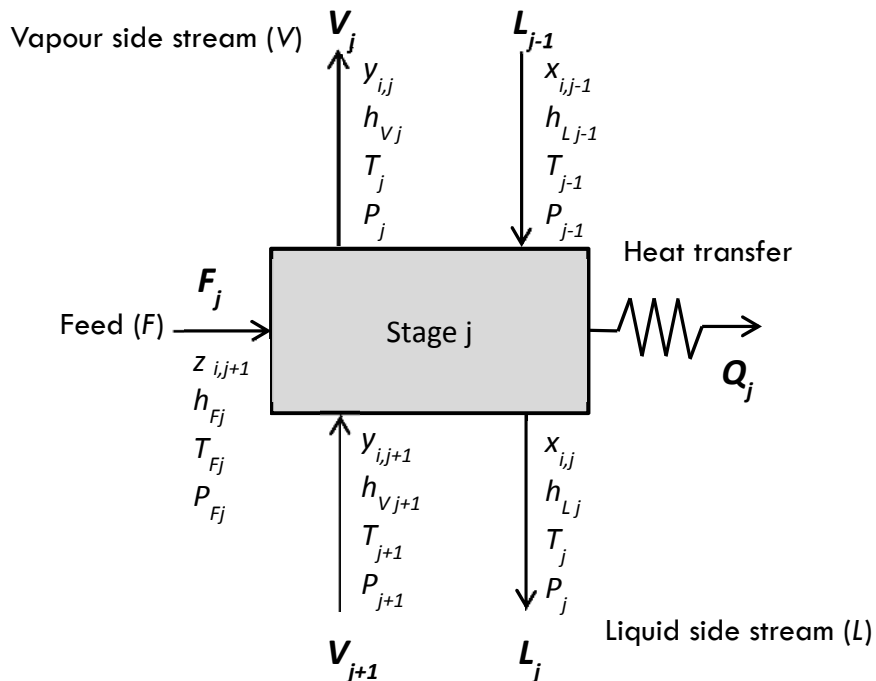


Figure 4.22. General equilibrium stage.

The Equilibrium Stage Model (Henley and Seader, 2006) considers a general, continuous, steady-state vapour liquid separator and assumes that (1) phase equilibrium is achieved, (2) no chemical reactions occur and (3) entrainment of liquid drops in vapour and occlusion of vapour bubbles in liquid are negligible. In this model, the Equations (4.22)-(4.26) must be satisfied for each stage.

Material mass balance for each component:

$$L_{j-1}x_{i,j-1} + V_{j+1}y_{i,j+1} + F_jz_{i,j} - L_jx_{i,j} - V_jy_{i,j} = 0 \quad (4.22)$$

Phase-Equilibrium relation for each component:

$$y_{i,j} - K_{i,j}x_{i,j} = 0 \quad (4.23)$$

where  $K_{i,j}$  is the phase equilibrium ratio.

Mole fraction summations:

$$\sum_{i=1}^c y_{i,j} = 1 \quad (4.24)$$

$$\sum_{i=1}^c x_{i,j} = 1 \quad (4.25)$$

Energy balance:

$$L_{j-1}h_{Lj-1} + V_{j+1}h_{Vj+1} + F_jh_{Fj} - L_jh_{Lj} - V_jh_{Vj} - Q_j = 0 \quad (4.26)$$

As described previously in *Section 4.1.2*, the phase equilibrium of the ternary mixture CO<sub>2</sub>-ethanol-water was modelled at the experimental conditions of 101 bar and 60 °C by the Peng-Robinson EoS. This model, together with the Equations (4.22)-(4.25) of the Equilibrium Stage Model Concept, was used to determine whether the equilibrium was achieved in the experiments carried out in this work. On the contrary, the energy balance (Equation (4.26)) was not considered.

Further on, the influence of the following parameters on the extraction process was studied: the feed concentration, the solvent flow rate (i.e. Solvent-to-Feed ratio), the length



of the capillary placed between the micro-mixer and separator, and the overall flow rate. The experimental results obtained for the SFE of ethanol from aqueous solutions with scCO<sub>2</sub> in micro-mixers are shown and discussed in the next sections of this chapter. In the following graphs, the results using the HPIMM micro-mixer will always be represented by filled symbols (●,■), while the results obtained with the Tee-mixer will be represented by hollow symbols (○,□). Moreover, it is important to point out that the standard deviation error is represented for every experimental result shown in the figures. However, this error is so small in some cases that it is not always appreciable in the graphs. As described in *Section 3.3.1*, during the extraction experiments, samples from extract and raffinate were taken regularly. The experimental results presented in this chapter correspond to the average value of the extract concentration and the raffinate concentration (ethanol's mass fraction) in each experiment. The standard deviation was used to assess the dispersion of the experimental data on the extract and raffinate concentrations for every experiment.

#### 4.3.1. Influence of the feed concentration

SFE experiments of ethanol from different aqueous solutions (namely, with different concentration) were performed in order to study whether equilibrium could always be achieved, regardless of the feed concentration. As discussed in *Section 4.2.3*, the properties of ethanol-water mixtures are heavily dependent on the concentration of ethanol, especially the interfacial tension between the ethanol-water mixture and scCO<sub>2</sub>, which increases drastically as the concentration of ethanol decreases. Budich and Brunner (2003) calculated HETS values for the extraction of ethanol from aqueous solutions at the same extraction conditions (100 bar and 60 °C) as in the experiments carried out here, and obtained different HETS values for different feed concentrations. In their work, a HETS value of 0.33 m was calculated for a feed with very high concentration of ethanol (94 wt.%); whereas, with feed mixtures of low ethanol content (~ 10 wt.%), HETS calculated values were in the range of 1 m. The authors concluded that HETS is influenced, among many factors, by the transport properties of both phases, such as viscosity and interfacial tension, as they can influence the mass transfer and backmixing. In our experimental apparatus, the mixing volume is given by the inner volume of the micro-mixer, which is fixed and cannot be changed. Therefore, it was the purpose of this first series of experiments to investigate whether a single stage of extraction could be

achieved in our high pressure micro-device apparatus for SFE when having different feed concentrations of ethanol, in the range of 10 wt.% - 90 wt.%.

The results in Figure 4.23 (HPIMM micro-mixer) and Figure 4.24 (Tee-mixer) show the product's ethanol mass fractions (raffinate and extract) for different feed concentrations at S-to-F ratios of 8, 11.5 and 13. In these figures, the experimental results are compared with the model developed in ASPEN Plus®. It is observed that they fit well with the compositions predicted using the model, especially for the raffinate phase. Therefore it was concluded that equilibrium was reached through the extraction process and one single stage was achieved, regardless of the feed concentration, at least in the S-to-F ratios considered, and with a constant feed flow rate of 30 mL/h.

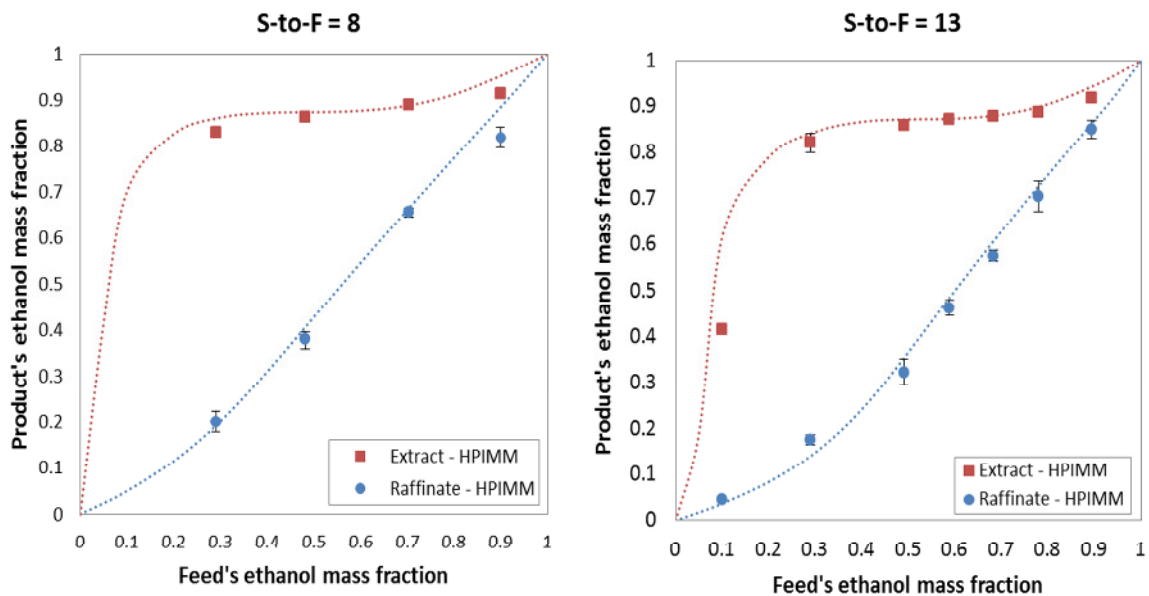


Figure 4.23. Experimental results of raffinate (•) and extract (■) compositions using the HPIMM micro-mixer and the prediction of a single theoretical stage model with mass S-to-F of 8 and 13.

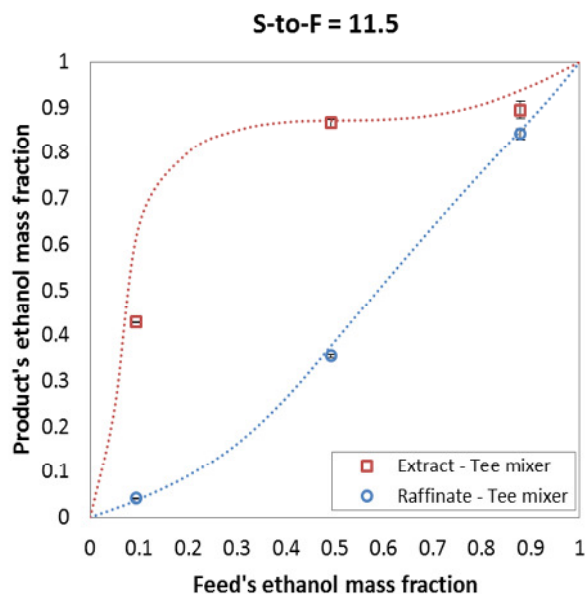


Figure 4.24. Experimental results of raffinate (o) and extract (□) compositions using the Tee-mixer and the prediction of a single theoretical stage model with mass S-to-F = 11.5.

### 4.3.2. Influence of the solvent flow rate

It is known that the extraction results are heavily dependent on the amount of solvent and therefore on the S-to-F ratio. Hence, experiments keeping constant the feed volume flow rate and varying the solvent volume flow rate were performed. Figure 4.25 shows the raffinate's and extract's ethanol mass fractions as a function of the total volume flow rate. The feed flow rate was the same in every case (30 mL/h), while the scCO<sub>2</sub> flow rate was changed. The total volume flow rate corresponds to the sum of feed plus solvent volume flow rates in the micro-mixer, at the conditions of 101 bar and 60 °C. It is observed that the experimental points, especially the raffinate's ethanol mass fraction, fit with the model well, which leads to the conclusion that in the range of total volume flow rate between 500 and 1500 mL/h equilibrium was always reached. It must be pointed out that in Figure 4.25, for the 90 wt.% feed composition, the raffinate phase fits very well with the model but the experimental results of the extract are slightly lower than the values predicted. The conclusion is that our model is less accurate for the prediction of the extract phase, as noted in *Section 4.1.2*, especially with feed solutions of high ethanol content.

Experimental data obtained with the HPIMM micro-mixer and the Tee-mixer are compared in Figure 4.26, showing the raffinate's and extract's ethanol mass fractions obtained for a feed composition of 50 wt.% of ethanol as a function of the total volume flow

rate. It is observed that results with the HPIMM micro-mixer and with the Tee-mixer fit the model well and moreover both present a similar behaviour in this range of total volume flow rate, between 500 and 1500 mL/h

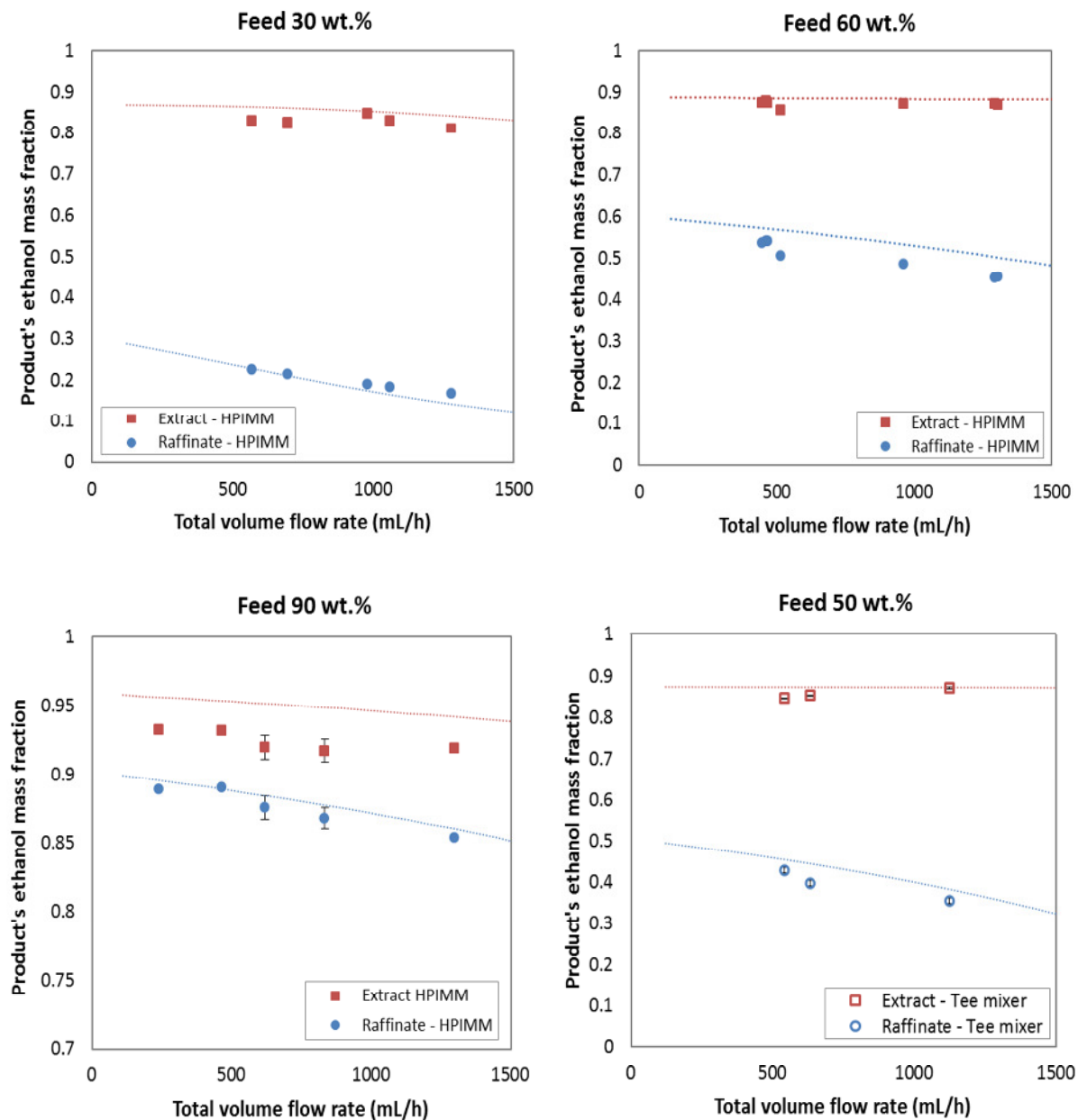


Figure 4.25. Product's ethanol mass fraction, raffinate (●, ○) and extract (■, □) and the prediction of a single theoretical stage model, as a function of the total volume flow rate in the micro-device (constant feed volume flow rate of 30 mL/h, variable CO<sub>2</sub> volume flow rate). Feed compositions are 30 wt.%, 60 wt.% and 90 wt.% (experiments with the HPIMM micro-mixer) and 50 wt.% (experiments with the Tee-mixer) of ethanol.

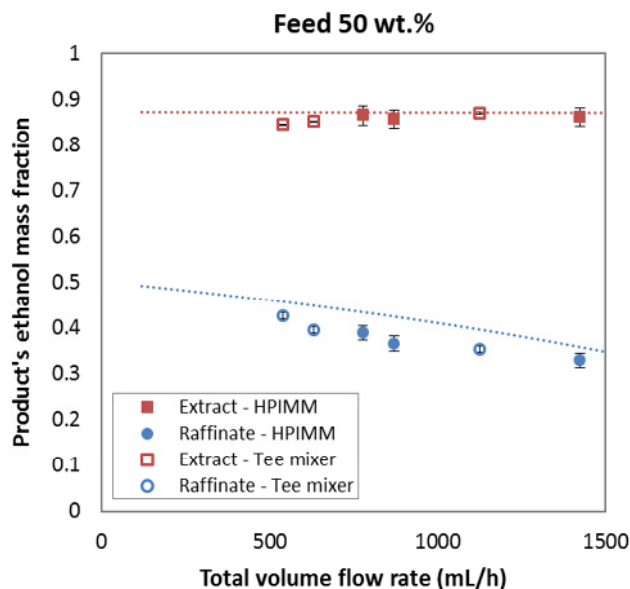


Figure 4.26. Comparison of both micro-mixers: product's ethanol mass fraction, raffinate (●, ○) and extract (■, □) and the prediction of a single theoretical stage model, as a function of the total volume flow rate in the micro-device (constant feed volume flow rate of 30 mL/h, variable CO<sub>2</sub> volume flow rate) for a feed composition of 50 wt.% ethanol.

#### 4.3.3. Influence of the Solvent-to-Feed ratio (S-to-F)

For the purpose of studying more in detail the influence of the ratio of solvent and feed, further experiments at different Solvent-to-Feed ratios were performed. Due to the flow rate limitation of the HPLC pump and the HPIMM micro-mixer (see *Sections 3.1.1* and *3.1.3*), both solvent and feed flow rates were varied in the experiments shown in this section in order to attain different Solvent- to-Feed ratios.

Figure 4.27 shows the raffinate's and extract's ethanol mass fractions as a function of the S-to-F ratios. The experiments with the HPIMM micro-mixer (right side in Figure 4.27) were focused on higher S-to-F ratios and lower flow rates: experiments were performed in a range of total volume flow rate of 500-980 mL/h. On the contrary, the experiments performed with the Tee-mixer were focused on lower values of S-to-F but higher flow rates, of a range of 600-1600 mL/h. In every case the experimental points, especially the raffinate's ethanol mass fraction, fit with the model well, which leads to conclude that the equilibrium was reached through the extraction process in the range of S-to-F values studied, with a maximum total volume flow rate of 980 mL/h and 1600 mL/h for the HPIMM micro-mixer and the Tee-mixer, respectively.

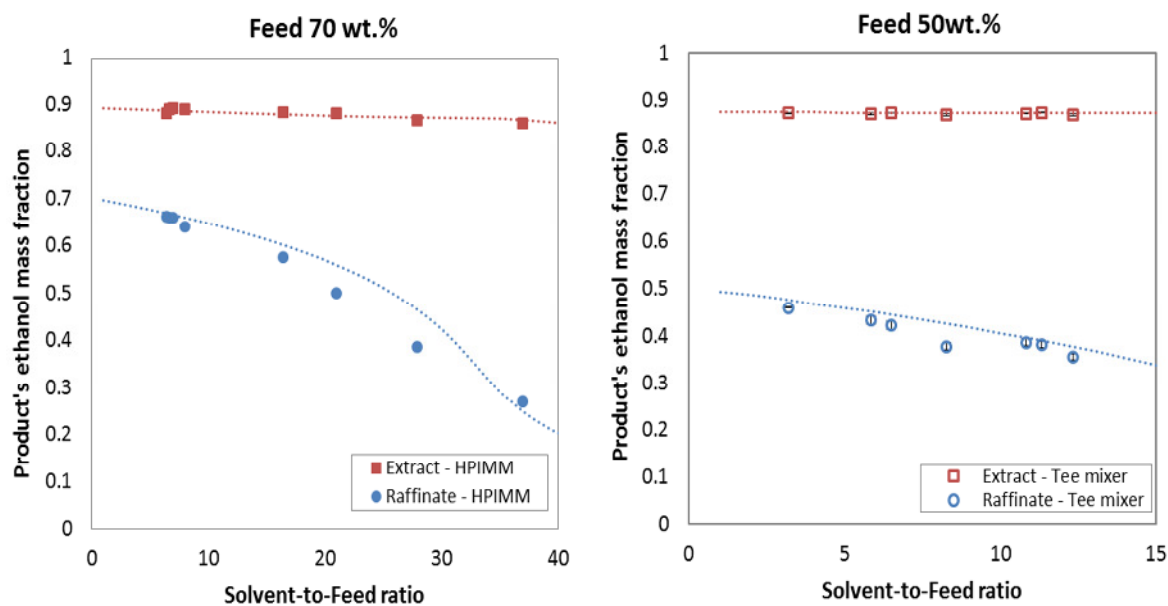


Figure 4.27. Product's ethanol mass fraction, raffinate (●, ○) and extract (■, □) and the prediction of a single theoretical stage model, as a function of the mass Solvent-to-Feed ratio (variable feed and CO<sub>2</sub> volume flow rates), for feed compositions of 70 wt.% (HPIMM micro-mixer) and 50 wt.% (Tee-mixer) of ethanol.

#### 4.3.4. Influence of the capillary length

As it can be expected from the remarkably small inner volume of the micro-mixers (see *Section 3.1.3*), the residence time in the contact zone, which comprises the micro-mixer and the capillary placed between the micro-mixer and the first separator (see Figure 4.28), is extremely short. In order to study how the capillary length influences the mixing and therefore the extraction process, the length of the capillary placed between the micro-mixer and the first separator was varied (all the results shown and explained above were obtained with a capillary length of 200 mm). As discussed by Jovanovic et al. (2012), the residence time in microsystems is usually changed by altering the flow rate. However, in multiphase systems (like the system studied here), variation of the flow rate to adjust the residence time can lead to changes of flow pattern. Thus, for the purpose of studying the influence of the residence time of solvent and feed mixture in the contact area (micro-mixer + capillary) without affecting the flow pattern, it was decided to change residence time by changing the capillary length at a constant flow rate. Therefore experiments with same volume flow rates (25 mL/min and 0.5 mL/min, for solvent and feed, respectively, except when otherwise noted) and same S-to-F ratios were performed using three different capillary lengths: 30 mm, 200 mm and 650 mm.

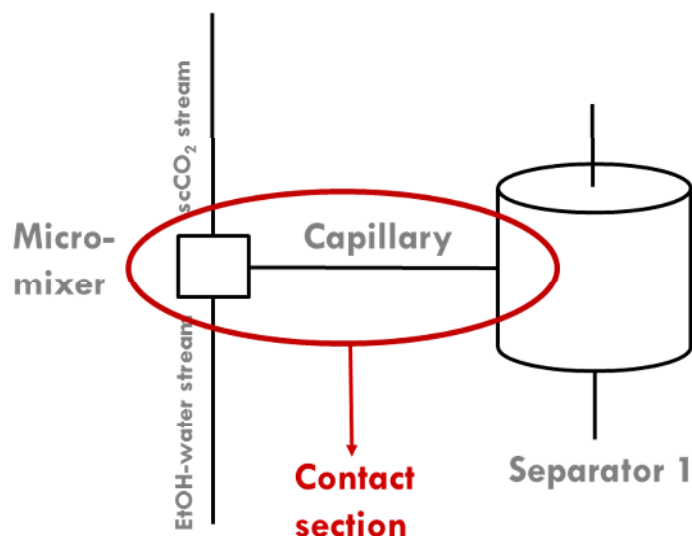


Figure 4.28. Schematic diagram of the contact section of the feed and the solvent in the high-pressure extraction apparatus. The contact section comprises the micro-mixer and the capillary.

Experiments with feed solutions of 10 wt.%, 50 wt.% and 90 wt.% ethanol were performed for a better comprehension of the influence of the capillary length on the mixing and extraction when having different physical properties of the liquid, such as density, viscosity or interfacial tension (see Sections 4.2.3 and 4.2.5).

The *K-factor* (Equation (4.27)) and the percentage of ethanol extracted (Equation (4.28)) were calculated in every case for a better comparison of the separation achieved. The *K-factor* is the quotient of the ethanol concentration in the extract and raffinate phases (CO<sub>2</sub>-free basis). The percentage of extracted ethanol is calculated as the amount of ethanol recovered in the extract in comparison with the amount of the ethanol in the feed. Obviously, the calculated percentage of extracted ethanol depends on the mass of extract recovered, which means that this value can be influenced by errors in the sampling. For the purpose of having a better notion of the accuracy of this value, the quotient of the mass of product (extract and raffinate) recovered and the mass of feed consumed was calculated for each experiment as percentage (Equation (4.29)) and represented together with the percentage of extracted ethanol in the Figures 4.29, 4.30 and 4.31. It is seen that this value was always around 90%.

$$K_{factor} = \frac{X_E}{X_R} \quad (4.27)$$

$$\text{Extracted ethanol (\%)} = \frac{m_{\text{EtOH extract}}}{m_{\text{EtOH feed}}} \cdot 100 \quad (4.28)$$

$$\text{Product recovered (\%)} = \frac{m_{\text{total raffinate}} + m_{\text{total extract}}}{m_{\text{total feed}}} \cdot 100 \quad (4.29)$$

In this series, experiments were run for 3 hours and extract and raffinate samples were taken every hour. The *K-factor* and the percentage of extracted ethanol were calculated for every hour of experiment (i.e. every time a sample was taken) and the average values with their corresponding standard deviation errors were calculated for each experiment. The results are shown in Figures 4.29-4.31. The dotted line in Figure 4.30 and 4.31 shows the *K-factor* value predicted by the model in ASPEN Plus®. However, this line is not shown in Figure 4.29 for a feed concentration of 10 wt.% ethanol, due to the lower accuracy of the model to predict the extract composition when a feed with low ethanol content is used (as commented in Section 4.1.2). The *K-factor* value predicted by the model for a feed solution of 10 wt.% ethanol and a S-to-F ratio of 13 was 17, which is very far from the experimental values. From Figures 4.29-4.31, it is concluded that the separation worsens slightly at longer residence times, i.e. with the larger capillary length, as the *K-factor* tends to decrease. It is observed that the equilibrium was only reached at short residence times (shorter than 200 ms). Regarding the extracted ethanol, we concluded that practically no great changes are found by increasing the residence time although it seems that it tends to slightly decrease at longer residence times. Moreover, the remarkably high standard deviation of the extraction efficiency with the lowest ethanol feed concentration (Figure 4.29) shows that, in this case, it takes some time to reach the equilibrium within the extraction process. It was found that still after one hour of experiment, the extracted ethanol was about 3-4% and the amount of extract was very small. During the experiment, the extracted ethanol per hour increased and reached the value of about 20% in the third hour of extraction. However, this behaviour was not observed when having an ethanol feed concentration of 50 wt.% and 90 wt.%. This shows that it takes longer to achieve the steady-state when the feed is 10 wt.% ethanol. This fact may be due to the high interfacial tension between the feed and the solvent in this case, which hinders the mixing. Furthermore, as concluded by Budich and Brunner (2003), the highest HETS calculated values were obtained with feed mixtures of low ethanol content (~ 10 wt.%). It is



also remarkable that, for a feed composition of 10 wt.% ethanol, the separation achieved by the Tee-mixer was better than by the HPIMM micro-mixer. However, in the experiments with a feed composition of 50 wt.% and 90 wt.% ethanol (Figures 4.30-4.31), the performance of both mixers was pretty similar, and no great differences could be recognized.

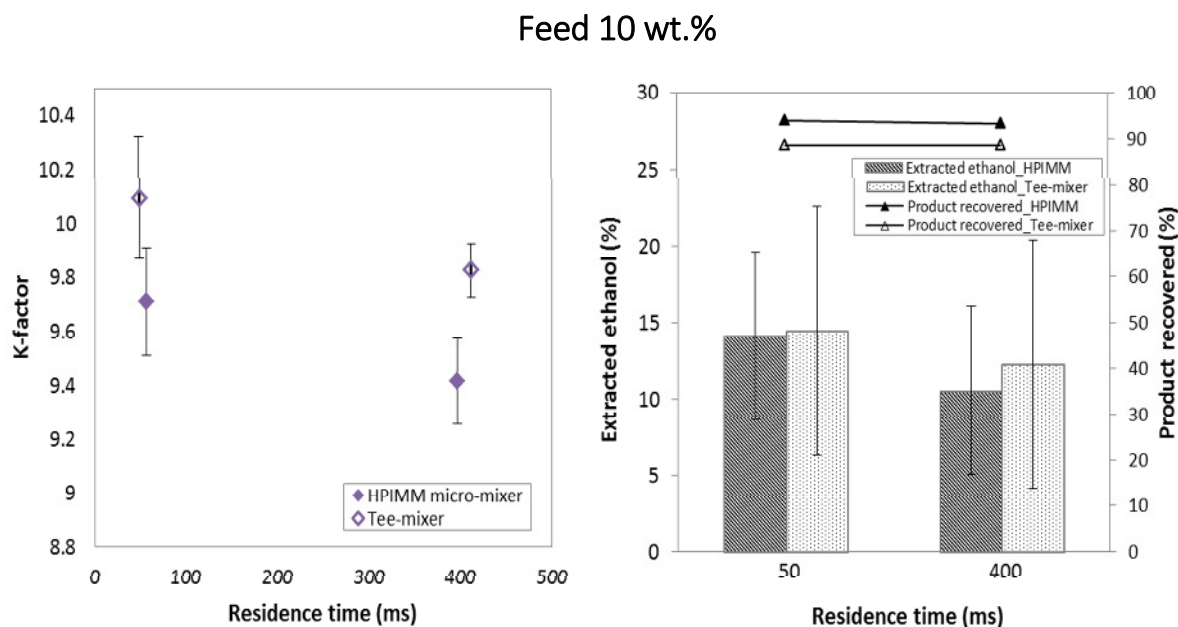


Figure 4.29. *K-factor* and extracted ethanol (%) as a function of the residence time for a feed composition of 10 wt.% of ethanol. S-to-F = 13; CO<sub>2</sub> flow rate = 20mL/min.

In summary, at first glance the results obtained indicate that the shorter the capillary, the better the separation at the experimental conditions considered here, which proves that the mixing effect inside the micro-mixer is good enough to reach equilibrium. These results can be explained by the fact that the mixing between the solvent and the feed occurs in the micro-mixer and, for this reason, even when the length of the capillary was extended and therefore the contact time was prolonged, the mixing would not be enhanced, as the structure or geometry of the capillary does not promote the mixing or “re-mixing” of the phases. Moreover, these results can confirm that one micro-mixer is equivalent to one theoretical extraction stage.

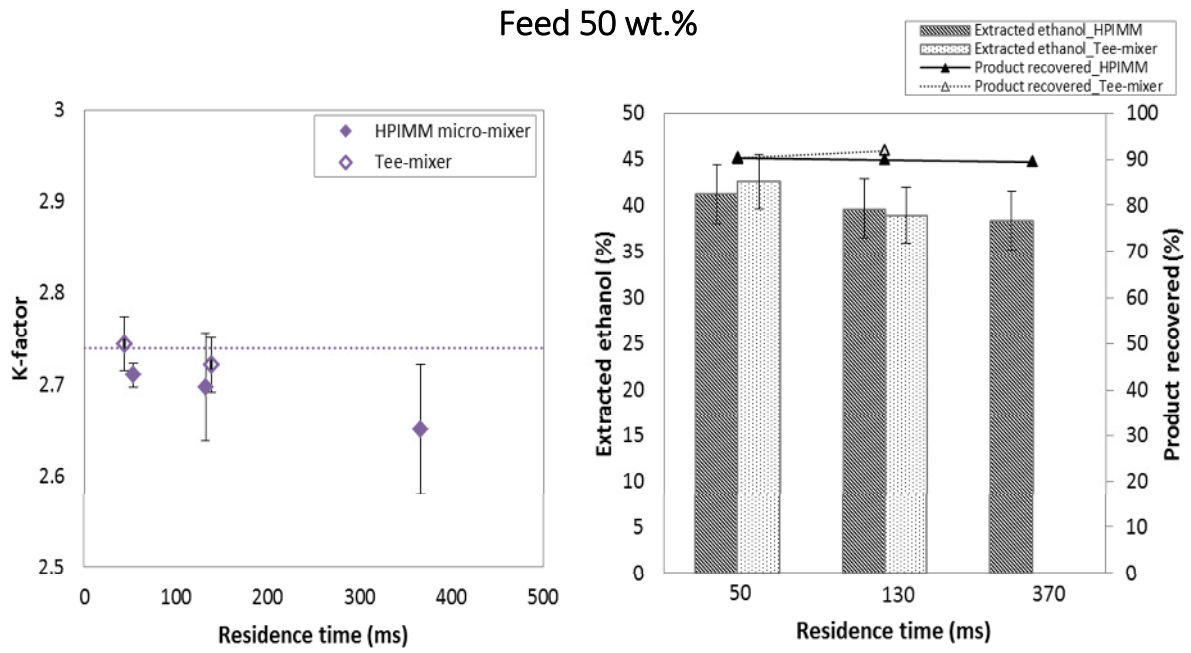


Figure 4.30. *K-factor* and ethanol extracted (%) as a function of the residence time for a feed composition of 50 wt.% ethanol. S-to-F = 16; CO<sub>2</sub> flow rate = 25mL/min.

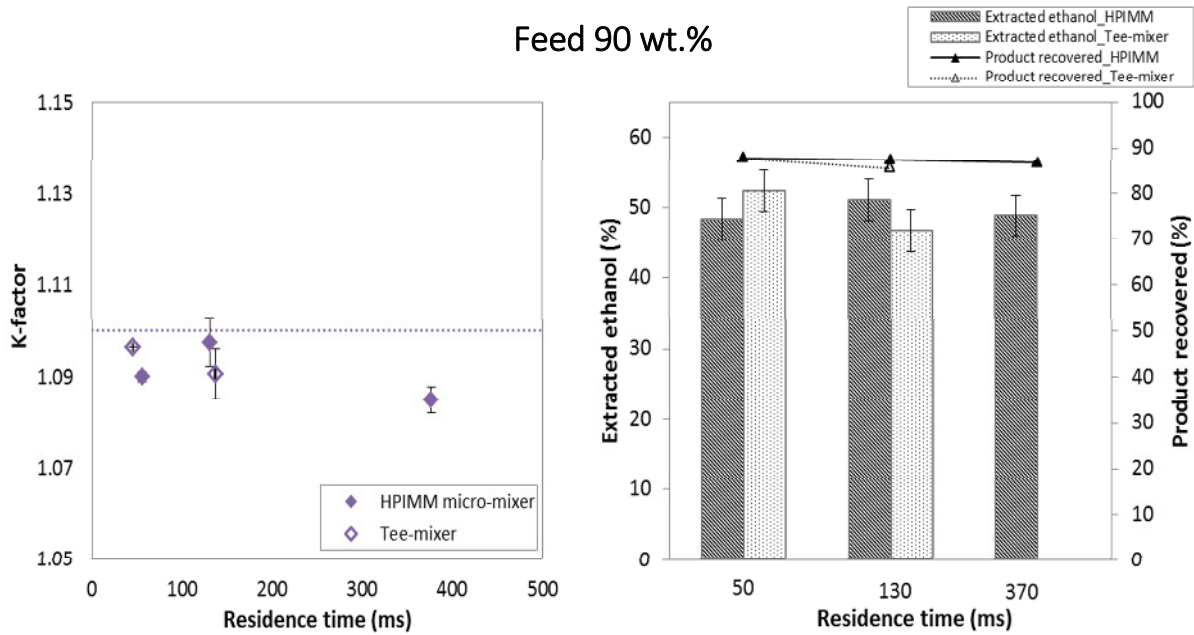


Figure 4.31. *K-factor* and ethanol extracted (%) as a function of the residence time for a feed composition of 90 wt.% of ethanol. S-to-F = 17; CO<sub>2</sub> flow rate = 25mL/min.

### 4.3.5. Influence of the overall volume flow rate

In the utilization of micro-mixers for liquid-liquid extraction, a high correlation between the total flow rate and the extraction efficiency has been found. For instance, Benz et al. (2001) evaluated the liquid-liquid extraction performance of micromixers and found the extraction efficiency to be a function of the volume flow rate. The authors studied the extraction of four different model systems for low and medium total volume flow rates of up to 1600 mL/h. Results showed better extraction efficiency at flow rates above 800 mL/h for two of the studied systems. The authors explained these results with the fact that the droplet diameter, as a measure of diffusional length, decreases with increasing flow rate. Furthermore, an increase in the flow rate also involves a drop of the residence time in the micro-mixer. Chasanis et al. (2010) stated that the superposition of these two effects (reduction of the droplet diameter and residence time) causes a minimum in the liquid-liquid extraction performance as a function of the total flow rate. Moreover, the variation of the flow rate can lead to changes in the flow pattern, as mentioned above (see *Section 4.3.4.*). Jovanovic et al. (2012) studied the liquid-liquid flow in a capillary micro-reactor and investigated the relation between the flow pattern in the capillary and the thermodynamic extraction efficiency. For the purpose of studying the relation between the extraction performance and the total flow rate in systems with a supercritical fluid as the solvent, experiments on the extraction of ethanol from aqueous solutions at different total volume flow rates but constant S-to-F ratio were performed. Once more, so as to study systems which considerably differ in the interfacial tension, three different feed solutions of 10 wt.%, 50 wt.% and 90 wt.% ethanol were used in these experiments.

In these series of experiments, the *K-factor* (Equation (4.27)) and the percentage of extracted ethanol (Equation (4.28)) were calculated in every case, unless otherwise indicated, for a better comparison of the separation achieved.

#### 4.3.5.1. Feed with 10 wt.% ethanol

Experiments on ethanol extraction from aqueous solutions with a content of 10 wt.% ethanol were performed at different total flow rates, keeping constant the S-to-F ratio. Due to the little amount of extract samples obtained during these experiments, especially in those with the lowest flow rates, the analysis of these samples was difficult and, in some cases, not

possible (see Section 3.3.1.3.). Therefore, the experimental results on the extract's mass fraction are not very accurate in this case. Figure 4.32 (A) shows the *K-factor* experimental results as a function of the total volume flow rate. It is observed that values notably differ from each other in a range between 8.8 and 10.8, with the clear tendency to decrease as the total volume flow rate increases. Besides, values of *K-factor* for the lowest flow rate investigated (390 mL/h) could not be calculated because extract's sample could not be analysed. This remarkable decrease in the *K-factor* when increasing the flow rate could be because of different reasons:

- (1) the total volume flow rate clearly influences the extraction performance;
- (2) experimental conditions were not reproducible enough, leading to large differences in the experimental results (in this point, the main parameter to bear in mind would be the CO<sub>2</sub> flow rate, as the HPLC pump could have had some technical problems to keep a constant flow rate, see Section 8.2);
- (3) the analysis of the extract's samples was not accurate enough, leading to small errors in the data of extract's mass fraction and therefore causing remarkable differences in the *K-factor* values calculated from these data.

In Figure 4.32 (B) the product's ethanol mass fraction as a function of the S-to-F ratio is represented for each experiment carried out in this series. In two cases, no extract's ethanol mass fraction is represented, as samples could not be analysed due to their small volume. In this figure, it is observed that the raffinate's ethanol mass fraction is practically the same in each experiment, whereas the extract's mass fraction values fluctuate in a range between 0.3 and 0.4 following no tendency with regard to the S-to-F ratio. Furthermore, no standard deviation is represented in the extract's mass fraction points, as only one sample was collected for each experiment, which could be analysed only once in most of the cases. Standard deviation values of raffinate's mass fraction data are represented, showing very small values. On the other hand, it is remarkable that, although the S-to-F ratio was not exactly the same in each experiment, the values were always in the range between 15 and 16. This means that this might not be the reason for having such as differing values of *K-factor* in the different experiments. Bearing all these facts in mind and with the purpose of having an appropriate comparison of the results of all the experiments carried out in this series with a feed of 10 wt.% ethanol, only the raffinate samples will be further used to compare and

discuss the extraction results. Furthermore, as the amount of extracted ethanol (in the extract) cannot be calculated by Equation (4.28), the percentage of ethanol removed from the feed was calculated instead, as indicated in Equation (4.30). This value highly depends on the amount of raffinate collected during the sampling. As explained in *Section 3.3.1.2*, although it was always tried to withdraw the total liquid amount from the separators, sometimes small amount of sample remained in the separators. The raffinate yield (Equation (4.31)), i.e. the amount of raffinate obtained in relation to the amount of feed consumed during the experiment, was therefore calculated and represented together with the percentage of removed ethanol to bear in mind this possible error caused by sampling (see Figure 4.33). With a feed solution of 10 wt.% ethanol, the ethanol content in the feed is low and thus the amount of collected extract in the second separator is very scarce, i.e. almost all the product obtained after the separation is raffinate. Therefore the values of raffinate yield obtained are around the 90%.

$$\text{Removed ethanol (\%)} = \frac{m_{\text{EtOH feed}} - m_{\text{EtOH raffinate}}}{m_{\text{EtOH feed}}} \cdot 100 \quad (4.30)$$

$$\text{Raffinate yield (\%)} = \frac{m_{\text{total raffinate}}}{m_{\text{total feed}}} \cdot 100 \quad (4.31)$$

In Figure 4.33.A, very tiny differences are observed in the raffinate's ethanol mass fraction as the flow rate increases. Here the dotted line represents the raffinate's ethanol mass fraction value in equilibrium, predicted by the model in ASPEN Plus®. It is seen that experimental values are closed to the predicted value but are slightly higher. However, due to the lower accuracy of the model in this range of feed ethanol content (as explained in *Section 4.1.2*), we concluded that experimental and predicted values are very similar. Therefore it was considered that equilibrium was achieved through the extraction process. Moreover, regarding the percentage of ethanol removed, small differences are observed but all the values are between 60 and 66%, which is a relatively small range. Summarising the results, at first glance it could be affirmed that the extraction performance seems to be highly influenced by the flow rate, as observed by comparing the *K-factor* values in Figure 4.32. However, a deeper evaluation and interpretation of the results led us to conclude that, with a feed solution of 10 wt.% ethanol, no remarkable differences are observed in the raffinate's

mass fraction as well as in the percentage of ethanol removed. Therefore, it was assumed that the extraction performance does not significantly vary at different flow rates up to 2000 mL/h.

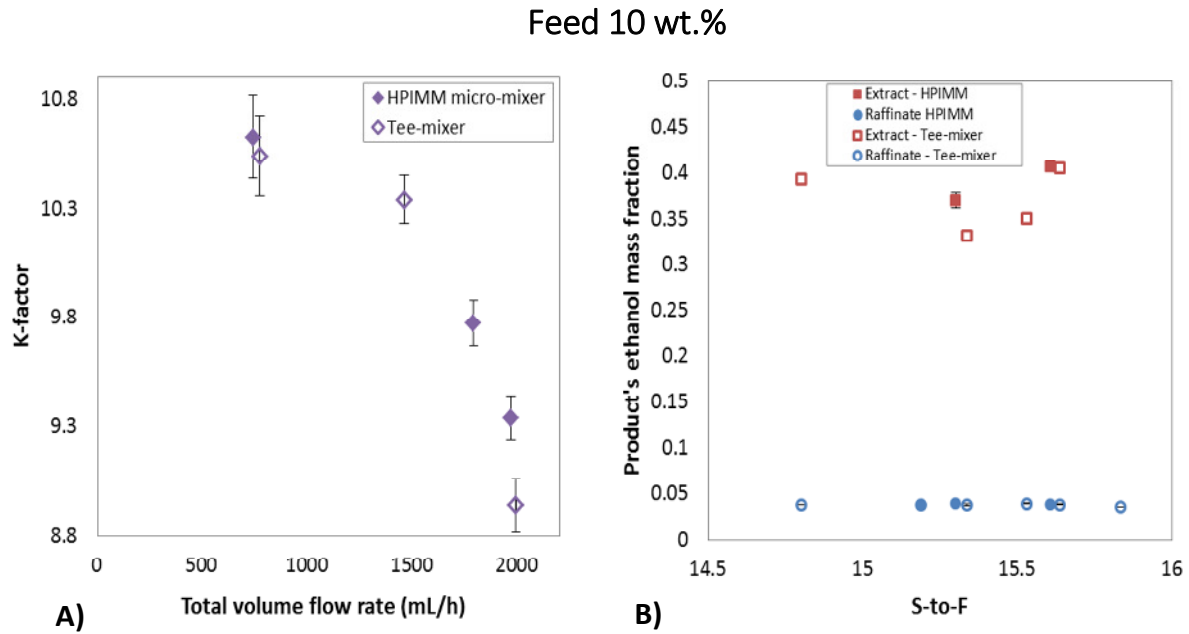


Figure 4.32. A) *K-factor* as a function of the total volume flow rate for a feed composition of 10 wt.% ethanol (left side). B) Product's ethanol mass fraction as a function of the S-to-F ratio for a feed composition of 10 wt.% ethanol (right side).

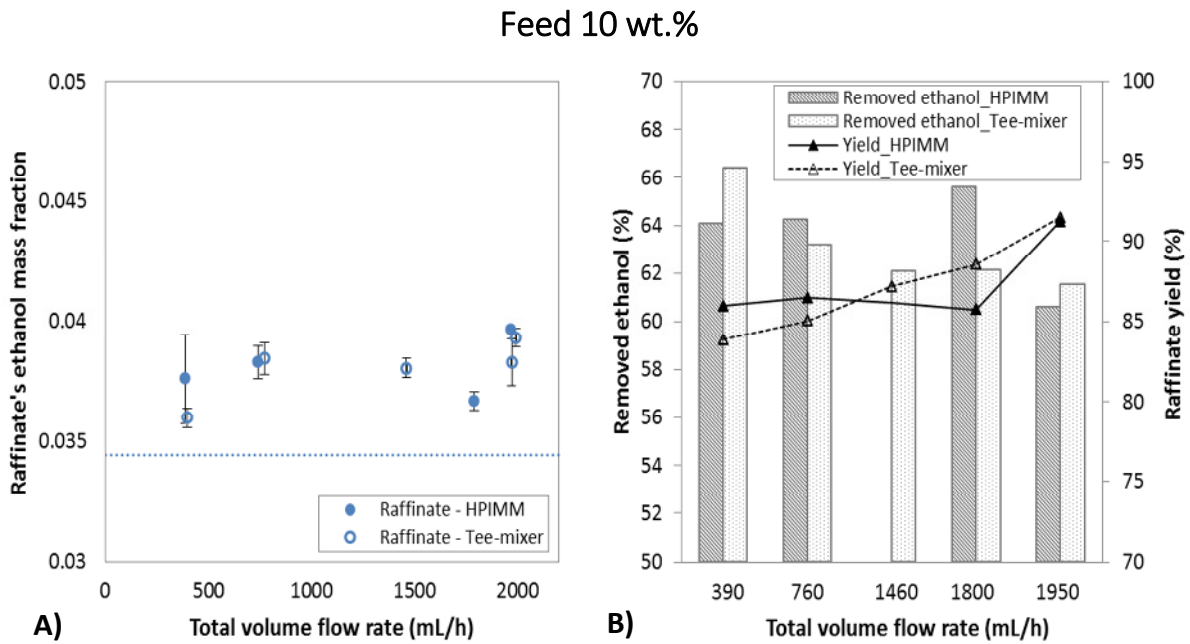


Figure 4.33. Raffinate's ethanol mass fraction (A) and removed ethanol (%) (B) as a function of the total volume flow rate for a feed composition of 10 wt.% ethanol.

#### 4.3.5.2. Feed with 50 wt.% ethanol

For the evaluation of these experimental results, with a feed of 50 wt.% ethanol, the *K-factor* (Equation (4.27)), the percentage of extracted ethanol (Equation (4.28)), and the product recovered (Equation (4.29)) were calculated and represented in Figure 4.34. As in the previous case (feed 10 wt.%), it is observed that the *K-factor* decreases as the total volume flow rate increases. In this case, the analysis of the samples did not pose a problem so the difference observed in the results might not be due to analysis nor sampling. Thus, the *K-factor* is represented as a function of the S-to-F ratio in Figure 4.35, to prove whether this variation of the *K-factor* could be caused by remarkable different S-to-F ratios (due to technical problems caused by the HPLC pump during the experiments). However, by carefully observing Figure 4.35, it is seen that even at the same S-to-F ratio (comparing, for instance, MMEFR1 to MMEFR2 and TEFR1 to TEFR3), higher values of *K-factor* were always obtained at the lowest flow rate studied here (~380 mL/h). It must be borne in mind that the *K-factor* values are in a range between 2.7 and 3. Considering the standard deviation, values are pretty similar. Nevertheless, it could be concluded that, with a feed of 50 wt.% ethanol content, the *K-factor* tends to decrease as the flow rate increases within the flow rate range studied here (between 380 and 2000 mL/h). Furthermore, if we focused on the Tee-mixer results in Figure 4.34. (A), it is observed that the *K-factor* decreases as the flow rates increases up to 1600 mL/h but then it tends to slightly increase again. This turning point might be the minimum to which Chasanis et al. (2010) referred as the result of the combination of the two effects of increasing the flow rate: drop of the residence time and decrease of the droplet diameter. For a better judgement, the *K-factor* is represented as a function of the residence time in the micro-mixer in Figure 4.36, in which it is observed that the two points at issue (encircled in red) present practically the same residence time in the Tee-mixer. On the other hand, this deviation in the *K-factor* from experiments TEFR3 and TEFR4 (i.e. with the two highest flow rates studied here) might be also due to the difference in the S-to-F ratio, as shown in Figure 4.35. Further study should be done at flow rates higher than 1500 mL/h for a better comprehension of the influence of the flow rate on the extraction performance in a Tee-mixer.

On the contrary, the HPIMM micro-mixer does not show a turning point but the *K-factor* seems to become constant at higher flow rates. This difference between the two mixers

might be due to the fact that we are already close to the maximum flow rate at which the HPIMM micro-mixer can operate (i.e. 2.5 L/h), whereas the Tee-mixer can still operate at much higher flow rates (we estimate that  $\sim 10$  L/h).

Moreover, it must also be pointed out that the experimental *K-factor* values at the lowest flow rate are slightly higher than the value predicted with the model (the dotted line in Figure 4.34 (A)). In this concentration range, our model presents a very accurate correlation to the VLE experimental data used for the calculation of the Peng Robinson parameters (see Section 4.1.2). Therefore, we attribute this deviation between our extraction experimental results and our model to some inaccuracy, not only in the model, but also in the experimental results used to calculate the model.

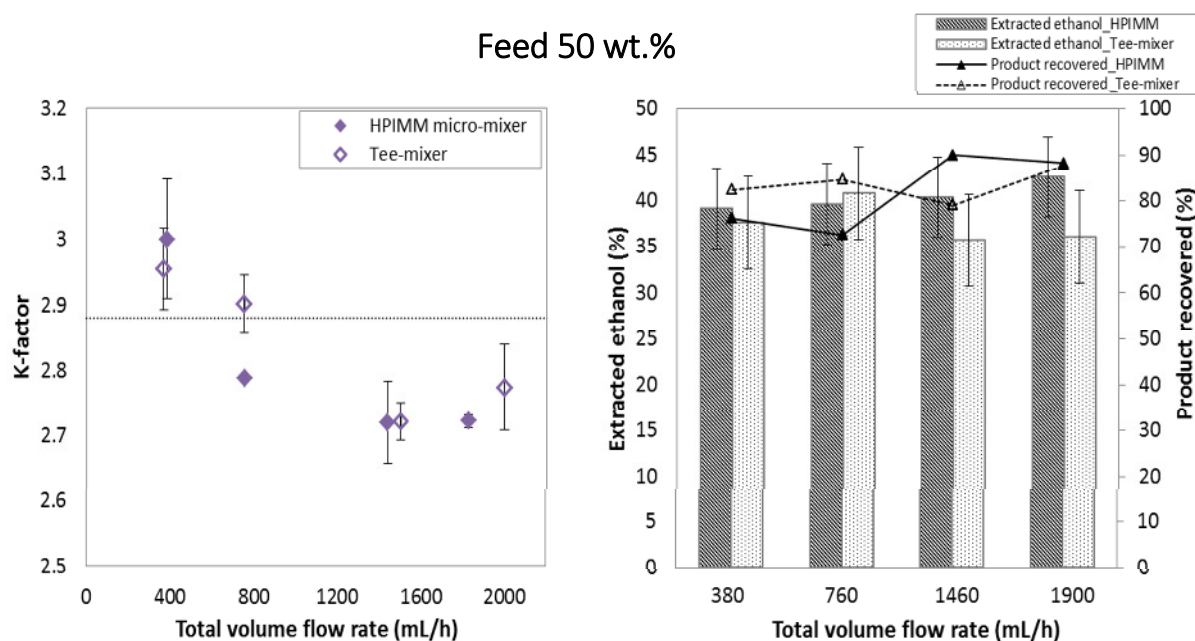


Figure 4.34. *K-factor* and extracted ethanol (%) as a function of the total volume flow rate for a feed composition of 50 wt.% of ethanol.



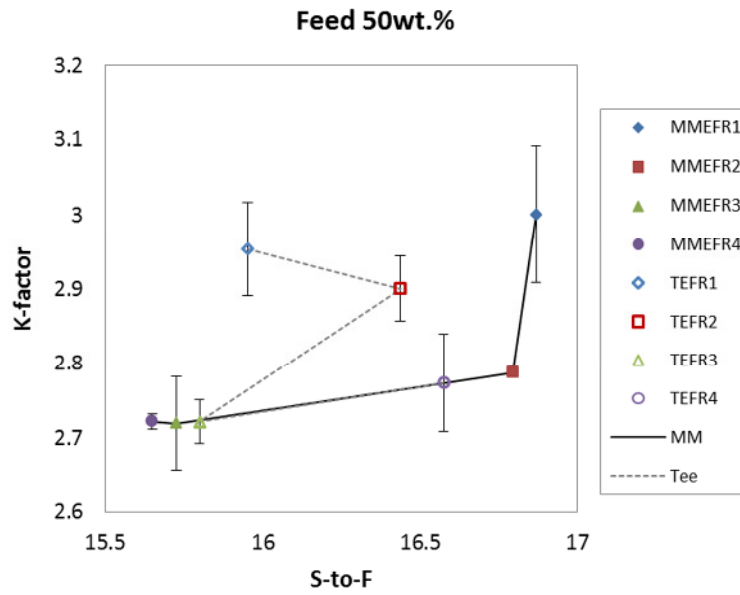


Figure 4.35. *K-factor* as a function of the S-to-F ratio for a feed composition of 50 wt.% ethanol. MME refers to HPIMM micro-mixer experiments, whereas TE refers to the experiments performed with the Tee-mixer. FR refers to the different flow rates studied, being 1 the lowest flow rate and 4 the highest one. The dotted line connects all the Tee-mixer experimental points, whereas the solid line connects the HPIMM micro-mixer experimental points.

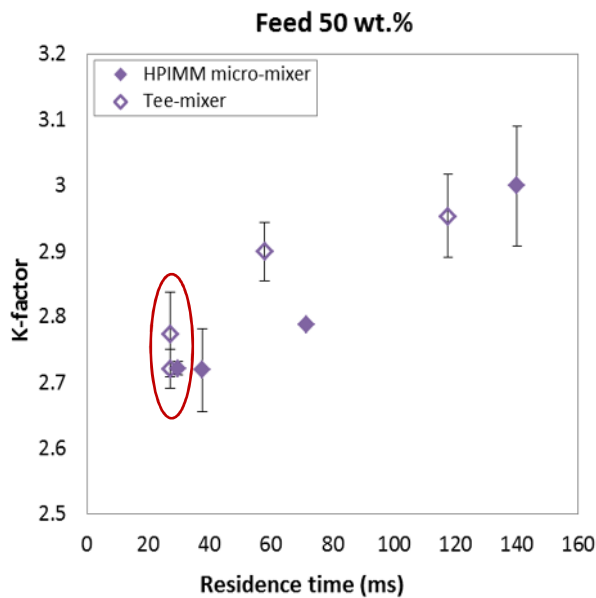


Figure 4.36. *K-factor* as a function of the residence time in the micro-mixer for a feed composition of 50 wt.% ethanol.

## 4.3.5.3. Feed with 90 wt.% ethanol

Lastly, the influence of the flow rate on the extraction performance was studied when using a feed of 90 wt.% ethanol. The *K-factor* and the percentage of ethanol extracted in every experiment are represented as a function of the flow rate in Figure 4.37. For a better evaluation of the results, the *K-factor* is represented as a function of the S-to-F ratio in Figure 4.38, in which it is seen that the S-to-F ratio was between 17 and 18 in practically every experiment. As it is shown in Figure 4.37 (A), all the *K-factor* results are in the narrow range between 1.09 and 1.11 so it is concluded that in this case, with a feed composition of 90 wt.% ethanol, the flow rate barely influences the extraction performance in a range between 360 – 1900 mL/h.

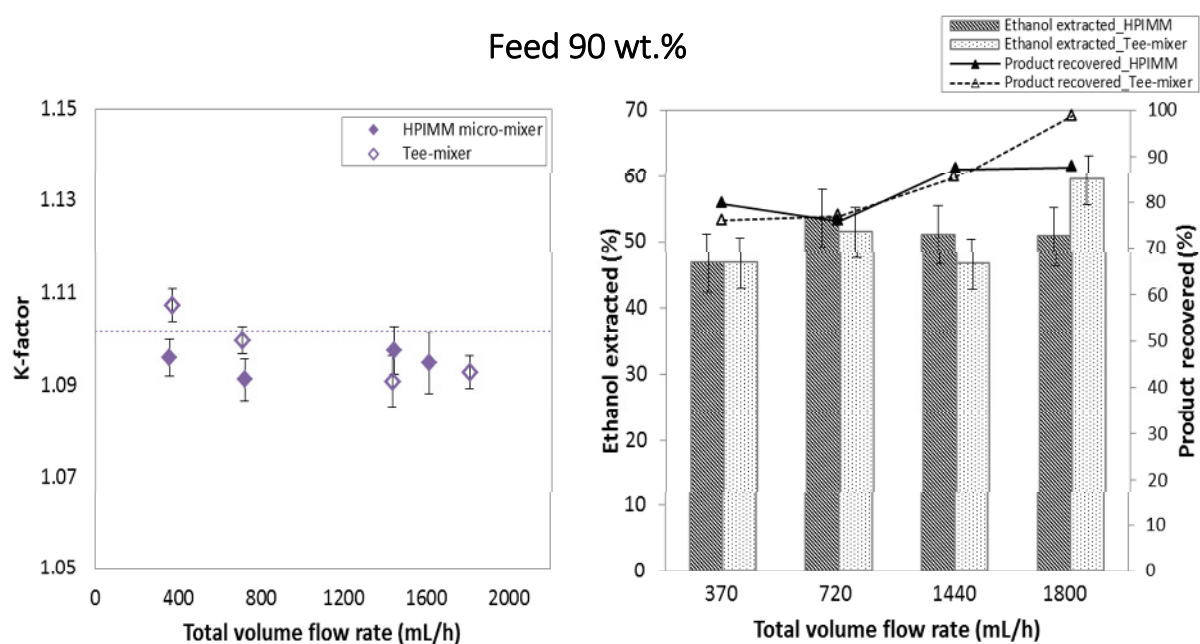


Figure 4.37. *K-factor* and extracted ethanol (%) as a function of the total volume flow rate for a feed composition of 90 wt.% of ethanol.

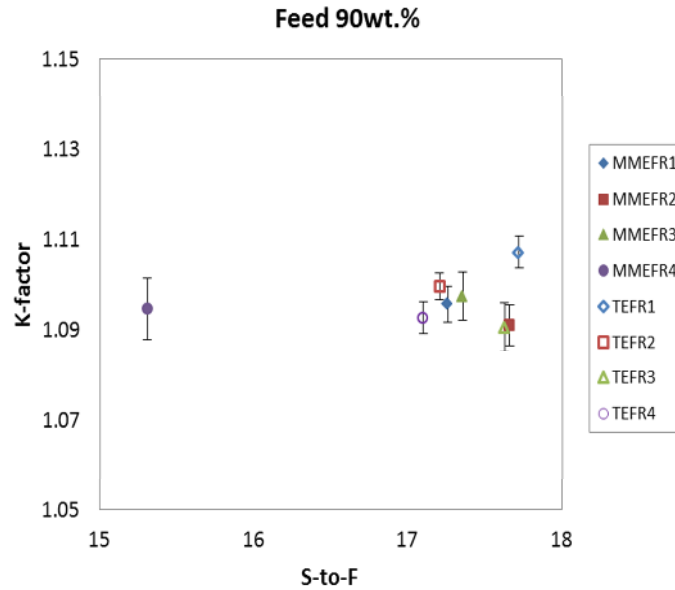


Figure 4.38. *K-factor* as a function of the S-to-F ratio for a feed composition of 90 wt.% ethanol. MME refers to HPIMM micro-mixer experiments, whereas TE refers to the experiments performed with the Tee. FR refers to the different flow rates studied, being 1 the lowest flow rate and 4 the highest one.

#### 4.4. Process design of a micro-mixer multi-stage extraction process and comparison with SFE in an extraction column

It has been previously mentioned in different sections that the main drawback of using micro-mixers or mixer-settlers for extraction purposes is the limitation to systems which require a relative small number of stages. In our experiments for the extraction of ethanol from aqueous solutions it was proven that one extraction stage can be reached in a micro-mixer. Based on this, extraction processes requiring more than one single stage could simply be designed as a number of micro-mixers (the same number as extraction stages are required) placed in series. The design of different multi-stage extraction cases was carried out here using ASPEN Plus®. The results were compared with experiments in an extraction column from literature (Pieck et al., 2015) as well as with simulations of an extraction column. Different factors such as feed concentration, the overall S-to-F ratio and the S-to-F ratio in each mixer were taken into account.

Pieck et al. (2015) carried out a multi-scale experimental study using the extraction of ethanol from ethanol-water mixtures by scCO<sub>2</sub> as the model system. The extraction conditions were the same as the conditions considered in our experiments: 101 bar and 60

°C. Moreover, the conditions chosen for the separation of the solvent and extract were also the same in both cases: 45 bar and 20 °C. The authors studied the extraction at laboratory scale, pilot scale and industrial scale, performing several experiments. In this work, only results at lab scale were considered. The column characteristics from Pieck et al. (2015) are shown in Table 4.13. The authors concluded that their experimental results are in good agreement with a single flash model, which means that not more than one single stage of extraction was achieved in the extraction columns. In this work, their experimental results were evaluated and compared with the results obtained in the ASPEN Plus® simulations with a mixer and 2 separators apparatus (see Figure 4.39) applying our thermodynamic model, in order to confirm the number of stages achieved in each column. The deviation between our calculated values and the experimental values from Pieck et al. (2015) was calculated according to Equation (4.32).

Table 4.13. Column characteristics from Pieck et al. (2015).

Scale	ID (mm)	Height (m)	Packing
Laboratory	19	2	VFF Interpack (10mm)

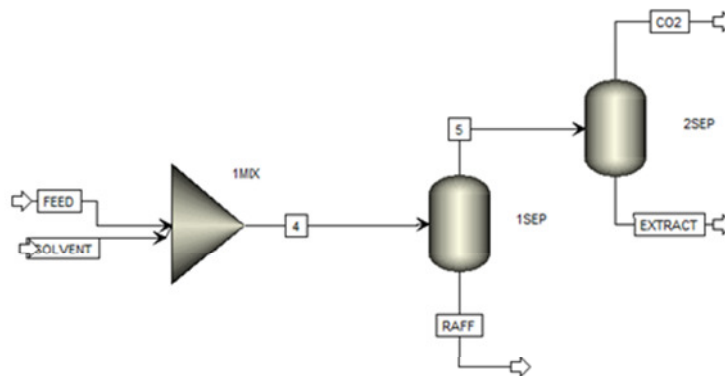


Figure 4.39. Mixer + 2 separators configuration in ASPEN Plus® used for the simulation of the experiments from Pieck et al. (2015).

As observed in Table 4.14, the highest deviations between the experimental results from Pieck et al. (2015) at lab scale and our calculations with the PR EoS model are found when the feed has a very low ethanol content (i.e. 10 wt.% ethanol). This is mainly attributed to the fact that the PR EoS model is less accurate in this feed concentration range. Besides that, the

experimental results at lab scale fit the thermodynamic calculations very well. This confirms that, as the authors stated, only one single stage of extraction was achieved in the experiments performed by Pieck et al. (2015).

Table 4.14. Comparison of experimental results from Pieck et al. (2015) with the PR EoS thermodynamic model.

Scale	Flow rate (kg/h)		S-to-F	Feed mass fraction	Extract mass fraction			Raffinate mass fraction		
	Solvent	Feed			Exp	Calc	Dev (%)	Exp	Calc	Dev (%)
Lab	6	0.237	25.3	0.1010	0.5301	0.3621	31.69	0.0437	0.0216	50.49
	6	0.295	25.1	0.1004	0.5294	0.4779	9.74	0.0430	0.0258	39.97
	12	0.589	20.4	0.1008	0.5704	0.4795	15.94	0.0417	0.0259	37.91
	9.6	0.576	16.7	0.2662	0.8075	0.8108	0.41	0.0934	0.0997	6.71
	12	0.573	20.9	0.2976	0.8080	0.8047	0.41	0.0996	0.0943	5.37
	6	1.097	5.5	0.4979	0.8640	0.8726	0.99	0.4464	0.4516	1.16
	12	0.164	73.2	0.5000	0.7455	0.6932	7.02	0.0436	0.0481	10.37
	12	0.526	22.8	0.6659	0.8812	0.8730	0.93	0.4100	0.4819	17.54
	12	1.043	11.5	0.6940	0.8842	0.8825	0.19	0.6054	0.6312	4.26
	12	0.493	24.3	0.8837	0.9300	0.9220	0.86	0.7587	0.8073	6.41

$$Deviation (\%) = \left| \frac{x_{calc} - x_{exp}}{x_{exp}} \right| \cdot 100 \quad (4.32)$$

Furthermore, different simulations were performed for the study and comparison of a multi-stage SFE process using either an extraction column or a multi-stage mixers configuration. The simulations were carried out using ASPEN Plus® and the PR EoS model described in Section 4.1.2. Figures 4.40 and 4.41 show the schematic diagram of both simulations: the extraction column and the mixers+separators configuration, respectively. The separation step (i.e. separation of the solvent and extract) was fixed at the conditions of 45 bar and 20 °C for in both cases. Therefore, this step was not taken into account in the comparison, as the main purpose here was just to compare the extraction step in the column with the extraction in a multi-mixer configuration.

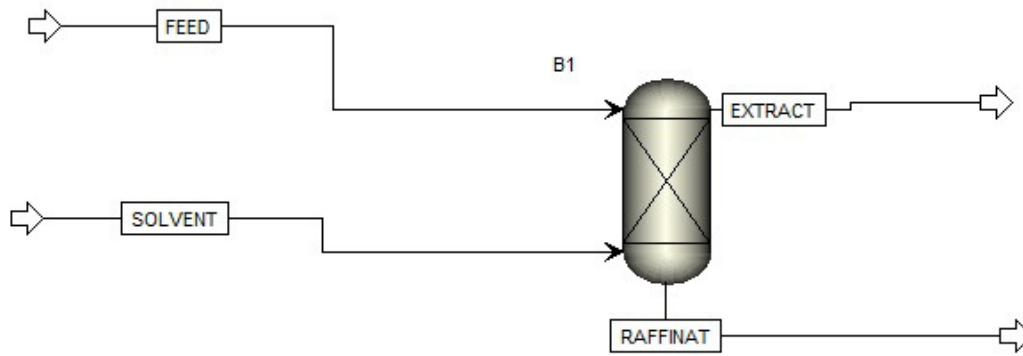


Figure 4.40. Schematic diagram of the extraction column in ASPEN Plus®.

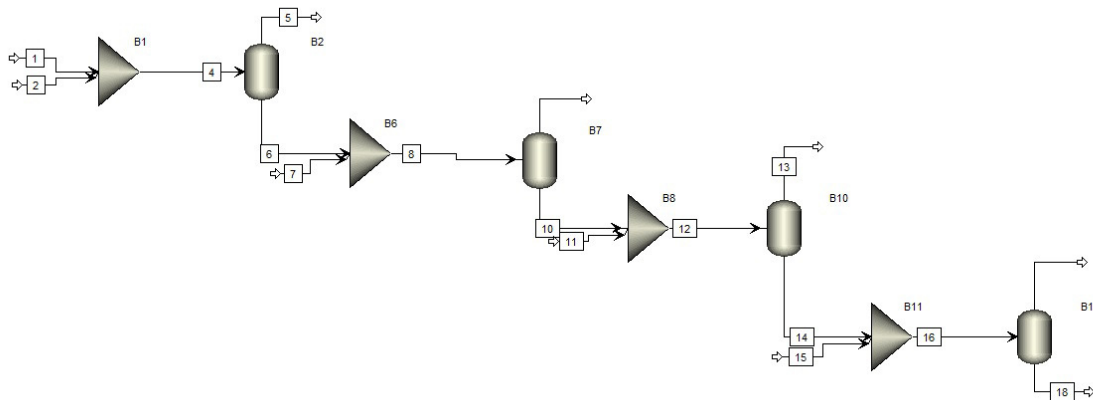


Figure 4.41. Schematic diagram of the multi-stage mixers+separators configuration for SFE in ASPEN Plus®.

Three different feed concentrations were again considered in these simulations: 10, 50 and 90 wt.% ethanol. The feed mass flow rate for every single simulation presented here was 0.25 kg/h. For the extraction column simulations the S-to-F ratio was always 20. Thus the solvent flow rate in the column simulations was always 5 kg/h. For the simulations of the mixers configuration, different cases were considered, as following explained:

- Case A: same solvent flow rate in every mixer, equal to 5 kg/h.
- Case B: same S-to-F ratio in every mixer, equal to 20.
- Case C: overall S-to-F ratio of the process equal to 20.

Table 4.15. CO<sub>2</sub>-free basis results of the different simulation cases with the multi-mixer configuration and a feed concentration of 10 wt.% ethanol.

Simulations	Stage	Raffinate's EtOH mass fraction	Extract's EtOH mass fraction	Solvent flow rate (kg/h)	S-to-F ratio
Case A	1	0.0261	0.6374	5	20
	2	0.0057	0.2965	5	32.8
	3	0.0012	0.0807	5	24.5
	4	0.0002	0.0168	5	25.9
	<b>Overall</b>	<b>0.0002</b>	<b>0.3657</b>	<b>20</b>	<b>80</b>
Case B	1	0.0261	0.6374	5	20
	2	0.0063	0.3175	4.4	20
	3	0.0015	0.1020	4.1	20
	4	0.00036	0.0265	3.9	20
	<b>Overall</b>	<b>0.00036</b>	<b>0.3976</b>	<b>17.4</b>	<b>67.7</b>
Case C	1	0.0627	0.7842	1.25	5
	2	0.0366	0.7025	1.25	5.3
	3	0.0203	0.5841	1.25	5.5
	4	0.0109	0.4399	1.25	5.7
	<b>Overall</b>	<b>0.0109</b>	<b>0.6728</b>	<b>5</b>	<b>20</b>

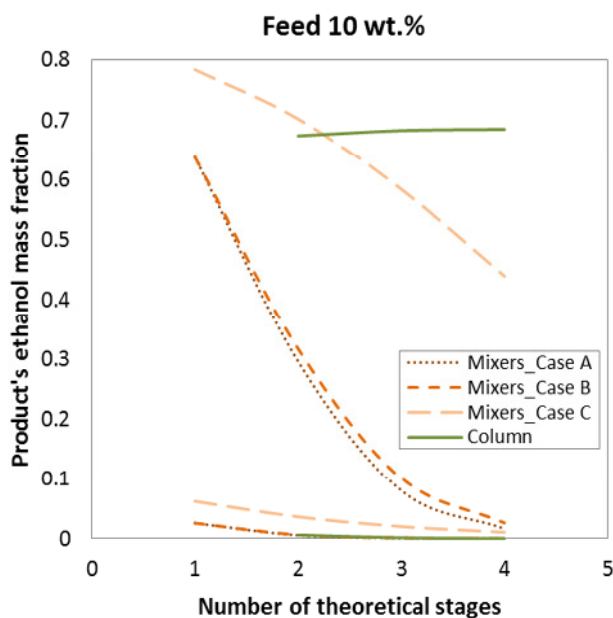


Figure 4.42. Prediction of the extract's and raffinate's ethanol mass fraction as a function of the number of theoretical stages considered in the simulations with a feed concentration of 10 wt.% ethanol.

Table 4.16. CO<sub>2</sub>-free basis results of the extraction column simulations with a feed concentration of 10 wt.% ethanol.

Column	Raffinate's EtOH mass fraction	Extract's EtOH mass fraction
2-stages column	0.0062	0.6745
3-stages column	0.0016	0.6832
4-stages column	0.0004	0.6853

The simulation results for feed concentration of 10 wt.% ethanol are shown in Tables 4.15 and 4.16. The results of the extraction column simulations are compared with the different multi-mixer configuration cases in Figure 4.42. In Table 4.15, the results of each extraction stage are shown. The values given are the raffinate's and extract's ethanol mass fraction after each mixer stage. Besides, the raffinate's and extract's concentration of the entire extraction process as well as the S-to-F ratio are also given, named *overall*. The overall raffinate's ethanol mass fraction is the final concentration of the raffinate after the last stage of extraction; whereas the overall extract's ethanol mass fraction is calculated according to Equation (4.33), considering the mass of extract and the extract's ethanol mass at each extraction stage.

$$\text{Overall extract's EtOH mass fraction} = \frac{\sum_i^n (m_{total\ extract} \cdot X_E)}{\sum_i^n m_{total\ extract}} \quad (4.33)$$

The results of the simulations performed with a feed concentration of 50 wt.% ethanol are shown in Tables 4.17 and 4.18. Figure 4.43 compares the extraction column results with the different multi-mixer configuration cases. As in Table 4.15, the results of each extraction stage (of a total of 4 stages) are also given in Table 4.17.



Table 4.17. CO<sub>2</sub>-free basis results of the different simulation cases with the multi-mixer configuration and a feed concentration of 50 wt.% ethanol.

Simulations	Stage	Raffinate's EtOH mass fraction	Extract's EtOH mass fraction	Solvent flow rate (kg/h)	S-to-F
Case A	1	0.2691	0.8794	5	20
	2	0.0502	0.7563	5	32.8
	3	0.0061	0.3089	5	46.6
	4	0.0006	0.0451	5	54.5
	<b>Overall</b>	<b>0.0006</b>	<b>0.7360</b>	<b>20</b>	<b>80</b>
Case B	1	0.2591	0.8794	5	20
	2	0.0808	0.8130	3.1	20
	3	0.0206	0.5876	2.3	20
	4	0.0049	0.2694	2.1	20
	<b>Overall</b>	<b>0.0049</b>	<b>0.8153</b>	<b>12.4</b>	<b>49.8</b>
Case C	1	0.4584	0.8832	1.25	5
	2	0.4050	0.8828	1.25	5.7
	3	0.3367	0.8823	1.25	6.4
	4	0.2495	0.8787	1.25	7.2
	<b>Overall</b>	<b>0.2495</b>	<b>0.8818</b>	<b>5</b>	<b>20</b>

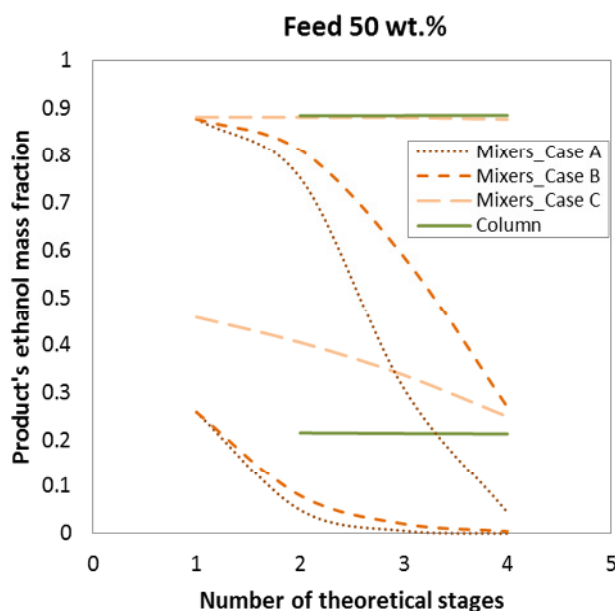


Figure 4.43. Prediction of the extract's and raffinate's ethanol mass fraction as a function of the number of theoretical stages considered in the simulations with a the feed concentration of 50 wt.% ethanol.

Table 4.18. CO<sub>2</sub>-free basis results of the extraction column simulations with a feed concentration of 50 wt.% ethanol.

Column	Raffinate's EtOH mass fraction	Extract's EtOH mass fraction
2-stages column	0.2155	0.8764
3-stages column	0.2143	0.8756
4-stages column	0.2135	0.8754

Likewise, the same simulations were carried out considering a feed solution of 90 wt.% ethanol. The results of the simulations are shown in Tables 4.19 and 4.20. Furthermore, Figure 4.44 compares the extraction column results with the different multi-mixer configuration cases. In Table 4.19, only two stages were considered for the case A. The reason of this is that the amount of raffinate after the second stage of extraction was so low (0.00745 kg/h) that no further extraction was possible.

Table 4.19. CO<sub>2</sub>-free basis results of the different simulation cases with the multi-mixer configuration and a feed concentration of 90 wt.% ethanol.

Simulations	Stage	Raffinate's EtOH mass fraction	Extract's EtOH mass fraction	Solvent flow rate (kg/h)	S-to-F
Case A	1	0.8471	0.9407	5	20
	2	0.3634	0.8827	5	46.6
	3	-	-	-	-
	4	-	-	-	-
	<b>Overall</b>	<b>0.3634</b>	<b>0.9165</b>	<b>10</b>	<b>40</b>
Case B	1	0.8471	0.9407	5	20
	2	0.7749	0.9177	2.2	20
	3	0.6758	0.8974	1.1	20
	4	0.5301	0.7503	0.6	20
	<b>Overall</b>	<b>0.5301</b>	<b>0.9300</b>	<b>12.4</b>	<b>49.8</b>
Case C	1	0.8907	0.9571	1.25	5
	2	0.8770	0.9518	1.25	6.5
	3	0.8584	0.9448	1.25	7.8
	4	0.8318	0.9354	1.25	9.7
	<b>Overall</b>	<b>0.8318</b>	<b>0.9473</b>	<b>5</b>	<b>20</b>

Table 4.20. CO<sub>2</sub>-free basis results of the extraction column simulations with a feed concentration of 90 wt.% ethanol.

Column	Raffinate's EtOH mass fraction	Extract's EtOH mass fraction
2-stages column	0.8095	0.9536
3-stages column	0.7918	0.9585
4-stages column	0.7842	0.9603

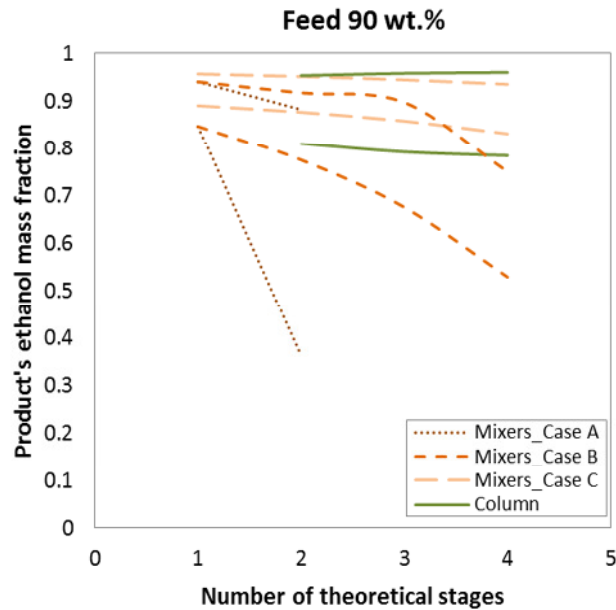


Figure 4.44. Prediction of the extract's and raffinate's ethanol mass fraction as a function of the number of theoretical stages considered in the simulations with a feed concentration of 90 wt.% ethanol.

A careful observation and comparison of the simulation results for the different feed concentrations shows that, in the multi-mixer configuration simulations, the case C is the most similar to the extraction column simulations, as the overall S-to-F ratio is the same in both processes (S-to-F ratio = 20). Very similar extraction results could be obtained with both, the extraction column and the multi-mixer configuration. However, the multi-mixer configuration gives a larger variety of options in the design of the extraction process. This means that, depending on the main purpose of the extraction process (e.g. the purification of a component in the extract, the removal of a component from the raffinate, etc.), the solvent flow rate in each stage can be varied and adjusted for a better and more precise design of the extraction process in order to achieve the desired concentrations on the easiest way or the fewest number of extraction stages. Moreover, the multi-mixer configuration arrangement

can be easily modified in accordance with the process demands. The main advantage of the multi-mixer configuration for extraction purposes over the extraction column is that it offers the possibility to adjust more parameters for a better, more optimized extraction process.

## 5. SFE of free fatty acids from olive oil

The feasibility of micro-mixers for the SFE of ethanol from aqueous solutions with scCO<sub>2</sub> was proved in *Chapter 4*. Nevertheless, for a better comprehension and knowledge of the applicability and efficiency of micro-mixers in SFE and SFF processes, a further in-depth study was necessary. Therefore, it was decided to investigate a second extraction system. After a literature review on SFE and SFF of liquids, the extraction of free fatty acids (FFA) from olive oil was chosen as the second system to test in our high pressure micro-device apparatus for SFE. Among many reasons, this system was chosen over the others because of the relatively extensive data available in literature and, moreover, because the olive oil presents physical properties very different from the properties of the ethanol-water mixtures, especially different viscosity, which will be discussed in *Section 5.2*. On top of this, the experimental conditions chosen for the extraction of FFA from olive oil are different from the experimental conditions for the separation of ethanol-water mixtures, which means that the density and viscosity of scCO<sub>2</sub> also change (discussion in *Section 5.2.1*). The main purpose was to study the use of micro-mixers for SFE under different fluid dynamic and hydrodynamic conditions and to verify whether equilibrium can also be reached for this different system. Therefore, the phase behaviour of CO<sub>2</sub> + olive oil as well as the fluid properties such as density, viscosity, interfacial tension and diffusion coefficient was studied in detail, and explained below. In this chapter, when comparing both extraction systems, system A will refer to the extraction of ethanol from aqueous solutions, whereas system B will allude to the extraction of FFA from olive oil, as noted in Table 3.1 (in *Chapter 3*).

### 5.1. Phase behaviour

The phase behaviour of vegetable oils and CO<sub>2</sub> at supercritical conditions has been extensively studied in the last years for different applications: deacidification of oils or extraction of minor components such as sterols, tocopherols, squalene, etc. This study was focused only on the deacidification of olive oil, i.e. the extraction of FFA from olive oil.

The measurement and modelling of the phase behaviour of olive oil and scCO<sub>2</sub> has been carried out by different authors in the last years (Bharath et al., 1992; Simões and Brunner, 1996; Gracia et al., 2009; Vázquez et al., 2009; Fernández-Ronco et al., 2010). Most of these

authors considered the olive oil as a simple pseudo-binary oleic acid-triolein mixture. As explained by Lozano Sánchez et al. (2009), olive oil consists of two different fractions:

- (1) the saponifiable fraction, which is composed of saturated and unsaturated fatty acids, mostly esterified forming triglycerides; to a much lesser extent, diglycerides and monoglycerides, and free fatty acids are also found.
- (2) the unsaponifiable fraction, which comprises minor compounds such as polyphenols, tocopherols, sterols, volatile compounds and pigments.

Moreover, the composition of the olive oil differs pretty much depending on the production area. The main factors which affect the fatty acids composition of the olive oil are: the latitude, the weather conditions, and the variety and degree of ripeness of the olives. Table 5.1 shows the olive oil fatty acids content according to the IOC (International Olive Council), where it is observed that oleic acid is the major component of the olive oil. In order to simplify, the olive oil was assumed to be an oleic acid-triolein pseudo-binary system in this work.

**Table 5.1. Limit fatty acids content in olive oil according to IOC.**

Fatty acid	Concentration (g per 100 g of total fatty acids)
Oleic acid (C18:1)	55 – 83
Linoleic acid (C18:2)	3.5 – 21
Palmitic acid (C16:0)	7.5 – 20
Stearic acid (C18:0)	0.5 – 5
Palmitoleic acid (C16:1)	0.3 – 3.5
Linoleic acid (C18:3)	0.0 - 1.5

Bharath et al. (1992) measured the phase equilibria of the binary systems carbon dioxide-oleic acid and carbon dioxide-triolein, and of the ternary system carbon dioxide-oleic acid-triolein, for the separation and fractionation of fatty oil components by scCO<sub>2</sub>. They concluded that the distribution coefficient (*K-factor*) of both oleic acid and triolein varies not only with the pressure but also with the feed composition. They found that an increase in the pressure results in a higher distribution coefficient of both oleic acid and triolein, and that the *K-factor* value of the oleic acid is ten times larger than that of triolein. This indicates that oleic acid is selectively soluble in scCO<sub>2</sub>. Their experimental results on the ternary system are shown in Figure 5.1.

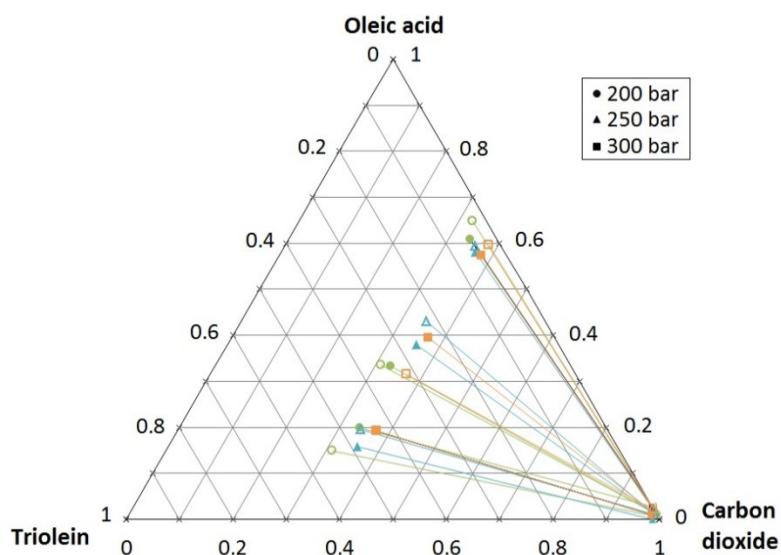


Figure 5.1. Vapour-liquid equilibria for the CO<sub>2</sub>-oleic acid-triolein system. Filled symbols (●, ■, ▲): T = 40 °C. Hollow symbols (○, □, △): T = 60 °C (data from Bharath et al., 1992).

Simões and Brunner (1996) studied the phase equilibria of an extra virgin olive oil in scCO<sub>2</sub> at temperatures between 40 and 80 °C and pressures up to 300 bar. The olive oil had a content of about 0.7 wt.% squalene, therefore they considered the multicomponent system FFA + triglycerides + squalene + CO<sub>2</sub>. The authors concluded that the multicomponent phase equilibria of olive oil in scCO<sub>2</sub> show a high selectivity of the CO<sub>2</sub> towards squalene and FFA in the studied range. Only at 80 °C the solvent was preferentially selective to the free fatty acids, as seen in Figure 5.2 from Simões and Brunner (1996). Moreover, they used the measured phase equilibria data to model the deacidification of olive oil in a counter-current packed column. The simulation results showed an increase of the extraction yield with the density of the CO<sub>2</sub>. At a constant density, the extraction yield was higher at high temperatures. Moreover, they observed that higher solvent-to-feed ratios (S-to-F) improved the extraction yield, resulting in lower raffinate acidities.

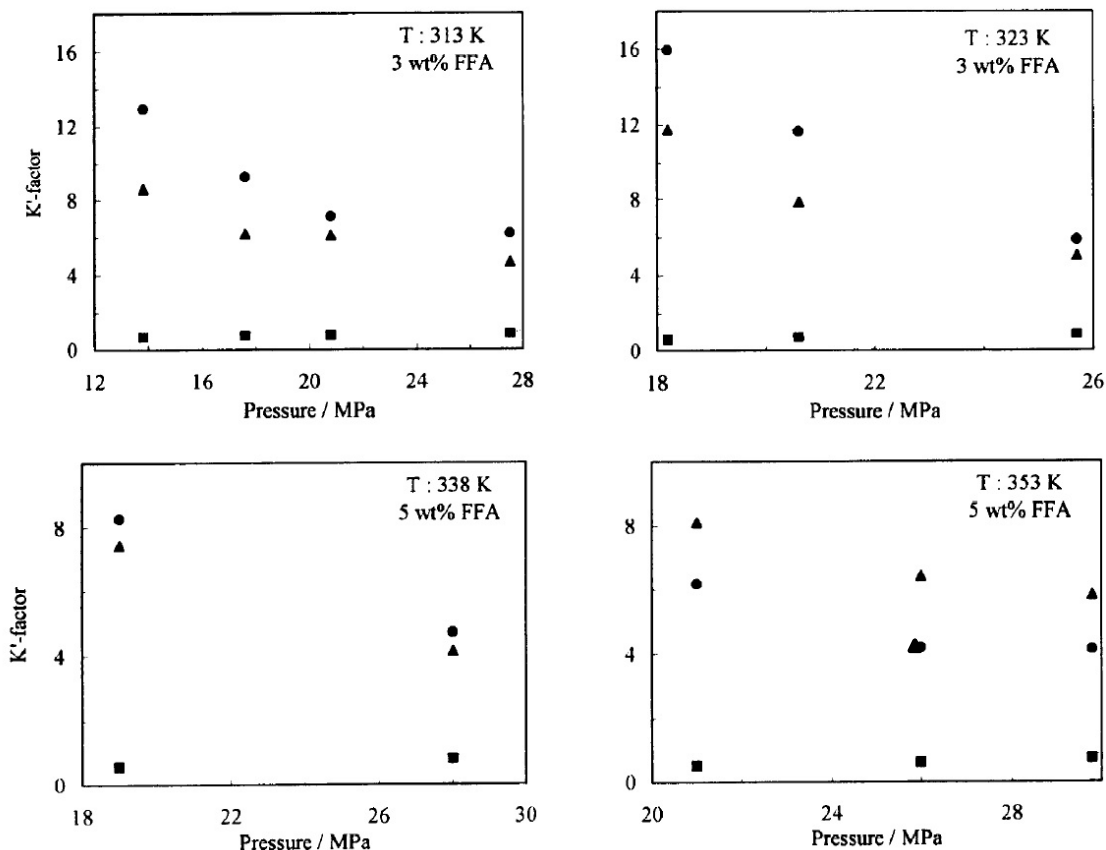


Figure 5.2. K-factor (on a solvent-free basis) of the pseudo components of olive oil as a function of the pressure and temperature at two different initial FFA contents. (▲) FFA, (■) triglycerides, and (●) squalene. Source: Simões and Brunner (1996).

On the other hand, Bondioli et al. (1992) used a scCO<sub>2</sub> counter-current extraction plant to refine lampante olive oil and studied the influence of different parameters such as pressure, temperature and solvent-to-feed ratios on the refining process. For the study of the temperature influence, they considered two different temperature conditions: 40 and 60 °C, and concluded that an increase of 20 °C seriously compromised the outcome of the process. At 60 °C and 130 bar, the FFA in refined oil was much higher (4.11 wt.%) than when carrying out the extraction at 40 °C and same pressure (0.70 wt.%). The authors pointed out that the decrease in the scCO<sub>2</sub> density due to the temperature increase could have been avoided by increasing also the pressure, but that would not be economical.

Taking into account all the factors explained above, 40 °C was chosen as the temperature to perform our experiments on the deacidification of olive oil in our high pressure micro-device apparatus. Moreover, most of the data available in literature on the extraction of FFA from vegetable oils were obtained at 40 °C (as previously reported in *Section 2.2.2*), which made the comparison of our experimental results using micro-mixers with the results on an



extraction column easier. The first purpose of the experiments on the extraction of FFA from olive oil using micro-mixers was to determine whether equilibrium was reached, so one-single extraction stage could be achieved. Therefore, the modelling of the phase behaviour was necessary to predict the vapour-liquid equilibria of the CO<sub>2</sub> – oleic acid – triolein system at our experimental conditions. Table 5.2 shows a brief summary of the equations of state and mixing rules used in literature to model this system. Considering the acceptable deviations and its simplicity, the Peng-Robinson-Boston-Mathias (PR-BM) EoS model by Gracia et al. (2009) was chosen and used in this work to determine whether equilibrium has been reached in our extraction experiments. The parameters calculated by Gracia et al. (2009) for the PR-BM EoS are shown in Table 5.3. In this model, olive oil is again characterized as a pseudo-binary system of oleic acid + triolein. This assumption considers that a vegetable oil is formed mainly by two key components: triglycerides and free fatty acids. The solubility differences between particular components of any family are small compared to the corresponding values between free fatty acids and triglycerides. Therefore one particular compound from each family was selected: triolein for triglycerides and oleic acid for free fatty acids.

**Table 5.2. Summary of the equations of state and mixing rules used in literature for the system CO<sub>2</sub>-oleic acid-triolein.**

Equation of State	Mixing rule(s)	References
Redlich-Kwong-Soave EoS	RKS-Aspen mixing rules	Gracia et al. (2009)
Peng-Robinson-Boston-Mathias	-	Gracia et al. (2009)
GC-EoS	-	Vázquez et al. (2009)
GC-EoS	-	Fernández-Ronco et al. (2010)

**Table 5.3. Estimated parameters for Peng-Robinson-Boston-Mathias EoS by Gracia et al. (2009).**

Compounds/ binary system	$k_{12}$	$\omega_i$
CO <sub>2</sub>		0.17640295
Oleic acid		2.15731602
Triolein		1.75567735
CO <sub>2</sub> -oleic acid	0.05264151	
Triolein-CO <sub>2</sub>	0.01409294	
Triolein-oleic acid	-0.0509409	

Figure 5.3 compares the experimental data on the phase equilibria of the ternary mixture CO<sub>2</sub>-oleic acid-triolein from Bharath et al. (1992) at 40 °C and different pressures with the values predicted by the model with the parameters calculated by Gracia et al. (2009) and ASPEN Plus®. As it is observed, the liquid phase fits the experimental data very well, whereas the vapour phase predicted by the model does not. Therefore, for the comparison of our experimental results with the model to determine whether equilibrium has been achieved in our extraction experiments, only the raffinate (liquid phase) compositions were compared. Figure 5.4 shows the phase behaviour of the ternary system predicted by the model at 40 °C and 150 bar, the pressure and temperature conditions at which our extraction experiments were performed.

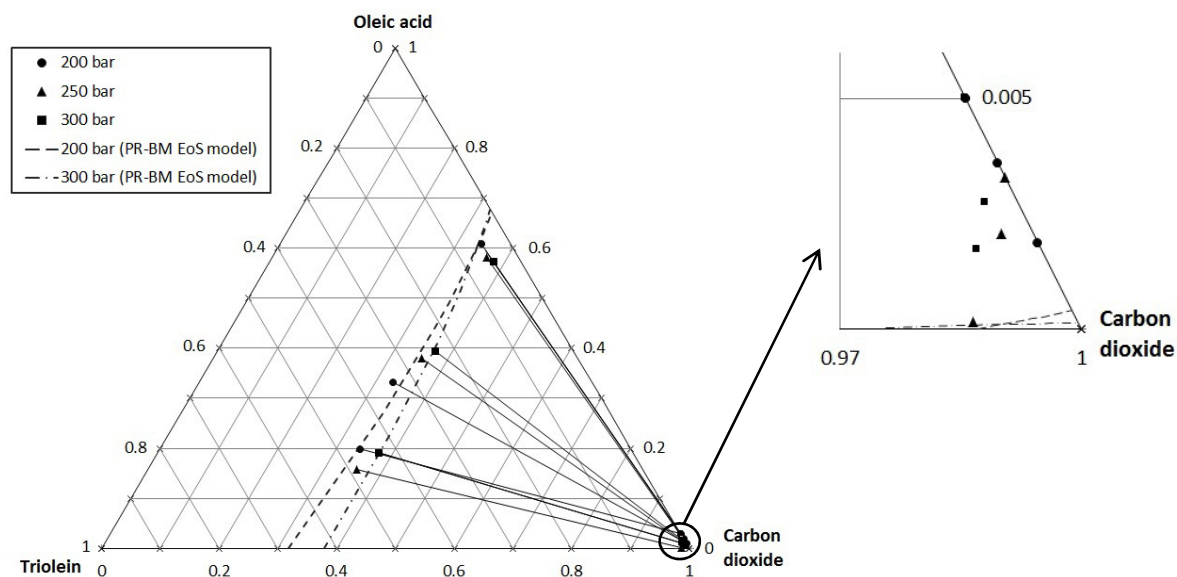


Figure 5.3. CO<sub>2</sub>-oleic acid-triolein phase equilibria (in mass fraction) at 40 °C. Symbols: experimental data from Bharath et al. (1992). Dotted lines: PR-BM EoS model.

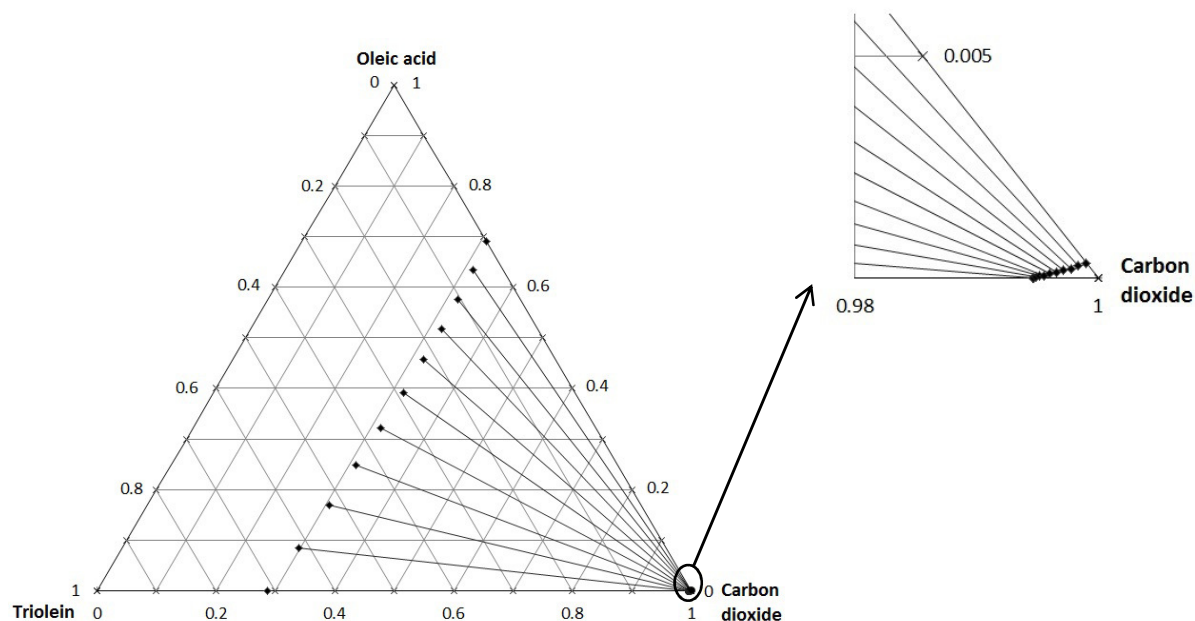


Figure 5.4. Prediction of the phase behaviour of the ternary mixture  $\text{CO}_2$ -oleic acid-triolein (in mass fraction) at  $40^\circ\text{C}$  and 150 bar using the PR-BM EoS model.

## 5.2. Physical properties

As discussed in *Chapter 4 (Section 4.2)*, the physical properties such as density, viscosity and surface or interfacial tension rule the behaviour of the fluids and certainly influence most of the chemical and physical processes. Olive oil presents different physical properties from ethanol-water binary systems. Moreover, the experimental conditions chosen for the extraction from olive oil are also different, leading to different viscosity and density of  $\text{scCO}_2$ . All these aspects influence the mixing of the solvent and feed in the micro-mixers and therefore the extraction process. The physical properties of the systems involved in the extraction of FFA from olive oil were deeply studied and are described here in order to have a better overview of their influence on the mixing of the phases and on the extraction process investigated in this work.

### 5.2.1. Supercritical $\text{CO}_2$

The solvent chosen for the extraction of FFA from olive oil is again  $\text{scCO}_2$ , so its fluid dynamic properties play an important role here as well. It has been already explained (see *Section 2.1*) that the density and some others properties of the supercritical fluids are extremely sensitive to minor changes in pressure and temperature near the critical point. As

mentioned above, the experimental conditions chosen for system B (40 °C and 150 bar) are different from the extraction conditions for system A (60 °C and 101 bar). Therefore, the properties of the scCO<sub>2</sub> are also different, as observed in Figures 5.5 and 5.6, where the density and viscosity of scCO<sub>2</sub> are represented as a function of the pressure at 40 °C and 60 °C for a better comparison. In Table 5.4, the density and viscosity of the scCO<sub>2</sub> at the experimental conditions chosen in this work for each system are shown. The increase in the solvent density and viscosity in system B in comparison to system A is obvious. Besides, it is important to highlight that the density difference between the feed and the solvent is much lower in system B (see Section 5.2.2) than in system A (see Table 4.7).

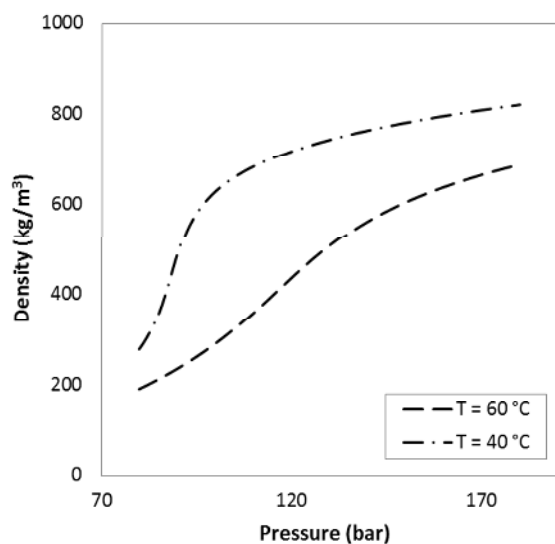


Figure 5.5. Density of scCO<sub>2</sub> as a function of the pressure at 40 and 60 °C. Data from NIST (2016).

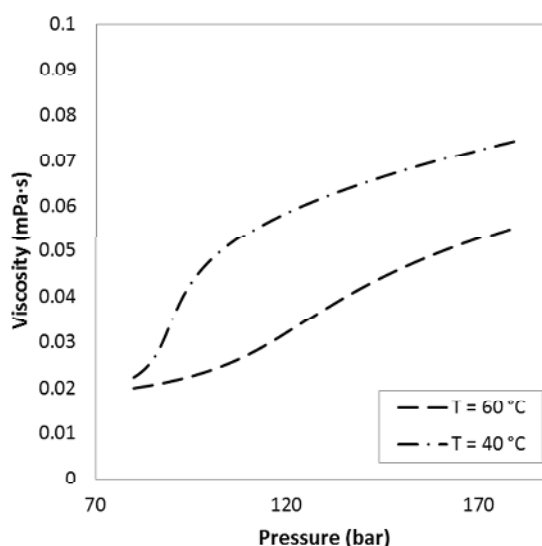


Figure 5.6. Viscosity of scCO<sub>2</sub> as a function of the pressure at 40 and 60 °C. Data from NIST (2016).

Table 5.4. CO<sub>2</sub> density and viscosity at the different extraction conditions studied in this work (NIST, 2016).

Extraction system	Temperature (°C)	Pressure (bar)	Density (kg/m <sup>3</sup> )	Viscosity (mPa·s)
System A	60	101	296	0.024
System B	40	150	780	4

### 5.2.2. Olive oil

Olive oil with different acidities (2.4 and 5 wt.%) was used as feed in these extraction experiments. Viscosity and density of the feed solutions at 20 and 40 °C and at ambient pressure were measured in our lab and results are shown in Table 5.5. As the acidity difference was very small and the density and viscosity values for the two different solutions were practically the same, the effect of this small acidity difference on the olive oil physical properties was assumed to be negligible.

**Table 5.5. Measured values of density and viscosity of olive oil at 20 and 40 °C (this work).**

Temperature (°C)	Olive oil acidity (wt.%)	Density (kg·m <sup>-3</sup> )	Viscosity (mPa·s)
20	2.5	911.3 ± 0.0	79.951 ± 0.045
	5.0	911.0 ± 0.0	78.952 ± 0.174
40	2.5	897.9 ± 0.0	34.646 ± 0.088
	5.0	897.5 ± 0.0	34.152 ± 0.024

Mean ± standard deviation based on duplicated measurements.

Acosta et al. (1996) studied the high-pressure *PVT* behaviour of natural fats and oils, olive oil among them, at different temperatures and pressures up to 1500 bar. Their experimental results at 40 °C and different pressures are represented in Figure 5.7. These data were correlated in order to estimate the density of olive oil at 150 bar and 40 °C (our experimental conditions) and a value of about 906 kg/m<sup>3</sup> was obtained.

On the other hand, Schaschke et al. (2006) measured the viscosity of olive oil at high pressure using a falling sinker type viscometer at 20 °C (Figure 5.9). As it is observed, in the range of 20 MPa (200 bar), marked with dotted lines, the change in the viscosity is very small. Therefore, as assumed for system A, the influence of pressure on the viscosity of the olive oil at our experimental conditions (150 bar) might be neglected as well. Valeri and Meirelles (1997) obtained viscosity data for fatty acids, triglycerides and their binary mixtures. In Figure 5.8, the viscosity of triolein and oleic acid (the two main components of the olive oil) is represented as a function of the temperature. Moreover, our measured data on the viscosity of olive oil at 20 and 40 °C are also represented, fitting with the density of triolein perfectly. This confirms that, as it has been assumed, triolein is the major component in olive oil.

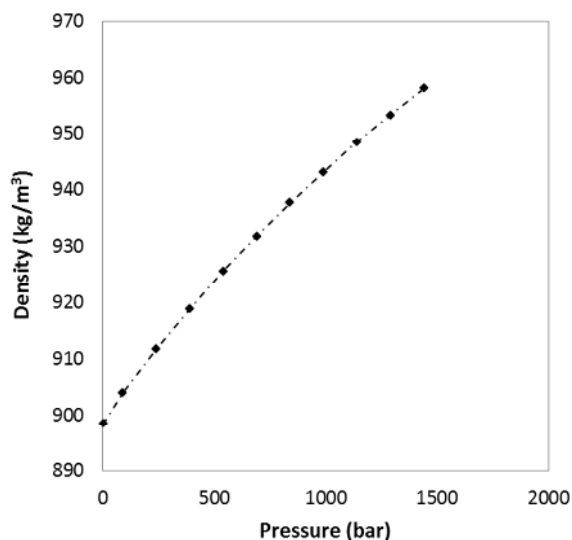


Figure 5.7. Density of olive oil as a function of the pressure at 40 °C. Data from Acosta et al. (1996).

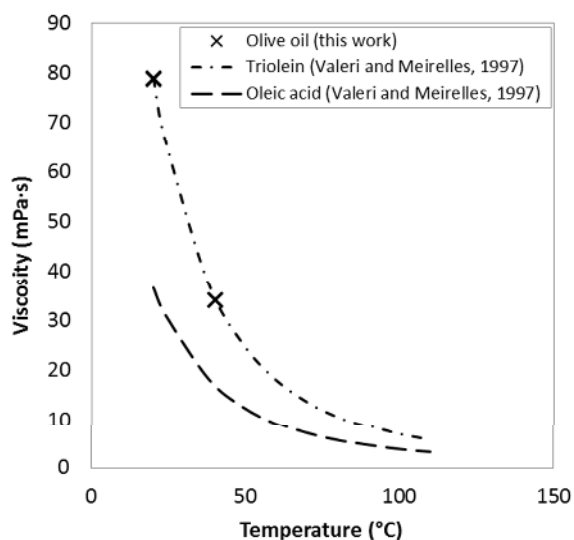


Figure 5.8. Viscosity of olive oil, triolein and oleic acid as a function of the temperature at ambient pressure.

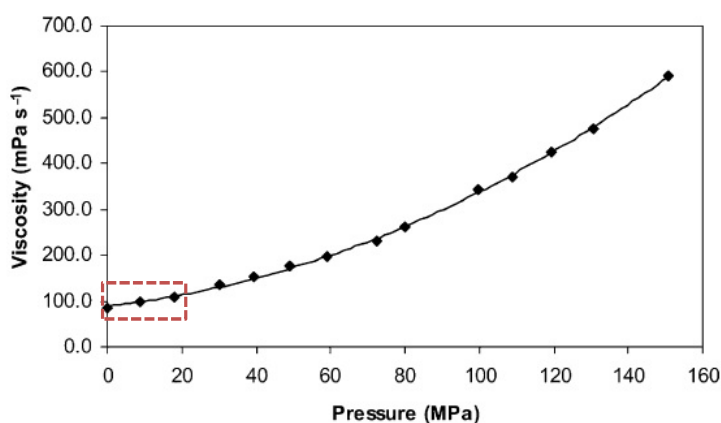


Figure 5.9. Viscosity of olive oil under pressure at 20 °C. Source: Schaschke et al. (2006).

### 5.2.3. CO<sub>2</sub> + olive oil

The system CO<sub>2</sub> + olive oil was considered as a pseudo ternary system CO<sub>2</sub>-oleic acid-triolein, which comprises the three fundamental components for the extraction of FFA from olive oil: solvent (CO<sub>2</sub>), solute (oleic acid) and key component of the phase from which the solute is extracted (triolein). Fluid properties such as viscosity and density of both fluids (olive oil and scCO<sub>2</sub>) have been explained in the previous sections (*Section 5.2.1* and *5.2.2*). Unlike system A, in which water (key component of the phase from which the solute is extracted) and scCO<sub>2</sub> (solvent) were considered immiscible and therefore ethanol was the only diffusing species, in system B triolein and scCO<sub>2</sub> are not immiscible, but partially miscible. This fact may

change the viscosity, density and volume of the olive oil in contact with CO<sub>2</sub> and therefore influence the flow and the mass transport. Thus, this factor must be taken into account in our study.

The viscosity and density of CO<sub>2</sub>-expanded canola oil was studied by Jenab and Temelli (2011) and Jenab and Temelli (2012), respectively. In Figure 5.10, the typical fatty acid compositions of olive oil and canola oil are compared (Gunstone, 1996). It is obvious that both compositions are pretty similar. Moreover, the density of pure canola oil at high pressure (Figure 5.11, from Jenab and Temelli, 2012) is compared to the density of pure olive oil (Figure 5.12) at 40 °C and in the same pressure range, showing that both oils present very similar density. Taking this into account, the behaviour of the canola oil in contact with CO<sub>2</sub> can be considered similar to the olive oil behaviour.

<b>Canola oil (rapeseed)</b>	<b>6% saturated</b>		<b>92% unsaturated</b>	
	4	palmitic 16:0	56	oleic 18:1 n-9
	2	stearic 18:0	26	linoleic 18:2 n-6
			10	linolenic 18:3 n-3
			2% other	
<b>Olive oil</b>	<b>12% saturated</b>		<b>86% unsaturated</b>	
	10	palmitic 16:0	78	oleic 18:1 n-9
	2	stearic 18:0	7	linoleic 18:2 n-6
			1	linolenic 18:3 n-3
			2% other	

Figure 5.10. Typical fatty acid composition of olive oil and canola oil (Gunstone, 1996).

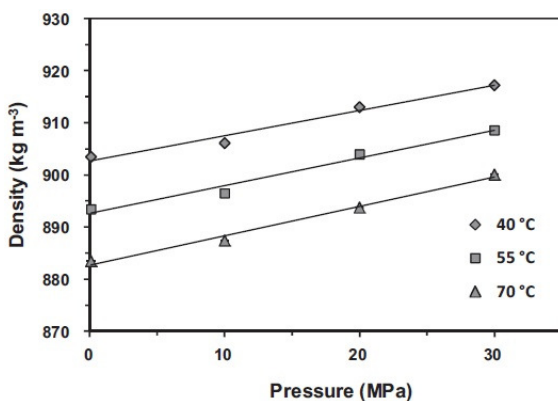


Figure 5.11. Density of pure canola oil as a function of the pressure at various temperatures. Source: Jenab and Temelli (2012).

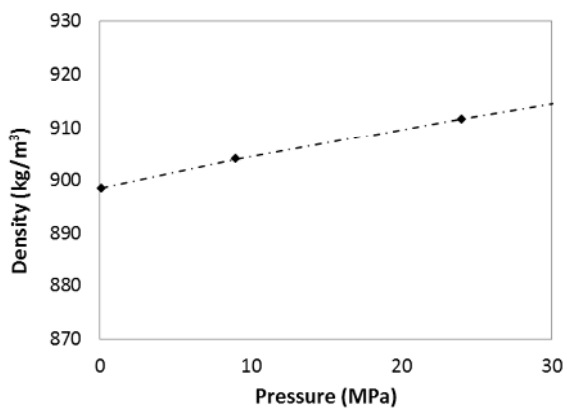


Figure 5.12. Density of pure olive oil as a function of the pressure at 40 °C. Data from Acosta et al. (1996).

Jenab and Temelli (2012) measured the density of CO<sub>2</sub>-expanded canola oil at different temperatures and pressures and determined that it increases with pressure and decreases with temperature at constant pressure. At 40 °C, the density of canola oil increased by 4.7% related to its value at atmospheric pressure. The authors observed that the solubilisation of CO<sub>2</sub> in the canola oil (liquid phase) increases the density of the liquid phase remarkably although the pure CO<sub>2</sub> density is lower than the canola oil density at the same conditions. They concluded that the density of the liquid phase in equilibrium with high pressure CO<sub>2</sub> is not only dependent on the solubility of CO<sub>2</sub> in the liquid phase but also on the compressibility of the liquid phase. Beforehand, Tegetmeier et al. (2000) had measured the density of corn oil in equilibrium with high pressure CO<sub>2</sub> and had observed a similar behaviour: the density of corn oil increases when increasing the pressure, and when decreasing the temperature. The maximum increase in density that they measured was about 5% (similar to Jenab and Temelli's measurements). Furthermore, Jenab and Temelli (2012) also measured the relative volumetric expansion of canola oil in equilibrium with high pressure CO<sub>2</sub> (Figure 5.15) and observed that at 40 °C the relative volumetric expansion of canola oil in equilibrium with high pressure CO<sub>2</sub> was about 40% at 150 bar (15 MPa).

On the other hand, the experimental data from Jenab and Temelli (2011) on the viscosity of canola oil in equilibrium with high pressure CO<sub>2</sub> (Figure 5.14) showed that the viscosity dramatically decreases with pressure up to 100 bar, and above that it reaches a constant level. The authors concluded that the mass fraction of CO<sub>2</sub> in the oil has substantial influence on the viscosity, due to the dilution of the oil with a component of very low viscosity. In any manner, comparing Figures 5.13 and 5.14 is concluded that the dilution of high pressure CO<sub>2</sub> in canola oil (or in a liquid lipid phase) has very different effects on the density and on the viscosity of the liquid phase.

In summary, the results from Jenab and Temelli (2011) and Jenab and Temelli (2012) together with the fact that Tegetmeier et al. (2000) obtained very similar results when measuring corn oil led us to assumed the behaviour of olive oil in contact with scCO<sub>2</sub> during our experiments to be similar to what is observed in Figures 5.13 and 5.14.



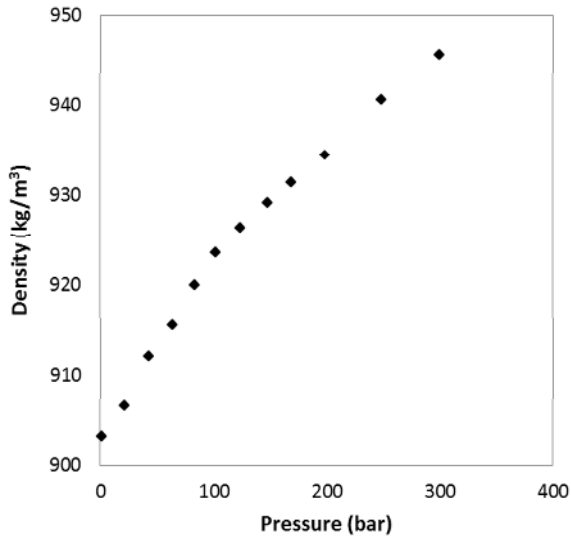


Figure 5.13. Density of canola oil in equilibrium with CO<sub>2</sub> as a function of the pressure at 40 °C. Data from Jenab and Temelli (2012).

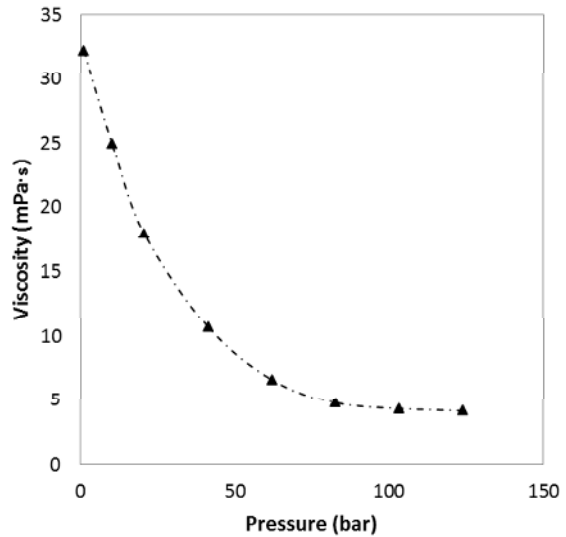


Figure 5.14. Viscosity of canola oil in equilibrium with CO<sub>2</sub> as a function of the pressure at 40 °C. Data from Jenab and Temelli (2011).

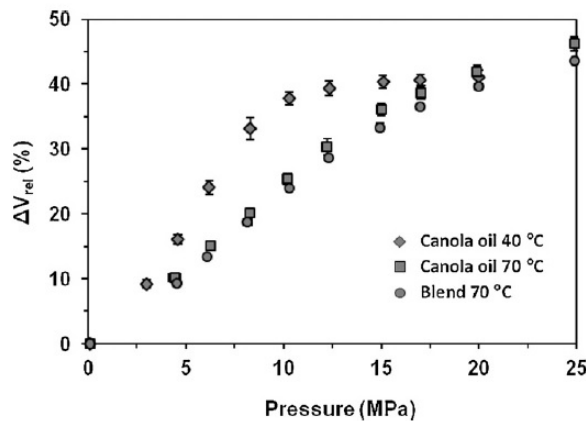


Figure 5.15. Relative volumetric expansion of canola oil in equilibrium with CO<sub>2</sub> as a function of the pressure at various temperatures (Jenab and Temelli, 2012).

These properties (viscosity and density), together with the interfacial tension between the two phases define the behaviour of the fluids in the mixing process as well as the flow pattern in the capillary. Figure 5.16 shows the interfacial tension of a virgin olive oil enriched to a free fatty acid content of 7.6 wt.% in scCO<sub>2</sub> atmosphere at 40 °C (313 K) and 80 °C (353 K), measured by Simões et al. (2000).

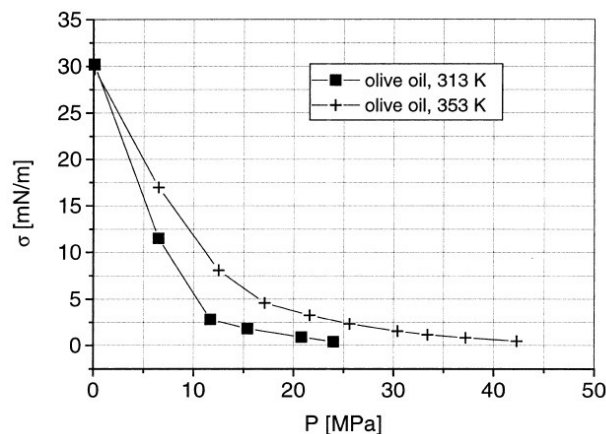


Figure 5.16. Interfacial tension of olive oil in CO<sub>2</sub> as a function of the pressure at 40 °C (313 K) and 80 °C. Source: Simões et al. (2000).

### 5.3. Experimental results

Experiments on the extraction of FFA from olive oil were carried out in our high pressure micro-device apparatus for SFE described in *Chapter 3* to study the feasibility of micro-mixers for a second extraction system. The experimental conditions were chosen based on the phase behaviour of the system (*Section 5.1*), the data available in literature and the characteristics of our experimental apparatus. As the separators can withstand only up to 250 bar, pressures in the range between 150 – 200 bar were considered for the conditions in the first separator. Two preliminary experiments were carried out at 150 and 180 bar and results were compared (see Table 5.6). As the extraction results from both experiments were extremely similar, showing that the influence of the pressure in this range is very low, the lowest pressure (150 bar) was chosen for our successive experiments. In Table 5.7, the experimental conditions chosen in this work for the extraction of FFA from olive oil are shown.

Table 5.6. Comparison of the experimental yield and acidity of the raffinate obtained in the SFE of olive oil at 40 °C.

Oil acidity	Extraction pressure (bar)	S-to-F	Raffinate yield (%)	Raffinate acidity
5	150	13	94.4	4.31 ± 0.03
5	180	13	93.5	4.28 ± 0.04

Mean ± standard deviation based on duplicated measurements.

Table 5.7. Experimental conditions for the extraction of FFA from olive oil by scCO<sub>2</sub> (system B).

	Pressure (bar)	Temperature (°C)
1 <sup>st</sup> separator	150	40
2 <sup>nd</sup> separator	55	40

As described in *Chapter 3*, in our SFE experimental apparatus, the micro-mixer is the only point in which solvent and feed get into contact. Thus, only one theoretical stage of extraction can be achieved within the extraction process. In this series of experiments, the objective was to determine whether the equilibrium was reached and therefore one theoretical stage could be achieved in the high pressure micro-device apparatus. For this, as commented above in *Section 5.1*, the phase equilibria of the ternary mixture CO<sub>2</sub>-oleic acid-triolein was studied and the model calculated by Gracia et al. (2009) was used, together with the Equations (4.22)-(4.25) of the Equilibrium Stage Model Concept (see *Chapter 4*), to determine whether the equilibrium has been achieved in the experiments carried out here.

In this series of experiments only two different feed concentrations (i.e. olive oil with different acidity) were under study. Brunetti et al. (1989) investigated the extraction of fatty acids from fatty acid + triglyceride mixtures using scCO<sub>2</sub> as solvent. They concluded that the selectivity factor for the fatty acid extraction increases as the concentration of the FFA in the oil decreases. Therefore SFE is particularly suitable for deacidification of olive oils with FFA content lower than 10 wt.%. Olive oils with acidity of 2.4 and 5 wt.% were used for the extraction experiments carried out in this work.

The experimental results obtained on the SFE of FFA from olive oil with scCO<sub>2</sub> in micro-mixers are shown and discussed here. In the following graphs, the results using the HPIMM micro-mixer will be again represented by filled symbols (●), while the results obtained with the Tee-mixer will be represented by hollow symbols (○). It is important to point out that the standard deviation error is represented for every experimental result shown in the figures. However, this error is so small in some cases that it is not always appreciable in the graphs. As mentioned in *Section 3.3.2*, raffinate samples were analysed twice and the mean value of the two analyses was taken as raffinate concentration. The standard deviation based on the duplicate measurements was also calculated and represented.

Although the extract concentration was not compared with the phase equilibria model (as explained in *Section 5.1*), the extract samples collected during the experiments were also analysed and weighed in order to calculate the mass balance. In each experiment, mass balance was calculated to validate the extraction results.

The experimental results obtained for the extraction of FFA from olive oil at different S-to-F ratios are represented in Figure 5.17(A). Moreover, the raffinate's acidity predicted by the PR-BM EoS model is also represented for comparison. It is observed that the experimental results using either the Tee-mixer or the HPIMM micro-mixer fit the model well. Furthermore, the raffinate's acidity is also represented as a function of the total volume flow rate in Figure 5.17 (B). Although the mass Solvent-to-Feed ratio range and the feed flow rate in this series of experiments is very similar to the ranges studied for system A (see *Sections 4.3.2.* and *4.3.3.*), the range of total volume flow rate is much lower in the experiments of system B: between 200 and 500 mL/h, whereas in the experiments for system A, the total volume flow rate range studied was from 200 to 1500 mL/h. This difference in the volume flow rate range is mainly attributed to the CO<sub>2</sub> density difference at the different experimental conditions (see Table 5.4). Furthermore, it is observed in Figure 5.17 that our experimental results fit the model pretty well in every case. Therefore it was concluded that equilibrium was achieved in the extraction of system B, as it was achieved in the extraction of system A as well.

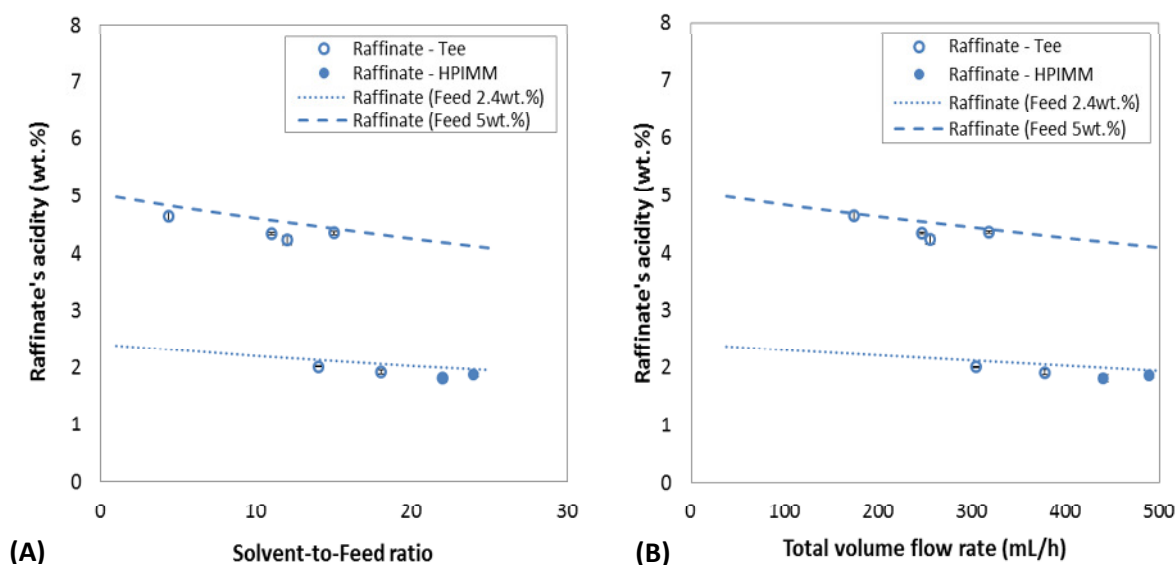


Figure 5.17. Raffinate's acidity and the prediction of a single theoretical stage model as a function of the mass Solvent-to-Feed ratio (A), and as a function of the total volume flow rate (B) for different feed acidity values (2.4 and 5 wt.%). Constant feed volume flow rate of 18 mL/h, variable CO<sub>2</sub> volume flow rate.

Furthermore, in Table 5.8, our experimental results are compared with the results obtained from the simulations in ASPEN Plus® with PR-BM EoS, and the deviation was calculated. It is observed that the experimental results in our high-pressure micro-device extraction apparatus fit the model extremely well, as the deviation is always lower than 10%. The case with the highest deviation (15.53%), when comparing the experimental to the calculated raffinate yield, was actually attributed to a sampling error. The raffinate yield was calculated according to Equation (4.31).

Table 5.8. Comparison of experimental data at 40 °C and 150 bar with the PR-BM EoS model used in this work.

Oil acidity (wt.%)	S-to-F	Raffinate yield (%)			Raffinate acidity (wt.%)		
		Experimental	Calculated	Deviation (%)	Experimental	Calculated	Deviation (%)
2.4	14	96.5	97.2	0.73	2.01	2.14	6.36
	18	95.9	96.3	0.35	1.92	2.07	7.68
	22	89.6	95.5	6.58	1.81	2.00	10.30
	24	92.5	95.1	2.81	1.87	1.96	5.02
5.0	5	85.6	98.9	15.53	4.65	4.80	3.25
	11	92.9	97.7	5.17	4.34	4.59	5.66
	12	93.5	97.4	4.17	4.24	4.55	7.41
	15	96.8	96.7	0.10	4.36	4.44	1.83

## 5.4. Validation of the model

In order to validate the thermodynamic model used here to assess our experimental results, the model was also compared with different experimental data from literature. On one hand, data from Vazquez et al. (2009) in a packed column of 3 m height and 18 mm ID were used (see Table 5.9). The cases in which the oil acidity was the most similar to those considered in our experiments were simulated in ASPEN Plus® using the PR-BM EoS model. Calculated results were compared with the experimental results from Vazquez et al. (2009). Taking into account that values of around 0.5-1.0 m have been obtained for the HETS in this system (Simões and Brunner, 1996), our simulations in ASPEN Plus® were performed using an extraction column with 3 stages. By comparing the calculated results with the experimental data, it is observed that they fit very well, as the deviation is around 10% or lower in every case.

Table 5.9. Comparison of experimental data from Vazquez et al. (2009) on the SFE of olive oil at 40 °C and S-to-F = 20 with the PR-BM EoS model used in this work.

Oil acidity (wt.%)	p (bar)	Raffinate yield (%)			Raffinate acidity (wt.%)		
		Experimental	Calculated	Deviation (%)	Experimental	Calculated	Deviation (%)
2.5	180	92.6	94.4	5.47	1.21	1.67	11.33
	250	85.8	95.6	10.90	0.93	0.96	7.87
4.0	180	92.9	94.0	5.03	2.31	2.70	10.20
	250	84.1	94.7	10.76	1.43	1.55	6.16

On the other hand, experimental results from Bondioli et al. (1992) in a packed column with Sulzer EX packing, 3 m height and an ID of 30 mm were also compared with the PR-BM EoS model. In Table 5.10, it is observed that although the calculated and experimental results do not fit as well as in the previous comparison, still the deviation obtained is acceptable, especially in the case at 150 bar, which is at the same experimental conditions than our experiments. The larger deviation in the results obtained at 130 bar could be attributed to the pressure range, which is already quite lower than the pressure range at which the thermodynamic data from Bharath et al. (1992) were obtained, i.e. 200-300 bar.

Even though, after comparing the model with our experimental results as well as with previous experimental results from literature, it was concluded that the PR-BM model results are in good agreement with the SFE experimental results.

Table 5.10. Comparison of experimental data from Bondioli et al. (1992) on the SFE of olive oil at 40 °C and oil acidity 6.3 wt.% with the PR-BM EoS model used in this work.

S-to-F	Pressure (bar)	Experimental		Calculated			Deviation (%)	
		Raffinate yield (%)	Raffinate acidity (wt.%)	N (number of stages)	Raffinate yield (%)	Raffinate acidity (wt.%)	Raffinate yield (%)	Raffinate acidity (wt.%)
100	150	68.7	2.07	2	77.8	2.17	13.25	4.83
				3	77.6	1.55	12.95	25.12
20	130	91.9	4.34	2	97.6	5.69	6.20	31.11
				3	97.6	5.69	6.20	31.11

## 6. Visualization of multiphase flows of supercritical carbon dioxide and liquid mixtures

Here, our main purpose was the investigation of the fluid behaviour of  $\text{scCO}_2$  with liquid mixtures in the both micro-devices studied in this work (HPIMM micro-mixer and Tee-mixer) and its influence on the extraction performance. Both micro-devices are made of stainless-steel, thus only the visualization of the fluid behaviour in the capillary placed in the section from the micro-device to the separator was possible. Therefore the multiphase flow behaviour of  $\text{scCO}_2$  with different liquid mixtures, ethanol-water mixtures (system A) and olive oil (system B), in a capillary was observed for a better comprehension of the mixing and extraction processes studied. The dimensions of the transparent Radel® Tubing used for the visualization experiments were the same as of the stainless steel micro-channel used for the extraction experiments (i.e. ID = 0.5 mm; OD = 1/16") as described in *Section 3.1.2*, in order to maintain the same conditions and characteristics. The effect of the mixing principle (multi-lamination or T-type lamination) and the total flow rate were investigated. The S-to-F ratio was kept constant. For a better understanding of the mixing of the phases in the micro-device and the behaviour through the capillary, the flow was observed at two different points: close to the inlet of the capillary (next to the micro-device) and in the middle of the capillary (at approx. 100-120 mm distance to the capillary inlet), as described in Figure 6.1.

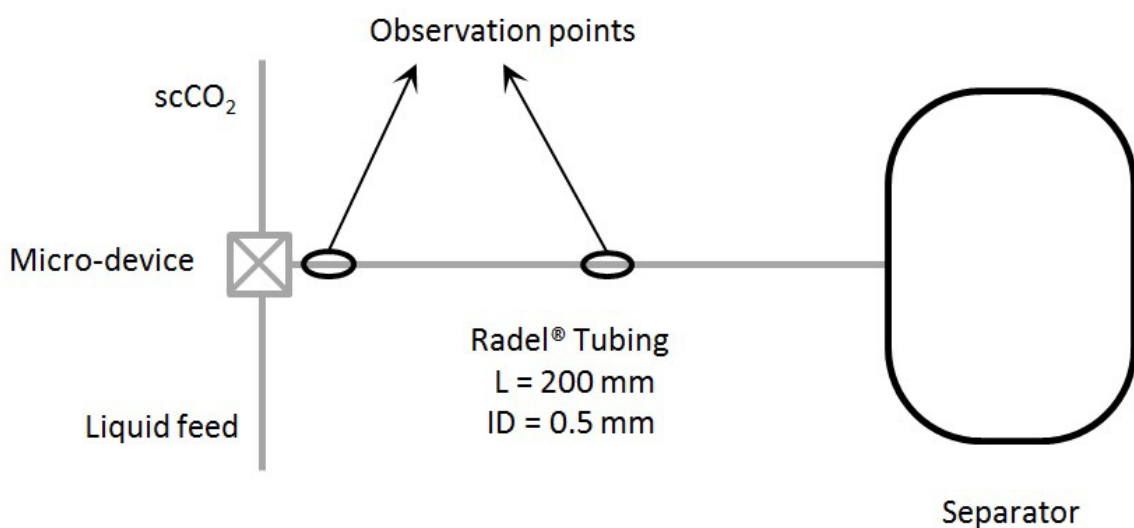


Figure 6.1. Schematic diagram of the two observation points in the visualization experimental apparatus.

Furthermore, for the assessment of the experimental results presented here two aspects must be taken into account:

(1) due to the pulsations in the HPLC pump, the flow patterns were not observed continuously but they were “appearing and disappearing” in a cyclic manner. Therefore, when a flow is classified in the further sections as wavy, annular or plug flow, it means that this type of flow was observed repeatedly in a stable manner at those conditions;

(2) at the highest flow rates studied here (i.e. FR3 in Table 6.1), the notably high flow velocity made the observation and classification of the flow pattern difficult in some cases, so the flow description given here at the highest flow rate might be less accurate than the rest.

## 6.1. Fluid behaviour of supercritical carbon dioxide with ethanol-water liquid mixtures (system A)

The purpose of these series of experiments was to study whether the hydrodynamics of the scCO<sub>2</sub>-liquid mixture flow patterns could have an influence on the extraction results. Therefore, the experimental conditions and feed solutions considered were the same as in the extraction experiments explained in *Section 4.3.5*, for a proper comparison and analysis of the results. The flow rates studied in these experiments are given in Table 6.1. Moreover, the feed solutions used in these experiments and their fluid properties together with the solvent (scCO<sub>2</sub>) fluid properties at the experimental conditions are shown in Table 6.2, the values are taken from the discussion in *Section 4.2*. On the other hand, as water is one of the components of the system studied here and, as described previously (see *Section 2.3.3*), the flow of scCO<sub>2</sub> and water has been studied by different authors in the last years, a series of experiments on the study of the flow of scCO<sub>2</sub> and liquid water was performed as well. Likewise, experiments on the flow of scCO<sub>2</sub> and liquid ethanol were also performed.

Table 6.1. Flow conditions in the experiments of the system A.

	Total flow rate (mL/min)	Flow velocity (mm/s)
FR1	6.125	0.51
FR2	12.25	1.02
FR3	24.5	2.04



$$Re = \frac{\text{inertial forces}}{\text{viscous forces}} = \frac{\rho \cdot v \cdot L}{\eta} \quad (6.1)$$

$$Ca = \frac{\text{viscous forces}}{\text{surface tension}} = \frac{\eta \cdot v}{\gamma} \quad (6.2)$$

$$We = \frac{\text{inertial forces}}{\text{surface tension}} = Re \cdot Ca = \frac{\rho \cdot v^2 \cdot L}{\gamma} \quad (6.3)$$

Table 6.2. Physical properties of the studied mixtures at the experimental conditions: 101 bar and 60°C.

Mixture	Density (kg/m <sup>3</sup> )	Viscosity (Pa·s)	Interfacial tension (N/m)
Water	987	4.69·10 <sup>-4</sup>	3.17·10 <sup>-2</sup>
10 wt.% ethanol	971	6.31·10 <sup>-4</sup>	3.08·10 <sup>-2</sup>
50 wt.% ethanol	882	9.17·10 <sup>-4</sup>	1.82·10 <sup>-2</sup>
90 wt.% ethanol	793	6.84·10 <sup>-4</sup>	5.63·10 <sup>-3</sup>
Ethanol	764	5.85·10 <sup>-4</sup>	1.03·10 <sup>-3</sup>
scCO <sub>2</sub>	296	2.41·10 <sup>-5</sup>	-

Table 6.3. Dimensionless numbers for the different liquid solutions used in the experiments with system A.

	Liquid			CO <sub>2</sub>		
	Re	Ca	We	Re	Ca	We
Water	11.2 – 44.7	1.57·10 <sup>-4</sup> – 6.28·10 <sup>-4</sup>	1.75·10 <sup>-3</sup> – 2.80·10 <sup>-2</sup>	3.16·10 <sup>3</sup> – 1.26·10 <sup>4</sup>	3.88·10 <sup>-4</sup> – 1.55·10 <sup>-3</sup>	1.22 – 19.6
10 wt.% ethanol	8.18 – 32.7	2.18·10 <sup>-4</sup> – 8.71·10 <sup>-4</sup>	1.78·10 <sup>-3</sup> – 2.85·10 <sup>-2</sup>	3.16·10 <sup>3</sup> – 1.26·10 <sup>4</sup>	3.99·10 <sup>-4</sup> – 1.60·10 <sup>-3</sup>	1.26 – 20.2
50 wt.% ethanol	5.12 – 20.5	5.41·10 <sup>-4</sup> – 2.16·10 <sup>-3</sup>	2.77·10 <sup>-3</sup> – 4.43·10 <sup>-2</sup>	3.16·10 <sup>3</sup> – 1.26·10 <sup>4</sup>	6.83·10 <sup>-4</sup> – 2.73·10 <sup>-3</sup>	2.15 – 34.5
90 wt.% ethanol	6.17 – 24.7	1.29·10 <sup>-3</sup> – 5.16·10 <sup>-3</sup>	7.96·10 <sup>-3</sup> – 1.27·10 <sup>-1</sup>	3.16·10 <sup>3</sup> – 1.26·10 <sup>4</sup>	2.18·10 <sup>-4</sup> – 8.73·10 <sup>-3</sup>	6.89 – 110
Ethanol	6.93 – 27.7	6.03·10 <sup>-3</sup> – 2.41·10 <sup>-2</sup>	4.18·10 <sup>-2</sup> – 6.68·10 <sup>-1</sup>	3.16·10 <sup>3</sup> – 1.26·10 <sup>4</sup>	1.19·10 <sup>-2</sup> – 4.77·10 <sup>-2</sup>	37.6 – 602

The velocities in Table 6.1 were estimated using the volume flow rates and the cross section of the capillary. Reynolds (Re), Capillary (Ca) and Weber (We) numbers were calculated for every mixture used as liquid phase in the experiments, values are shown in Table 6.3. Dimensionless numbers were calculated according to Equations (6.1) – (6.3), where

$\rho$  is the fluid density,  $v$  is the fluid velocity,  $L$  is the characteristic length of the system (in this case, the capillary inner diameter),  $\eta$  is the dynamic viscosity of the fluid, and  $\gamma$  is the interfacial tension between the two fluids. Weber number can be calculated combining the Reynolds and the Capillary numbers according to Equation (6.3) when the viscosities in the fluid are kept constant. In this study, the viscosity change of the fluids through the capillary was neglected to simplify the system.

### 6.1.1. Mixing in HPIMM micro-mixer

The flow behaviour of scCO<sub>2</sub>-liquid water and scCO<sub>2</sub>-liquid aqueous ethanol solutions with different ethanol concentrations in a capillary with an inner diameter of 0.5 mm was investigated. Both supercritical and liquid phases were mixed in the HPIMM micro-mixer and this mixture flowed then through the capillary, where the flow was studied. The classification of the flow patterns observed in the experiments is shown in Table 6.4, where inlet refers to the observation point at the inlet of the capillary (just after the mixing in the HPIMM micro-mixer) and middle refers to the observation point located in the middle of the capillary (as shown in Figure 6.1). Moreover, the different flow patterns observed are described in Table 6.5. As it observed in Table 6.4, plug flow and inverse annular flow (in which the liquid is the inner phase and the scCO<sub>2</sub> the outer phase) were observed only in the experiments performed with water and the 10 wt.% ethanol solution. These are the cases with a higher interfacial tension between the phases and besides, the two cases in which either there is not mass transfer (scCO<sub>2</sub>-water flow) or the ethanol transfer is the lowest (scCO<sub>2</sub>-10 wt.% ethanol flow). Therefore the composition of the both phases barely changes through the capillary in these two cases. It must be mentioned that, due to the large length of the plugs observed, it was not possible to show an entire plug in Table 6.5 (A). Besides, the asterisks in Table 6.4 are used to remark the cases in which it was not easy to discern whether the liquid phase was flowing forming big plugs (plug flow) or in an inverse annular flow.

On the other hand, in the cases in which the liquid phase is a solution with a higher concentration of ethanol (i.e. 50 wt.% and 90 wt.% ethanol) and therefore more ethanol is transferred from the liquid phase to the supercritical phase, the annular flow and “wavy” annular flow were the most observed flow patterns. Besides, wavy flow was also visualized at these conditions. It is important to mention that the “wavy” annular flow visualized in our

experiments (shown in Table 6.5 (E)) is similar to the flow simulated by Hardt and Schönfeld (2003) for the slit-shaped micro-mixer when they studied the laminar mixing in different interdigital micro-mixers. Hardt and Schönfeld (2003) investigated by computational fluid dynamics (CFD) the flow patterns and mixing properties of different multi-lamination micro-devices, including the multi-lamination slit-shaped micro-mixer among them. Figure 6.2 shows the lamellae profile for different Reynolds numbers obtained in their CFD simulations, where the geometric arrangement and the deformation of the liquid lamellae are observed. We considered that the “wavy” annular flow observed at the inlet of the capillary in some of our experiments is quite similar to the model from Hardt and Schönfeld (2003).

Moreover, it must be pointed out that in the experiments with the 90wt.% ethanol solution, the interface between the two phases was very hard to identify, especially at the inlet of the capillary, zone which we considered as a very high mass transfer zone (according to our experimental results shown in *Section 4.3.4*). Further, in the middle of the capillary the interface was clearer and the two phases, liquid and supercritical, were more distinguishable, showing an annular flow in which the liquid phase was the outer phase and the supercritical phase (with ethanol dissolved) was the inner phase. It is also important to mention that annular flow was observed at some point in practically every experiment here. We attribute this to the “discontinuous” liquid flow due to the HPLC pump pulsations. That means that the liquid is not pumped in a continuous form but it is a “pulsed” flow, which makes the flow to appear and disappear (as mentioned above). In the time intervals in which no liquid was pumped (between the pulses of the HPLC pump), still liquid was observed in the capillary (but less on quantity), forming an annular flow with the supercritical phase. Moreover, after every “pulsation” when liquid was pumped, very small droplets were formed and observed at the inlet of the capillary (see (F) in Table 6.5), as the liquid flow seemed to break in small droplets. On the other hand, a flow classification for the scCO<sub>2</sub>-ethanol flow was not made as it was not possible to discern two phases nor an interface in all the experiments performed with ethanol in this work.

Summarizing, in our experiments plug flow was observed at low flow rates when there was a high interfacial tension between the two phases and no mass transfer or very low mass transfer occurred. An increase in the flow rate shifted the flow from plug to inverse annular flow. Nevertheless, in systems with low interfacial tension as well as systems in which more

ethanol is transferred from one phase to the other (because the initial concentration of ethanol in the liquid phase is higher), then annular and wavy flow prevailed.

Table 6.4. Flow patterns observed in the experiments with the HPIMM micro-mixer on the flow of scCO<sub>2</sub> with liquid ethanol+water mixtures.

Liquid phase	Flow rate	Inlet	Middle
Water	FR1	Plug flow	Wavy flow
	FR2	Inverse annular flow*	Wavy flow
	FR3	Inverse annular flow	Inversed annular flow
10 wt.% ethanol	FR1	Plug flow	Plug flow
	FR2	Inverse annular flow*	Inversed annular flow
	FR3	Inverse annular flow	Inversed annular flow
50 wt.% ethanol	FR1	“Wavy” annular flow	Wavy flow
	FR2	“Wavy” annular flow	Wavy flow
	FR3	“Wavy” annular flow	Wavy flow
90 wt.% ethanol	FR1	“Wavy” annular flow	Annular flow
	FR2	“Wavy” annular flow	Annular flow
	FR3	-	Annular flow

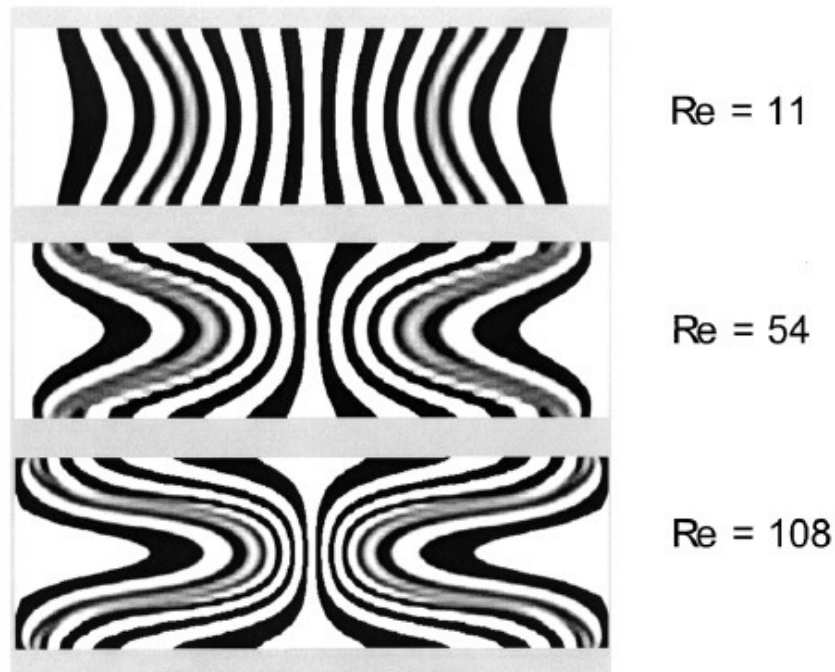
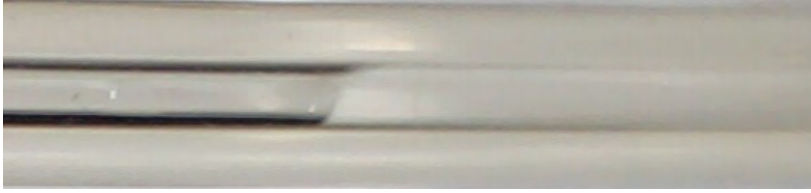







Figure 6.2. Orientation of liquid lamellae in the mixing channel of the slit-shaped micro-mixer. (Source: Hardt and Schönfeld, 2003).

Table 6.5. Flow patterns observed in our experiments with system A and the HPIMM micro-mixer.

---

	(A) Plug flow
	(B) Wavy flow
	(C) Inverse annular flow
	(D) Annular flow
	(E) "Wavy" annular flow
	(F) Droplets formation

---

### 6.1.2. Mixing in Tee-mixer

The results presented here are focused on the flow behaviour of  $\text{scCO}_2$ -liquid water and  $\text{scCO}_2$ -liquid aqueous ethanol solutions with different ethanol concentration in a capillary with an inner diameter of 0.5 mm after mixing in a Tee-mixer. Both supercritical and liquid phases were mixed in the Tee-mixer and this mixture flowed then through the capillary where the flow was studied. The classification of the flow patterns experimentally observed is shown in

Table 6.6, where again inlet refers to the observation point at the inlet of the capillary (just after the mixing in the Tee-mixer), and middle refers to the observation point located in the middle of the capillary (as shown in Figure 6.1). Moreover, the different flow patterns observed are described in Table 6.7. For a better definition of the chaotic thin striations flow, as the photography from our experiments in Table 6.6 (C) might not be clear enough, a photography from Zhao et al. (2006) describing the chaotic thin striations is also shown. As observed in Table 6.6, plug flow was again observed only in the experiments performed with water and with 10 wt.% ethanol solution. As mentioned above, these are the cases with the highest interfacial tension between the phases and moreover, the two cases in which either there is not mass transfer (scCO<sub>2</sub>-water flow) or the mass transfer is the lowest (scCO<sub>2</sub>-10 wt.% ethanol flow). Therefore the composition as well as the volume of the both phases barely changes through the capillary in these two cases. Chaotic thin striations flow was also observed in the experiments performed with water and 10 wt.% ethanol and, at the highest flow rates, with the 50 wt.% ethanol solution. In the latter case, in spite of the ethanol transfer from the liquid to the supercritical phase, the volume of the liquid phase is still relatively high, as the volume flow rate is very high. Besides, the asterisk in Table 6.6 is used to remark that in that case (medium flow rate and water as liquid phase) the flow observed was a parallel flow combined intermittently with plug flow. On the other hand, when the liquid phase has a higher concentration of ethanol (i.e. 50 wt.% and 90 wt.% ethanol), more ethanol is transferred from the liquid phase to the supercritical phase, and therefore the volume of the liquid phase significantly decreases through the capillary. In these cases, bubbly flow and annular flow were observed in the middle of the capillary where, according to our extraction results, the thermodynamic equilibrium must have been already reached and therefore the mass transfer has occurred. Wavy flow was also visualized, at lower flow rates. In these experiments, it must be pointed out again that when having 90 wt.% ethanol solution, the interface between the two phases was very hard to identify, especially at the inlet of the capillary, zone which was considered as a very high mass transfer zone (according to our experimental results shown in *Section 4.3.4*). Further, in the middle of the capillary, the interface was clearer and the two phases, liquid and supercritical, were more distinguishable, showing annular flow regime in which the liquid phase was the outer phase and the supercritical phase (with ethanol dissolved) was the inner phase. It must also be mentioned

that in the bubbly flow observed when the solution with a 50 wt.% ethanol was the liquid phase, generally the diameter of the droplets decreased when increasing the flow rate, as shown in Figure 6.3. These results agree with Benz et al. (2001), who observed that for the liquid-liquid extraction in micro-mixers, the droplet diameter decreases as the flow rate increases. On the other hand, a flow classification for the scCO<sub>2</sub>-ethanol flow was not made as it was not possible to discern two phases nor an interface.

Table 6.6. Flow patterns observed in the experiments with the Tee-mixer on the flow of scCO<sub>2</sub> with liquid ethanol + water mixtures.

Liquid phase	Flow rate	Inlet	Middle
Water	FR1	Plug flow	Plug flow
	FR2	Parallel flow*	Chaotic thin striations flow
	FR3	Parallel flow	Chaotic thin striations flow
10 wt.% ethanol	FR1	Plug flow	Plug flow
	FR2	Plug flow	Chaotic thin striations flow
	FR3	Chaotic thin striations flow	Chaotic thin striations flow
50 wt.% ethanol	FR1	Wavy flow	Slug/bubbly flow
	FR2	Wavy flow	Bubbly flow
	FR3	Chaotic thin striations flow	Bubbly flow
90 wt.% ethanol	FR1	Annular flow	Annular flow
	FR2	-	Annular flow
	FR3	-	Annular flow

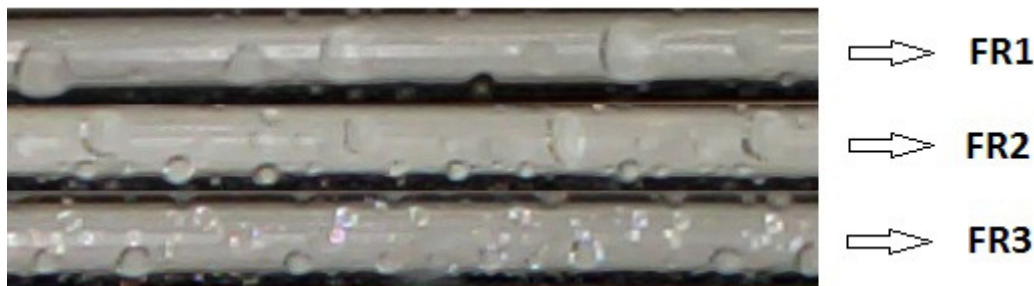



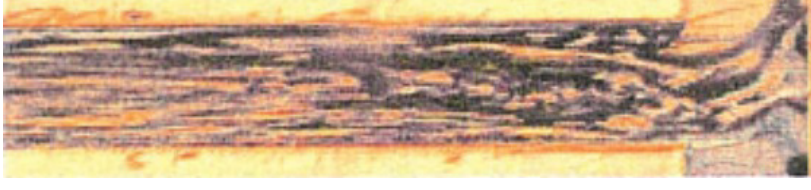






Figure 6.3. Droplet size of liquid phase (with an initial concentration of 50 wt.% ethanol) in scCO<sub>2</sub> at different flow rates.

Table 6.7. Flow patterns observed in our experiments with system A and the Tee-mixer.

---

	(A) Plug flow
	(B) Parallel flow
	(C) Chaotic thin striations flow
	[Chaotic thin striations flow, picture from Zhao et al., 2006]
	(D) Wavy flow
	(E) Slug flow
	(F) Annular flow
	(G) Bubbly flow

---



### 6.1.3. Comparison HPIMM micro-mixer vs. Tee-mixer

By comparing Tables 6.4 and 6.6, it is observed that the flow of  $\text{scCO}_2$  with liquid ethanol-water solutions presented similarities as well as differences when using either the HPIMM micro-mixer or the Tee-mixer. For instance, at the lowest flow rates studied here and when the liquid phase was water or the 10 wt.% ethanol solution, plug flow was observed at the inlet of the capillary in both circumstances, with the difference that the plugs observed with the Tee-mixer have a remarkably shorter length than the plugs formed with the HPIMM micro-mixer. However, when increasing the flow rates, the flow was shifting from plug flow to inverse annular flow with the HPIMM micro-mixer, whereas with the Tee-mixer, the flow shifted from plug flow to chaotic thin striations flow. Moreover, when the liquid phase was a solution with 90 wt.% ethanol, annular flow was observed with both micro-devices. Although the “wavy” annular flow was observed at the inlet only in the experiments with the HPIMM micro-mixer and not in the experiments with the Tee-mixer, as this “liquid lamellae” is typical of the multi-lamination principle slit-shaped micro-mixers.

On the other hand, in the cases when the liquid phase was a 50 wt.% ethanol solution, the fluid behaviour differs the most between the HPIMM micro-mixer and the Tee-mixer: in the case of the HPIMM micro-mixer, “wavy” annular flow was again observed at the inlet of the capillary, just after the mixing, and the flow shifted then to wavy flow through the capillary, as the volume of the liquid phase diminished due to the transfer of ethanol from the liquid to the supercritical phase. Nevertheless, when the Tee-mixer was used for mixing, the wavy flow was observed at the inlet of the capillary and the flow shifted then to bubbly flow in the middle of the capillary.

Furthermore, by comparing the flow behaviour in the capillary after the mixing either in the Tee-mixer or in the HPIMM micro-mixer, it seems that the flow is much more affected by the HPLC pump pulsations when having the Tee-mixer than in the case of the HPIMM micro-mixer. Pulsations were observed in both cases, but in the case of the Tee-mixer, the observed flow was generally more “chaotic”. This might be the reason why chaotic thin striations flow was observed with the Tee-mixer but not with the HPIMM micro-mixer. Besides, this could also explain the fact that the plugs observed in the experiments with the Tee-mixer are shorter than the plugs visualized in the experiments with the HPIMM micro-mixer. It might be

that the inner geometry of the HPIMM micro-mixer helps to slightly buffer the pulse flow. On the contrary, the fact of having a “convergence point” between the Tee-mixer and the capillary, as the diameter decreases from the Tee-mixer (inner diameter: 1mm) to the capillary (inner diameter: 0.5 mm), see *Section 3.1.3*, might result in a more chaotic and unstable flow.

## 6.2. Fluid behaviour of supercritical carbon dioxide with olive oil (system B)

The purpose here was the visualization of the scCO<sub>2</sub> - olive oil flow and the comparison with the flow patterns observed with system A, since the fluid properties of systems A and B differ considerably. The experimental conditions were the same as in the extraction experiments explained in *Section 5.3*, and the olive oil had an acidity of 2.4 wt.%. The flow rates studied in these experiments are given in Table 6.8, only two flow rates were studied for this system. The velocities were estimated using the volume flow rates and the cross section of the capillary. Moreover, the fluid properties of the liquid phase and supercritical phase (scCO<sub>2</sub>) at the experimental conditions are shown in Table 6.9, the values are taken from the discussion in *Section 5.2*. For a better understanding of the process, the fluid properties of the olive oil as well as the fluid properties of the olive oil in equilibrium with the scCO<sub>2</sub> are shown.

**Table 6.8. Flow conditions in the experiments of the system B.**

	Total flow rate (mL/min)	Flow velocity (mm/s)
FR1	5.0	0.42
FR2	10.0	0.84

**Table 6.9. Physical properties of the studied mixtures at the experimental conditions: 150 bar and 40°C.**

Mixture	Density (kg/m <sup>3</sup> )	Viscosity (Pa·s)	Interfacial tension (N/m)
Olive oil	906	$3.4 \cdot 10^{-2}$	$2 \cdot 10^{-3}$
Olive oil in equilibrium with scCO <sub>2</sub>	930	$4.0 \cdot 10^{-3}$	
scCO <sub>2</sub>	780	$6.8 \cdot 10^{-5}$	-

The Reynolds (Re), Capillary (Ca) and Weber (We) numbers in our experiments were calculated and the ranges are shown in Table 6.10. Equations (6.1) – (6.3) were used to

calculate the dimensionless numbers. Due to the significant changes in the density and viscosity of olive oil when it is in equilibrium with scCO<sub>2</sub>, the dimensionless numbers were calculated for both cases (i.e. olive oil as liquid phase, and olive oil in equilibrium with scCO<sub>2</sub> as liquid phase) so the difference in the dimensionless numbers can be known. It is observed in Table 6.10 that the largest differences are observed in the Reynolds and Capillary numbers, as the biggest change is observed in the viscosity (in Table 6.9).

**Table 6.10. Dimensionless numbers in the system B experiments.**

	Liquid			CO <sub>2</sub>		
	Re	Ca	We	Re	Ca	We
Olive oil	0.17 – 0.34	0.22 – 0.44	3.67·10 <sup>-2</sup> – 1.47·10 <sup>-1</sup>	2.36·10 <sup>3</sup> – 4.72·10 <sup>3</sup>	1.40·10 <sup>-2</sup> – 2.80·10 <sup>-2</sup>	33.0 – 132
Olive oil in equilibrium with CO <sub>2</sub>	1.48 – 2.96	2.55·10 <sup>-2</sup> – 5.09·10 <sup>-2</sup>	3.77·10 <sup>-2</sup> – 1.51·10 <sup>-1</sup>	2.36·10 <sup>3</sup> – 4.72·10 <sup>3</sup>	1.40·10 <sup>-2</sup> – 2.80·10 <sup>-2</sup>	33.0 – 132

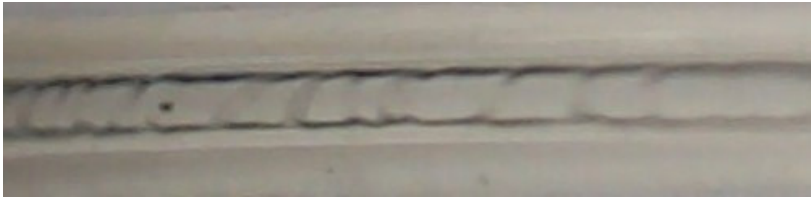

### 6.2.1. Mixing in HPIMM micro-mixer

The flow behaviour of scCO<sub>2</sub>-liquid olive oil in a capillary with an inner diameter of 0.5 mm was investigated. Both supercritical and liquid phases were mixed in the HPIMM micro-mixer and the mixture flowed then through the capillary where the flow was visualized and studied. The classification of the flow patterns observed in the experiments is given in Table 6.11, where inlet and middle refer to the points described before (as shown in Figure 6.1). Moreover, the different flow patterns observed in our experiments are described in Table 6.12. As shown in Table 6.11, in this system and in the studied range, the increase in the flow rate does not affect the flow pattern. The only flow regime observed for the flow of scCO<sub>2</sub> with olive oil mixed by the HPIMM micro-mixer was the annular flow, which at the inlet of the capillary, just after the mixing, is very “wavy” (see Table 6.12 (A)) and then became smoother along the capillary. As explained above in *Section 6.1.1.*, this “wavy” annular flow is a very characteristic orientation of liquid lamellae of multi-lamination slit-shaped micro-mixers, as described Hardt and Schönfeld (2003). This flow was previously observed in some cases of system A.

Table 6.11. Flow patterns observed in the experiments with the HPIMM mixer on the flow of scCO<sub>2</sub> with olive oil.

Liquid phase	Flow rate	Inlet	Middle
Olive oil	FR1	“Wavy” annular flow	Annular flow
	FR2	“Wavy” annular flow	Annular flow

Table 6.12. Flow patterns observed in our experiments with system B and the HPIMM micro-mixer.

	(A) “Wavy” annular flow
	(B) Annular flow

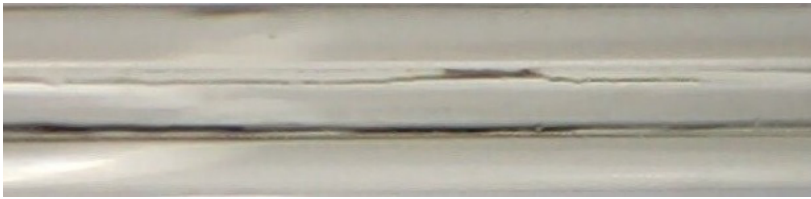


### 6.2.2. Mixing in Tee-mixer

The results presented here show the flow behaviour of scCO<sub>2</sub> and olive oil in a capillary with an inner diameter of 0.5 mm after mixing in a Tee-mixer. The classification of the flow patterns experimentally observed is shown in Table 6.13. Moreover, the different flow patterns visualized are described in Table 6.14. In the experiments with system B and the Tee-mixer only annular flow was observed with the remark that, droplets flowing simultaneously with the annular flow were observed at the inlet of the capillary (see Table 6.14 (B)). It must be pointed out that, due to the HPLC pulsations, the flow was not continuous (as explained above), which means that the annular flow was not observed continuously but intermittently. Furthermore, in the middle of the capillary, when the annular flow was not appearing, some olive oil droplets were flowing through the capillary instead, as Table 6.14 (C) shows.

Table 6.13. Flow patterns observed in the experiments with the Tee-mixer on the flow of scCO<sub>2</sub> with olive oil.

Liquid phase	Flow rate	Inlet	Middle
Olive oil	FR1	Annular flow with droplets	Annular flow
	FR2	Annular flow with droplets	Annular flow

Table 6.14. Flow patterns observed in our experiments with system B and the Tee-mixer.

	(A) Annular flow
	(B) Annular flow with droplets
	(C) Small droplets

### 6.2.3. Comparison HPIMM micro-mixer vs. Tee-mixer

When Tables 6.11 and 6.13 are compared, it is observed that the flow of  $\text{scCO}_2$  and olive oil in a capillary does not present major differences when the phases are mixed either in the HPIMM micro-mixer or in the Tee-mixer. The main difference observed between the two micro-devices is that the “wavy” annular flow was only visualized in the experiments with the HPIMM micro-mixer because, as modelled and explained by Hardt and Schönfeld (2003), this liquid lamellae behaviour is characteristic of slit-shaped micro-mixers. On the other hand, droplets were observed only in the experiments that the phases were mixed in the Tee-mixer. The droplets were visualized in two cases: simultaneously with the annular flow (in the inlet of the capillary), or in the middle of the capillary during time intervals in which annular flow was not appearing because of the pulsations of the HPLC pump. However, besides these differences, the flow regime prevailing in the flow of  $\text{scCO}_2$  with olive oil was the annular flow.

## 6.3. Comparison of the fluid behaviour of system A and system B

By comparing the fluid behaviour of system A and B, the first observation was that although the different dimensionless numbers ranges for the supercritical phase are similar (mainly for  $Re$  and  $We$  numbers), the values for the liquid phases differ remarkably. If Tables 6.3 and 6.10 are compared, it is seen that the Reynolds numbers for the olive oil phase are

remarkably lower in comparison to the Reynolds numbers for the different liquid phases studied in system A. On one hand, this is because the flow velocities studied in system B are slightly smaller than in system A (as seen in Tables 6.1 and 6.8); but on the other hand this difference is principally because of the remarkably higher viscosity of olive oil in comparison with the different liquid phases considered in system A. This difference in the viscosity leads not only to different ranges of Reynolds but also of Capillary number in the liquid phases, as observed when comparing Tables 6.3 and 6.10. Moreover, regarding the interfacial tension between the liquid phase and the scCO<sub>2</sub> phase, in system A, only the liquid phases of 90 wt.% ethanol and the (pure) ethanol present similar values to olive oil at the experimental conditions studied here.

Annular flow was the main flow regime observed in system B, which was also observed in system A, but only in the middle of the capillary and with the 90 wt.% ethanol liquid phase (which also presents a very low interfacial tension with the scCO<sub>2</sub>). Therefore, by comparing the Weber numbers of both phases (liquid and supercritical) for these two different cases, olive oil and 90 wt.% ethanol, it can be considered that both ranges are pretty similar. This fact, together with the dimensionless number ranges of both liquid and supercritical phases in each system led us to conclude that among the different forces, the surface tension (or interfacial tension between the phases) is one of the main factors to define the flow pattern regime in the capillary.

## 7. CFD modelling of the multiphase flow of supercritical carbon dioxide and liquid mixtures

For a better understanding of the mixing process of supercritical fluids with liquids, CFD was used to model the flow of  $\text{scCO}_2$  and liquid mixtures when they are mixed in a Tee-mixer, as well as the mass transfer of alcohol from the liquid to the supercritical phase. The model explained here was performed by Prof. Ricardo Santos and his research group from the University of Porto, Portugal, in collaboration with our project.

As pointed out previously in *Chapters 3 and 6*, the micro-devices used in this work are made of stainless-steel. Therefore the visualization of the mixing and the fluid behaviour inside the micro-devices was not possible. Thus, the model developed and described here helped us to have a better comprehension of the mixing step in the Tee-mixer studied here.

### 7.1. CFD model of the flow behaviour

#### 7.1.1. 3D domain

A 3D Tee-mixer with a similar cylindrical geometry to the one used in our experiments was made for the CFD simulations of water and  $\text{scCO}_2$  mixing. The inner diameter of the jets was kept as in our experiments: 1 mm. The dimensions considered for the length of the jets are  $L_1 = 14.5$  mm and  $L_2 = 10$  mm (see Figure 7.1). The mesh data are collected in Tables 7.1 - 7.4. The computational grids (Figure 7.2) consisted of tetrahedral and hexahedral cells with different sizes and a spatial discretization  $\Delta x \leq 65\mu\text{m}$ . The geometrical domain and simulation grid were generated with the software packages *DesignModeler* and *Meshing* included in Ansys 17 suite.

Table 7.1. Mesh domain extents.

	x-coordinate	y-coordinate	z-coordinate
Minimum (m)	-5e-04	-5e-04	0
Maximum (m)	5e-04	1.5e-02	1e-02

Table 7.2. Mesh size.

Level	Cells	Faces	Nodes	Partitions
0	505726	1155647	196131	2

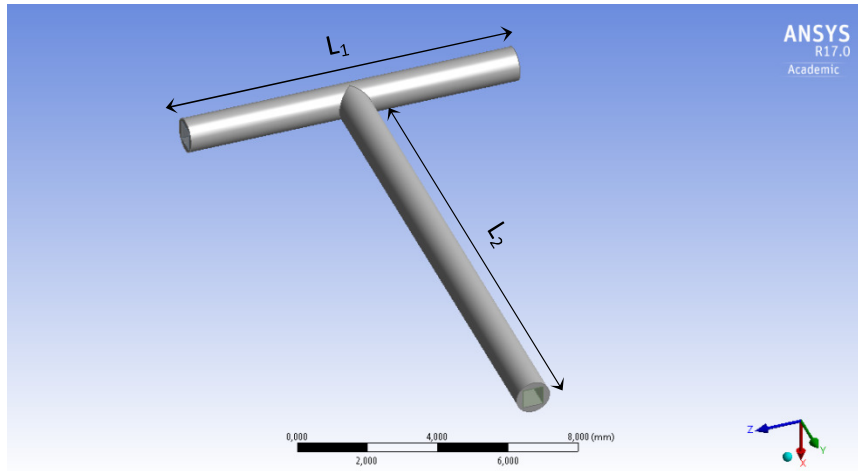


Figure 7.1. Mesh geometry used for CFD simulations.

Table 7.3. Mesh volume statistics.

Minimum volume (m <sup>3</sup> )	6.6e-16
Maximum volume (m <sup>3</sup> )	2.8e-13
Total volume (m <sup>3</sup> )	1.9e-08

Table 7.4. Mesh face area statistics.

Minimum face area (m <sup>2</sup> )	1.2e-10
Maximum face area (m <sup>2</sup> )	5.6e-09

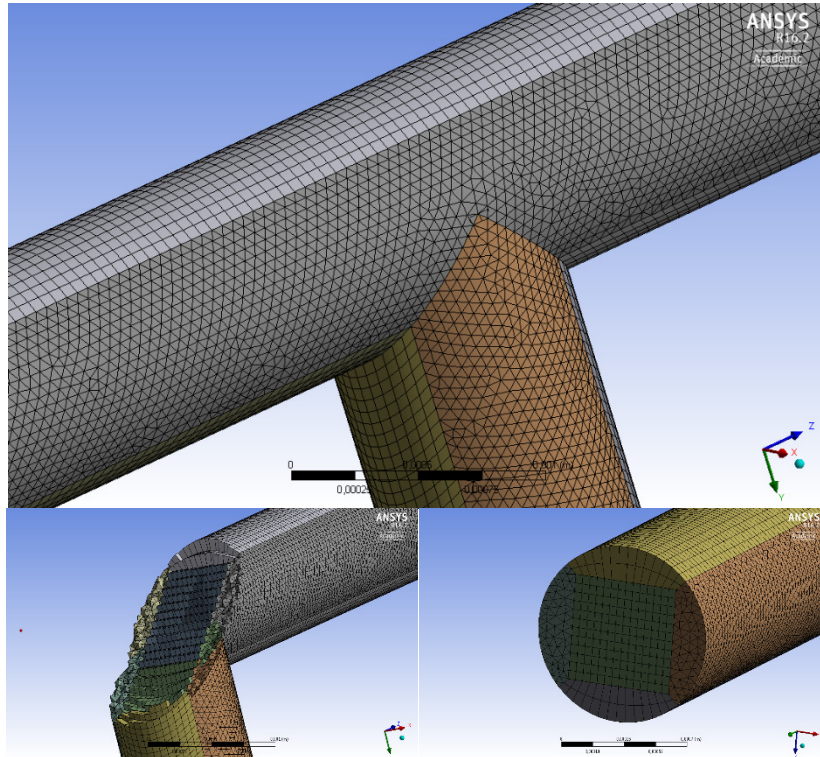


Figure 7.2. Simulation grid.



### 7.1.2. VOF model

In a first step, due to the available experimental data on the mixing of water and scCO<sub>2</sub> in literature (Ogden et al. 2014; Knaust et al. 2015), the mixing of this binary system was modelled at the experimental conditions of our extraction experiments (i.e. 101 bar and 60 °C). The VOF (Volume of Fluid) model was chosen to simulate the multiphase flow pattern of water and scCO<sub>2</sub> in a Tee-mixer. This model can be used for two or more immiscible fluids and allows tracking the volume fraction of each of the fluids throughout the domain. The volume fraction is denoted as  $\alpha_q$ , for fluid  $q$ . A value of  $\alpha_q=1$  denotes that a cell (a finite volume in the discretized domain) is full of fluid  $q$ ; on the other hand, a value of  $\alpha_q=0$  denotes that the cell is empty of fluid  $q$ . When the cell contains the interface between the fluid  $q$  and one or more fluids,  $\alpha_q$  assumes a value  $0 < \alpha_q < 1$ , depending on the amount of each phase present in that finite volume. Moreover, the primary-phase volume fraction is computed based on the constraint  $\sum_{q=1}^n \alpha_q = 1$ . Thus, as a binary system was simulated in this case, the volume fraction of Phase 1 (scCO<sub>2</sub>),  $\alpha_1$ , is obtained using the constraint  $\alpha_1 = 1 - \alpha_2$ .

The tracking of the interfaces is solved by a continuity equation (Equation (7.1)) for the volume fraction of the phases. In our case, as mass transfer does not occur, the equation for a  $q^{th}$  phase is as follows:

$$\frac{1}{\rho_q} \left[ \frac{\partial}{\partial t} (\alpha_q \rho_q) + \nabla \cdot (\alpha_q \rho_q \vec{v}_q) \right] = 0 \quad (7.1)$$

The VOF model solves a single momentum equation (Equation (7.2)) throughout the domain, dependent on the volume fraction of all phases through the properties  $\rho$  and  $\mu$ , shown below:

$$\frac{\partial}{\partial t} (\rho \vec{v}) + \nabla \cdot (\rho \vec{v} \vec{v}) = -\nabla p + \nabla \cdot [\mu (\nabla \vec{v} + \nabla \vec{v}^T)] + \rho \vec{g} + \vec{F} \quad (7.2)$$

The physical properties used in the simulation to define each phase are collected in Table 7.5, close to the properties discussed previously in Section 4.2. The interfacial tension between the two phases was assumed to be 29 mN/m.

Table 7.5. Physical properties of each phase.

	Phase 1 (scCO <sub>2</sub> )	Phase 2 (water)
Density (kg/m <sup>3</sup> )	299	998.2
Viscosity (Pa·s)	2.4e-05	1.003e-03
Inlet velocity (m/s)	0.21	0.01

In our case, Equation (7.1) is solved for the following boundary conditions at the inlets:

$$\begin{cases} \alpha_1 = 1; \alpha_2 = 0 & \text{at the inlet 1} \\ \alpha_1 = 0; \alpha_2 = 1 & \text{at the inlet 2} \end{cases}$$

Table 7.6 shows the Solution Methods chosen for the simulations. In order to shorten the time of the CFD simulation, the channel of inlet 2 was completely filled with water as initial condition. All the CFD simulations of the mixing of scCO<sub>2</sub> and water in a Tee-mixer are summarized in Table 7.7.

Table 7.6. Simulation Solution Methods

Pressure-Velocity Coupling			
Scheme	Simple		
Spatial Discretization			
Gradient	Least Squares based	Squares	Cell
Pressure	PRESTO!		
Momentum	Third-Order MUSCL		
Volume Fraction	Geo-Reconstruct		

Table 7.7. Summary of simulations of the mixing of scCO<sub>2</sub> and water in a Tee-mixer using VOF model.

Simulation	Wall adhesion (contact angle)	Time step size	Max iteration/time step
TSCa	Not set	1e-05	10
TSCb	90°	1e-05	10
TSCc	20°	1e-05	20
TSCd	20°	1e-06	10
TSCe	160°	1e-05	100

Figures 7.4a and 7.4b show the results from simulation TSCa, in which liquid water enters the Tee-mixer at Inlet 2 (left side), whereas the  $\text{scCO}_2$  enters at Inlet 1 (right side). In the figure, the volume fraction of Phase 1 is represented in a contour of the plane YZ of the physical domain. The contour map (the colour scale is at the top left corner of the figure) shows the colour legend to identify the value of the volume fraction of Phase 1 throughout the contour plane represented. The blue colour means that the Phase 1 volume fraction is 0, therefore no  $\text{scCO}_2$  is present at Inlet 2. Contrary, the red colour represents the Phase 1 volume fraction value of 1. The green colour shows an isosurface used to identify the interphase between the water and the  $\text{scCO}_2$  phases. As seen in the figures, in this isosurface the volume fraction of Phase 1 is 0.5 (and therefore the volume fraction of Phase 2 is also 0.5), hence the interphase area is defined. By focusing on the interphase in Figures 7.4a-b, it is observed that the water forms a droplet as it enters the mixing chamber and this droplet flows through the mixing chamber. In this simulation, the wall adhesion was not set, what means that ANSYS takes automatically  $90^\circ$  as contact angle. In any manner, the case TSCb was simulated setting a water contact angle of  $90^\circ$  so it was confirmed that the results were the same, as it is seen by comparing Figures 7.4a-7.4b to Figure 7.5, where the cylindrical shape of the droplets in both cases is clear and equal. On the other hand, Figures 7.6a-d and 7.7a-b show the results of the simulation TSCc, in which the wall adhesion was  $20^\circ$ . In this simulation, it is seen how the water phase forms a liquid film on the channel wall instead of droplets. In Figure 7.6a-b the flow is shown from the opposite perspective, so it is clearly observed how the thin water film flows on the channel wall. Therefore, according to these results, the wall adhesion has a big influence on the flow of the both phases in the Tee mixing channel, since by changing only the contact angle, the flow shifted from slug flow (with distinct droplets) to annular flow.

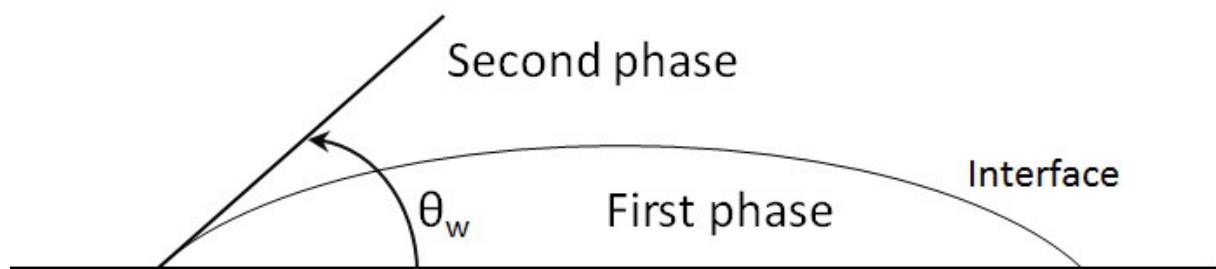


Figure 7.3. Schematic illustrating the contact angle.

Figure 7.8 shows the results from simulation TSCd, in which the wall adhesion set was the same as in simulation TSCc, but in TSCd the time step size was smaller ( $1e-06$  instead of  $1e-05$ ), and the maximum number of iterations per time step was decreased from 20 to 10. If Figure 7.8 is compared to Figures 7.6 and 7.7, it is observed that the results from simulations TSCc and TSCd are the same, though the time step size and number of the iterations were varied.

Further, another simulation with a contact angle higher than  $90^\circ$  was run. Figures 7.10a-b show the results from the simulation TSCe, in which the wall adhesion was set to  $160^\circ$ . It is observed that in TSCe the water phase again forms droplets when mixing with the  $scCO_2$  phase. However, when comparing carefully the droplets formed in simulation TSCa and in simulation TSCe, differences were observed. In Figure 7.9, the droplets from simulations TSCa and TSCe are enlarged for a better comparison. It is seen that the shape of both droplets is different: while the droplet from simulation TSCa presents a flat interphase, the droplet from TSCe has a spherical shape. This led us to conclude that changes in the wall adhesion may not only cause changes in the flow, but can also define the shape of the droplets in the cases in which there is droplet formation. In Figure 7.3, the explanation of the contact angle is illustrated. It is shown that the contact angle is smaller than  $90^\circ$  (for instance  $20^\circ$ , as in simulation TSCd), this means that the wall has a better affinity to the water phase (Phase 2) than to the  $CO_2$  phase (Phase 1). On the other hand, when the wall adhesion is set with a contact angle larger than  $90^\circ$  (for instance,  $160^\circ$  as in simulation TSCe), the affinity of the wall with the  $CO_2$  phase is better than with the water phase. Therefore, in the simulation TSCe, the water droplet had a more spherical shape, since due to the affinity of the wall with the  $CO_2$ , the latter was “surrounding” the water phase, i.e. the water droplet.

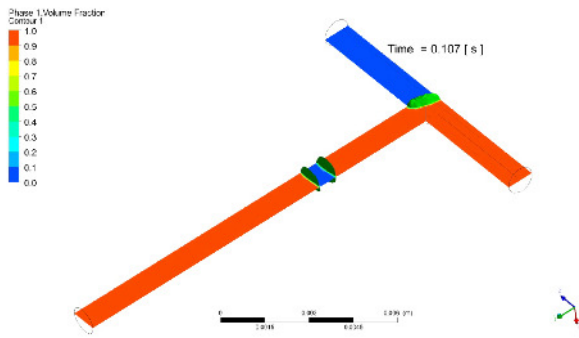


Figure 7.4a. Simulation TSCa (t = 0.107 s).

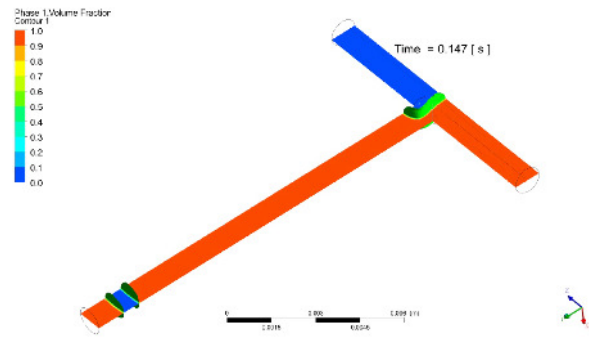


Figure 7.4b. Simulation TSCa (t = 0.147 s).

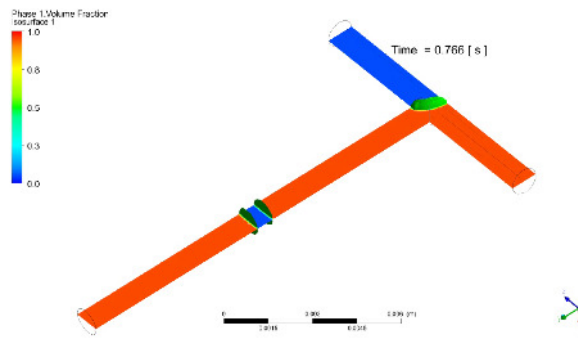


Figure 7.5. Simulation TSCb (t = 0.766 s).

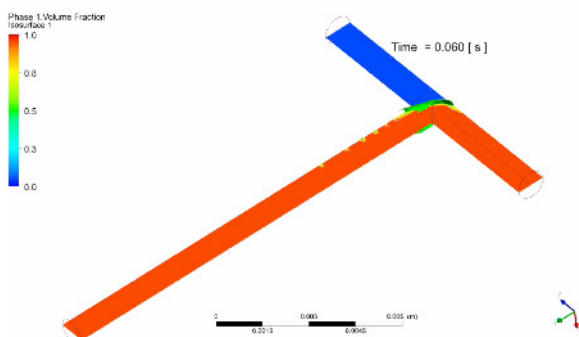


Figure 7.6a. Simulation TSCc (t = 0.060 s).

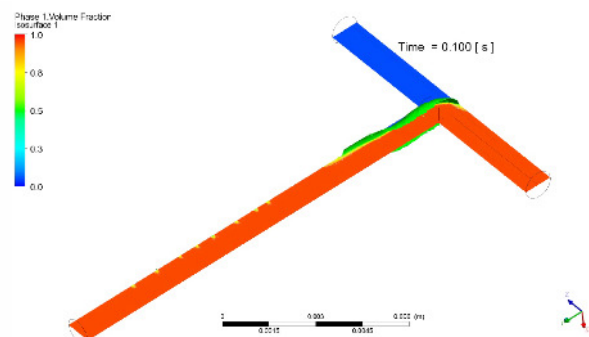


Figure 7.6b. Simulation TSCc (t = 0.100 s).

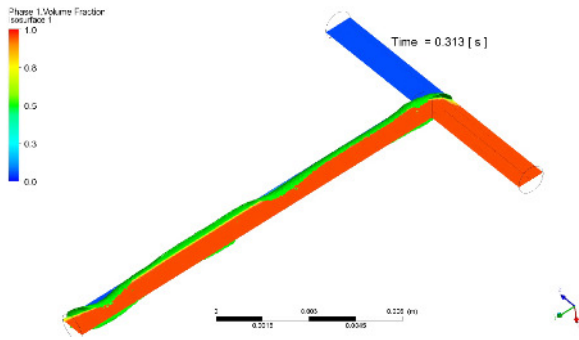


Figure 7.6c. Simulation TSCc (t = 0.313 s).

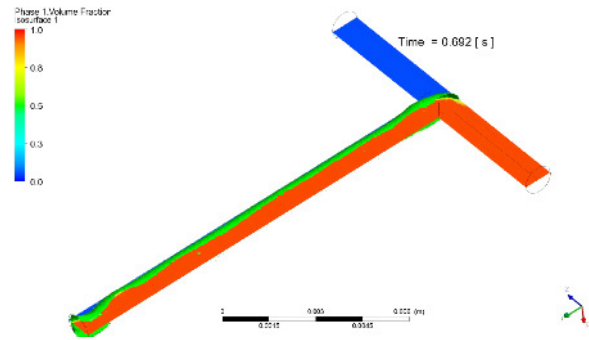


Figure 7.6d. Simulation TSCc (t = 0.692 s).

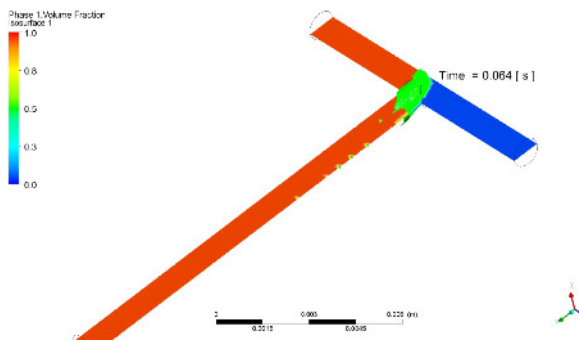


Figure 7.7a. Simulation TSCc from another perspective.

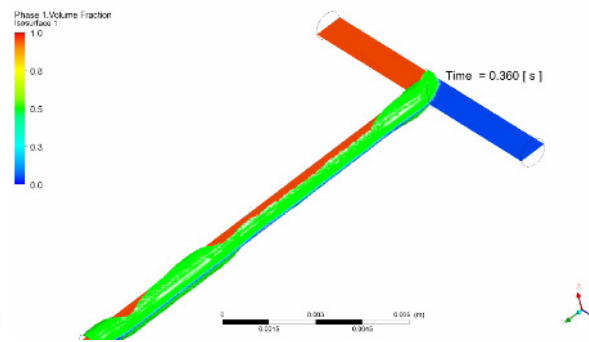


Figure 7.7b. Simulation TSCc from another perspective.

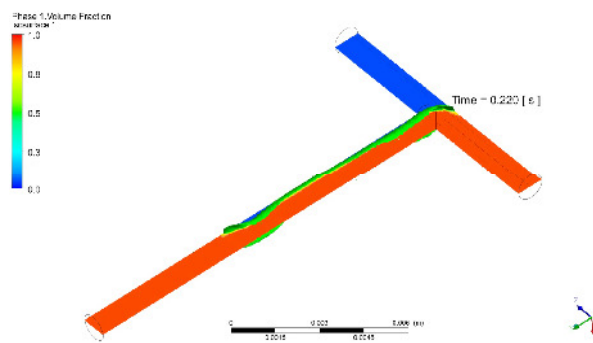


Figure 7.8. Simulation TSCd (t = 0.220 s).

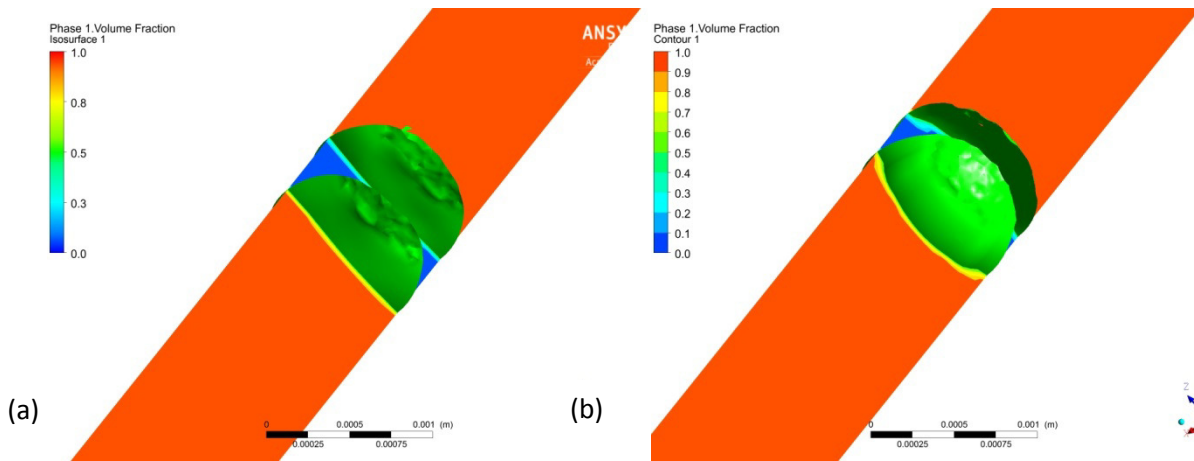


Figure 7.9. Droplet of water in scCO<sub>2</sub> from simulation TSCa (a), on the left side, and simulation TSCe (B), on the right side.

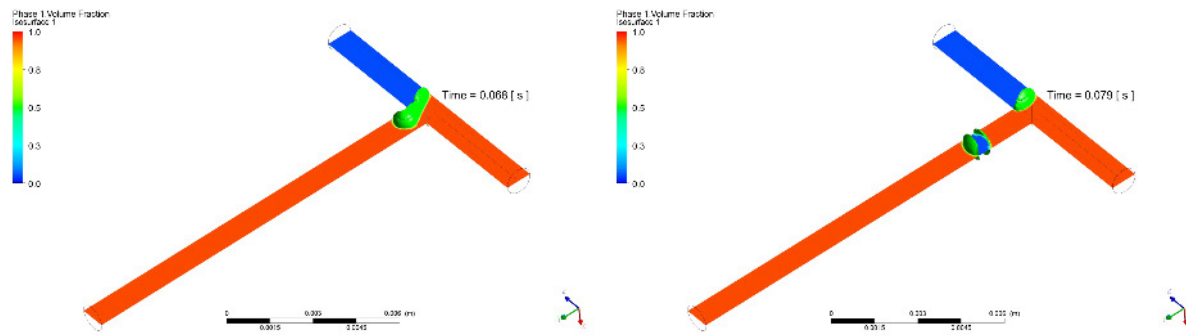


Figure 7.10a. Simulation TSCe (t = 0.068 s).

Figure 7.10b. Simulation TSCe (t = 0.079 s).

## 7.2. CFD model of the mass transfer

After simulating the flow behaviour of scCO<sub>2</sub> and water in a Tee-mixer and validating the results, the modelling of the mass transfer was the next step. Here, the mass transfer of ethanol from water (Phase 2) to scCO<sub>2</sub> (Phase 1) in a Tee-mixer was simulated. The 3D domain used was the same as for the simulations of the flow behaviour (see Figures 7.1-7.2 and Tables 7.1-7.4). For the modelling of the mass transfer, the Eulerian multiphase model was chosen. As it is observed in Figure 7.11, the Eulerian multiphase flow can be modelled in ANSYS Fluent using and combining different models or equations. In this work, the mass transfer was initially simulated applying the Eulerian-Eulerian approach.

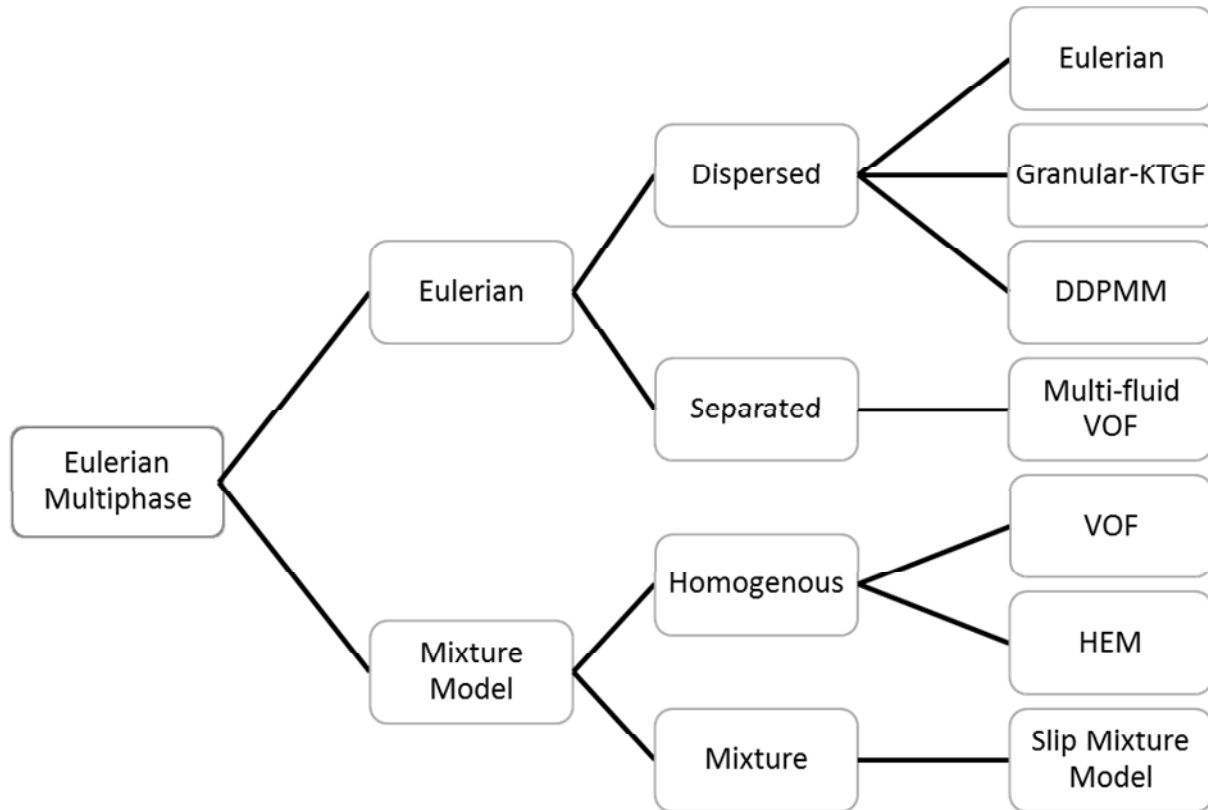


Figure 7.11. Modelling strategies in ANSYS Fluent for the Eulerian multiphase flow.

### 7.2.1. Eulerian-Eulerian model

This model allows the modelling of multiple separate, interacting phases. In the Eulerian-Eulerian mode, momentum and continuity equations are solved for each of the phases. For the case studied here, a fluid-fluid multiphase flow, the equations for the general case of a  $n$ -phase flow are given in Equations (7.3) and (7.4).

Continuity equation:

$$\frac{1}{\rho_{rq}} \left( \frac{\partial}{\partial t} (\alpha_q \rho_q) + \nabla \cdot (\alpha_q \rho_q \vec{v}_q) = \sum_{p=1}^n (\dot{m}_{pq} - \dot{m}_{qp}) \right) \quad (7.3)$$

Fluid-fluid momentum equation:

$$\begin{aligned} \frac{\partial}{\partial t} (\alpha_q \rho_q \vec{v}_q) + \nabla \cdot (\alpha_q \rho_q \vec{v}_q) = & -\alpha_q \nabla p + \nabla \cdot \bar{\tau}_q + \alpha_q \rho_q \vec{g} \\ & + \sum_{p=1}^n (K_{pq} (\vec{v}_p - \vec{v}_q) + \dot{m}_{pq} \vec{v}_{pq} - \dot{m}_{qp} \vec{v}_{qp}) \\ & + (\vec{F}_q + \vec{F}_{lift,q} + \vec{F}_{wl,q} + \vec{F}_{vm,q} + \vec{F}_{td,q}) \end{aligned} \quad (7.4)$$



Where:

$\dot{m}_{pq}$	characterizes the mass transfer from the $p^{th}$ to the $q^{th}$ phase
$\bar{\tau}_q$	is the stress-strain tensor
$K_{pq}$	is an interphase momentum exchange coefficient
$\vec{F}_q$	represents an external body force
$\vec{F}_{lift,q}$	is a lift force
$\vec{F}_{wl,q}$	represents a wall lubrication force
$\vec{F}_{td,q}$	is a turbulence dispersion force

Furthermore, the mass transfer coefficient (noted as  $k_{pq}$ ) can be modelled in ANSYS Fluent either as a constant, as a user-defined function, or as a function of the Sherwood number. This latter was the option chosen here. The Sherwood number (Sh) is a dimensionless number, used in mass transfer operation, and can be defined as the ratio of convective to diffusive mass transfer, as shown in Equation (7.5), where  $L$  is the characteristic length (m),  $D$  represents the mass diffusivity ( $m^2/s$ ) and  $k$  is the mass transfer coefficient (m/s).

Two different simulations on the mass transfer of ethanol from water to  $scCO_2$  were run using the Eulerian-Eulerian model. As Table 7.8 shows, in both simulations, the initial mass fraction of ethanol in Phase 2 (liquid phase) was the same: 0.1; while the Sherwood number and the inlet velocity of Phase 2 were varied in order to test the importance of the diffusion rate in the bubble formation of the liquid phase. The results of both TSCf and TSCh simulations were pretty similar and are shown in Figures 7.12a-b and 7.13a-b. In these figures, the colour legend (located at the top left corner of the figures) shows the values of the ethanol mass fraction of Phase 1 throughout the contour plane represented. The blue colour means that the ethanol mass fraction in Phase 1 is 0. Again, the green colour shows an isosurface used to identify the interphase between the liquid (water+ethanol) and the  $scCO_2$  phases.

$$Sh = \frac{kL}{D} = \frac{\text{Mass transfer}}{\text{Diffusion rate}} \quad (7.5)$$

Table 7.8. Summary of simulations of the mass transfer of ethanol from water to scCO<sub>2</sub> in a Tee-mixer using the Eulerian model.

Simulation	Wall adhesion (contact angle)	Time step size	Max iteration/time step	Sh	Phase 2	
					Inlet velocity (m/s)	Initial EtOH mass fraction
TSCf	160°	1e-05	20	2	0.01	0.1
TSCh	160°	1e-05	20	1	0.02	0.1

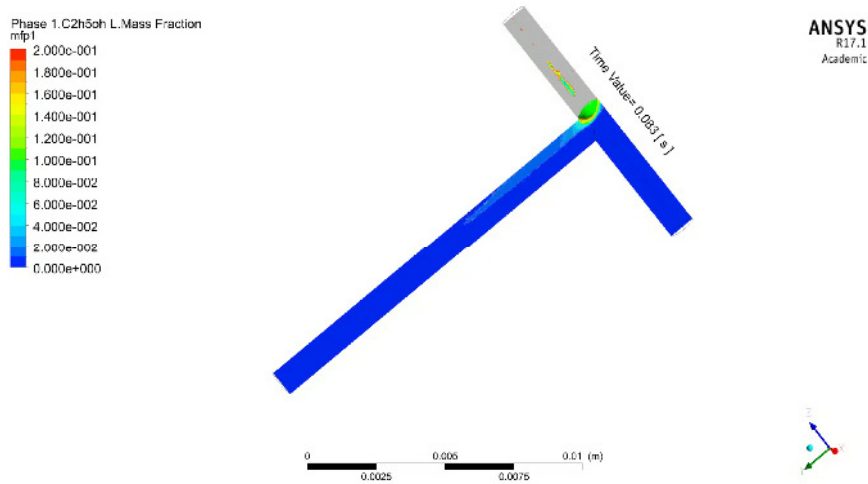


Figure 7.12a. Simulation TSCf (t = 0.083 s).

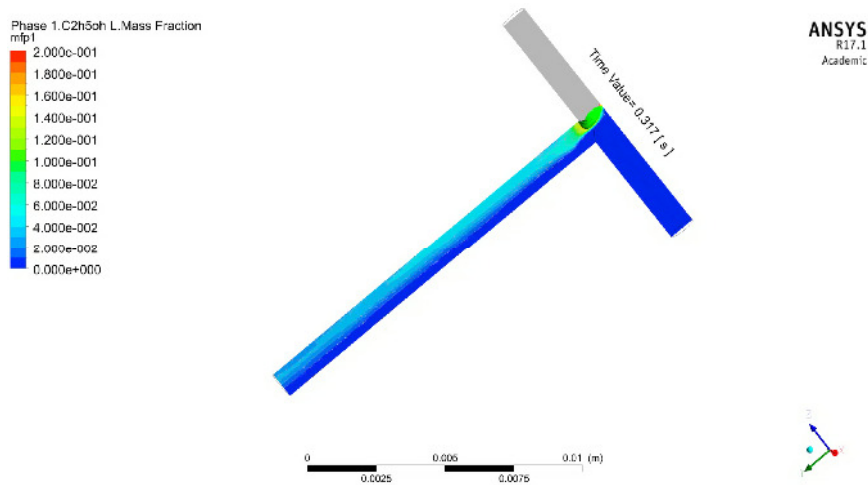


Figure 7.12b. Simulation TSCf (t = 0.317 s).

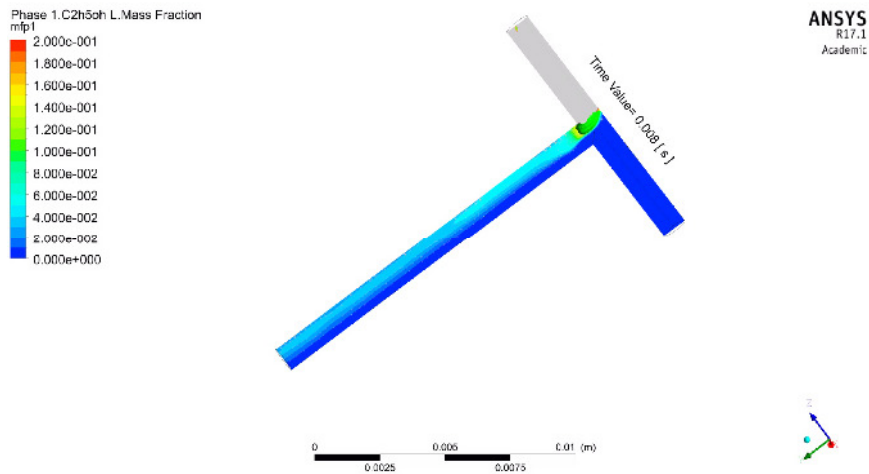


Figure 7.13a. Simulation TSCh (t = 0.008 s).

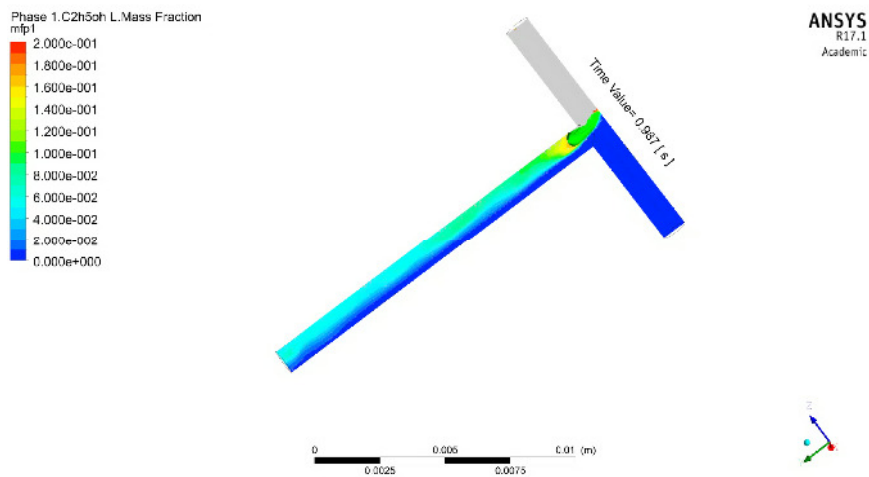


Figure 7.13b. Simulation TSCh (t = 0.987 s).

It is seen that in both simulations, as soon as Phase 2 gets into contact with Phase 1 in the mixing chamber, the first one diffuses completely into the latter one and no interface is further observed. These results proved therefore that the mass transfer of ethanol from water to  $\text{scCO}_2$  could not be successfully simulated using the Eulerian-Eulerian model, due to the excessive numerical diffusion affecting the mass transfer between the two phases.

### 7.2.2. Eulerian model with Multi-fluid VOF

According to the ANSYS Fluent Theory Guide, the multi-fluid VOF model provides a framework to couple the VOF and Eulerian multiphase models. Due to the good performance of the VOF model to simulate the flow behaviour of the  $\text{scCO}_2$ -water system and, as the Eulerian-Eulerian model did not provide reliable results for the mass transfer modelling, it was

decided that the next step here would be the simulation of the mass transfer of ethanol from water to scCO<sub>2</sub> by combining the Eulerian multiphase model with the multi-fluid VOF model. For the interface tracking, the Geo-Reconstruct scheme was selected. This scheme tracks the interface based on geometrical information and is the most accurate. Regarding the mass transfer, the Two-Resistance model was chosen, which models the species mass transfer based on equilibrium at the phase interface. This model considers separate mass transfer processes with different mass transfer coefficients on either sides of the phase interface, as Figure 7.14 shows. Therefore, in this work, the mass transfer from the FROM-phase (Phase 2) to the interface was calculated using the Ranz-Marshall model, whereas for the mass transfer from the interface to the TO-phase (Phase 1) the zero-resistance condition was specified. The Ranz-Marshall model is a correlation for the calculation of the Sherwood number as a function of the Reynolds and the Schmidt numbers (see Equation (7.6)). On the other hand, the zero-resistance condition implies that the species transport across the interface is instantaneous and therefore equilibrium conditions prevail at the phase interface at all times.

Although only preliminary results from this simulation (TSCi) can be shown here, as the simulation was still running at the moment this chapter was written, it seems like results are promising.

In Figures 7.15a-b, the first results from the simulation TSCi are shown. It is observed that some aspects have been improved in comparison with simulations TSCf and TSCh from Section 7.2.1. First of all, still both phases are distinguished after they get into contact in the mixing chamber. Moreover, the ethanol mass transfer can be observed in Phase 1, in the vicinity of the interface. These preliminary results show that the Eulerian model combined with the multi-fluid VOF model might be appropriate for modelling the mass transfer of ethanol from water to scCO<sub>2</sub>. Therefore, more simulations and a deeper study will be performed following this research line.

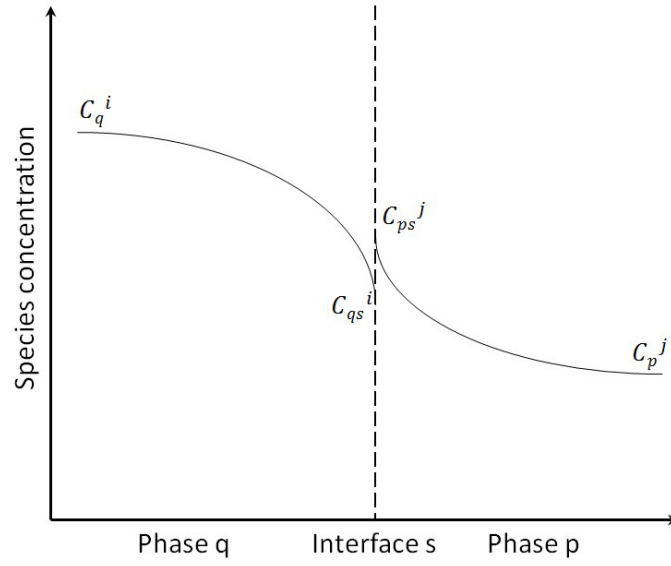


Figure 7.14. Distribution of molar concentration in the Two-Resistance Model.

$$Sh_q = 2 + 0.6Re_q^{1/2} Sc_q^{1/3} \quad (7.6)$$

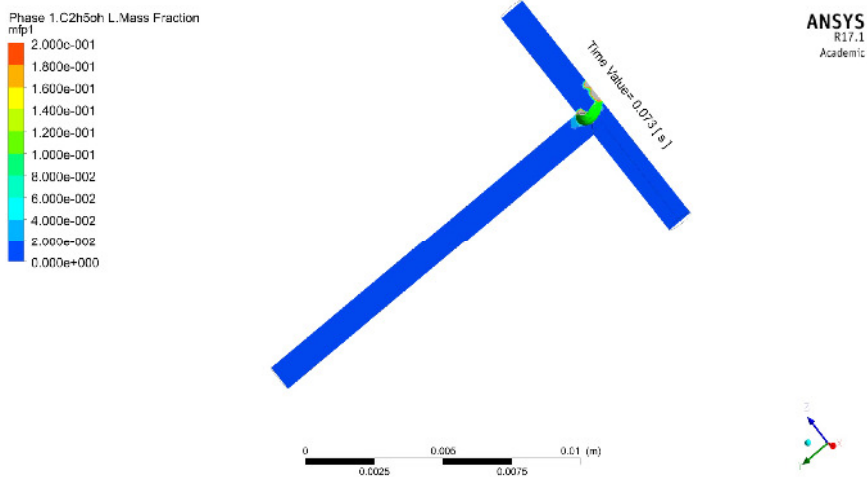


Figure 7.15a. Simulation TSCi (t = 0.073 s).

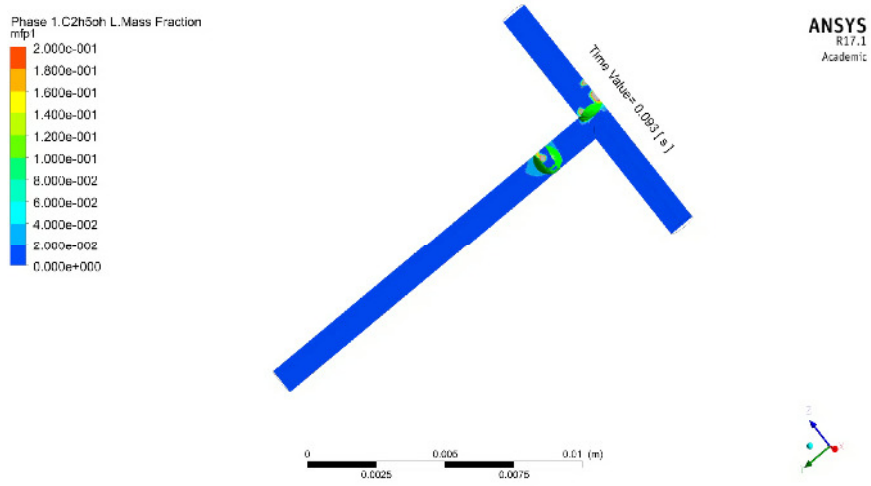


Figure 7.15b. Simulation TSCi (t = 0.093 s).

## 8. Conclusions, remarks and outlook

### 8.1. Conclusions

The applicability, feasibility and efficiency of micro-mixers for SFE and SFF processes have been investigated in this work. Two different extraction processes were tested in the high-pressure micro-mixer apparatus designed for this purpose: the extraction of ethanol from aqueous solutions and the deacidification of olive oil, both by  $\text{scCO}_2$ . Two different mixing principles were studied: T-type lamination and multilamination principles. The Peng-Robinson EoS has been demonstrated to be a good choice for the modelling of phase equilibria mixtures with  $\text{scCO}_2$ : this EoS has been used here for the prediction of the two systems under study, and has shown very good results and accurate predictions, especially for the liquid phase. In the extraction of ethanol from aqueous solutions by  $\text{scCO}_2$ , different factors (feed concentration; solvent flow rate and Solvent-to-Feed ratio; length of the capillary placed between the micro-mixer and separator; and overall flow rate) were considered and their influence on the extraction performance and efficiency was investigated. The experimental results confirmed that thermodynamic equilibrium could be reached through the extraction process when having different feed ethanol concentrations as well as Solvent-to-Feed ratios. Nevertheless, the study of the capillary length showed that at the longest length under study (i.e. 650 mm), the extraction results worsen. These experiments confirmed that the thermodynamic equilibrium is reached in the micro-mixer and therefore the extraction cannot be enhanced by increasing the capillary length, on the contrary, the separation achieved worsens. Regarding the study on the influence of the total volume flow rate, changes in the *K-factor* were observed when using a feed of 50wt.%: the *K-factor* decreased as the total volume flow increased. Nevertheless, for the feed concentrations of 10wt.% and 90wt.% of ethanol, no significant changes were observed as the total flow rate was increased. Further on, experiments on the deacidification of olive oil were carried out and the results proved that equilibrium could be achieved as well at distinct physical properties and therefore hydrodynamics conditions. It was proved that one micro-mixer can be equivalent of a theoretical extraction stage. Moreover, by comparing the results obtained with both mixing principles studied here, it was concluded that the extraction results were not influenced by the mixing principle.

Nevertheless, the mixing principle as well as the physical properties was found to influence the flow behaviour of the fluids through the mixing process and in the capillary. The multiphase flow behaviour of scCO<sub>2</sub> with different liquid mixtures (ethanol-water mixtures and olive oil) in a capillary placed at the outlet of the micro-mixer was observed. In the mixing of scCO<sub>2</sub> with ethanol-water mixtures, even at the same pressure and temperature conditions, different flow patterns were observed when varying the ethanol concentration of the liquid mixture. This was attributed to that physical properties such as density, viscosity and, more importantly, interfacial tension change with the ethanol concentration.

Regarding the CFD simulations, the VOF model provided good results for the modelling of the flow behaviour of scCO<sub>2</sub> and water. The contact angle was found to be a key factor in this model. However, the results were validated and the model was confirmed to be precise: according to Egger and Jaeger (1994), contact angle values of 90°, 135° and 165° were measured at the pressure of 60, 180 and 250 bar, respectively, and temperature of 40 °C, for the CO<sub>2</sub>-water system. This confirms that the contact angle of our system is higher than 90° and therefore, according to the CFD model, the flow must be a plug flow (or in other words, a big droplet of water is formed in the mixing chamber). These results were in accordance with our experimental results on the visualization of the flow of scCO<sub>2</sub>-water system, as shown in *Section 6.1.2*. Furthermore, the mass transfer of ethanol from water to scCO<sub>2</sub> was also studied using CFD. The Eulerian-Eulerian method was found not to be suitable for this purpose. However, promising results were obtained by combining the Eulerian model with the Multi-flow VOF model. Nevertheless, further work is required to improve this model.

To summarize, very satisfactory extraction results were obtained, as it was confirmed that one theoretical stage could be achieved with both micro-mixers in the extraction of both systems under study. Therefore, the choice between these two mixing principles for SFF purposes seems to be trivial. Moreover, the influence of the hydrodynamics on the extraction process was investigated by varying physical properties of the fluids, and flow rates. Practically in every experiment performed, good extraction performance was observed. This work concludes that the use of micro-mixers for SFE and SFF is a competitive alternative to current processes, as the extraction can be achieved in much smaller volumes and shorter time. Thus, the use of micro-mixers for SFF can be applied at short-term for the investigation



at lab scale of new extraction systems, mixtures or processes as well as for the determination of extraction conditions and some others experimental factors.

## 8.2. Remarks

During the course of this research study, some issues have arisen and several assumptions have been taken which are worthy of mention:

- As described in *Section 3.1.1*, in the experimental setup, the liquid CO<sub>2</sub> is pumped by a HPLC pump, which is actually designed to pump liquids. Thus, in order to ensure that the CO<sub>2</sub> was in liquid state when pumped, a special cooling device was coupled to the HPLC pump head. However, when the flow rate set in the pump was close to its limit (i.e. 10 mL/min), it was very difficult to keep the low temperature in the head pump due to the heat generated by the friction of the piston. As a consequence, the CO<sub>2</sub> flow rate was not completely constant in some experiments. Even so, as the CO<sub>2</sub> flow was double-checked (at the inlet of the experimental set up by a Coriolis mass flow meter and at the outlet by a Ritter volumetric gas flow meter), the mass of CO<sub>2</sub> passing through the system was always known.
- The characterization of the olive oil for the modelling in ASPEN Plus® of the phase behaviour led to different problems and errors. Therefore, several assumptions must be taken to simplify and solve the issues, as described in *Chapter 5*. Nevertheless, all these assumptions had already been covered in literature. It was finally confirmed that the thermodynamic model fit the phase behaviour experimental data very well, at least concerning the liquid phase.
- One drawback of the SCFs is the difficulty to measure physical properties at high pressure, as special and complex equipment is usually required. Therefore, practically all the data on physical properties at high pressure given and used in this work are from literature. Besides, data on interfacial tension and diffusion coefficients are very scarce, thus some of the values given here were obtained by correlation of experimental data or by predictive equations.
- In the experiments performed for the visualization of the multiphase flow of scCO<sub>2</sub> with liquid mixtures, the pulsations caused by both HPLC pumps (both for the liquid phase and the CO<sub>2</sub> phase) raised an issue. On one hand, it was difficult in some cases

to determine and classify the flow pattern, as it showed a discontinuous and pulsed flow. On the other hand, this fact clearly influences the mixing as well as the flow, thus it must be borne in mind that the mixing and the extraction results presented in this work might be influenced not only by the mixing principle of the micro-mixers, but also by the pulsations caused by the HPLC pumps.

### 8.3. Outlook

In this work, it has been proved that one micro-mixer can be equivalent of a theoretical stage and therefore extraction processes which require more than one single stage can simply be designed as a number of micro-mixers (the same number as extraction stages are required) placed in series. The design of a multi-stage SFF with micro-mixers has been made in this work (see *Section 4.4*). Nevertheless, further experimental work should be done for a proper study and design of the process, and the apparatus.

Scale-up of the process is another goal for the future. The scale-up of a process which implies the concept “micro” is tricky. The advantage of the micro-mixers over other mixing devices is their small inner volume as well as their inner geometry. When designing an industrial scale production process, these facts must be borne in mind and therefore two main possibilities are possible: either increasing the number of micro-mixer units to increase the flow rate capacity of the equipment (external numbering-up) or increasing the size and therefore capacity of the mixers but keeping the same or very similar internal geometry (internal numbering-up). Kashid et al. (2010) investigated the numbering-up, both internal and external, of micro-structured reactors for the extraction of acetic acid from kerosene into water, see Figure 8.1.

Regarding the internal numbering-up for the multi-lamination principle studied here, some options are already on the market: LH1000, manufactured by Ehrfeld AG (see Figures 8.2 and 8.3). The inner geometry of the LH1000 Ehrfeld mixer consists of the superposition of plates which divide the streams into smaller blocks, as Figure 8.3 shows, to ensure an efficient, constant mixing of the two fluids. Nonetheless, to our knowledge, the LH1000 Ehrfeld manufactured at the moment has a maximum allowable fluid pressure of 30 bar (at 25 °C), therefore it is not suitable for processes with scCO<sub>2</sub>.

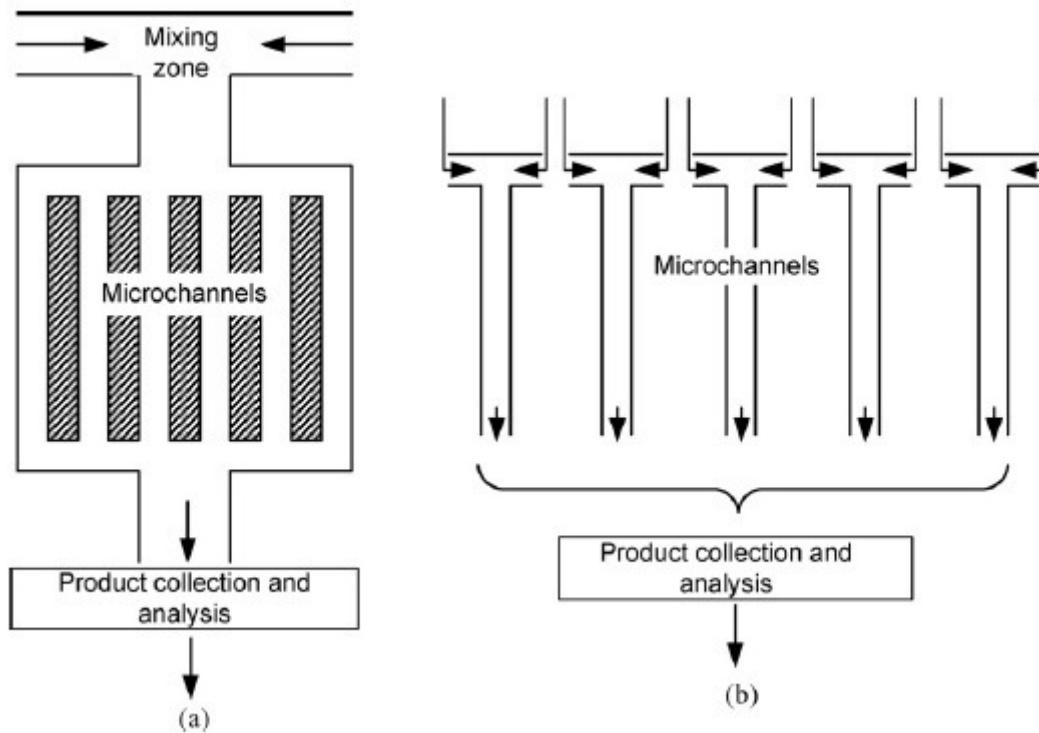


Figure 8.1. Numbering-up concept according to Kashid et al. (2010). (a) Represents the internal numbering-up, whereas (b) is the external numbering-up. Source: Kashid et al. (2010).

On the other hand, mixers with different mixing principle and higher capacity in relation to the ones studied here have already been designed to hold relative high pressures: the NETmix<sup>®</sup> (see Figure 8.4). As Fonte et al. (2012) described, this mixer or reactor, developed by the LSRE (Laboratory of Separation and Reaction Engineering) from the University of Porto, Portugal, consists of a network of mixing chambers interconnected by transport channels. Networks are generated by the repetition of unit cells where each unit cell consists of one chamber with two inlet and two outlet channels oriented at a 45° angle from the main flow direction. The chambers can be either constructed from cylindrical chambers and rectangular cross section area channels (2D unit cell) or from spherical chambers and cylindrical channels (3D unit cell), as shown in Figure 8.5.

Otherwise, concerning the external numbering-up, several aspects must be taken into account for the design of the apparatus. In this work, the influence of the length of the capillary placed at the outlet of the micro-mixer was studied (see Section 4.3.4) and it was observed that the extraction tended to worsen, as the capillary length increased. This and other factors which might also influence the extraction performance must be considered when designing the external numbering-up.

Those are just some ideas to scale-up the process, however, in-depth study and further work are required to investigate the different possibilities and conclude which is the best.

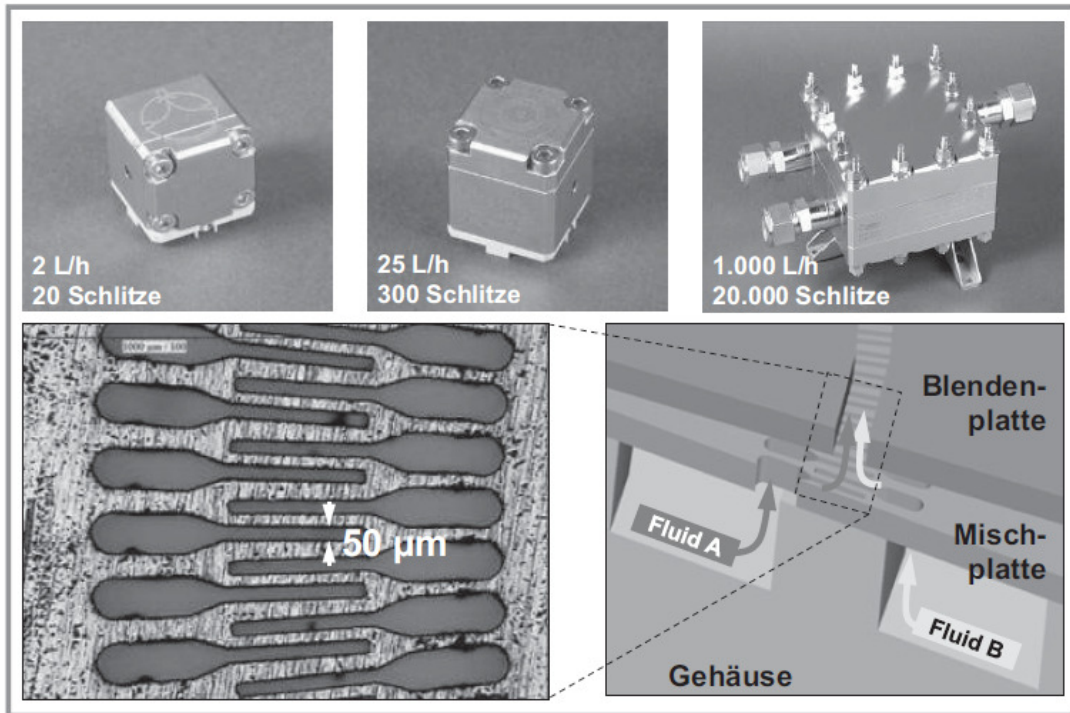


Figure 8.2. Operating principle of multi-lamination mixers. Source: Grünewald and Heck (2015).

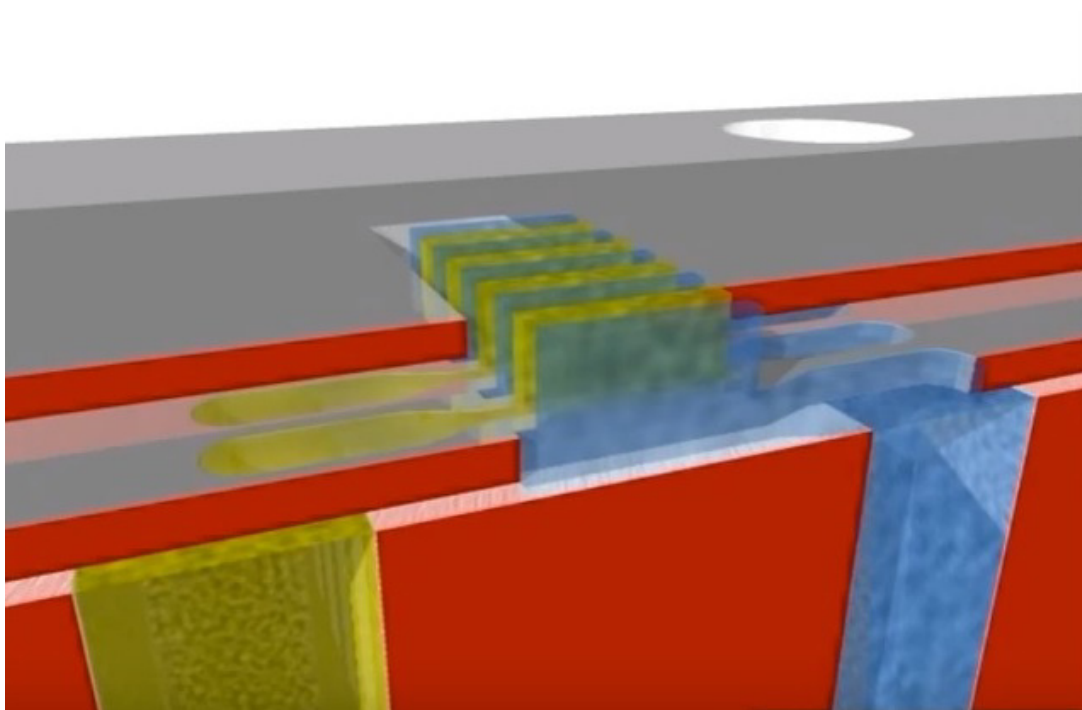


Figure 8.3. Operating principle and inner geometry of the LH1000 mixer, manufactured by Ehrfeld AG. Source: Ehrfeld AG.



Figure 8.4. NETmix reactor.

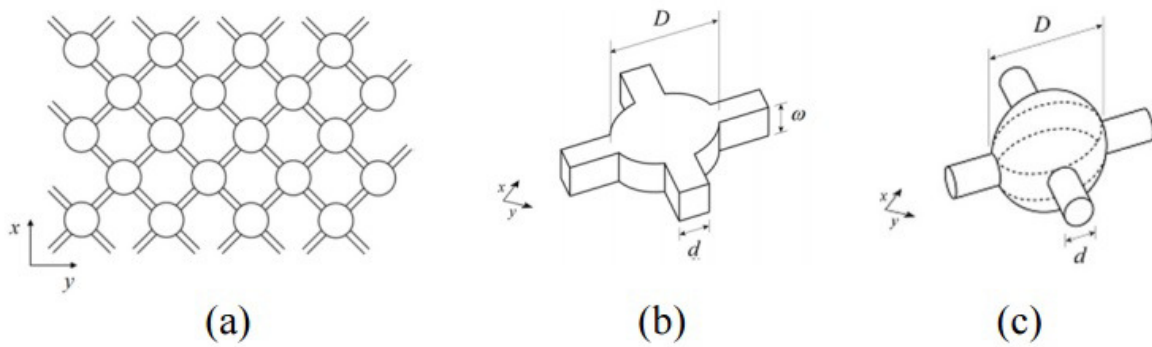


Figure 8.5. Illustration of the NETmix<sup>®</sup> network (a), the 2D unit cell (b), and the 3D unit cell (c). Source: Fonte et al. (2012).

Although the use of micro-mixers for SFF processes has been proved in this study to be a good alternative to traditional methods, still further work must be done. Study of more extraction systems and other mixing principles are some of the research fronts that must be

adequately addressed. Moreover, a deeper knowledge of the flow behaviour and the mass transfer in microfluidics with  $\text{scCO}_2$  is required. For this purpose, experiments combined with CFD are a good option. CFD has shown good results on the modelling of the flow behaviour of liquids with  $\text{scCO}_2$ , and promising results on the modelling of the mass transfer. This, together with the fact that the data on CFD and SCFs in literature is very scarce, makes it an intriguing, challenging research line.

## 9. Summary

The study of the process intensification for SFF and SFE by means of micro-mixers was the main purpose of this work. The benefits of micro-mixers for liquid-liquid extraction had been proved in literature within the last two decades. However, their utilization for SFE and SFF had been barely investigated. In this work, the applicability, feasibility and efficiency of micro-mixers for SFE and SFF processes were studied. First of all, a high-pressure micro-device extraction apparatus was designed and assembled. The design of this apparatus was made so that different mixing principles could be tested. Because of the experimental conditions required, the selection of the mixing principles was quite limited. Finally, a multi-lamination micro-mixer and a Tee-mixer were chosen. Furthermore, because it is a widely studied process for applications such as dealcoholisation of beverages, ethanol production or ethanol recovery from fermentation broth, the extraction of ethanol from aqueous solutions by  $\text{scCO}_2$  was chosen as a model system. One of the main first goals of this investigation was to determine whether equilibrium could be reached and therefore one theoretical stage could be achieved within the extraction process in the high-pressure micro-device apparatus. Thus, the phase behaviour of the  $\text{CO}_2$ -ethanol-water mixture was modelled in ASPEN Plus® by the Peng-Robinson EoS. According to experimental data from other authors, the model presented good accuracy. The influence of different parameters on the extraction process was studied: feed concentration, solvent flow rate and Solvent-to-Feed ratio, length of the capillary placed between the micro-mixer and separator, and overall flow rate. Experimental results showed that one theoretical stage was always reached at the different feed ethanol concentrations and Solvent-to-Feed ratios studied. Nevertheless, the study of the capillary length showed that the K-factor slightly decreases as the capillary length increases. These results confirmed that at the flow rates considered, the mixing in the micro-mixers is enough to reach the thermodynamic equilibrium. On the other hand, the study of the influence of the overall flow rate on the extraction process showed that at some ethanol feed concentrations, the separation worsens as the total flow rate increases. However, it must be remarked that this behaviour was observed only at certain feed ethanol concentrations, but not always.

Further on, the extraction of FFA from olive oil with micro-mixers was also studied and so the extraction process in micro-mixers under different hydrodynamic conditions could be

assessed. The thermodynamic model calculated by Gracia et al. (2009) in ASPEN Plus® using the PR-BM EoS was used to predict the phase behaviour of the CO<sub>2</sub>-oleic acid-triolein system. The extraction results proved that equilibrium could be achieved as well at distinct physical properties and therefore different hydrodynamics conditions. It was concluded that one micro-mixer can be equivalent of a theoretical extraction stage. By comparing the results obtained with both mixing principles studied here, it was observed that the extraction results were not influenced by the mixing principle.

Besides the extraction process, the mixing of liquids with scCO<sub>2</sub> was also studied here. The multiphase flow behaviour of scCO<sub>2</sub> with different liquid mixtures (ethanol-water mixtures and olive oil) in a capillary placed at the outlet of the micro-mixer was observed. The results showed that the mixing principle as well as the physical properties influences the flow behaviour of the fluids through the mixing process and in the capillary. In the mixing of scCO<sub>2</sub> with ethanol-water mixtures, even at the same pressure and temperature conditions, different flow patterns were observed when varying the ethanol concentration of the liquid mixture. This was attributed to that physical properties such as density, viscosity and, more importantly, interfacial tension change with the ethanol concentration.

The multiphase flow of scCO<sub>2</sub> with water and ethanol-water mixtures was modelled by CFD. The VOF model provided good results for the modelling of the flow behaviour of scCO<sub>2</sub> and water. The contact angle was found to be a key factor in the model. However, the results were validated and the model was confirmed to be precise. The model results were in accordance with our experimental results on the visualization of the flow of scCO<sub>2</sub>-water system. Besides, the mass transfer of ethanol from water to scCO<sub>2</sub> was also studied and simulated using CFD. The Eulerian-Eulerian method was found not to be suitable for this purpose. However, promising results were obtained by combining the Eulerian model with the Multi-flow VOF model. Nevertheless, further work is required to improve the model.

Some other aspects such as the design of a multi-stage extraction process with micro-mixers as well as the scale-up of the process (internal and external numbering-up) have also been discussed.

The experimental results of this work confirmed that one theoretical stage could be achieved with both micro-mixers. Therefore, the choice between these two mixing principles



for SFF purposes seems to be trivial. The influence of the hydrodynamics on the extraction process was also investigated by varying physical properties of the fluids and flow rates. Practically in every experiment performed, good extraction performance was observed. Therefore, this work concludes that the use of micro-mixers for SFE and SFF is a competitive alternative to current processes, as the extraction can be achieved in smaller volumes and shorter time. According to this results, the use of micro-mixers for SFF can be applied at short-term for the investigation at lab scale of new extraction systems, mixtures or processes as well as for the determination of extraction conditions and some others experimental factors, for instance.

# Abbreviations

AAD	Average Absolute Deviation
calc.	calculated
CFD	Computational Fluid Dynamics
dev.	deviation
DGF	Deutsche Gesellschaft für Fettwissenschaft
EoS	Equation of State
EtOH	ethanol
exp.	experimental
FFA	Free Fatty Acids
FR	Flow Rate
HETS	Height Equivalent to one Theoretical Stage
HPIMM	High-Pressure Interdigital Micro-Mixer
HPLC	High-Performance Liquid Chromatography
ID	Inner Diameter
IL	Ionic Liquids
IOC	International Olive Council
PR	Peng-Robinson
PR-BM	Peng-Robinson-Boston-Mathias
scCO <sub>2</sub>	Supercritical carbon dioxide
SCF	Supercritical Fluid
SFC	Supercritical Fluid Chromatography
SFE	Supercritical Fluid Extraction
SFF	Supercritical Fluid Fractionation
S-to-F	Solvent-to-Feed ratio [g/g]
VOF	Volume of Fluid (CFD model)
wt. %	Weight percentage

# Nomenclature

$a, b$	species-dependent constants (Peng-Robinson EoS)
$c$	Peneloux volume term correction (Peng-Robinson EoS)
Ca	Capillary number
$D$	mass diffusivity
$F$	Force
$g$	gravity
$h$	enthalpy
$k_{ij}, l_{ij}$	binary interaction parameters in Peng-Robinson EoS
$L$	length
$m$	mass
$\dot{m}$	mass flow
$M$	Molar weight
$N$	Avogadro's number
$p$	pressure
$r$	radius
$R$	universal gas constant
Re	Reynolds number
Sc	Schmidt number
Sh	Sherwood number
System A	Ethanol+water+CO <sub>2</sub> system
System B	Olive oil+CO <sub>2</sub> system
$t$	time
$T$	temperature
$v$	velocity
$V$ or $V_m$	molar volume
We	Weber number
$x$	mole fraction (liquid phase)
$X$	(ethanol) mass fraction
$y$	mole fraction (vapour phase)
$Z_{RA}$	Racket parameter
<b>Greek letters</b>	
$\alpha$	volume fraction (in VOF model)
$\gamma$	interfacial tension
$\eta$	dynamic viscosity
$\theta$	contact angle
$\rho$	density
$\omega$	acentric factor in Peng-Robinson EoS

### *Subscripts*

c	critical
E	extract
F	feed
m	mixture
r	reduced
R	raffinate

## References

- Acosta, G. M., Smith, R. L., Arai, K., 1996. High-pressure PVT behavior of natural fats and oils, trilaurin, triolein, and n-tridecane from 303 K to 353 K from atmospheric pressure to 150 MPa. *J. Chem. Eng. Data*, 41(5), 961-969.
- Assmann, N., Kaiser, S., von Rohr, P. R., 2012. Supercritical extraction of vanillin in a microfluidic device. *J. Supercrit. Fluids*, 67, 149-154.
- Assmann, N., Ładosz, A., von Rohr, P. R., 2013. Continuous Micro Liquid-Liquid Extraction. *Chem. Eng. Tech.*, 36(6), 921-936.
- Assmann, N., Werhan, H., Ładosz, A., von Rohr, P. R., 2013. Supercritical extraction of lignin oxidation products in a microfluidic device. *Chem. Eng. Sci.*, 99, 177-183.
- Becht, S., Franke, R., Geißelmann, A., Hahn, H., 2007. Micro process technology as a means of process intensification. *Chem. Eng. Technol.*, 30(3), 295-299.
- Bejarano, A., Simões, P. C., del Valle, J. M., 2016. Fractionation technologies for liquid mixtures using dense carbon dioxide. *J. Supercrit. Fluids*, 107, 321-348.
- Benz, K., Jäckel, K. P., Regenauer, K. J., Schiewe, J., Drese, K., Ehrfeld, W., Hessel, V., Löwe, H., 2001. Utilization of micromixers for extraction processes. *Chem. Eng. Tech.*, 24(1), 11-17.
- Bernad, L., Keller, A., Barth, D., 1993. Separation of ethanol from aqueous solutions by supercritical carbon dioxide—comparison between simulations and experiments. *J. Supercrit. Fluids* 6, 9–14.
- Bharath, R., Inomata, H., Adschiri, T., Arai, K., 1992. Phase equilibrium study for the separation and fractionation of fatty oil components using supercritical carbon dioxide. *Fluid Phase Equilib.*, 81, 307-320.
- Bikkina, P. K., Shoham, O., Uppaluri, R., 2011. Equilibrated interfacial tension data of the CO<sub>2</sub>–water system at high pressures and moderate temperatures. *J. Chem. Eng. Data*, 56(10), 3725-3733.
- Blanch-Ojea, R., Tiggelaar, R. M., Pallares, J., Grau, F. X., Gardeniers, J. G. E., 2012. Flow of CO<sub>2</sub>–ethanol and of CO<sub>2</sub>–methanol in a non-adiabatic microfluidic T-junction at high pressures. *Microfluidics Nanofluidics*, 12(6), 927-940.
- Bondioli, P., Mariani, C., Lanzani, A., Fedeli, E., Mossa, A., Muller, A., 1992. Lampante olive oil refining with supercritical carbon dioxide. *J. Am. Oil Chem. Soc.*, 69(5), 477-480.
- Brennecke, J. F., Eckert, C. A., 1989. Phase equilibria for supercritical fluid process design. *AIChE J.*, 35(9), 1409-1427.

Brown, Z. K., Fryer, P. J., Norton, I. T., Bakalis, S., Bridson, R. H., 2008. Drying of foods using supercritical carbon dioxide—Investigations with carrot. *Innov. Food Sci. Emerg. Technol.*, 9(3), 280-289.

Bröll, D., Kaul, C., Krämer, A., Krammer, P., Richter, T., Jung, M., Vogel, H., Zehner, P., 1999. Chemistry in supercritical water. *Angew. Chem. Int. Ed.*, 38(20), 2998-3014.

Brunetti, L., Daghetta, A., Fedell, E., Kikic, I., Zanderighi, L., 1989. Deacidification of olive oils by supercritical carbon dioxide. *J. Am. Oil Chem. Soc.*, 66(2), 209-217.

Brunner, G., 2010. Applications of supercritical fluids. *Annu. Rev. Chem. Biomol. Eng.*, 1, 321-342.

Brunner, G., 2013. Gas extraction: an introduction to fundamentals of supercritical fluids and the application to separation processes (Vol. 4). Springer Science & Business Media.

Budich, M., Brunner, G., 2003. Supercritical fluid extraction of ethanol from aqueous solutions. *J. Supercrit. Fluids* 25, 45–55.

Catchpole, O. J., Simões, P., Grey, J. B., Nogueiro, E. M., Carmelo, P. J., Nunes da Ponte, M., 2000. Fractionation of lipids in a static mixer and packed column using supercritical carbon dioxide. *Ind. Eng. Chem. Res.*, 39(12), 4820-4827.

Chasanis, P., Kern, J., Grünewald, M., Kenig, E. Y., 2010. Mikrotrenntechnik: Entwicklungsstand und Perspektiven. *Chem. Ing. Tech.* 82(3), 215-228.

Chun, B. S., Wilkinson, G. T., 1995. Interfacial tension in high-pressure carbon dioxide mixtures. *Ind. Eng. Chem. Res.* 34 (12), 4371-4377.

De Lucas, A., Rincon, J., Gracia, I., 2002. Influence of operating variables on yield and quality parameters of olive husk oil extracted with supercritical carbon dioxide. *J. Am. Oil Chem. Soc.*, 79(3), 237-243.

De Marco, C., Credi, C., Briatico-Vangosa, F., Bianchi, E., Ciftlik, A. T., Gijs, M., Dubini, G., Levi, M., Turri, S., 2014. Fabrication of biocompatible monolithic microchannels with high pressure-resistance using direct polymerization of PEG-modified PMMA. *J. Appl. Polym. Sci.*, 131(21).

DeSimone, J. M., 2002. Practical approaches to green solvents. *Science*, 297(5582), 799-803.

DeSimone, J. M., Tumas, W., 2003. Green chemistry using liquid and supercritical carbon dioxide. Oxford University Press.

Dittmar, D., Bijosono Oei, S., Eggers, R., 2002. Interfacial tension and density of ethanol in contact with carbon dioxide. *Chem. Eng. Technol.* 25(1), 23-27.

Dortmund Data Bank, DDBST GmbH, 2010. Oldenburg, Germany, [www.ddbst.de](http://www.ddbst.de)

- Durling, N.E., Catchpole, O.J., Tallon, S.J., Grey, J.B., 2007. Measurement and modelling of the ternary phase equilibria for high pressure carbon dioxide–ethanol–water mixtures. *Fluid Phase Equilib.* 252, 103–113.
- Easteal, A. J., Woolf, L. A., 1985. Pressure and temperature dependence of tracer diffusion coefficients of methanol, ethanol, acetonitrile, and formamide in water. *J. Phys. Chem.* 89 (7), 1066-1069.
- Eckert, C. A., 1996. Supercritical fluids as solvents for chemical and materials processing. *Nature*, 383, 313-318.
- Eggers, R., Jaeger, P. T., 1994. Der Einfluß von Grenzflächenerscheinungen auf den Stoffübergang und die Prozeßführung in Gegenstromkolonnen mit überkritischem CO<sub>2</sub>. *Wärme-und Stoffübertragung*, 29(6), 373-377.
- Fernandes, J., Lisboa, P. F., Simões, P. C., Mota, J. P., Saadjan, E., 2009. Application of CFD in the study of supercritical fluid extraction with structured packing: wet pressure drop calculations. *J. Supercrit. Fluids*, 50(1), 61-68.
- Fernandes, J., Simões, P. C., Mota, J. P., Saadjan, E., 2008. Application of CFD in the study of supercritical fluid extraction with structured packing: dry pressure drop calculations. *J. Supercrit. Fluids*, 47(1), 17-24.
- Fernández-Ronco, M. P., Cismondi, M., Gracia, I., De Lucas, A., Rodríguez, J. F., 2010. High-pressure phase equilibria of binary and ternary mixtures of carbon dioxide, triglycerides and free fatty acids: measurement and modeling with the GC-EOS. *Fluid Phase Equilib.*, 295(1), 1-8.
- Fonte, C. M., Leblebici, M. E., Dias, M. M., Lopes, J. C. B., 2012. The NETmix<sup>®</sup> reactor: 3D CFD modelling and pressure drop measurements. Paper presented at the 14<sup>th</sup> European Conference on Mixing, Warszawa, 10-13 September (pp. 107-112).
- Fornari, T., Hernandez, E.J., Ruiz-Rodriguez, A., Senorans, F.J., Reglero, G., 2009. Phase equilibria for the removal of ethanol from alcoholic beverages using supercritical carbon dioxide. *J. Supercrit. Fluids* 50, 91–96.
- Furuta, S., Ikawa, N., Fukuzato, R., Imanishi, N., 1989. Extraction of ethanol from aqueous solutions using supercritical carbon dioxide. *Kagaku Kogaku Ronbunshu* 15, 519–525.
- Gamse, T., Rogler, I., Marr, R., 1999. Supercritical CO<sub>2</sub> extraction for utilisation of excess wine of poor quality. *J. Supercrit. Fluids*, 14(2), 123-128.
- Gilbert, M.L., Paulaitis, M.E., 1986. Gas-liquid equilibrium for ethanol–water–carbon dioxide mixtures at elevated pressures. *J. Chem. Eng. Data* 31, 296–298.

- Gracia, I., García, M. T., Rodríguez, J. F., Fernández, M. P., De Lucas, A., 2009. Modelling of the phase behaviour for vegetable oils at supercritical conditions. *J. Supercrit. Fluids*, 48(3), 189-194.
- Gros, H. P., Bottini, S. B., Brignole, E. A., 1997. High pressure phase equilibrium modeling of mixtures containing associating compounds and gases. *Fluid Phase Equilib.* 139(1), 75-87.
- Grünewald, M., Heck, J., 2015. Modulare Verfahrenstechnik: Neue Anforderungen an die Apparateentwicklung. *Chem. Ing. Tech.*, 87(9), 1185-1193.
- Gunstone, F. D., 1996. Fatty acid and lipid chemistry. Blackie Academic & Professional.
- Güvenc., A., Mehmetoglu, Ü., Calimli, A., 1998. Supercritical CO<sub>2</sub> extraction of ethanol from fermentation broth in a semicontinuous system. *J. Supercrit. Fluids*, 13, 325–329.
- Han, X., Koelling, K. W., Tomasko, D. L., Lee, L. J., 2002. Continuous microcellular polystyrene foam extrusion with supercritical CO<sub>2</sub>. *Polym. Eng. Sci.*, 42(11), 2094-2106.
- Hardt, S., Schönfeld, F., 2003. Laminar mixing in different interdigital micromixers: II. Numerical simulations. *AIChE J.*, 49(3), 578-584.
- He, C. H., 1998. Infinite-dilution diffusion coefficients in supercritical and high-temperature liquid solvents. *Fluid Phase Equilib.* 147(1), 309-317.
- He, S., Kim, W. S., Jackson, J. D. 2008. A computational study of convective heat transfer to carbon dioxide at a pressure just above the critical value. *Appl. Therm. Eng.*, 28(13), 1662-1675.
- Henley, E.J., Seader, J.D.. 2006. Separation process principles, second edition. New York: Wiley.
- Hessel, V., Hardt, S., Löwe, H., Schönfeld, F., 2003. Laminar mixing in different interdigital micromixers: I. Experimental characterization. *AIChE J.*, 49(3), 566-577.
- Hessel, V., Löwe, H., Schönfeld, F., 2005. Micromixers—a review on passive and active mixing principles. *Chem. Eng. Sci.*, 60(8), 2479-2501.
- Hessel, V., Noël, T., 2012. Micro process technology, 2. Processing. Wiley-VCH Verlag GmbH & Co. KGaA.
- Hurtado-Benavides, A. M., Señoráns, F. J., Ibáñez, E., Reglero, G., 2004. Countercurrent packed column supercritical CO<sub>2</sub> extraction of olive oil. Mass transfer evaluation. *J. Supercrit. Fluids*, 28(1), 29-35.
- Hyatt, J. A., 1984. Liquid and supercritical carbon dioxide as organic solvents. *J. Org. Chem.*, 49(26), 5097-5101.



Ibanez, E., Palacios, J., Senorans, F. J., Santa-Maria, G., Tabera, J., Reglero, G., 2000. Isolation and separation of tocopherols from olive by-products with supercritical fluids. *J. Am. Oil Chem. Soc.*, 77(2), 187-190.

Ikawa, N., Nagase, Y., Tada, T., Furuta, S., Fukuzato, R., 1993. Separation process of ethanol from aqueous solutions using supercritical carbon dioxide. *Fluid Phase Equilib.* 83, 167–174.

Jenab, E., Temelli, F., 2011. Viscosity measurement and modeling of canola oil and its blend with canola stearin in equilibrium with high pressure carbon dioxide. *J. Supercrit. Fluids*, 58(1), 7-14.

Jenab, E., Temelli, F., 2012. Density and volumetric expansion of carbon dioxide-expanded canola oil and its blend with fully-hydrogenated canola oil. *J. Supercrit. Fluids*, 70, 57-65.

Jovanovic, J., Rebrov, E. V., Nijhuis, T. A., Kreutzer, M. T., Hessel, V., Schouten, J. C., 2011. Liquid–liquid flow in a capillary microreactor: hydrodynamic flow patterns and extraction performance. *Ind. Eng. Chem. Res.*, 51(2), 1015-1026.

Kashid, M. N., Gupta, A., Renken, A., Kiwi-Minsker, L., 2010. Numbering-up and mass transfer studies of liquid–liquid two-phase microstructured reactors. *Chem. Eng. J.*, 158(2), 233-240.

Kikic, I., Vecchione, F., 2003. Supercritical impregnation of polymers. *Curr. Opin. Solid State Mater. Sci.*, 7(4), 399-405.

King, J. W., Favati, F., Taylor, S. L., 1996. Production of Tocopherol Concentrates by Supercritical Fluid Extraction and Chromatography. *Sep. Sci. Technol.*, 31(13), 1843-1857.

Kjellow, A. W., Henriksen, O., 2009. Supercritical wood impregnation. *J. Supercrit. Fluids*, 50(3), 297-304.

Klesper, E., Corwin, A. H., Turner, D. A., 1962. High pressure gas chromatography above critical temperatures. *J. Org. Chem.*, 27(2), 700.

Knapp, H., Döring, R., Oellrich, L., Plöcker, U., Prausnitz, J.M., 1982. Vapor-Liquid Equilibria for Mixtures of Low Boiling Substances. *Dechema In Chem. Data Series* 6.

Knaust, S., Andersson, M., Rogeman, N., Hjort, K., Amberg, G., Klintberg, L., 2015. Influence of flow rate, temperature and pressure on multiphase flows of supercritical carbon dioxide and water using multivariate partial least square regression. *J. Micromech. Microeng.*, 25(10), 105001.

Knez, Z., Weidner, E., 2003. Particles formation and particle design using supercritical fluids. *Curr. Opin. Solid State Mater. Sci.*, 7(4), 353-361.

Kong, C. Y., Funazukuri, T., Kagei, S., 2006. Binary diffusion coefficients and retention factors for polar compounds in supercritical carbon dioxide by chromatographic impulse response method. *J. Supercrit. Fluids*, 37(3), 359-366.

- Lévai, G., Martín, Á., de Paz, E., Rodríguez-Rojo, S., Cocero, M. J., 2015. Production of stabilized quercetin aqueous suspensions by supercritical fluid extraction of emulsions. *J. Supercrit. Fluids*, 100, 34-45.
- Li, J., Rodrigues, M., Matos, H. A., Gomes de Azevedo, E., 2005. VLE of carbon dioxide/ethanol/water: applications to volume expansion evaluation and water removal efficiency. *Ind. Eng. Chem. Res.*, 44 (17), 6751-6759.
- Lim, J.S., Lee, Y.Y., Chun, H.S., 1994. Phase equilibria for carbon dioxide–ethanol–water system at elevated pressures. *J. Supercrit. Fluids* 7, 219–230.
- Lim, J.S., Lee, Y.W., Kim, J.D., Lee, Y.Y., 1995. Mass-transfer and hydraulic characteristics in spray and packed extraction columns for supercritical carbon dioxide–ethanol–water system. *J. Supercrit. Fluids*, 8, 127–137.
- Lisboa, P. F., Fernandes, J., Simões, P. C., Mota, J. P., Saadjan, E., 2010. Computational-fluid-dynamics study of a Kenics static mixer as a heat exchanger for supercritical carbon dioxide. *J. Supercrit. Fluids*, 55(1), 107-115.
- Lopes, J. M., Sánchez, F. A., Reartes, S. B. R., Bermejo, M. D., Martín, Á., Cocero, M. J., 2016. Melting point depression effect with CO<sub>2</sub> in high melting temperature cellulose dissolving ionic liquids. Modeling with group contribution equation of state. *J. Supercrit. Fluids*, 107, 590-604.
- Loppinet-Serani, A., Aymonier, C., Cansell, F., 2008. Current and foreseeable applications of supercritical water for energy and the environment. *ChemSusChem*, 1(6), 486-503.
- Lorber, N., Sarrazin, F., Guillot, P., Panizza, P., Colin, A., Pavageau, B., Hany, C., Maestro, P., Marre, S., Delclos, T., Aymonier, C., Subra, P., Prat, L., Gourdon, C., Mignard, E., 2011. Some recent advances in the design and the use of miniaturized droplet-based continuous process: Applications in chemistry and high-pressure microflows. *Lab on a Chip*, 11(5), 779-787.
- Lozano Sánchez, J., Segura Carretero, A., Fernández Gutiérrez, A., 2009. El aceite de oliva virgen: tesoro de Andalucía. 13 perspectivas concatenadas. Unicaja Editorial.
- Luther, S. K., Braeuer, A., 2012. High-pressure microfluidics for the investigation into multi-phase systems using the supercritical fluid extraction of emulsions (SFEE). *J. Supercrit. Fluids*, 65, 78-86.
- Luther, S. K., Schuster, J. J., Leipertz, A., Braeuer, A., 2013. Microfluidic investigation into mass transfer in compressible multi-phase systems composed of oil, water and carbon dioxide at elevated pressure. *J. Supercrit. Fluids*, 84, 121-131.
- Marre, S., Aymonier, C., Subra, P., Mignard, E., 2009. Dripping to jetting transitions observed from supercritical fluid in liquid microflows. *Appl. Phys. Lett.*, 95(13), 134105.

Martin, A., Cocero, M. J., 2004. Numerical modeling of jet hydrodynamics, mass transfer, and crystallization kinetics in the supercritical antisolvent (SAS) process. *J. Supercrit. Fluids*, 32(1), 203-219.

Mathias, P.M., Klotz, H.C., Prausnitz, J.M., 1991. Equation of state mixing rules for multicomponent mixtures: the problem of invariance. *Fluid Phase Equilib.* 67, 31–44.

McHugh, M.A., Krukonis, V.J., 1994. *Supercritical Fluid Extraction*, second ed. Butterworth-Heinemann, Boston, MA.

Medina, I., 2012. Determination of diffusion coefficients for supercritical fluids. *J. Chromatogr. A* 1250, 124-140.

Merzkirch, W., 1987. *Flow visualization* (2<sup>nd</sup> Edition). Academic Press, New York.

Miller, C. C., 1924. The Stokes-Einstein Law for diffusion in solution. *Proceedings of the Royal Society of London. Series A, Containing Papers of a Mathematical and Physical Character*, 106(740), 724-749.

Müller, E., Berger, R., Blass, E., Sluyts, D., Pfennig, A., 2012. Liquid–liquid extraction. *Ullmann's Encyclopedia of Industrial Chemistry*.

Müller, T. E., Leitner, W., 2015. CO<sub>2</sub> chemistry. *Beilstein J. Org. Chem.*, 11(1), 675-677.

NIST Chemistry Webbook, 2016: <http://webbook.nist.gov/chemistry/fluid/>

Nguyen, N.T., 2012. *Micromixers: Fundamentals, Design and Fabrication*, second ed. Elsevier, Waltham, MA.

Ogden, S., Bodén, R., Do-Quang, M., Wu, Z. G., Amberg, G., Hjort, K., 2014. Fluid behavior of supercritical carbon dioxide with water in a double-Y-channel microfluidic chip. *Microfluidics Nanofluidics*, 17(6), 1105-1112.

Ohashi, A., Sugaya, M., Kim, H. B., 2011. Development of a microfluidic device for measurement of distribution behavior between supercritical carbon dioxide and water. *Anal. Sci.*, 27(6), 567.

Omprakash, H. N., 2016. Food Processing by Supercritical Carbon Dioxide-Review. *EC Chemistry* 2.1, 111-135.

Ortega, A. B., Škerget, M., Knez, Ž., 2016. Separation of xanthohumol from hop extracts by supercritical fluid chromatography. *Chem. Eng. Res. Des.*, 109, 335-345.

de la Ossa, E. M., Brandani, V., Del Re, G., Di Giacomo, G., Ferri, E., 1990. Binary and ternary phase behaviour of the system water-ethanol-carbon dioxide. *Fluid Phase Equilib.* 56, 325-340.

de la Ossa, E.M., Serrano, M.A.G., 1990. Extracción con fluidos supercríticos (I): fundamentos. *Ingeniería química*, (256), 169-175.

Pantić, M., Knez, Ž., Novak, Z., 2016. Supercritical impregnation as a feasible technique for entrapment of fat-soluble vitamins into alginate aerogels. *J. Non-Cryst. Solids*, 432, 519-526.

Peach, J., Eastoe, J., 2014. Supercritical carbon dioxide: a solvent like no other. *Beilstein J. Org. Chem.*, 10(1), 1878-1895.

Pečar, D., Doleček, V., 2005. Volumetric properties of ethanol–water mixtures under high temperatures and pressures. *Fluid phase equilib.* 230(1), 36-44.

Pecnik, R., Rinaldi, E., Colonna, P., 2012. Computational fluid dynamics of a radial compressor operating with supercritical CO<sub>2</sub>. *J. Eng. Gas Turb. Power*, 134(12), 122301.

Peng, D.Y., Robinson, D.B., 1976. A new two-constant equation-of-state. *Ind. Eng. Chem. Fundam.* 15, 59–64.

Perakis, C., Voutsas, E., Magoulas, K., Tassios, D., 2006. Thermodynamic modeling of the vapor–liquid equilibrium of the water/ethanol/CO<sub>2</sub> system. *Fluid Phase Equilib.* 243(1), 142-150.

Perrut, M., 2000. Supercritical fluid applications: industrial developments and economic issues. *Ind. Eng. Chem. Res.* 39(12), 4531-4535.

Perry H.R., Green D.W., 1997. *Perry's Chemical Engineers Handbook (7th Edition)* McGrawHill, New York, USA.

Pieck, C.A., Crampon, C., Charton, F., Badens, E., 2015. Multi-scale experimental study and modelling of the supercritical fractionation process. *J. Supercrit. Fluids* 105, 158–169.

Pratt, K. C., Wakeham, W. A., 1974. The mutual diffusion coefficient of ethanol-water mixtures: determination by a rapid, new method. In *Proceedings of the Royal Society of London A: Mathematical, Physical and Engineering Sciences* Vol. 336, No. 1606, pp. 393-406.

Raventós, M., Duarte, S., Alarcón, R., 2002. Application and possibilities of supercritical CO<sub>2</sub> extraction in food processing industry: an overview. *Food Sci. Technol. Int.*, 8(5), 269-284.

Reverchon, E., De Marco, I., 2006. Supercritical fluid extraction and fractionation of natural matter. *J. Supercrit. Fluids* 38 (2), 146–166.

Rozzi, N. L., Singh, R. K., 2002. Supercritical fluids and the food industry. *Comp. Rev. Food Sci. Food Safety*, 1(1), 33-44.

Ruivo, R., Cebola, M. J., Simões, P. C., Nunes da Ponte, M., 2001. Fractionation of edible oil model mixtures by supercritical carbon dioxide in a packed column. Part I: experimental results. *Ind. Eng. Chem. Res.*, 40(7), 1706-1711.

- Ruivo, R., Cebola, M. J., Simões, P. C., Nunes da Ponte, M., 2002. Fractionation of edible oil model mixtures by supercritical carbon dioxide in a packed column. 2. A mass-transfer study. *Ind. Eng. Chem. Res.*, 41(9), 2305-2315.
- Savage, P. E., Gopalan, S., Mizan, T. I., Martino, C. J., Brock, E. E., 1995. Reactions at supercritical conditions: applications and fundamentals. *AIChE J.*, 41(7), 1723-1778.
- Schaschke, C. J., Allio, S., Holmberg, E. (2006). Viscosity measurement of vegetable oil at high pressure. *Food and bioproducts processing*, 84(3), 173-178.
- Simões, P. C., Brunner, G., 1996. Multicomponent phase equilibria of an extra-virgin olive oil in supercritical carbon dioxide. *J. Supercrit. Fluids*, 9(2), 75-81.
- Simões, P. C., Eggers, R., Jaeger, P. T., 2000. Interfacial tension of edible oils in supercritical carbon dioxide. *Eur. J. Lipid Sci. Technol.*, 102(4), 263-265.
- Stankiewicz, A. I., Moulijn, J. A. (2000). Process intensification: transforming chemical engineering. *Chem. Eng. Prog.*, 96(1), 22-34.
- Stavroulias, S., Panayiotou, C., 2005. Determination of optimum conditions for the extraction of squalene from olive pomace with supercritical CO<sub>2</sub>. *Chem. Biochem. Eng. Q.*, 19(4), 373-381.
- Takishima, S., Saiki, K., Arai, K., Saito, S., 1986. Phase equilibrium for CO<sub>2</sub>-C<sub>2</sub>H<sub>5</sub>OH-H<sub>2</sub>O system. *J. Chem. Eng. Jpn.* 19, 48-56.
- Tanaka, Y., Matsuda, Y., Fujiwara, H., Kubota, H., Makita, T., 1987. Viscosity of (water+ alcohol) mixtures under high pressure. *Int. J. Thermophys.* 8(2), 147-163.
- Taylor, L.T., 2009. Supercritical fluid chromatography for the 21st century. *J. Supercrit. Fluids*, 47(3), 566-573.
- Tegetmeier, A., Dittmar, D., Fredenhagen, A., Eggers, R., 2000. Density and volume of water and triglyceride mixtures in contact with carbon dioxide. *Chem. Eng. Process.*, 39(5), 399-405.
- Temelli, F., 2009. Perspectives on supercritical fluid processing of fats and oils. *J. Supercrit. Fluids*, 47(3), 583-590.
- Valeri, D., Meirelles, A. J., 1997. Viscosities of fatty acids, triglycerides, and their binary mixtures. *J. Am. Oil Chem. Soc.*, 74(10), 1221-1226.
- Varga, D., Alkin, S., Gluschitz, P., Péter-Szabó, B., Székely, E., Gamse, T., 2016. Supercritical Fluid Dyeing of Polycarbonate in Carbon Dioxide. *J. Supercrit. Fluids*, 116, 111-116.
- Vázquez, L., Hurtado-Benavides, A. M., Reglero, G., Fornari, T., Ibáñez, E., Señoráns, F. J., 2009. Deacidification of olive oil by countercurrent supercritical carbon dioxide extraction: experimental and thermodynamic modelling. *J. Food Eng.*, 90(4), 463-470.

Vázquez da Silva, M., 2010. Supercritical Fluids and Its Applications. Recent Progress in Chemical Engineering, Chapter 10. Editor JMPQ Delgado.

Weidner, E., Petermann, M., Knez, Z., 2003. Multifunctional composites by high-pressure spray processes. *Curr. Opin. Solid State Mater. Sci.*, 7(4), 385-390.

Wong, S. H., Ward, M. C., Wharton, C. W., 2004. Micro T-mixer as a rapid mixing micromixer. *Sens. Actuator B-Chem.*, 100(3), 359-379.

Yoon, J. H., Lee, H., Chung, B. H., 1994. High pressure three-phase equilibria for the carbon dioxide-ethanol-water system. *Fluid Phase Equilib.* 102(2), 287-292

Zhang, Z.Y., Yang, J.C., Li, Y.G., 2000. Prediction of phase equilibria for CO<sub>2</sub>-C<sub>2</sub>H<sub>5</sub>OH-H<sub>2</sub>O system using the SAFT equation of state. *Fluid Phase Equilib.* 169, 1-18.

Zhao, Y., Chen, G., Yuan, Q., 2006. Liquid-liquid two-phase flow patterns in a rectangular microchannel. *AIChE J.*, 52(12), 4052-4060.

Zhao, Y., Chen, G., Yuan, Q., 2007. Liquid-liquid two-phase mass transfer in the T-junction microchannels. *AIChE J.*, 53(12), 3042-3053.

## V6.3

## Hochdruckinaktivierung: Unterschiedliches Druckprofil – gleicher Zellschaden?

M. Izydor<sup>1)</sup> (E-Mail: iz@ipat.uni-erlangen.de), M. Hainthaler<sup>1)</sup>, Prof. Dr.-Ing. E. Schlücker<sup>1)</sup>

<sup>1)</sup>Friedrich-Alexander-Universität Erlangen-Nürnberg, Lehrstuhl für Prozessmaschinen und Anlagentechnik, Cauerstraße 4, 91058 Erlangen, Deutschland

DOI: 10.1002/cite.201550038

Die Behandlung von Lebensmitteln und Pharmazeutika mithilfe von Hochdruck stellt heutzutage eine schonende Alternative zu konventionellen Konservierungsverfahren dar. Sie bietet die Möglichkeit, Mikroorganismen und Pathogene zu inaktivieren, ohne dabei die wertgebenden Inhaltsstoffe und damit die Produktqualität zu schädigen [1–3]. Die Anwendung dynamischer Hochdruckprofile ermöglicht dabei eine innovative Prozessvariante dieses Verfahrens, die am Lehrstuhl für Prozessmaschinen und Anlagentechnik der Universität Erlangen entwickelt wurde. Sie erlaubt durch die Anwendung mehrerer aufeinanderfolgender Druckzyklen sowohl eine Intensivierung des Inaktivierungseffekts als auch eine quasi-kontinuierliche Fahrweise des Prozesses (Abb.), wodurch Energie- und Prozesskosten eingespart werden können [4].

Zur Optimierung dieses neuen Verfahrens ist es notwendig, die unterschiedlichen, flexibel gestalteten Druckprofile zu betrachten und gleichzeitig den durch den Hochdruck verursachten Zellschaden zu untersuchen. Um den Entstehungsmechanismus druckinduzierter Schäden untersuchen zu können, muss in das Innere der Mikroorganismen geblickt werden. Mittels verschiedener Fluoreszenzfärbeverfahren wird am Beispiel der Bier- und Bäckerhefe

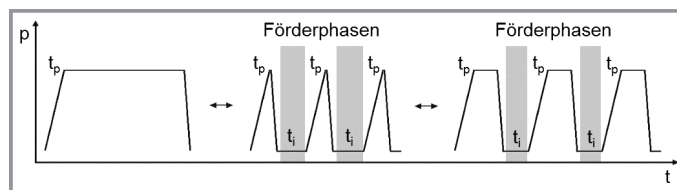
*Saccharomyces cerevisiae* der Hochdruckeinfluss auf relevante Zellbereiche analysiert. Somit können zusätzlich zum klassischen Ausplattieren, welches die genaue Anzahl an überlebenden, vermehrungsfähigen Zellen erfasst, auch Aussagen über den Entstehungsort der letalen Schädigung in der Zelle getroffen werden. Es zeigte sich, dass neben dem Maximaldruck und der Druckhaltezeit auch das Druckprofil (statisch, gepulst oder dynamisch) unterschiedliche Auswirkungen auf die Zellmembran und die Mitochondrien hat. Des Weiteren wurde untersucht, ob die Schädigung der Mitochondrien zu einer apoptotischen, programmierten Form des Zelltods führt, die sich deutlich von der beispielsweise durch Hitze verursachten nekrotischen Form unterscheidet.

Aufbauend auf der Erkenntnis, dass neben Druckhöhe und -haltezeit auch die

Ausgestaltung des Druckprofils und der dynamischen Prozessparameter eine entscheidende Rolle spielen, ergibt sich ein großes Forschungs- und Entwicklungspotenzial sowie erheblicher Spielraum zur weiteren Prozessoptimierung.

Diese Forschungsarbeit wurde von der Alfred Kärcher-Förderstiftung unterstützt.

- [1] D. M. Considine, A. L. Kelly, G. F. Fitzgerald, C. Hill, R. Sleator, *FEMS Microbiol. Lett.* **2008**, *281*, 1–9.
- [2] D. Knorr, A. Froehling, H. Jaeger, K. Reineke, O. Schlueter, K. Schoessler, *Annu. Rev. Food Sci. Technol.* **2011**, *2*, 203–235.
- [3] B. Rademacher, *Chem. Ing. Tech.* **2006**, *78 (11)*, 1674–1981.
- [4] N. Ebel, *Dissertation*, Friedrich-Alexander-Universität Erlangen-Nürnberg **2012**.



**Abbildung.** Vom statischen (1 Zyklus) zum dynamischen, quasi-kontinuierlichen Druckprofil ( $n$  Zyklen): während der Haltezeit  $t_p$  wird das Produkt mit Druck beaufschlagt und kann anschließend während der drucklosen Intervallzeit  $t_i$  gefördert werden.

## V6.4

## Prozessintensivierung der Hochdruckextraktion flüssiger Ausgangsmaterialien durch Mikromischer

C. Campos Dominguez<sup>1)</sup> (E-Mail: camposdominguez@tugraz.at), Prof. Dr. T. Gamse<sup>1)</sup>

<sup>1)</sup>Technische Universität Graz, Institut für Chemische Verfahrenstechnik und Umwelttechnik, Inffeldgasse 25/C/II, 8010 Graz, Österreich

DOI: 10.1002/cite.201550052

Die Anwendung überkritischer Gase für die Hochdruckextraktion ist eine gute Alternative zur Verwendung organischer Lösungsmittel. Die Prozessintensivierung

der Hochdruckextraktion flüssiger Ausgangsmaterialien mithilfe von Mikromischern wurde untersucht. Die Mikromischer bewirken eine Verkleinerung der

Produktionsanlage, was zur Erhöhung der Prozesssicherheit sowie zur Reduktion der Prozesskosten führt. Die Mikrokanäle innerhalb des Mikromischers besitzen

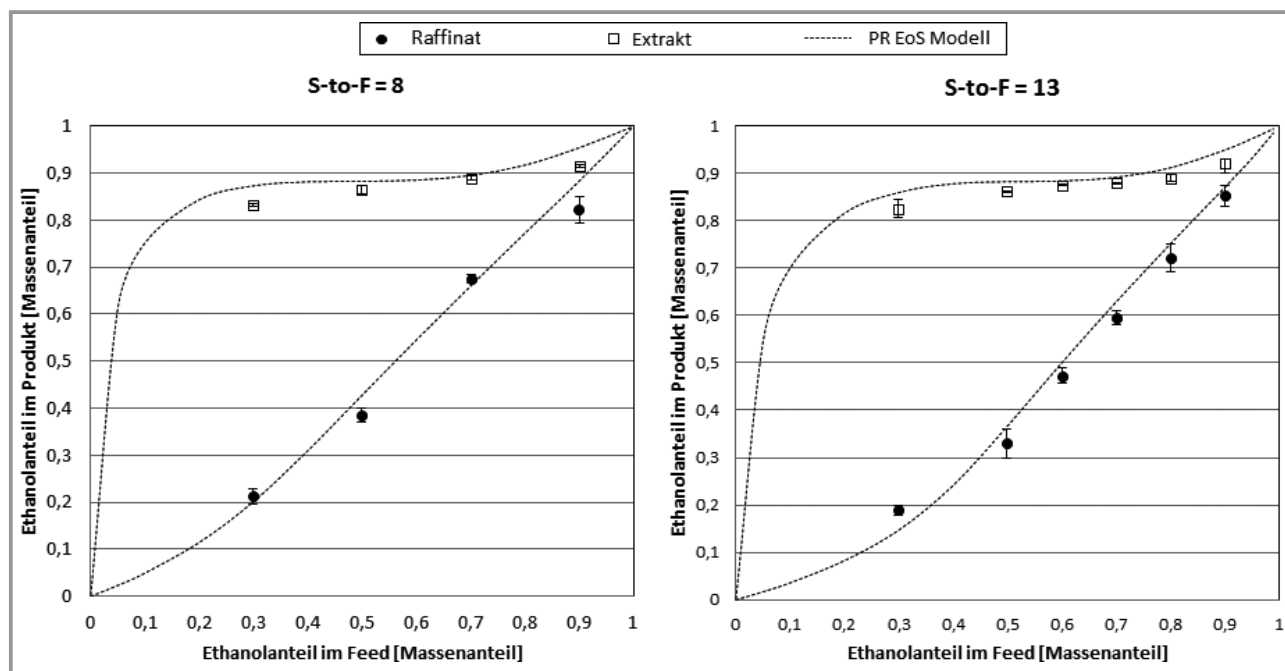
extrem kleine Durchmesser von ca.  $45\ \mu\text{m}$ , wodurch ein guter Stoffübergang erreicht werden kann, der vergleichbar oder besser ist als in Extraktionskolonnen.

Zur Untersuchung der Durchführbarkeit des Extraktionsprozesses mittels Mikromischer anstelle einer Extraktionskolonne wurde eine Hochdruckanlage konzipiert und im Labor aufgebaut. Bei dieser Anlage ist der Mikromischer das Kernstück, in dem das Lösungsmittel (überkritisches  $\text{CO}_2$ ) und das flüssige Ausgangsmaterial intensiv gemischt werden. Die Abtrennung von Raffinat und Extrakt findet in zwei aufeinander folgenden Separatoren statt. Eingesetzt wurde ein Hochdruck-Schlitz-Interdigital-Mikromischer HPIMM von Fraunhofer ICT-IMM, der nach dem Multilaminations-Mischprinzip arbeitet.

Die Hochdruckextraktion von Ethanol aus wässrigen Lösungen wurde in den vergangenen Jahren umfassend untersucht. Aufgrund der großen in der Literatur verfügbaren Datenmenge über Trennergebnisse sowie Phasengleichgewichte wurde die Ethanol-Wasser-Trennung mit überkritischem  $\text{CO}_2$  als Lösungsmittel gewählt, um die Wirtschaftlichkeit der Mikromischer-Hochdruckextraktionsanlage zu ermitteln. Experimente wurden bei 101 bar,  $60^\circ\text{C}$ , unterschiedlichen Feedzusammensetzungen sowie verschiedenen Verhältnissen von Lösemittel zu Feed durchgeführt. Um zu prüfen, ob eine Gleichgewichtseinstellung in einer Trennstufe bei der Mikromischeranlage erreicht wird, wurden die Phasengleichgewichtsberechnungen mit der Peng-Robinson-Zustandsgleichung in ASPEN simuliert

[1–3]. Die Proben wurden mittels Paardichtemessgerät analysiert und die Zusammensetzungen wurden mit Tabellen aus der Literatur [4] ermittelt. Die experimentellen Ergebnisse wurden mit der Modellierung verglichen. Diese Ergebnisse sind sehr zufriedenstellend und bestätigen, dass in der Mikromischeranlage eine theoretische Stufe erreicht werden kann.

- [1] M. Budich, G. Brunner, *J. Supercrit. Fluids* **2003**, 25, 45–55.
- [2] S. Furuta, N. Ikawa, R. Fukuzato, N. Imanishi, *Kagaku Kogaku Ronbunshu* **1989**, 15, 519–525.
- [3] J. S. Lim, Y. Y. Lee, H. S. Chun, *J. Supercrit. Fluids* **1994**, 7, 219–230.
- [4] R. H. Perry, C. H. Chilton, *Chemical Engineers' Handbook*, McGraw-Hill, New York **1973**.



**Abbildung.** Änderungen der Extrakt- und Raffinatkonzentration bei unterschiedlichen Ethanolkonzentrationen im Feed und unterschiedlichen Verhältnissen von Lösemittel zu Feed (S-to-F).





ELSEVIER

Contents lists available at ScienceDirect

Chemical Engineering Research and Design

journal homepage: [www.elsevier.com/locate/cherd](http://www.elsevier.com/locate/cherd)IChemE  
ADVANCING  
CHEMICAL  
ENGINEERING  
WORLDWIDE

# Process intensification by the use of micro devices for liquid fractionation with supercritical carbon dioxide

Candela Campos Domínguez\*, Thomas Gamse

Graz University of Technology, Institute of Chemical Engineering and Environmental Technology, Inffeldgasse 25 C, Graz 8010, Austria

## ARTICLE INFO

### Article history:

Received 30 July 2015

Received in revised form 20 November 2015

Accepted 8 January 2016

Available online 21 January 2016

### Keywords:

Supercritical fluid extraction

Micro-mixer

Multi-lamination principle

Supercritical CO<sub>2</sub>

Peng Robinson equation of state

## ABSTRACT

The present study is focused on the process intensification of extraction with supercritical fluids by using micro-devices. The main purpose is to investigate the efficiency and applicability of micro-mixers in supercritical fluid extraction processes. Two micro-devices with different mixing principles, multilamination and T-type lamination, were used and results were compared. The extraction experiments were carried out in a micro-device apparatus designed for high-pressure processes, in which the micro-device is the unit where the solvent and the liquid feed come into contact. Experiments on the continuous extraction of ethanol from aqueous solutions using supercritical CO<sub>2</sub> as solvent were performed to study the feasibility of the extraction process in a micro-device apparatus. The separation of both liquid and vapour phases was achieved by changes of temperature and pressure. The experiments were carried out at 101 bar and 60 °C. Different ethanol concentrations in the feed and solvent-to-feed ratio values were considered. Results obtained with the two different micro-devices were compared. A phase equilibrium model using Peng Robinson equation of state was developed in ASPEN-Plus® and calculations were performed to confirm that equilibrium was achieved through the extraction process and that one theoretical stage can be reached in a micro-device stage.

© 2016 The Institution of Chemical Engineers. Published by Elsevier B.V. All rights reserved.

## 1. Introduction

In the last decades, Supercritical Fluid Extraction (SFE) and Supercritical Fluid Fractionation (SFF) are becoming a convenient, significant alternative to other conventional techniques. Due to its moderate critical parameters ( $T_c = 31\text{ °C}$ ,  $P_c = 73.8\text{ bar}$ ), good solvent power, non-toxicity, non-flammability and low-cost, supercritical CO<sub>2</sub> (scCO<sub>2</sub>) is the most common solvent for SFE. The use of supercritical solvents provides enhanced extraction rates and solvent-free extracts, as product recovery happens via simple pressure reduction. Moreover, because of the low temperature conditions, less degradation of solutes occurs. McHugh and

Krukonis (1994) explained the fundamentals and industrial applications of this technique. In Reverchon and De Marco (2006) SFE and SFF techniques of natural matter carried out within the last decades were analysed.

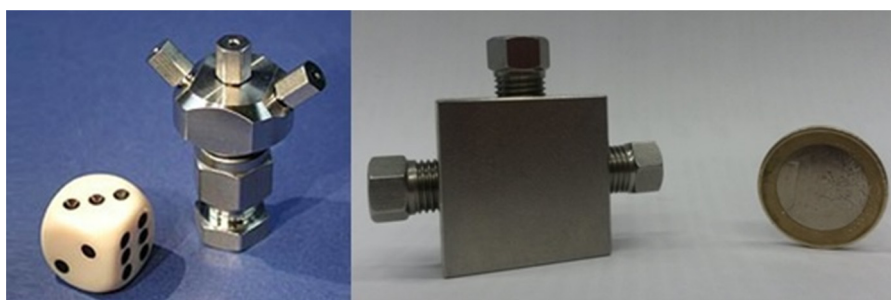
This study is focused on the utilization of micro-devices for SFE and SFF purposes. Micro-process technology has gained more attention in the past years because of its advantages in different processes. Nguyen (2012) introduced the design and applications of micro-mixers in chemical engineering processes. In particular, the use of micro-mixers in extraction and separation is becoming of interest in the last years (Benz et al., 2001; Assmann et al., 2013; Kenig et al., 2013) and it has been proved that liquid–liquid extraction process can

\* Corresponding author. Tel.: +43 3168737482.

E-mail address: [camposdominguez@tugraz.at](mailto:camposdominguez@tugraz.at) (C. Campos Domínguez).

<http://dx.doi.org/10.1016/j.cherd.2016.01.011>

0263-8762/© 2016 The Institution of Chemical Engineers. Published by Elsevier B.V. All rights reserved.



**Fig. 1 – Micro-mixers used in this work: HPIMM micro-mixer from Fraunhofer ICT-IMM (on the left) and Tee-mixer (on the right).**

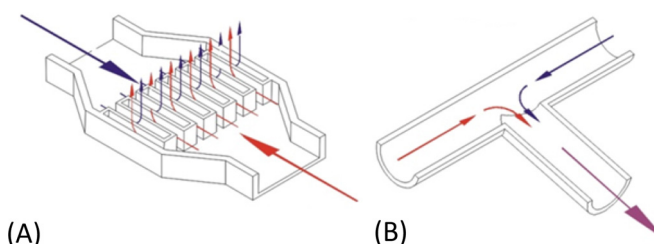
benefit from microfluidics: the short path lengths as well as the large interfacial area due to the extremely small size of the micro-channels can enhance mass transfer and equilibrium can be reached within seconds. Nevertheless, the use of micro-mixers for SFE and SFF applications has been barely studied to date and only some results are available in the literature: Assmann et al. (2012) carried out successfully the extraction of vanillin in a microfluidic device using  $\text{scCO}_2$ . In this work, a high pressure micro-device extraction apparatus has been designed and assembled in order to evaluate the feasibility and efficiency of SFE process using micro-mixers. The continuous extraction of ethanol from aqueous solutions using  $\text{scCO}_2$  as solvent has been chosen as an example.

The removal or extraction of ethanol by  $\text{scCO}_2$  is a widely studied process for applications such as dealcoholisation of beverages (Fornari et al., 2009), ethanol production or ethanol recovery from fermentation processes (Güvenç et al., 1998). Therefore, the  $\text{CO}_2$ -ethanol-water ternary mixture has been extensively investigated, as well the phase equilibrium behaviour of the system (Gilbert and Paulaitis, 1986; Takishima et al., 1986; Nagahama et al., 1988; Furuta et al., 1989; Lim et al., 1994; Budich and Brunner, 2003; Durling et al., 2007), the extraction and the mass transfer rates (Bernad et al., 1993; Ikawa et al., 1993; Lim et al., 1995; Budich and Brunner, 2003; Pieck et al., 2015). For several years, the ethanol-water azeotrope, with a composition of 89.4 mol% of ethanol (DDBST GmbH, in press), had been a perpetual limit of the distillation: a concentration of ethanol higher than the azeotrope composition could not be achieved within one distillation column. Lim et al. (1994) determined that the upper limit of ethanol concentration in the  $\text{scCO}_2$  phase was attributed to the existence of a plait point, the point in which both liquid and vapour phases coincide and therefore no separation is possible. Hence, they postulated that ethanol could be concentrated above its atmospheric azeotropic composition if the extraction is performed below the critical pressure of the  $\text{CO}_2$ -ethanol system at the given temperature. Experimental conditions considered in this work had been chosen according to this.

## 2. Experiments

### 2.1. Mixing principles

The selection of the micro-mixer and therefore the type of mixing can affect the mass transfer as well as the extraction efficiency within the process. In this work, two different mixing principles are studied. Because of the experimental conditions required, the selection was quite limited. In the end, a multi-lamination micro-mixer and a Tee-mixer



**Fig. 2 – Description of the mixing principles studied in this work: multi-lamination (A) and T-type lamination (B). Source Löwe et al. (2000).**

were chosen (Fig. 1). The mixing principles are represented and explained in Fig. 2. HPIMM (High-Pressure Interdigital Micro-Mixer) is a passive micro-mixer, whose mixing principles rely on the pumping energy, with multi-laminating flow configurations consisting of the generation of an alternating arrangement of thin fluid compartments – *multilamellae* – which are then mixed by diffusion. On the other hand, the mixing in the Tee-mixer (T-type lamination) occurs by contacting both streams together on a third perpendicular jet. Operating conditions of both micro-mixers are compared in Table 1, it can be observed that inner volumes are similar but the HPIMM micro-mixer presents some limitations on flow rate and viscosity.

### 2.2. Materials and analytical methods

Distilled water and high-purity ethanol (>99.9%) were used for the preparation of feed solutions. Technical grade carbon dioxide (>99.5%) supplied by Linde was used as the solvent.

All water-ethanol compositions were determined by density measurements using an Anton Paar DMA 45 density-meter. The ethanol mass fraction of feed, extract and raffinate was calculated from literature density tables (Perry and Green, 1997).

**Table 1 – Comparison of operating conditions of HPIMM and Tee micro-mixers.**

	HPIMM	Tee
Temperature range (°C)	–40–500	–50–180
Pressure stability (up to)	600	1000
Flow rate (L/h)	0.04–2.5	–
Residence time (ms)	27–1350	–
Mixing channels $W \times L$ ( $\mu\text{m}$ )	$45 \times 200$	–
Inner volume ( $\mu\text{L}$ )	15	12.1
Max. viscosity (mPa s)	1000	–

**Table 2 – Experimental conditions, S-to-F and feed composition values of this work.**

Feed flow rate (in the pump)	0.5 mL/min
Feed composition	10–90% (w/w) ethanol
Mass Solvent-to-Feed ratio	5–25
Temperature 1st separator	60 °C
Pressure 1st separator	101 bar
Temperature 2nd separator	20 °C
Pressure 2nd separator	45 bar

### 2.3. Experimental conditions

All experiments in this work were performed at same conditions of pressure and temperature. Mass Solvent-to-Feed ratio (S-to-F) as well as feed concentration were varied. All experimental values are presented in Table 2.

### 2.4. Experimental setup

A high pressure micro-device apparatus was designed and assembled in our lab. It mainly comprises two HPLC pumps, two separators, two regulation valves and a micro-mixer. A schematic diagram of the experimental setup is shown in Fig. 3. The separators are able to withstand up to 400 bar and have an inner volume of 0.14 L. The temperature and pressure in both are maintained constant by thermostated water baths (represented in Fig. 3 by the dotted lines) and the two KAMMER regulation valves located just beyond each separator (12, 16). To test the mixing capacity of each micro-mixer and its feasibility for use in the high-pressure extraction process, two series of extraction experiments were performed, using either the Tee mixer or the HPIMM micro-mixer, which were installed in the experimental apparatus (8 in Fig. 3).

The flow chart of the experimental apparatus shows that either the micro-mixer or the Tee-mixer is the unit where the solvent and the liquid feed come into contact. After this contact, the feed and solvent mixture flows through a capillary with a diameter of 0.5 mm and a length of 20 cm, and enters the first separator for separation of the raffinate. The solvent phase is then expanded into a second separator for separating the extract. In this way, the separation of both phases, liquid and vapour, is achieved by changes of temperature and pressure, obtaining a raffinate and an extract.

Experiments were carried out as follows. Liquid CO<sub>2</sub> from the bottle (at approx. 50 bar) is cooled to 5 °C in a heat exchanger (4) before being pumped and heated to the working temperature. Once the system is pressurized and heated at the desired conditions (101 bar, 60 °C in the first separator and 45 bar, 20 °C in the second separator), the experiment is started and liquid feed is fed into the system. Both the solvent and feed are pumped continuously by two Gilson 305 HPLC pumps (5, 6) and flow rate of CO<sub>2</sub> is double-checked at the entrance and the exit of the system (3, 17). Continuous extraction experiments lasted for 4 h, raffinate and extract samples were collected through two valves (10 and 14, respectively).

## 3. Results

### 3.1. Equilibrium model

One of the main objectives of this work was to determine whether the equilibrium is reached and therefore one theoretical stage can be achieved within the extraction process in the micro-device apparatus. By knowing this, extraction processes which require more than one single stage could simply be designed as a number of micro-devices (the same number as extraction stages are required) placed in series. Therefore, the phase behaviour of the CO<sub>2</sub>–ethanol–water mixture was studied and modelled using ASPEN-Plus® and the Peng–Robinson Equation of State (Peng and Robinson, 1976; Mathias et al., 1991; Knapp et al., 1982), which is defined in ASPEN® as:

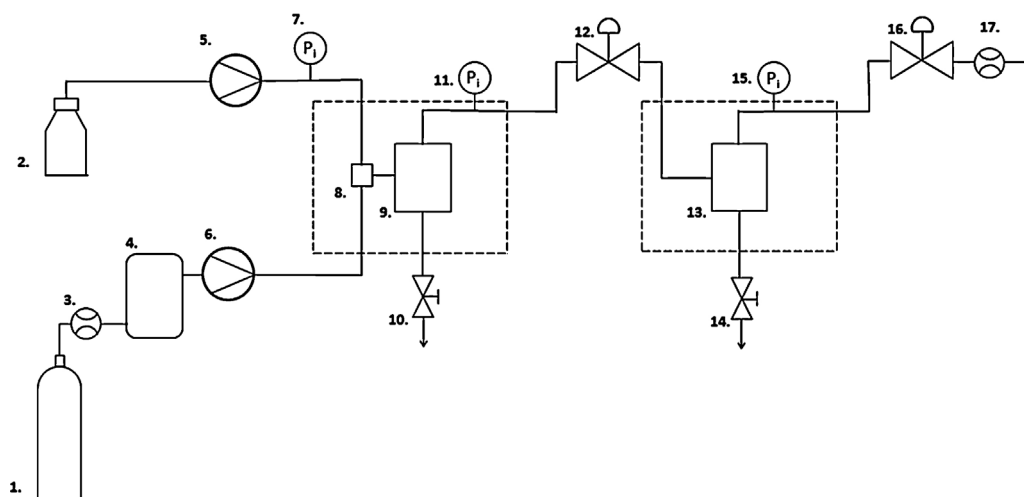
$$P = \frac{RT}{(c + V_m) - b} - \frac{a}{(V_m + c)(V_m + c + b) + b(V_m + c - b)} \quad (1)$$

$$b = \sum_i x_i b_i \quad (2)$$

$$c = \sum_i x_i c_i \quad (3)$$

$$a = a_0 + a_1 \quad (4)$$

$$a_0 = \sum_i \sum_j x_i x_j (a_i a_j)^{0.5} (1 - k_{ij}) \quad (5)$$



**Fig. 3 – Schematic diagram of high-pressure extraction apparatus. (1) CO<sub>2</sub> cylinder, (2) liquid feed flask, (3) flow meter, (4) cooler, (5, 6) HPLC pumps, (7, 11, 15) pressure regulators, (8) micro-mixer, (9, 13) separators, (10, 14) valves, (12, 16) regulation valves, (17) gas meter.**

**Table 3 – Binary interaction parameters for the PR EoS at 101 bar and 60 °C.**

	CO <sub>2</sub> –ethanol	CO <sub>2</sub> –water	Ethanol–water
$k_{12} = k_{21}$	0.11196	−0.01950	−0.09680
$l_{12}$	−0.08228	0.13973	0.02310
$l_{21}$	0.02295	−0.37128	0.11160

$$k_{ij} = k_{ij}^{(1)} + k_{ij}^{(2)}T + \frac{k_{ij}^{(3)}}{T} \quad k_{ij} = k_{ji} \quad (6)$$

$$a_i = \sum_{i=1}^n x_i \left( \sum_{j=1}^a x_j \left( (a_i a_j)^{1/2} l_{ij} \right)^{1/3} \right)^3 \quad (7)$$

$$l_{ij} = l_{ij}^{(1)} + l_{ij}^{(2)}T + \frac{l_{ij}^{(3)}}{T} \quad l_{ij} \neq l_{ji} \quad (8)$$

$$a_i = \text{fcn}(T, T_{ci}, p_{ci}, \omega_i) \quad (9)$$

$$b_i = \text{fcn}(T_{ci}, p_{ci}) \quad (10)$$

$$c_i = 0.40768 \left( \frac{RT_{ci}}{P_{ci}} \right) (0.29441 - z_{RAi}) \quad (11)$$

The factor  $z_{RAi}$  in (11) represents the Rackett parameter, which estimates the molar volume. The  $k_{ij}$ ,  $l_{ij}$  and  $l_{ji}$  binary interaction parameters were calculated in ASPEN from experimental results obtained by different authors (Furuta et al., 1989; Lim et al., 1994; Budich and Brunner, 2003) at the experimental conditions chosen in this work (101 bar, 60 °C). The obtained values are shown in Table 3. This model fits the experimental results from the authors well, as it is observed in Fig. 4. However, looking at the slope of the tie lines and comparing the model with the experimental results, it can be observed that the model fits the liquid phase better than the vapour phase compositions.

The relative deviation (RD) was used as an error criterion to assess the model. RD is defined in (12), where  $N$  is the number of data point,  $x_{EtOHexp}$  (mole fraction) is the experimental value and  $x_{EtOHcal}$  corresponds to the value calculated with the model.

$$RD = \frac{100}{N} \sum \frac{|x_{EtOHexp} - x_{EtOHcal}|}{x_{EtOHexp}} \quad (12)$$

The relative deviation of the vapour phase and the liquid phase data is 18% and 4%, respectively. Thus, we assumed that the raffinate composition (liquid phase) is more representative than the extract composition (vapour phase) for comparison of our experimental extraction results with the model.

### 3.2. Extraction results

In the following graphs, the results obtained with the HPIMM micro-mixer will be always represented by filled symbols (●, ■), while the results obtained with the Tee-mixer will be represented by hollow symbols (○, □). The results in Fig. 5 (HPIMM micro-mixer) and Fig. 6 (Tee-mixer) show the product's ethanol mass fractions (raffinate and extract) for different feed concentrations at given S-to-F of 8, 11.5 and 13. In these figures, the experimental results are compared with the model developed in ASPEN® so it can be observed that they fit well with the compositions predicted using the model, especially in the raffinate phase. Therefore it is concluded that equilibrium is reached through the extraction process and one single stage is achieved. It is important to point out that the standard deviation error is represented for every experimental point. However, this error is so small in some cases that it is not always appreciable in the graphs.

It is known that the extraction results are heavily dependent on the amount of solvent and therefore on the S-to-F. Hence, experiments keeping constant the feed volume

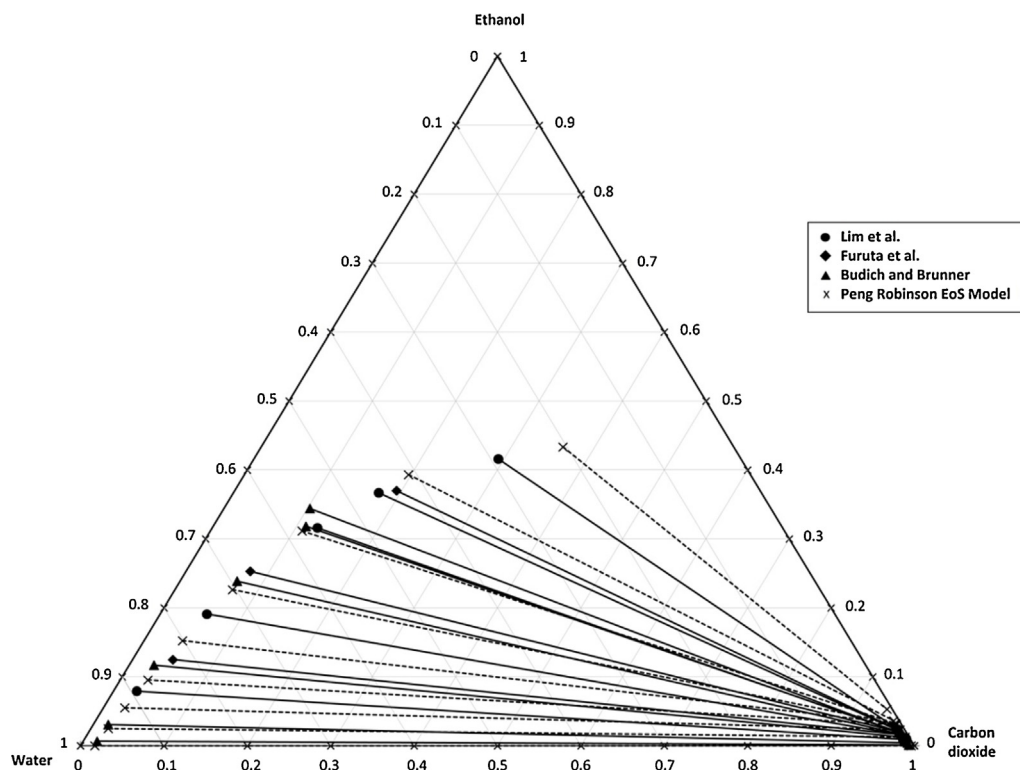


Fig. 4 – Phase behaviour of the ternary mixture CO<sub>2</sub>–ethanol–water at 60 °C and 101 bar.



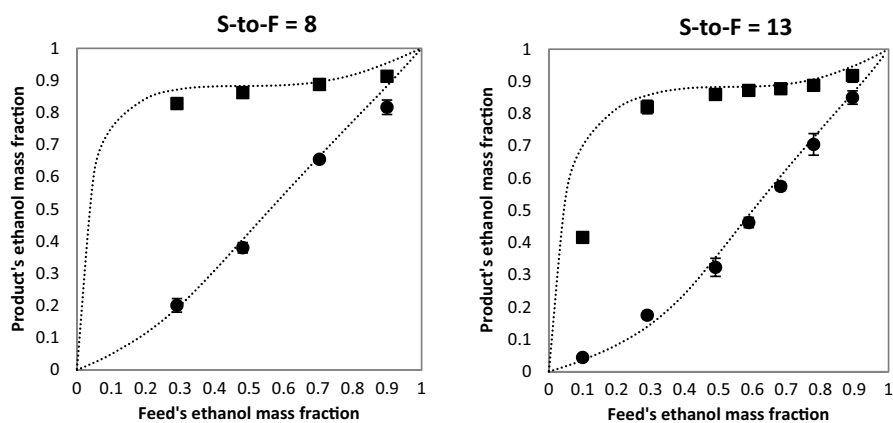


Fig. 5 – Experimental results of raffinate (●) and extract (■) compositions using the HPIMM micro-mixer and the prediction of a single theoretical stage model with mass S-to-F of 8 and 13.

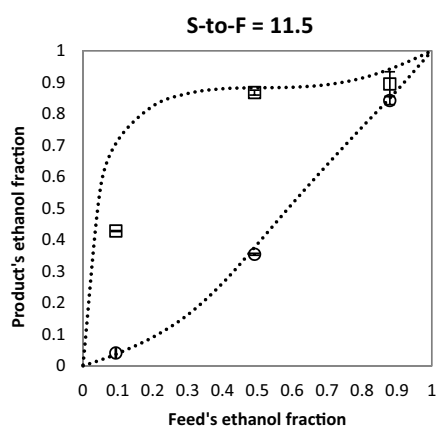


Fig. 6 – Experimental results of raffinate (○) and extract (□) compositions using the Tee-mixer and the prediction of a single theoretical stage model with mass S-to-F = 11.5.

flowrate and varying the solvent volume flowrate were performed. Fig. 7 shows the raffinate's and extract's ethanol mass fractions as a function of the total volume flowrate. The liquid feed flow rate is the same in every experiment (30 mL/h), while the scCO<sub>2</sub> flow rate is changed. The total volume flowrate corresponds to the sum of feed and solvent volume flowrates in the micro-device, at the conditions of 101 bar and 60 °C. It is observed that the experimental points, especially the raffinate's ethanol mass fraction, fit with the model well, which leads to conclude that in the range of total

volume flowrate between 500 and 1300 mL/h the equilibrium was always reached through the extraction process.

Furthermore, the residence time in the contact phase is inversely related to the volume flowrate. Due to that both micro-devices have similar inner volumes (see Table 1) and the capillary placed between the micro-device and the separator is the same in every experiment, the residence time range for both micro-devices is similar: between 120 ms and 650 ms. From Fig. 7 it is concluded that in this residence time range, the equilibrium is reached in the extraction process with each micro-device and therefore a single extraction stage is achieved.

### 3.2.1. Comparison: HPIMM micro-mixer vs. Tee-mixer

Results obtained in this work show that when using either the HPIMM micro-mixer or the Tee-mixer, separation of liquid and vapour phase was possible. Experimental results discussed above prove that extraction was performed successfully in the micro-device apparatus as, according to the model developed here using Peng–Robinson EoS and ASPEN<sup>®</sup>, equilibrium was reached through the process and one single extraction stage could be achieved. In Fig. 8, experimental data obtained with the HPIMM micromixer and the Tee-mixer are compared. Fig. 8(A) shows the product's ethanol mass fractions (raffinate and extract) obtained with the HPIMM micro-mixer and the Tee-mixer as a function of the feed concentration at S-to-F = 16 and a total volume flowrate of 1400 mL/h. It is seen that, for the same feed concentration, the products concentrations practically overlap, indicating that, at least at these experimental

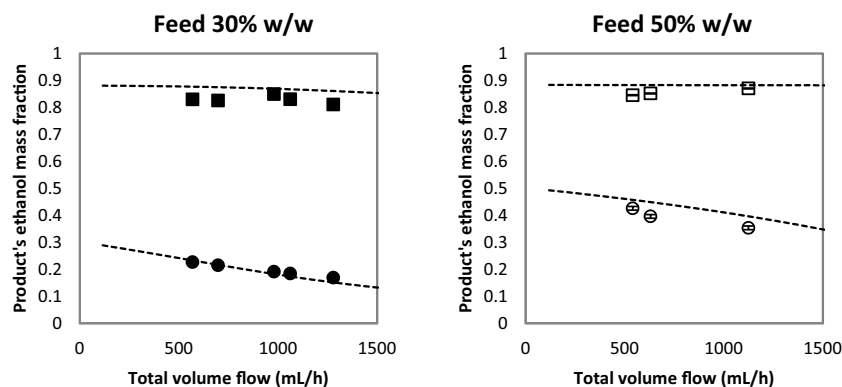
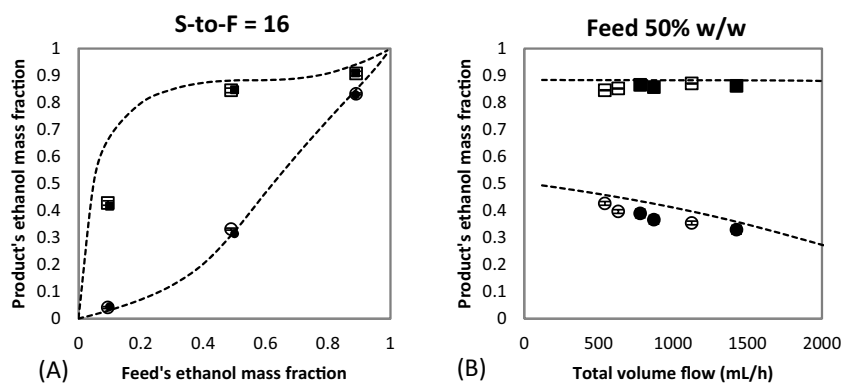


Fig. 7 – Product's ethanol mass fraction, raffinate (●, ○) and extract (■, □) and the prediction of a single theoretical stage model, as a function of the total volume flowrate in the micro-device (constant feed volume flowrate of 30 mL/h, variable CO<sub>2</sub> volume flowrate). Feed compositions are 30% w/w on the left (experiments with the HPIMM micro-mixer) and 50% w/w on the right (experiments with the Tee-mixer).



**Fig. 8 – Comparison of both micro-devices. On the left side (A), comparison of experimental results of raffinate and extract compositions using the HPIMM (●,■) and the Tee-mixer (○,□) with the model result of one single theoretical stage (S-to-F = 16). On the right side (B), product's ethanol mass fraction, raffinate (●, ○) and extract (■, □) and the prediction of a single theoretical stage model, as a function of the total volume flowrate in the micro-device (constant feed volume flowrate of 30 mL/h, variable CO<sub>2</sub> volume flowrate) for a feed composition of 50% w/w.**

conditions and with this total volume flowrate (1400 mL/h), the feasibility of both micro-devices for the SFE process is comparable in the three different cases compared (i.e. feed concentrations of 10%, 50% and 90% w/w of ethanol). Furthermore, in Fig. 8(B), which shows the raffinate's and extract's ethanol mass fractions obtained for a feed composition of 50% w/w of ethanol as a function of the total volume flowrate, it is observed that results with the HPIMM micro-mixer and with the Tee-mixer fit well with the model and moreover both micro-devices present a similar behaviour in this range of total volume flowrate, between 500 and 1500 mL/h.

#### 4. Conclusions

The feasibility of a SFE process using micro-devices and the effects of the mixing principle in the extraction results were investigated at a lab scale. Experimental results obtained in this work concluded that separation of ethanol–water binary mixtures using scCO<sub>2</sub> as solvent in a high pressure micro-device extraction plant by apparatus is possible and that thermodynamic equilibrium is achieved in the extraction process. Two different mixing principles were considered: multi-lamination and T-type lamination. Satisfactory results were obtained with both micro-devices, as it has been proved that equilibrium could be reached when using either one or the other one. Extraction was performed at different total volume flowrates, keeping always constant the feed volume flowrate at 30 mL/h and varying the solvent volume flowrate. It was found that in the range between 500 and 1500 mL/h, equilibrium could be reached in both micro-devices.

#### Acknowledgements

The authors want to thank the People programme (Marie Curie Actions) of the European Union's Seventh Framework Programme FP7/2007–2013/ under REA grant agreement no. 316959 (DoHip project, "Training Program for the Design of Resource and Energy Efficient Products by High Pressure Processes"). The authors would also like to thank Dániel Varga for his help and assistance.

#### References

Assmann, N., Kaiser, S., Rudolf von Rohr, P., 2012. [Supercritical extraction of vanillin in a microfluidic device](#). *J. Supercrit. Fluids* 67, 149–154.

- Assmann, N., Ładosz, A., Rudolf von Rohr, P., 2013. [Continuous Micro Liquid-Liquid Extraction](#). *Chem. Eng. Technol.* 36 (6), 921–936.
- Benz, K., Jäckel, K.P., Regenauer, K.J., Schiewe, J., Drese, K., Ehrfeld, W., Hessel, V., Löwe, H., 2001. [Utilization of micromixers for extraction processes](#). *Chem. Eng. Technol.* 24 (1), 11–17.
- Bernad, L., Keller, A., Barth, D., 1993. [Separation of ethanol from aqueous solutions by supercritical carbon dioxide—comparison between simulations and experiments](#). *J. Supercrit. Fluids* 6, 9–14.
- Budich, M., Brunner, G., 2003. [Supercritical fluid extraction of ethanol from aqueous solutions](#). *J. Supercrit. Fluids* 25, 45–55.
- Dortmund Data Bank, DDBST GmbH, 2010. Oldenburg, Germany, [www.ddbst.de](http://www.ddbst.de).
- Durling, N.E., Catchpole, O.J., Tallon, S.J., Grey, J.B., 2007. [Measurement and modelling of the ternary phase equilibria for high pressure carbon dioxide–ethanol–water mixtures](#). *Fluid Phase Equilib.* 252, 103–113.
- Fornari, T., Hernandez, E.J., Ruiz-Rodriguez, A., Senorans, F.J., Reglero, G., 2009. [Phase equilibria for the removal of ethanol from alcoholic beverages using supercritical carbon dioxide](#). *J. Supercrit. Fluids* 50, 91–96.
- Furuta, S., Ikawa, N., Fukuzato, R., Imanishi, N., 1989. [Extraction of ethanol from aqueous solutions using supercritical carbon dioxide](#). *Kagaku Kogaku Ronbunshu* 15, 519–525.
- Ikawa, N., Nagase, Y., Tada, T., Furuta, S., Fukuzato, R., 1993. [Separation process of ethanol from aqueous solutions using supercritical carbon dioxide](#). *Fluid Phase Equilib.* 83, 167–174.
- Gilbert, M.L., Paulaitis, M.E., 1986. [Gas-liquid equilibrium for ethanol–water–carbon dioxide mixtures at elevated pressures](#). *J. Chem. Eng. Data* 31, 296–298.
- Güvenç, A., Mehmetoglu, Ü., Çalimli, A., 1998. [Supercritical CO<sub>2</sub> extraction of ethanol from fermentation broth in a semicontinuous system](#). *J. Supercrit. Fluids* 13, 325–329.
- Kenig, E.Y., Su, Y., Lautenschleger, A., Chasanis, P., Grünwald, M., 2013. [Micro-separation of fluid systems: a state-of-the-art review](#). *Sep. Purif. Technol.* 120, 245–264.
- Knapp, H., Döring, R., Oellrich, L., Plöcker, U., Prausnitz, J.M., 1982. [Vapor-Liquid Equilibria for Mixtures of Low Boiling Substances](#). *Dechema In Chem. Data Series* 6.
- Löwe, H., et al., 2000. [Micromixing technology](#). In: *Fourth International Conference on Microreaction Technology, IMRET 4, Topical Conference Proceedings, Atlanta, USA. A.I.Ch.E.*, pp. 31–47.
- Lim, J.S., Lee, Y.Y., Chun, H.S., 1994. [Phase equilibria for carbon dioxide–ethanol–water system at elevated pressures](#). *J. Supercrit. Fluids* 7, 219–230.
- Lim, J.S., Lee, Y.W., Kim, J.D., Lee, Y.Y., 1995. [Mass-transfer and hydraulic characteristics in spray and packed extraction columns for supercritical carbon dioxide–ethanol–water system](#). *J. Supercrit. Fluids* 8, 127–137.

- Mathias, P.M., Klotz, H.C., Prausnitz, J.M., 1991. Equation of state mixing rules for multicomponent mixtures: the problem of invariance. *Fluid Phase Equilib.* 67, 31–44.
- McHugh, M.A., Krukonis, V.J., 1994. *Supercritical Fluid Extraction, second ed.* Butterworth-Heinemann, Boston, MA.
- Nagahama, K., Suzuki, J., Suzuki, T., 1988. High pressure vapor-liquid equilibrium for the supercritical CO<sub>2</sub> + ethanol + water system. In: *Proceedings of the First International Symposium on Supercritical Fluids, Nice, France*, pp. 143–150, vol. 1.
- Nguyen, N.T., 2012. *Micromixers: Fundamentals, Design and Fabrication, second ed.* Elsevier, Waltham, MA.
- Peng, D.Y., Robinson, D.B., 1976. A new two-constant equation-of-state. *Ind. Eng. Chem. Fundam.* 15, 59–64.
- Perry, H.R., Green, D.W., 1997. *Perry's Chemical Engineers Handbook, seventh ed.* McGrawHill, New York, NY.
- Pieck, C.A., Crampon, C., Charton, F., Badens, E., 2015. Multi-scale experimental study and modelling of the supercritical fractionation process. *J. Supercrit. Fluids* 105, 158–169.
- Reverchon, E., De Marco, I., 2006. Supercritical fluid extraction and fractionation of natural matter. *J. Supercrit. Fluids* 38 (2), 146–166.
- Takishima, S., Saiki, K., Arai, K., Saito, S., 1986. Phase equilibrium for CO<sub>2</sub>-C<sub>2</sub>H<sub>5</sub>OH-H<sub>2</sub>O system. *J. Chem. Eng. Jpn.* 19, 48–56.